Characterisation of Endometrial Gland Defects Associated with Recurrent Missed Miscarriage

Komal Makwana

A thesis submitted to the University of Warwick for the degree of Doctor of Philosophy.

Division of Biomedical Sciences
Warwick Medical School
University of Warwick

August 2021

Contents

List of Figures

Chapter 1: Introduction

Chapter 2: Material and Methods

Chapter 3: Analysis of the Luteal Endometrium in Recurrent Missed Miscarriage

List of Tables

Acknowledgements

First, I thank my supervisor Professor Jan Brosens for his guidance throughout my PhD project. Your commitment and passion to reproductive science and high standards have moulded me into a better scientist and I thank you for your mentorship. Next, I thank Dr Emma Lucas for your supervision, scientific advice and for being the person I looked up to in the lab. I am extremely grateful for all your kindness and support. I also thank Professor Mark Christian for your supervision and continued support during my PhD.

From the lab, I thank first and foremost, Dr Thomas Rawlings. From undergrad students to becoming the 'OG' of Brosens' Team Organoid, I thank you for being the best lab partner. I am grateful for all your endless support and motivation, especially in the moments I doubted myself. The collaborative nature of the Brosens' lab group has been essential for helping me build my thesis and came with a large amount of support and generosity over the past four years. Therefore, I thank Dr Joanne Muter, Dr Maria Diniz da Costa, Dr Tauqeer Alam, Dr Paul Brighton, Dr Pavle Vrljicak, Dr Katherine Fishwick, Chow Seng Kong and Maria Tryfonos. To the Implantation Clinic team and all the hundreds of women who have donated research samples, this thesis would not be possible without you, so thank you.

To everyone in my family, I thank you for your love, support, and constant motivation. I also thank Olga and Jason Nearchou for being my 'home away from home' for the past three years. I am immensely grateful to all the support, endless encouragement and laughs you provided through my PhD, especially during my writing period. To my dearest friends, Paulina Porkorska, Frances Stannard, Sophie Lay, Fathima Mohammed, Maria Diniz da Costa and Thomas Rawlings I cannot put into words how grateful I am for your endless support and friendship. Finally, I would like to thank Chris Hemsworth for his motivational video that was replayed several times in my PhD, and a special thank you to BTS for being the happy place of my thesis.

Declaration

This thesis is submitted to the University of Warwick in support of my application for the degree of Doctor of Philosophy. It has been composed by myself and has not been submitted in any previous application for any degree.

The work presented (including data generated and data analysis) was carried out by the author expect in the cases outlined below:

1) Gland LCM RNA-seq data collection was conducted by Dr Flavio Barros for his thesis, 'Characterisation of human endometrial glandular epithelium *in vitro* and *in vivo*' (2017). Data was reanalysed for this thesis (Chapter 3).
2) Collaboration with Dr Tauqeer Alam in the bioinformatic analysis of both LCM gland RNA-seq datasets (Chapter 3) and the gland organoid dataset (Chapter 5).
3) Collaboration with Dr Joanne Muter in data collection of transcript levels of molecular timing genes in endometrial biopsies (Chapter 3).
4) Collaboration with Dr Katherine Fishwick in data collection regarding immunohistochemistry of uNK and $p16^{INK4a}$ in endometrial biopsies (Chapter 3 and 5).
5) Collaboration with Dr Thomas Rawlings in data collection regarding the minimal differentiation medium experiment and immunohistochemical analysis of endometrial gland organoids and assembloids (Chapter 6).
6) Collaboration with Dr Emma Lucas in the preparation of the assembloid scRNA-seq experiment and the bioinformatic analysis of the scRNA-seq dataset (Chapter 6).

Parts of this thesis have been published by the author:

Rawlings, T. M., **Makwana, K.**, Taylor, D. M., Molè, M. A., Fishwick, K. J., Tryfonos, M., Odendaal, J., Hawkes, A., Zernicka-Goetz, M., Hartshorne, G. M., Brosens, J. J. & Lucas, E. S. 2021. Modelling the impact of decidual senescence on embryo implantation in human endometrial assembloids. *Elife*, 10, e69603.

Rawlings, T. M., **Makwana, K.**, Tryfonos, M. & Lucas, E. S. 2021. Organoids to model the endometrium: implantation and beyond. *Reproduction and Fertility*, 2, R85-R101.

Abstract

Recurrent pregnancy loss, defined as multiple miscarriages, is a distressing condition associated with significant physical trauma and psychological morbidity. Miscarriage often causes bleeding in early gestation, reflecting the breakdown of the emerging maternal-fetal interface. However, bleeding is not a prominent feature in missed miscarriage, which typically involves very early-onset fetal growth restriction, fetal bradycardia and ultimately fetal demise. I hypothesised that recurrent missed miscarriage (RMM), defined here as 3 or more 'silent' miscarriages, reflects an endometrial glandular defect that compromises histotrophic nutrition before the onset of placental perfusion around 12 weeks of pregnancy.

To test this hypothesis, RNA-sequencing data of laser-captured mid-luteal endometrial glands from RMM patients and control subjects were subjected to metabolic modelling using flux variability and balance analysis. Computational modelling revealed a notable metabolic signature in RMM, characterised by heightened oxidative phosphorylation and fatty acid oxidation and decreased glycolysis, which was not attributable to glandular asynchrony. To explore the drivers of this endometrial defect in RMM, I optimised a robust organoid protocol to assess glandular differentiation *in vitro*. RMM organoids not only recapitulated the *in vivo* metabolic signature but displayed a multitude of defects caused by more naïve progenitor cells, including attenuated Wnt and Notch signalling, and impaired specification of epithelial cells into differentiated and senescent subpopulations upon progesterone-induced cell cycle arrest and differentiation. Importantly, senescent epithelial cells, which are a major source of growth factors and extracellular matrix proteinases, may critically regulate endoglandular trophoblast invasion and access to glandular secretions in early gestation. Quantification of $p16^{INK4}$ immuno reactivity in 48 biopsies confirmed that RMM is associated with lack of glandular senescence during the peri-implantation window. Collectively, the data indicate that aberrant metabolic programming of endometrial epithelial progenitor cells compromises glandular function, thus revealing a novel therapeutic target for RMM prevention.

List of Abbreviations

8-bromo-cAMP	8-Bromoadenosine-3', 5'-cyclic monophosphate
2D	Two-dimensional
3D	Three-dimensional
ACADSB	Short/branched chain specific acyl-CoA dehydrogenase
Acetyl-CoA	Acetyl coenzyme A
ACONT	Aconitase
ADP	Adenosine diphophosphate
AKGD	α-ketoglutarate dehydrogenase
ALD	Aldolase
ATP	Adenosine triphosphate
ASRM	American Society of Reproductive Medicine
AXIN2	Axis inhibition protein 2
BM	Base medium
BMI	Body Mass Index
BMP	Bone morphogenetic growth factor
BSA	Bovine serum albumin
CI	Complex I
CII	Complex II
CIII	Complex III
CIV	Complex IV
CV	Complex V
C1/C2/C3/C4	Cycle 1/2/3/4
C160CPT1	Carnitine O-palmitoyltransferase
C160CPT2	C160 transport into the mitochondria
C226CPT1	Carnitine C22:6 transferase
C226CPT2	C226 transport into the mitochondria
cAMP	Cyclic adenosine monophosphate
Cas9	CRISPR associated protein 9
cDNA	Complementary DNA
CDX2	Caudal Type Homeobox #
CO_2	Carbon dioxide
CoA-SH	Coenzyme A
COX-2	Cyclooxygenase-2
CRISPR	Clustered Regularly Interspaced Short Palindromic Repeats

CS	Citrate synthase
Ct	Cycle threshold
CXCL14	Cytokine chemokine (C-X-C) ligand 14
$cytC_{oxid}$	cytochrome c (oxidised)
$cyctC_{red}$	cytochrome (reduced)
DCC-FBS	Dextran-coated charcoal treated foetal bovine serum
dCt	Delta CT
DEGs	Differentially expressed genes
DIO2	Type II iodothyronine deiodinase
DNase I	Deoxyribonuclease type 1
DPP4	Dipeptidyl-peptidase 4
DMEM	Dulbecco's Modified Eagle Medium
DMSO	Dimethyl sulphoxide
E.coli	*Escherichia coli*
E-cadherin	Epithelial cadherin
E_2	Oestradiol
ECM	Extracellular matrix
EDTA	Ethylenediaminetetraacetic acid
EGF	Epithelial growth factor
ELF5	E74-like factor 5
EMT	Epithelial-mesenchymal transition
ENO	Enolase
EnSC	Stromal cells
EpC	Epithelial cells
EPCAM	Epithelial cell adhesion molecule
ER	Oestrogen receptor
ERA	Endometrial Receptivity Analysis
ERK	Extracellular signal regulated
EVT	Endovascular trophoblast
ExM	Expansion Media
$FADH_2$	Flavin adenine dinucleotide (reduced form)
FAO	Fatty acid oxidation
FAOCx	Fatty acid oxidation (carbon chain)
FBA	Flux balance analysis
FBS	Foetal bovine serum
FGF	Fibroblast growth factor

FOXA2	Forkhead box A2
FSH	Follicle stimulating hormone
FUM	Fumerase
FVA	Flux variability analysis
ESHRE	European Society of Human Reproduction and Embryology
G6PDH2	Glucose 6-phosphate dehydrogenase
GAPDH	Glyceraldehyde 3-phosphate dehydrogenase
GEO	Gene Expression Omnibus
GDP	Guanosine diphosphate
GLUT	Glucose transporter
GND	6-phosphogluconate dehydrogenase
GO	Gene ontology
GPX3	Glutathione peroxidase 3
GTP	Guanosine triphosphate
H^+	Hydrogen ion
H_2O	Water
hCG	Human chorionic gonadotrophin hormone
HES5	Hes family bHLH transcription factor 5
HEX1	Hexokinase
HGF	hepatocyte growth factor
hPL	Human placental lactogen hormone
IHC	Immunohistochemistry
ICD	Isocitrate dehydrogenase
IGF1	Insulin-like growth factor 1
IGF2	Insulin-like growth factor 2
iPSC	Induced pluripotent stem cells
L19	Ribosomal L19
LCM	Laser capture microdissection
LDH	Lactate dehydrogenase
LEF1	Lymphoid enhancer binding factor 1
LGR5	Leucine Rich Repeat Containing G Protein-Coupled Receptor 5
LH	Luteinising hormone
LHR	Luteinising hormone receptor
IL	Interleukin
LIF	Leukaemia inhibitory factor
LIFR	LIF receptor subunit alpha

LRIG1	Leucine rich repeats and immunoglobulin like domains 1
MAML2	Mastermind like transcriptional coactivator 2
MAML3	Mastermind like transcriptional coactivator 3
Max	Maximum
MDH	Malate dehydrogenase
MDM	Minimal differentiation medium
MET	Mesenchymal to epithelial transition
Min	Minimum
MMP	Matrix Metalloproteinases
MPA	Medroxyprogesterone acetate
N-cadherin	Neural cadherin
NAC	N-Acetyl-L-Cysteine
NAD^+	Nicotinamide adenine dinucleotide (oxidised form)
NADH	Nicotinamide adenine dinucleotide (reduced form)
$NADP^+$	Nicotinamide adenine dinucleotide phosphate (oxidised form)
NADPH	Nicotinamide adenine dinucleotide phosphate (reduced form)
NK	Natural killer
OFE	Organoid forming Efficiency
P_4	Progesterone
p16	$p16^{iNK4a}$
PAEP	Progestagen-associated endometrial protein
P0/P1/P2/P3	Passage 1/2/3/4
PBS	Phosphate buffered saline
PCA	Principal component analysis
PDH	Pyruvate dehydrogenase
PFK	Phospho-fructokinase-1
PGE_2	Prostaglandin E2
PGR	Progesterone receptor
PGI	Phosphohexose isomerase
PGK	Phosphoglycerate kinase
PGL	6-phosphogluconolactonase
PGM	Phosphoglycerate mutase
P_i	Phosphate
PRL	Prolactin
PRLR	Prolactin receptor
PROM1	Prominin 1

PPARGC1A	PPARG coactivator 1 alpha
PPP	Pentose phosphate pathway
PUGKO	Progestin uterine gland knockout
PUL	Pregnancy of unknown location
PYK	Pyruvate kinase
Q	Ubiquinone
QH_2	Ubiquinol
RIN	RNA integrity number
RMM	Recurrent Missed Miscarriage
RNA-seq	RNA-sequencing
RPI	Ribose 5-phosphate isomerase
RPE	Ribulose 5-phosphate 3 – epimerase
RPL	Recurrent Pregnancy Loss
RT	Reverse Transcriptase
RT-qPCR	Reverse Transcriptase Quantitative Polymerase Chain Reaction
ROS	Reactive oxygen species
SASP	Senescence-associated secretory phenotype
SAT1	Diamine acetyltransferase 1
scRNA-seq	Single-cell RNA-sequencing
SCARA5	Scavenger receptor class A member 5
SCD	Stearoyl-CoA desaturase
SD	Standard deviation
SDH	Succinate dehydrogenase
SLC15A2	Solute carrier family 15 member 2
snDC	Senescent decidual cells
SNN	Shared Nearest Neighbour
SPP1	Osteopontin
SSEA-1	Stage-specific embryonic antigen 1
SOX9	SRY-Box transcription factor 9
SUCOAS1	Succinyl Co-A synthetase
TAD	Transaldolase
TCA	Tricarboxylic acid cycle
TBS	Tris-buffered saline
TBS-T	Tris-buffered saline-Tween 20
TKT	Transketolase

TGF	Transforming growth factor
TPI	Triose phosphate isomerase
TPM	Transcripts per million
UGKO	Uterine gland knockout
VEGF	Vascular endothelial growth factor
UMAP	Uniform Manifold Approximation and Projection
uNK	Uterine Natural Killer
Wnt	Wingless/Integrated
WNT3A	Wnt Family Member 3A
WNT7A	Wnt Family Member 7A

Chapter 1:
Introduction

1.1 Miscarriage

1.1.1 Recurrent Pregnancy Loss

Guidelines from the European Society of Human Reproduction and Embryology (ESHRE) as well as the American Society of Reproductive Medicine (ASRM) define recurrent pregnancy loss (RPL) as the failure of two or more pregnancies confirmed by ultrasonography or histopathology, but not including ectopic and molar pregnancies (Bender Atik et al., 2018, Practice Committee of the American Society for Reproductive, 2012) (Table 1.1.). These miscarriages can be sub-classified as early miscarriage including anembryonic, yolk sac, embryonic; and fetal miscarriage (Bender Atik et al., 2018, Dimitriadis et al., 2020) (Table. 1.1). However, the inclusion of non-consecutive losses, biochemical losses and failed pregnancy of unknown location (PUL) is debatable (Dimitriadis et al., 2020). The upper gestation limit of miscarriage classification is dependent on legal definition of fetal viability in each country (20-24 weeks) (Dimitriadis et al., 2020). The average prevalence of RPL is estimated to be between 1 and 4% of all women who achieve pregnancy based on large-scale studies in Europe and USA (Rasmark Roepke et al., 2017, Magnus et al., 2019, Dimitriadis et al., 2020).

Maternal age at conception has shown to be associated with pregnancy loss rates (Risch et al., 1988, Berkowitz et al., 1990, Fretts et al., 1995, Andersen et al., 2000, Magnus et al., 2019). A recent population-based study demonstrated age-associated risk of pregnancy loss followed a J-shaped curve (Magnus et al., 2019). Women aged 25-29 years had the lowest risk of pregnancy loss (9.8%), which increased in women aged 30-35 years and rose even more so in women aged 40-44 years (33.2%) (Magnus et al., 2019). The primary driver of age-associated pregnancy loss is chromosome errors (aneuploidy) in the conceptus, with more than 90% of aneuploid miscarriages caused by errors in meiosis, occurring mainly at meiosis I in the oocyte (Hassold and Hunt, 2001, Nagaoka et al., 2012). Likewise, the incidence of age-associated meiotic error in preimplantation embryos and oocytes follows the J-shaped curve of age-associated pregnancy loss risk (Capalbo et al., 2017, Gruhn et al., 2019).

Another risk factor for RPL is the number of previous pregnancy losses, independent of maternal age, potentially accounted for by uterine factors (Dimitriadis et al., 2020). Evidence from population-based studies shows that after adjusting for age, the odds ratio for miscarriage increases stepwise after each loss (Knudsen et al., 1991,

Ogasawara et al., 2000, Maconochie et al., 2007, Kolte et al., 2021). Notably, women who have experienced six or more miscarriages have an odds ratio as high as 63% (Coomarasamy et al., 2020). One of these studies also demonstrated a previous live birth had a positive impact on the chance of success in the next pregnancy despite the number of previous losses, suggesting a live birth resets the endometrial environment (Kolte et al., 2021).

Other risk factors include genetic factors, maternal health (obesity, uterine malformations, antiphospholipid syndrome, overt hyperthyroidism, chronic endometritis and impaired decidualisation), and environmental and lifestyle factors (stress, smoking and excessive alcohol consumption) (Dimitriadis et al., 2020). However, in 50-70% of couples with RPL, no risk factors are identified (Ford and Schust, 2009, Jaslow et al., 2010). Some of these risk factors for RPL can be modified with lifestyle choices (Dimitriadis et al., 2020). However, the current evidence for most treatments is limited and conflicting. The strongest evidence was concluded from a recent large multicentre trial (PRISM) that found micronized progesterone (P_4) prevented miscarriages in women with a history of more than three losses or those with threatened miscarriage (Coomarasamy et al., 2019). However, the mechanism is unclear. A loss of endometrial mesenchymal stem cells has been associated with RPL (Lucas et al., 2016) and treatment with sitagliptin, a dipeptidyl-peptidase 4 (DPP4) inhibitor, was found to increase the abundance of these cells in RPL patients in a pilot study (Tewary et al., 2020). However, further trials are required.

1.1.2 Recurrent Missed Miscarriage

The current classification of RPL considers different types of miscarriage with the inclusion or exclusion of certain types of miscarriage varying for each region (Bender Atik et al., 2018, Quenby et al., 2021). However, there is no distinction between a patient who may have three types of miscarriage, e.g., a biochemical loss, an early miscarriage, and a fetal loss, and another patient who has three repeated fetal losses. Despite there being subtypes, patients are diagnosed with RPL without subcategorization. It is plausible the aetiology of these patients is distinct, but most studies have not distinguished subgroups within RPL by following the current definition (Tewary et al., 2020, Smits et al., 2020, Coomarasamy et al., 2020, Quenby et al., 2021).

Missed miscarriage is an intrauterine pregnancy loss with an empty gestational sac with a mean sac diameter of 25mm or more, or with an embryo that has a crown-rump

length more than 7 mm without cardiac activity (Quenby et al., 2021). Therefore, this pregnancy loss occurs without bleeding and pain, and expulsion of pregnancy tissue (Ghosh et al., 2021). At the Implantation Clinic, a research clinic based at University Hospital Coventry and Warwickshire, a subgroup of RPL patients with a distinct phenotype were identified by an experienced gynaecologist. These patients are herein referred to as recurrent missed miscarriage (RMM). Since 2015, approximately 14% of all RPL patients that visited the clinic were classified as RMM. Unlike most RPL, RMM is not associated with overt breakdown of the maternal-fetal interface and bleeding. Instead, RMM is defined here as a recurrent pattern of pregnancy loss that typically involves early-onset fetal growth restriction (defined by ultrasound dating based on crown-rump measurement being less advanced compared to dating on the basis of their last menstrual period) followed by fetal demise and, not infrequently, delayed breakdown of the decidua and expulsion of the conceptus. Medical, or surgical management is required. RMM does not include pregnancy losses with an empty gestational sac.

A few studies were conducted to understand the pathology of missed miscarriages, which demonstrated potential defects in development of the placenta (Jauniaux et al., 2003b, Chen et al., 2015, Zhu et al., 2020) as well as disrupted metabolic pathways using NMR-based serum metabolomics approach (Wu et al., 2018). There are also studies that suggest of a similar phenotype to RMM using terms such as ‘recurrent early missed abortion’ or ‘recurrent missed abortions’ (Halder and Fauzdar, 2006, Radović Janošević et al., 2016). However, the terminology used was unclear and did not have a clear definition like RMM. The studies did not state if the miscarriages were repeated missed miscarriages and one included different types of miscarriages by describing them as ‘missed’, ‘blighted ovum’ and even ‘spontaneous’ (Halder and Fauzdar, 2006, Radović Janošević et al., 2016). The literature on RMM using the criteria above is limited to a preliminary study, which found an upregulated mitochondrial gene signature in glands isolated by laser capture microdissection (LCM) from endometrial biopsies of RMM patients (Barros, 2017). A plausible, but as yet unsubstantiated, cause of RMM is a failure of the endometrial glands to provide sufficient histotrophic nutrition to support ongoing fetal development.

Table 1.1: Types of miscarriage. Early miscarriage can be sub-classified into anembryonic, yolk sac and embryonic miscarriage. *Not included in RPL.

Terms	Presentation	References
Early Miscarriage	An intrauterine pregnancy loss before 10 weeks of gestation.	(Kolte et al., 2015)
Anembryonic	An intrauterine pregnancy loss with an empty gestation sac.	(Kolte et al., 2015, Dimitriadis et al., 2020)
Yolk Sac	An intrauterine pregnancy loss with a gestation sac and yolk sac but no fetal pole.	(Kolte et al., 2015, Dimitriadis et al., 2020)
Embryonic	An intrauterine pregnancy loss with an embryo without cardiac activity.	(Kolte et al., 2015, Dimitriadis et al., 2020)
Fetal Miscarriage	Pregnancy loss on or after 10 weeks of gestation with a fetus (≥33 mm) on ultrasound.	(Stephenson and Kutteh, 2007, Kolte et al., 2015)
Missed (or silent) miscarriage	Pregnancy loss with an empty gestational sac with a mean sac diameter of ≥ 25mm or with an embryo with a crown-rump length >7 mm without cardiac activity.	(Quenby et al., 2021)
Biochemical loss	Pregnancy loss of a non-visualised pregnancy that was only documented by a positive pregnancy test.	(Dimitriadis et al., 2020)
Pregnancy of Unknown Location (PUL)	Pregnancy loss of a non-visualised pregnancy with resolution of serum β-hCG after spontaneous or required medical (treated) or surgical (resolved) management.	(Barnhart et al., 2011)
Ectopic Miscarriage*	Implantation of embryo outside the uterine cavity.	(Dimitriadis et al., 2020)
Molar Miscarriage*	A pregnancy with excessive placental growth due to an abnormal embryo.	(Dimitriadis et al., 2020)

1.2 Development and Regeneration of Endometrial Glands

1.2.1 Human Endometrium

A single uterine body is found in humans, developed from the fusion of the paramesonephric (Müllerian) ducts around 8 weeks of gestation that gives rise to the female reproductive tract (Gray et al., 2001). Derived from the inner layer of ductal mesenchyme, the endometrium is the inner mucosal lining of the uterus. The endometrium is formed of the dynamic superficial *stratum functionalis*, which is almost entirely lost during menstruation in non-pregnant cycles, and the stable lower *stratum basalis* (Fig. 1.1). The endometrial functional layer consists of a zone of luminal epithelium and subjacent stroma (zone I), and a second zone of sparse stroma surrounded by the straight portion of endometrial glands (zone II) (Padykula, 1989). The basal layer functions as the germinal compartment of the endometrium that is not shed during menstruation and contains the stem/progenitor cells that regenerate the functional layer (Padykula, 1989). Two additional zones can be found in the basalis, which contain loose stroma and the bodies of the glands (zone III) as well the final zone where the glands terminate (zone IV). Many different cell types can be found in the endometrium including luminal and glandular epithelial (EpC), stromal (EnSC), endothelial, and immune cells. This dynamic tissue plays a pivotal role in reproduction as it is essential for the preparation of implantation and if pregnancy occurs, provides a protective and nutritious environment (Critchley et al., 2020).

1.2.2 Development of Endometrial Glands

Growing evidence has demonstrated an indisputable role for uterine glands and their secretions as principal regulators of stromal decidualisation, implantation, placentation as well as conceptus development and survival (Kelleher et al., 2019). Histological analysis of uterine gland development, or adenogenesis, has revealed that simple columnar epithelium gives rise to numerous invaginations, representing the primordial glandular epithelium buds in the undifferentiated uterus (Koff, 1933, Gray et al., 2001). Adenogenesis is regulated intrinsically through proliferation, cell-cell interactions, growth factors and their inhibitors, including WNTs (Wingless/Integrated), transcription factors such as forkhead box A2 (FOXA2) as well as through extrinsic factors originating from the ovary, pituitary and mammary gland (Kelleher et al., 2019) (Table 1.2).

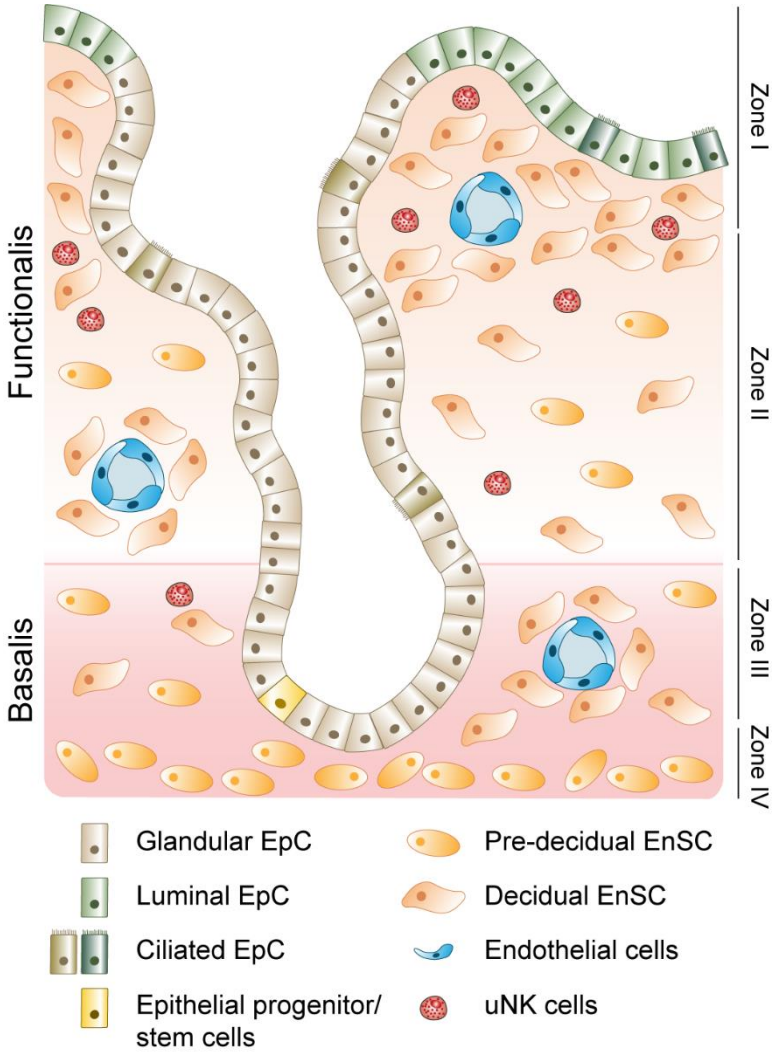

Figure 1.1. ***A schematic of the human endometrium.***

The endometrium is comprised of two layers: the superficial *stratum functionalis* and the lower *stratum basalis*. Clonal endometrial glands grow out from the basalis through the proliferative phase into the luminal and glandular epithelium of the adult endometrium. The glands are surrounded by EnSC and immune cells, such as uNK cells. The endometrium is vascularised with sub-mucosal capillary network and spiral arteries. Cell types are labelled in the key below the diagram.

Table 1.2: Factors involved in endometrial adenogenesis. Distilled information from (Kelleher et al., 2019)

Factors	Function	References
Wnt signalling	Canonical signalling stimulates epithelial adhesion and proliferation. Wnt7a coordinates several cell development pathways for postnatal uterine differentiation and growth.	(Carta and Sassoon, 2004, Kelleher et al., 2019)
FOXA2	A conserved critical transcription factor controlling differentiation and function of uterine glands. Regulates cell-cycle, cell junction, focal adhesion and WNT signalling in the neonatal mouse uterus.	(Filant and Spencer, 2013a, Filant et al., 2014)
Oestrogen receptor α	Maintenance of developed uterine glands and proliferation. Mediated by stromal paracrine signalling (EGF, IGF1 and IGF2).	(Nanjappa et al., 2015, Cooke et al., 1998)
Prolactin	Stimulates differentiation.	(Carpenter et al., 2003)
Progesterone (an endocrine disruptor)	Inhibits uterine gland development.	(Bartol et al., 1988, Gray et al., 2000, Filant et al., 2012)

At birth, endometrial histoarchitecture resembles that of an adult but is less developed as the luminal epithelium is low columnar or cuboidal and the glandular epithelium is sparse in comparison to the adluminal stroma (O'Rahilly, 1973, Gray et al., 2001). Gland proliferation in humans is completed postnatally and develops slowly until puberty. By the age of 6 years, endometrial glands extend from one-third to one-half the distance to the myometrium (Gray et al., 2001). Menstrual changes are rare before puberty. For endometrium maturation, responsiveness needs to be acquired by the endometrium and an immature endometrium persists in majority of girls until menarche or early adolescence (Brosens et al., 2015). At puberty, the mature uterine histoarchitecture can be observed with glands extending to the inner circular layer of the myometrium (Valdes-Dapena, 1973, Gray et al., 2001). The genesis of the glands in the human fetus is a result of glandular epithelium differentiating from the luminal epithelium through the stroma (Gray et al., 2001). However, the glands in postmenstrual human adults develop adluminally from the basalis during the proliferative phase.

The adult human endometrial functionalis goes through three phases. The menstrual cycle begins with menstruation and overlaps with the proliferative phase (aligned to the follicular phase) as it regenerates from the basalis, followed by a secretory phase in preparation for implantation (aligned with luteal phase) (Wynn, 1989) (Fig.1.2). If pregnancy does not take place, the cycle begins again with menstrual shedding. The endometrium will go through approximately 450 cycles during a woman's reproductive lifespan, highlighting the remarkable capacity of endometrial regeneration (Chavez-MacGregor et al., 2008). These phases are orchestrated by sex steroid hormones but endometrial responses are cell and zone specific (Ferenczy et al., 1979). After menstruation, pregnancy loss, parturition, and even iatrogenic destruction (e.g., curettage), the endometrium regenerates like no other tissue, beginning at a thickness of 1-2 mm and growing up to 14 mm (Fleischer, 1999). This regenerative capacity is attributed to stem/progenitor cells (Cousins et al., 2021).

1.2.3 Endometrial Epithelial Stem/Progenitor Cells

Endometrial epithelial stem/progenitor cells can be distinguished from other cell types in the tissue by their functional attributes, including self-renewal, high proliferative potential, the capacity to differentiate into one or more cell types and to regenerate the tissue after injury (Potten and Loeffler, 1990). Clonogenic endometrial epithelial stem/progenitor cells were found to comprise 0.22% of single cell suspensions of $EpCAM^{+}$ (Epithelial cell adhesion molecule) cells from hysterectomy samples (Chan

et al., 2004). Due to the endometrium regenerating from the basalis, the location of these cells was hypothesised to be in this layer. Thus, most of the focus on identifying stem/progenitor cell markers has been in the basalis.

Nuclear *AXIN2* (axis inhibition protein 2) was the first basalis-specific epithelial stem/progenitor cell marker to be identified (Nguyen et al., 2012). A gene microarray analysis of EPCAM$^+$ EpC from full thickness, pre- and post-menopausal hysterectomy endometrium was conducted with the assumption post-menopausal endometrial EpC have a similar expression to the pre-menopausal basalis. Post-menopausal endometrium is capable of regeneration in the presence of exogenous hormones; hence, stem/progenitor cells are expected to still reside in the basalis. The Wnt signalling pathway plays an essential role in maintenance and the activity of the stem cell reservoir (Nusse et al., 2008). Therefore, as anticipated, many Wnt-associated genes, including *AXIN2*, a negative regulator of β-catenin in the canonical Wnt signalling pathway (Jho et al., 2002), and SRY-Box transcription factor 9 (*SOX9*) a transcriptional factor, were differentially expressed between pre- and post-menopausal endometrium (Nguyen et al., 2012). Nuclear *AXIN2* presence was confirmed in the pre- and post-menopausal basalis using immunofluorescence and confocal microscopy, whereas cytoplasmic AXIN2 was found in the functionalis (Nguyen et al., 2012).

However, to demonstrate functional activity, live EpC need to be isolated, and nuclear markers are not suitable for this, thus surface markers are required. Recent work has identified two surface epithelial stem/progenitor cell markers, stage-specific embryonic antigen 1 (SSEA-1 encoded by *FUT4*) and N-cadherin (neural cadherin encoded by *CDH1*). SSEA-1$^+$ cells have been found in the basal layer. This study demonstrated large spheroids formed from isolated SSEA-1$^+$ cells in three-dimensional (3D) cultures and exhibited properties of quiescent progenitor cells such as greater telomerase activity, longer telomeres, and lower proliferative rates than SSEA-1$^-$ cells (Valentijn et al., 2013). Another study showed N-cadherin$^+$ cells also exhibit these properties (Nguyen et al., 2017). *In vivo*, N-cadherin$^+$ EpC were rarely positive for Ki-67, a proliferation marker, suggesting cellular quiescence. Interestingly, SSEA-1$^+$ were found to be positive for nuclear SOX9, with some positive for nuclear β-catenin, signifying active Wnt signalling to maintain an undifferentiated epithelial state (Valentijn et al., 2013). N-cadherin$^+$ cells were found not to colocalise with SOX9 (Nguyen et al., 2017).

A differentiation hierarchy was suggested of these markers (Nguyen et al., 2017). N-cadherin^{+} SSEA-1^{-} cells were found located deep in the basalis near the myometrium, thus were labelled as the most primitive cells. As these cells move closer to the functional layer, N-cadherin may be lost, and cells differentiate into transit amplifying SSEA-1^{+} cells before differentiating fully into the gland EpC found in the functional layer. However, the observation that SSEA-1^{+} cells are also found in the luminal epithelium argues against this proposed idea, but their stem/progenitor cell functions have not been tested.

Leucine Rich Repeat Containing G Protein-Coupled Receptor 5 (LGR5), an R-spondin receptor functioning as part of the canonical Wnt signalling pathway, has been proposed as an additional stem/progenitor cell marker. However, expression profiles for LGR5 during the menstrual cycle are conflicting (Gil-Sanchis et al., 2013, Tempest et al., 2018a) and the highest expression is seen in the luminal epithelium (Tempest et al., 2018a, Garcia-Alonso et al., 2021). No functional validation of LGR5^{+} cells has been reported to confirm stem/progenitor cell expression.

Epithelial stem cells residing in the terminal ends of endometrial glands in the basalis rejuvenate the glands of the functional layer (Valentijn et al., 2013, Tempest et al., 2020). Although the traditional view describes endometrium re-epithelialisation from the remaining gland stumps in the basalis, 3D reconstructions of the basalis have shown that glands form a complex horizontally inter-connecting network (Tempest et al., 2020, Yamaguchi et al., 2021). Interestingly, of those glands that share a branching point, 86% shared a branching point in the basalis (Yamaguchi et al., 2021). This plexus formation is suggested to be more difficult to eradicate at shedding, thus giving the glands a functional advantage in the conservation of stem/progenitor cells (Tempest et al., 2020, Yamaguchi et al., 2021). It has been speculated that the most primitive cells, such as N-cadherin^{+} cells are likely to be located in the horizontal branches (Cousins et al., 2021).

There is strong evidence for monoclonality in endometrial glands such that the cell population of a gland are descendants from a single stem/progenitor cell (Tanaka et al., 2003, Moore et al., 2020). However, recent work using *in vivo* lineage tracing of mitochondrial mutations has identified polyclonal glands (Tempest et al., 2020). These polyclonal glands were speculated to arise from upward perpendicular growth of progeny of two adjacent stem cells situated in parallel/branching glands.

1.2.4 Menstrual Cycle

1.2.4.1 Endometrial glands in the proliferative phase

Repair processes begin within 48 hours after initiation of menses within a steroid hormone and oestrogen receptor (ER) depleted environment (Ferenczy and Bergeron, 1991, Cousins et al., 2021). The remaining superficial gland stumps re-epithelises the denuded endometrial surface (Ludwig and Spornitz, 1991) and the surface epithelium of peritubal/isthmic regions of the endometrial cavity (Ferenczy and Bergeron, 1991). New luminal epithelium is found adjacent to the shedding functionalis, highlighting that the two processes of shedding and repair work concurrently in a piecemeal fashion (Garry et al., 2009). These cells resemble fibroblasts with cell migration features such as intracellular microtubular systems and pseudopodial projections but their basement membrane formation and intercellular desmosomes are in line with their epithelial structure (Ferenczy and Bergeron, 1991). As these luminal EpC closely relate to the underlying EnSC, mesenchymal to epithelial transition (MET) has been proposed as a potential mechanism to explain the rapid repair process (Owusu-Akyaw et al., 2019). Complete re-epithelialisation of the endometrial surface coincides with the end of menstruation (Ferenczy and Mutter, 2008).

Proliferation of the endometrium begins around day 3 of the cycle before menstruation is finished but is oestradiol (E_2)-independent. Despite an increase in DNA activity, plasma levels of the steroid hormones and their receptors in the endometrium remain low (Ferenczy and Mutter, 2008). However, as E_2 production from the growing ovarian follicles increases, proliferative activity is increased (Groothuis et al., 2007) with highest proliferative rates (maximum DNA synthesis) recorded on cycle day 8 and 10 in the upper one-third of the functional layer (Ferenczy et al., 1979). Zonal variations are observed in response to hormonal stimuli with the more intense proliferation in the top two-thirds of the functional layer than in the lower third and even less in the basalis (Ferenczy and Guralnick, 1983). As expected, ER and progesterone receptor (PGR) concentrations are highest during the proliferative phase (Ferenczy and Bergeron, 1991, Wang et al., 1998).

Histological analysis of the proliferative endometrium highlighted ultrastructural evidence of proliferation in gland EpC by the increase in free and bound ribosomes, mitochondria, Golgi and primary lysosomes (Ferenczy and Bergeron, 1991). These organelles provide protein matrix, energy and synthesis of other factors, including

glycolytic pathway enzymes (Ferenczy and Bergeron, 1991). A feature of proliferating EpC is oestrogen-dependent cilio- and micro-villogenesis (Ferenczy and Bergeron, 1991). Morphologically, the glands are short, straight, and lined with pseudostratified nuclei in the early proliferative phase with narrow lumens but as they proliferate the glands elongate and become tortuous (Padykula, 1989, Ferenczy and Mutter, 2008). By the end of the proliferative phase, the glands are coiled tightly and branched. In a non-pregnant state, a high density of glands are found in the endometrium with approximately 15 openings per mm^2 (Filant and Spencer, 2014).

1.2.4.2 Endometrial glands in the secretory phase

As ovarian E_2 levels continue to rise, the follicle stimulating hormone (FSH) that had been stimulated due to the lack of P_4 in the proliferative phase is downregulated due to negative feedback of E_2 (Reed and Carr, 2015). This leads to the selection of the dominant follicle and the regression of the other follicles. High levels of E_2 secretion induce positive feedback on the anterior pituitary, stimulating the luteinising hormone (LH) surge, which marks the transition from the proliferative to secretory phase (Reed and Carr, 2015). The LH surge signals for the activation of the proteolytic enzymes and prostaglandins that results in the release of the oocyte-cumulus complex, known as ovulation (Reed and Carr, 2015) (Fig. 1.2).

After ovulation, the endometrium enters the secretory phase, aligned to the ovarian luteal phase. During this period, the E_2-primed endometrium is under P_4 stimulation produced by the corpus luteum (CL), and undergoes secretory differentiation (Ferenczy and Bergeron, 1991). The development of subnuclear glycogen vacuoles in gland EpC and palisading of their nuclei is one of the first histological signs of ovulation that occurs three days post ovulation and has been used to date the endometrium (Wynn, 1989, Ferenczy and Bergeron, 1991). Two other features found in the endometrial glands are giant mitochondria for cellular steroid metabolism as well as a nucleolar channel system formed by the infolding of nuclear membranes by P_4 stimulation (Armstrong et al., 1973, Ferenczy and Bergeron, 1991). As the glands develop their secretory phenotype, DNA synthesis and mitosis decrease and disappear, respectively (Ferenczy and Bergeron, 1991).

Endometrial gland differentiation is regulated by the increasing levels of P_4. Two distinct subtypes of PGR are found in the glands in the menstrual cycle, PGR_A and PGR_B. Both receptors are present in the glands during the proliferative phase, reaching a maximum in the mid- and late-proliferative phase and just after ovulation

(Wang et al., 1998). Conversely, as P_4 levels rise, the transcription and translation of the receptors are downregulated (Chauchereau et al., 1992, Wang et al., 1998). The initial presence of PGR in the luteal phase is consistent with P_4-mediated inhibition of mitosis in the glands (Wang et al., 1998, Ferenczy et al., 1979). Hence, the downregulation of PGR in the glands results in significant changes in gene expression referred to as secretory transformation (Wang et al., 1998, Kelleher et al., 2019).

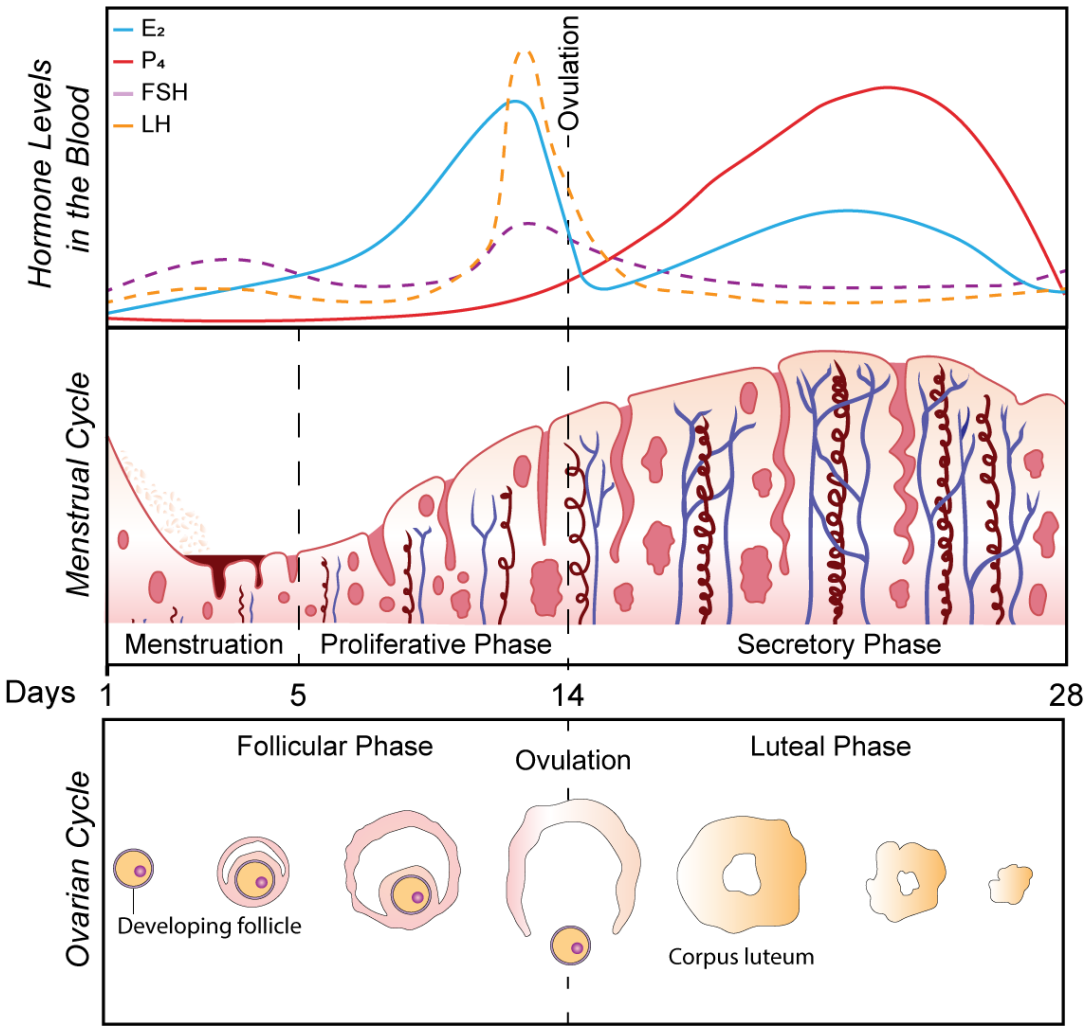

Figure 1.2. ***The menstrual cycle.***

The human menstrual cycle is divided into three phases: menstrual, proliferative, and secretory. The cycle begins on the first day of menstruation known as Day 0 and lasts for 3-5 days in most women. During this time, the endometrium also begins to regenerate. As menstruation ends, the proliferative phase begins, and the re-growth of the endometrium is assisted by the increase in E_2 produced by the follicles. The follicles are stimulated by the FSH produced by the pituitary. The rise in E_2 results in LH secretion, which induces ovulation and the formation of the CL. This step follows into the secretory phase, which is dominated by P_4, produced by the CL. FSH and LH levels drop in this phase but small amounts of E_2 are also secreted by the CL. During the secretory phase, the endometrium differentiates and prepares for implantation. If no, embryo implants, the P_4 levels fall, and the endometrium breaks down, before the cycle starts again. Adapted from (Wira et al., 2015).

1.3 Endometrial Glands and Pregnancy

1.3.1 Uterine Receptivity

Successful embryo implantation is dependent on species-specific strategies (Brighton et al., 2017). For example, in mice, implantation of multiple embryos is synchronised and is dependent on rising circulating E_2 (Paria et al., 1998). The rise of E_2 renders the P_4-primed endometrium receptive as well as activating dormant blastocysts for implantation (Paria et al., 1998). The human endometrium also acquires a receptive phenotype in the mid-luteal phase of the cycle, which lasts for 2-4 days but is not controlled by a nidatory surge in E_2 (De Ziegler et al., 1992, Groll et al., 2009), possibly due to synchronised implantation of multiple human embryos not being required (Brighton et al., 2017).

Endometrial glandular factors essential for embryo implantation were found through animal studies. Postnatal P_4 exposure for 8 weeks resulted in permanent inhibition of uterine gland differentiation in sheep, thereby establishing a uterine gland knock-out (UGKO) model (Gray et al., 2000, Gray et al., 2002). In this model, fertilisation takes place, but embryos fail to survive due to the absence of the glands and their secretions, leading to recurrent early pregnancy loss and complete infertility (Gray et al., 2002, Kelleher et al., 2019). Additionally, in both progestin uterine gland knockout (PUGKO) mice and a *Foxa2* conditional deletion model, implantation failure is observed in association with reduced expression of key implantation factors (Jeong et al., 2010, Filant and Spencer, 2013b).

LIF, which encodes for leukaemia inhibitory factor (LIF), is one of the critical implantation genes perturbed in gland dysfunction models (Stewart et al., 1992). LIF belongs to the interleukin cytokine family, and is found explicitly in the glandular epithelium after the nidatory surge of E_2 (Stewart et al., 1992). Studies on LIF in mice provided the initial evidence that endometrial glands secrete factors required for receptivity and implantation (Stewart et al., 1992, Rosario and Stewart, 2016). *Lif*-null mice are infertile due to impaired embryo implantation but exposure to recombinant mouse LIF, embryo implantation can take place and pregnancy is rescued (Stewart et al., 1992). Other null and conditional mutant mice that lack uterine glands and have implantation failures are attributed to diminished or absent *Lif* expression (Kelleher et al., 2019). Additionally, osteopontin and glycodelin (encoded by *SPP1* and *PAEP*, respectively) are both secreted by the glands and facilitate blastocyst adhesion to the luminal epithelium (Singh and Aplin, 2009, Uchida et al., 2007).

1.3.2 Stromal Decidualisation

1.3.2.1 Decidualisation

Decidualisation is an essential process characterised by local oedema, differentiation of the EnSC into specialised decidual cells and the influx of uterine NK (uNK) cells that coordinate trophoblast invasion and placenta formation to take place during and after embryo implantation (Christian et al., 2002, Gellersen and Brosens, 2014). Unlike in mice, where decidualisation takes place once murine embryos breach the luminal epithelium, human stromal decidualisation is an embryo-independent process. Instead, decidualisation occurs in response to elevated P_4 levels and intracellular cyclic adenosine monophosphate (cAMP) production in the mid-luteal phase of each cycle (Gellersen and Brosens, 2014).

As observed in the endometrial glands, PGR_B levels fall after ovulation in EnSC (Wang et al., 1998). However, PGR_A levels persist through the menstrual cycle in EnSC (Mote et al., 1999). EnSC differentiation is suspected not to be initiated by P_4 due to the lag period following the onset of morphological differentiation and rising P_4 circulation (Gellersen and Brosens, 2003). Notably, *in vitro* studies of primary EnSC have demonstrated that P_4 treatment alone induces very few genes (Brosens et al., 1999) and other factors are necessary for decidualisation including endocrine and paracrine cues, interleukins and lipids (Gellersen and Brosens, 2014).

Several gland-derived factors have been implicated in promoting decidualisation. Maximum expression of *LIF* is observed in the luminal and glandular epithelium during the mid-secretory phase (Aghajanova et al., 2003, Paiva et al., 2009). The timing of expression suggests the glands may influence the decidualisation prior to implantation in women (Kelleher et al., 2019). In agreement, *in vitro*, LIF was found to enhance stromal decidualisation in both human and mice EnSC (Shuya et al., 2011). Additionally, glands produce a large amount of prostaglandin E_2 (PGE_2) (Smith and Kelly, 1988), which is known to enhance stromal decidualisation by increasing intracellular cAMP (Gellersen and Brosens, 2014). Determining glandular factors and their potential paracrine actions in promoting stromal decidualisation is essential to further understanding the endometrium.

1.3.2.2 Decidual Divergence

Recent studies have shown decidualisation is a multistep differentiation process. After cell cycle exit at G0/G1, an evolutionary conserved acute cellular stress

response starts decidualisation with a burst of free radicals and secretion of chemokines and inflammatory mediators (Erkenbrack et al., 2018, Al-Sabbagh et al., 2011, Brighton et al., 2017). Multiple receptivity genes were activated in the mouse uterus with the exposure of this inflammatory secretome, suggesting the E_2 surge in mice is superseded by an inflammatory signal in humans (Salker et al., 2012). Coinciding with the window of implantation, this inflammatory phase is further characterised by the accumulation of uNK cells (Brighton et al., 2017). After 4 days, EnSC no longer have a fibroblastic appearance, instead emerge as secretory decidual cells with abundant cytoplasm and prominent endoplasmic reticulum (Gellersen and Brosens, 2014). These decidual cells are P_4-dependent (Brosens et al., 1999) and are resistant to oxidative and metabolic stress (Leitao et al., 2010, Muter et al., 2018) and highly responsive to embryonic signals (Weimar et al., 2012, Teklenburg et al., 2010). The inflammatory reprogramming of EnSC leads to permanent cell cycle arrest and the emergence of acute senescent decidual cells (Brighton et al., 2017, Lucas et al., 2020).

Unlike chronic senescence, which is associated with ageing, acute senescence is tightly coordinated process required for tissue remodelling such as embryo development, placenta formation and wound healing (Muñoz-Espín and Serrano, 2014). Senescent decidual cells are found in close proximity to the luminal epithelium, implying the cells arise from significant replication stress endured during the proliferative phase (Lucas et al., 2020). Morphologically, these cells are similar to decidual cells, but senescent decidual cells are P_4-resistant and secrete many extracellular matrix (ECM) remodelling proteins and proteinases, proinflammatory cytokines, chemokines, growth factors, known as senescence-associated secretory phenotype (SASP) (Brighton et al., 2017, Lucas et al., 2020). SASP was found to be critical for the amplification of the initial decidual inflammatory response that drives differentiation of the EnSC and controls the temporal expression of receptivity genes for implantation (Salker et al., 2012). Upon pregnancy and continuous P_4 signalling, decidual cells secrete interleukin 15 (IL-15) and other factors to recruit and activate uNK cells for the clearance of senescent decidual cells by perforin- and granzyme-containing granule exocytosis (Brighton et al., 2017, Lucas et al., 2020, Kong et al., 2021). In the absence of an implanting embryo, the fall in P_4 levels in the late-luteal phase leads to majority senescent cells, influx of leukocytes, ECM breakdown and menstrual shedding (Critchley et al., 2020).

The default trajectory of decidual cells is towards cellular senescence, which must be cleared by uNK cells through granule exocytosis or lead to chronic senescence (Lucas et al., 2020) (Fig. 1.3). Removal of senescent decidual cells may promote recruitment of bone-marrow derived decidual precursor cells for rapid decidual expansion in early pregnancy (Diniz-da-Costa et al., 2021). Importantly, RPL was found to have a pro-senescent decidual response and lack clonogenic decidual precursor cells (Lucas et al., 2016, Lucas et al., 2020, Tewary et al., 2020). This aberrant decidual response would lead to chronic senescence in the endometrium during the implantation window and result in an intrinsically unstable decidual-placental interface (Lucas et al., 2020). Additionally, it is plausible an aberrant decidual response can also impact glandular secretions. Moreover, senescent cells have been observed in endometrial luminal and glandular epithelium but little is yet known about their function (Brighton et al., 2017).

1.3.3 Histotrophic Nutrition

1.3.3.1 Endometrial glands at pregnancy

The primary role of the endometrial glands is to provide nutritional support for the conceptus during the first trimester (Burton et al., 2002, Hempstock et al., 2004). Histotrophic nutrition can be defined as the requirement of nutrients by the developing conceptus from the secretions of oviductal and uterine glands (Wooding and Burton, 2008, Filant and Spencer, 2014). Maternal arterial circulation to the placenta is not established until 10-12 weeks of pregnancy once organogenesis is complete, hence, histotrophic nutrition is the initial source of nutrition for the conceptus (Jauniaux et al., 2003a, Burton et al., 2011).

Adherence to the endometrial surface results in the transformation of the trophectoderm into the syncytiotrophoblast, which penetrates the endometrium. After complete embryo implantation, the enlarging syncytiotrophoblast erodes into the neck of nearby endometrial glands, resulting in the loss of their epithelial lining (Burton et al., 2020). Hence, the syncytiotrophoblast is in direct contact with secretions in the lumen of the glands as early as day 10-12 post-fertilization (Hamilton and Boyd, 1960). Histological studies (Moser et al., 2018) and *in vitro* models (Moser et al., 2010, Moser et al., 2015) highlighted endoglandular trophoblasts as a putative subpopulation of extravillious trophoblast cells that invade into the endometrial glands, replacing glandular EpC at the margin of the developing placenta. It has been

speculated that paracrine factors from the two cell types are responsible for the migration of the trophoblast cells and breakdown of the glands (Moser et al., 2015).

At this stage, the syncytiotrophoblast invades into the sub-mucosal capillary network but the spiral arteries do not penetrate the superficial third of the endometrium. Thus, the conceptus must enlarge and once contact is made with the tips of the arteries, endovascular trophoblast (EVT) migrate into the vessels forming plugs that block blood flow (Burton et al., 2011). Consequently, the intervillous space in the first trimester has low oxygen concentrations (Jauniaux et al., 2001). At the end of the first trimester, the plugs dissipate resulting in the switch from histotrophic to hemotrophic nutrition as the blood flows into the intervillous space from the placenta (Burton et al., 2002), but until this stage, nutritional support must be provided locally.

The nutritive role of the glands is evident from the accumulations of glycogen in the syncytiotrophoblast covering the surface of the villi facing the endometrium (Burton et al., 2002). The maternally-derived glycoprotein, glycodelin, is phagocytosed by the syncytiotrophoblast, highlighted by vesicles containing glycodelin in these cells (Burton et al., 2002, Burton et al., 2007). Throughout the first trimester the endometrial glands remain highly active, continuing to secrete into the intervillous space (Burton et al., 2002, Hempstock et al., 2004). Connections between the intervillous space of the placenta and lumen of the glands persist during this period (Burton et al., 2002). Notably, the glands near the conceptus become hypersecretory, termed the Arias-Stella reaction (Arias-Stella, 1954).

1.3.3.2 Regulation of endometrial gland secretions

Uterine gland secretory activity must be maintained during early pregnancy. Animal studies have revealed that factors from both the ovary and conceptus are required for appropriate glandular development and function at pregnancy (Kelleher et al., 2019) and an equivalent mechanism is likely present in humans (Fig. 1.4) (Burton et al., 2007, Burton et al., 2011). This method ensures the conceptus has a direct impact on the supply of nutrients from the mother until the onset of placental perfusion.

One of the first products produced by the syncytiotrophoblast is human chorionic gonadotrophin hormone (hCG). hCG acts on the CL by the LH receptor (LHR) in an endocrine manner to maintain P_4 secretion (Kelleher et al., 2019), required for stromal decidualisation (Zhou et al., 1999). hCG also acts in a paracrine manner on endometrial glands to increase their secretory function (Hausermann et al., 1998),

including increasing *PTGS2* expression (encodes cyclooxygenase-2, COX-2), which consequently increases the secretion of PGE_2 (Zhou et al., 1999). PGE_2 potentiates stromal decidualisation. Other lactogenic hormones that act on endometrial glands include human placental lactogen (hPL) secreted by the placental, and prolactin (PRL), the P_4-regulated secretory product of decidualised EnSC. The PRL receptor (PRLR) is found in abundance in the glands during both the secretory phase and early pregnancy (Jones et al., 1998). Together with hCG, these lactogenic hormones are believed to stimulate gland secretory functions and in turn, glandular secretions regulate development and function of the placenta (Burton et al., 2007, Kelleher et al., 2019).

1.3.3.3 Impact of gland secretions

Endometrial glands synthesise and secrete or selectively transport a wide variety of substances into the lumen, including ions, sugars, amino acids, extracellular vesicles, lipids, and proteins (Kelleher et al., 2019). During early pregnancy, a notable feature of the endometrial gland EpC is the accumulation of large quantities of glycogen in the apical side (Demir et al., 2002). As with many tissues, glucose is an essential source of energy for the developing placenta. High rates of glycolysis are maintained in the placenta through reoxidation of pyridine nucleotides by polyol pathways instead of fermentation of pyruvate to lactate (Burton et al., 2017). This alternative pathway ensures protection for the embryo from free radical-mediated teratogenesis. Additionally, less ATP is produced via glycolysis, however, the plentiful source of glucose from glands ensures placental requirements are met. Moreover, carbon skeletons are preserved for nucleotide synthesis and the rapid cell proliferation (Burton et al., 2020).

Evidence from transmission electron microscopy indicated that glycogen vesicles bud off into the lumen, rupturing the apical membrane in an apocrine fashion (Demir et al., 2002). Glycogen is released into the lumen by the breakdown of the vesicles and is broken down into glucose by α-amylase on the surface of the syncytiotrophoblast (Burton et al., 2020). An alternative method suggested that glycogen may be broken down by glycogen phosphorylase detected in EpC and then secreted into the lumen (Jones et al., 2015). Glucose transporters, GLUT3 and GLUT12 are present at high levels on the apical membrane of the syncytiotrophoblast (Brown et al., 2011) and syncytium (Gude et al., 2003), respectively during the first trimester. After uptake, glucose can be then be converted into glycogen by glycogen synthase as large

deposits of glycogen are found in the syncytium, specifically on the villous surface facing the gland openings (Burton et al., 2002, Burton et al., 2020).

An abundance of glycoproteins is found in the gland secretions. One of the best characterised glycoproteins is glycodelin. Glycodelin has been shown to affect the maternal immune cells which aids with early placental development by inhibiting the activation and proliferation of T cells (Scholz et al., 2008) and dendritic cells (Lee et al., 2011) alongside stimulating the conversion of peripheral natural killer (NK) cells to decidual NK (Lee et al., 2019). Also, glycodelin suppresses the invasiveness of trophoblast cell line by the downregulation of extracellular signal regulated (ERK)/c-Jun signalling pathway, which results in downregulation of matrix metalloproteinases (MMP) and urokinase plasminogen activator (Lam et al., 2011). Another glycoprotein component of glandular secretions is osteopontin, which, among other roles acts as both a pro- and anti-inflammatory cytokine (Johnson et al., 2003), as well as modulating cell migration and invasion within the placental bed by regulating integrin binding, cell-cell and cell-matrix adhesion (Burton et al., 2020). The latter role may influence invasion of extravillous trophoblast and spiral artery remodelling.

Lipid droplets are another common feature of gland secretions during early pregnancy. Lipids are an essential source of cholesterol required for cells and organelle membranes, steroid synthesis, and regulation of signal transduction, such as sonic hedgehog, which is vital during embryogenesis (Long et al., 2015, Burton et al., 2020). A range of growth factors including LIF, vascular endothelial growth factor (VEGF) and epidermal growth factor (EGF) are supplied to the conceptus from the glands (Hempstock et al., 2004). These growth factors have been implicated to stimulate cell proliferation and vasculogenesis in the developing placenta (Burton et al., 2020). Taken together, defects in glandular secretion could have detrimental effects on implantation and the developing conceptus.

1.3.4 Placentation

After approximately 10 weeks of gestation, nutrition switches from histotrophic to hemotrophic, as it is supplied by the fully formed placenta. Placentation is essential for a successful pregnancy and health of the fetus (Burton and Jauniaux, 2017). In humans, normal placentation is a highly invasive process of trophoblast cells remodelling the maternal spiral arteries, which results in the complete transformation of the decidual and myometrial segments of approximately 100 spiral arteries, known as ‘deep placentation’ (Brosens et al., 2011). The process of spiral artery remodelling

involves inert fibrinoid material replacing the smooth muscle and elastic material in the walls of the vessels (Burton and Jauniaux, 2017). In turn, the arteries dilate to allow for a constant high volume, low velocity maternal blood flow to the placenta (Burton et al., 2009). Malperfusion of the placenta due to impaired trophoblast invasion and deficient arterial remodelling are linked to a spectrum of disorders including fetal growth restriction and early onset pre-eclampsia (Brosens et al., 2011). The poor formation of the cytotrophoblastic shell has also been linked to miscarriages (Burton and Jauniaux, 2017).

1.3.4.1 Cytotrophoblastic shell

As the conceptus embeds into the superficial endometrium during implantation, placentation begins at an initial rate that is more advanced than the embryo (Burton and Jauniaux, 2017). The chorionic sac is soon covered by a mass of developing villi, each composed of a core of mesodermal cells and a bilaminar trophoblastic epithelium arranged with an outer layer of syncytiotrophoblast and an underlayer of progenitor cytotrophoblast cells (Burton and Jauniaux, 2017). Instead of syncytiotrophoblast, an elongated mass of cytotrophoblast cells known as the cytotrophoblast cell columns form at the distal ends of the villi, where they contact the decidua. These cells are derived from the proliferative zone at the proximal end of the columns. At their furthest points, contact is made with decidua basalis, and they spread laterally to merge with other columns to form the cytotrophoblastic shell (Burton and Jauniaux, 2017).

Currently, two intrauterine factors are believed to be key for regulating cytotrophoblast cell proliferation. Histotrophic support provided by the endometrial glands supply mitogenic growth factors, including EGF and insulin-like growth factor (IGF), which have demonstrated to increase proliferation of the cytotrophoblast cells in first trimester villus explants (Maruo et al., 1992, Forbes et al., 2008). As mentioned previously, signalling from the trophoblast to the glands is speculated to enhance the expression of these factors but experimental evidence is limited (Filant and Spencer, 2014). Notably, at the proximal end of the columns, the proliferative stem cells label positively for fibroblast growth factor receptor 2. The signalling from this receptor results in increased expression of two transcription factors, *Caudal Type Homeobox 2* (*CDX2*) and *E74-like factor 5* (*ELF5*), which are key for trophoblast stem cells (Hemberger et al., 2010). Secondly, the low oxygen concentration during early pregnancy may aid proliferation of cytotrophoblast progenitor cells (Zhou et al., 2011). The transition from histotrophic to hemotrophic nutrition increases the oxygen

concentration and results in the fall of trophoblast stem cell transcription factors levels, suggesting a large reduction in the proliferative capacity of trophoblast cells (Hemberger et al., 2010, Burton and Jauniaux, 2017). Hence, poor histotrophic support or an early rise in oxygen tension could be detrimental in the development of the placenta.

There are several reasons why the cytotrophoblastic shell is essential for early pregnancy, including providing the anchorage to the ECM of the endometrium, but more importantly, its role in the onset of the maternal arterial circulation (Aplin et al., 1998, Burton and Jauniaux, 2017). First, the cells at the outer surface undergo a partial epithelial-mesenchymal transition (EMT) to form interstitial trophoblast cells, which migrate through the decidua into the myometrium (Davies et al., 2016). They are found in abundance around the spiral arteries where they appear to be important in vascular remodelling (Kam et al., 1999). Increased rates of apoptosis of these cells and reduced invasiveness, or limited supply of cells from the shell have been suggested to cause deficient remodelling of the arteries in fetal growth restriction and pre-eclampsia (Burton and Jauniaux, 2017). Furthermore, the shell provides the EVT cells over a broad area that migrate down the lumen of any maternal arteries encountered and form the plugs during the first six weeks of pregnancy (Burton and Jauniaux, 2017). At the central region of the implantation site the shell is thickest, whereas towards the periphery the shell is thinner. Thus, the opportunity for plugging of the arteries here is less, resulting in the onset of the maternal circulation in this region and local levels of oxidative stress (Jauniaux et al., 2003b). This is believed to lead to villus regression and the formation of the smooth membranes of the definitive placenta, which takes place in all ongoing pregnancies (Burton and Jauniaux, 2017).

1.3.4.2 Defects of the cytotrophoblastic shell

Even though developmental differences are found in the shell of normal pregnancies due to variations in timing of the onset of maternal circulation, the pathology of spontaneous miscarriage is associated with gross impairments in the cytotrophoblastic shell (Burton and Jauniaux, 2017). The shell is found to be thin and fragmented in 70% of these cases, resulting in deficient EVT migration and incomplete plugging of the arteries (Hustin et al., 1990). This is independent of the trophoblastic karyotype. In missed miscarriages, early intervillous flow is commonly observed in the central regions or throughout the placenta, rather than peripheral regions (Jauniaux et al., 2003b). Trophoblastic stress presents as absence of microvilli, a thin layer of syncytiotrophoblast with infrequent, and flattened underlying

cytotrophoblast cells and is found in the periphery of normal placenta. However, in missed miscarriage, trophoblastic stress is found in the central regions as well as an avascular stromal core (Jauniaux et al., 2003b). By 12 to 13 weeks when fetal demise will have already occurred, the placenta of missed miscarriage patients are extremely atrophic as the villi has regressed and intervillous blood flow is less frequently detected on ultrasound/Doppler examination (Jauniaux et al., 2003b). Also, the intervillous space will have primarily collapsed, and filled with clotted maternal blood. Hence, onset of maternal circulation is early and spatially unorganised, leading to placental oxidative stress and secondary degeneration of the placenta (Jauniaux et al., 2003b, Burton and Jauniaux, 2017).

Spiral artery remodelling deficiency is also found in fetal growth restriction and pre-eclampsia, but to a lesser extent than in early pregnancy failure (Gerretsen et al., 1981, Brosens et al., 2011). Hence, these cases also reflect reduced trophoblast invasion, which suggest less extensive arterial plugging in early pregnancy and thus, the onset of maternal circulation may have been atypical, both temporally and spatially (Burton and Jauniaux, 2017). However, there are currently no studies to support or refute this hypothesis.

Defects in the development of the shell may impact the integrity of the maternal-fetal interface, leading to poor anchorage between the two tissues (Aplin et al., 1998). This is observed in threatened miscarriage, where regression of around two-thirds of the early placenta creates a mechanical weakness in the periphery (Burton and Jauniaux, 2017). As the spiral arteries are unplugged, bleeding takes places between the membranes and the decidua basalis at the end of the first trimester. In sub-chorionic hematomas, crescentic hypoechogenic areas are present between the placental membranes and the decidua that can cause complete detachment of the placenta (Burton and Jauniaux, 2017). In approximately 10% of these cases, a full miscarriage takes place within 48 hours of the first bleeding episode (Johns and Jauniaux, 2006, Burton and Jauniaux, 2017). The pregnancies that continue have an increased risk of premature rupture of the membrane and pre-term delivery (Jauniaux et al., 2010, Burton and Jauniaux, 2017). It has been speculated that the blood clot lying against the membranes stimulates oxidative stress, which induces senescence and premature rupture of the membranes; or an inflammatory response in the uterus, that leads to premature delivery (Menon, 2016, Dutta et al., 2016, Burton and Jauniaux, 2017).

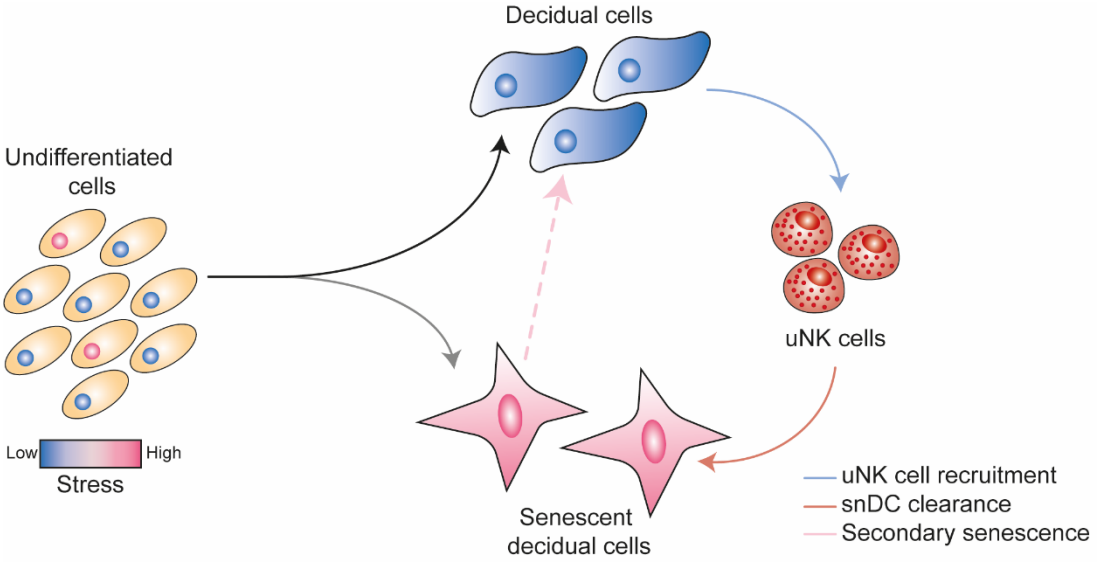

Figure 1.3. ***Fate divergence of decidual cells.***

Diagram illustrating the decidual pathway. Levels of replicative stress (highlighted by nuclear shading) sustained during the proliferative stage by individual EnSC results in the fate divergence of decidual EnSC. uNK cells are recruited by stress resistant decidual cells to eliminate senescent (stressed) decidual cells (snDC) by exocytosis. If senescent cells persist, by juxtracrine signalling can induce senescence in neighbouring cells (termed ‘secondary’ or ‘bystander’ senescence) that leads to the loss of tissue function. Adapted from (Lucas et al., 2020).

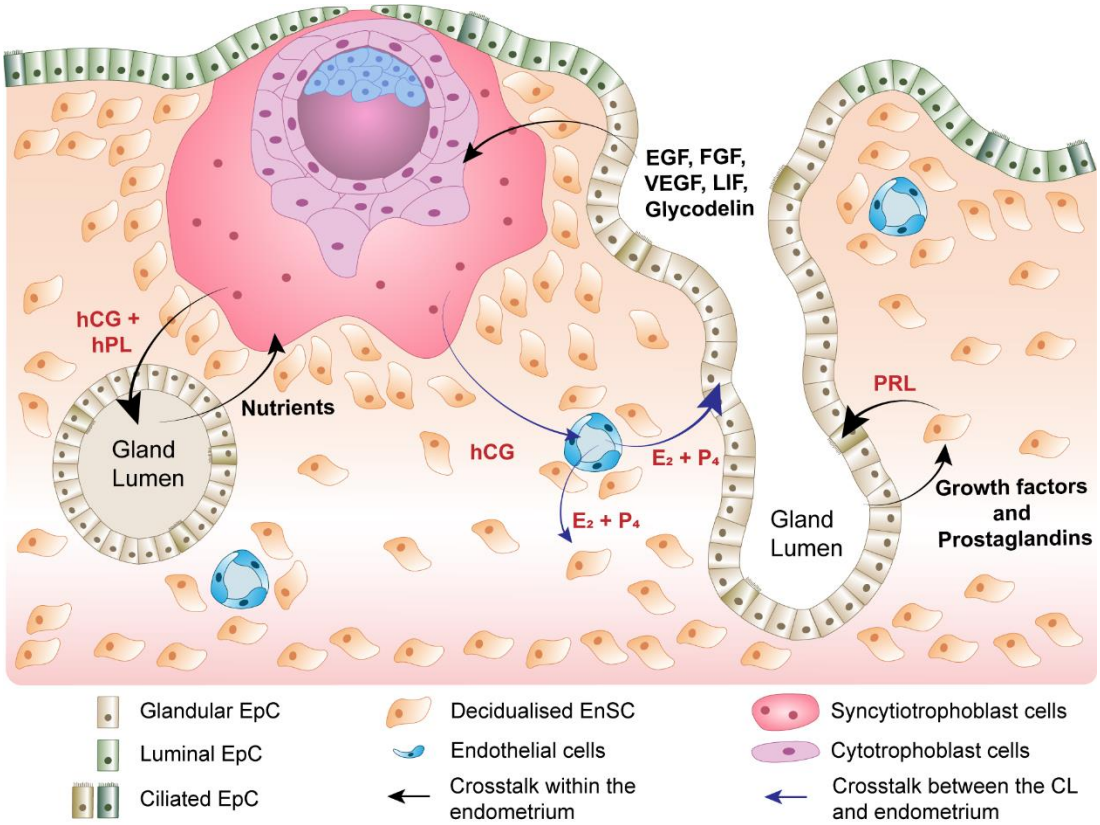

Figure 1.4. ***Regulation of glandular secretions at pregnancy.***

Schematic representation of the crosstalk between endometrial glands, decidualised EnSC, CL and trophoblasts cells of the invading embryo. During pregnancy, the syncytiotrophoblast produces hCG to maintain the CL so P_4 can be continually produced. P_4 is essential for the maintenance of the decidualised EnSC and differentiated glands. A key secretion of the decidual cells at implantation is PRL, which acts on the glands through PRLR to maintain the glandular secretory phenotype. Glands may also secrete factors that aid stromal decidualisation such as growth factors (EGF, FGF, VEGF, LIF) and PGE_2. Additionally, the trophoblast cells act directly on the glands through hCG and hPL, resulting in the production of growth factors (EGF, FGF, VEGF), nutrients (amino acids, lipids, proteins, and sugars), and receptivity markers such as LIF and glycodelin. In turn, these factors improve trophoblast invasion, thus forming a positive feedback loop. Black arrows represent crosstalk within the endometrium and blue arrows represent crosstalk between CL and the endometrium. Adapted from (Burton et al., 2007, Rawlings et al., 2021b).

1.4 Three-dimensional Endometrial Gland Models

1.4.1 Epithelial Gland Cultures

While animal models have provided important insights into the endometrial glands, laboratory animals do not fully recapitulate the human endometrium. Historically, two-dimensional (2D) cultures have been used to study the human endometrial cell types (EnSC, EpC, and endothelial cells) *in vitro* using tissue-derived cultures, stem cells and immortalised cell lines. These approaches have improved our understanding of the endometrium, however, primary EpC cannot be cultured long-term as they lose their phenotype by dedifferentiating (Hombach-Klonisch et al., 2005) and do not represent the normal physiological and architectural state of glands *in vivo*. When grown on plastic, primary EpC culture was limited to less than 2 weeks, with longer maintenance associated with a loss in cell integrity, indicated by intracellular vacuoles and squamoid morphology (Arnold et al., 2001), and with reduced protein synthesis, resulting in a loss of epithelial functionality (Mulholland et al., 1988). Extended cultures have been achieved by using gelatin-coated plates but medium supplementation with endothelial growth supplement essential to maintain the cultures, resulted in the loss of the 'classic epithelial cobblestone' morphology (Zhang et al., 1995)

Thus, 3D culture approaches were developed to produce a model using isolated primary EpC, grown first as small monolayer colonies that enlarge into organoid structures (Rinehart et al., 1988). The gland structures were enzymatically digested and transferred onto a Matrigel layer to provide a supportive matrix to form spheroidal structures. These structures had a highly polar columnar epithelia with microvilli lining a lumen and could be maintained long-term. However, the study was limited to mimicking the proliferative stage and therefore, the differentiation and functional capacity is unknown.

1.4.2 Organoids of the Reproductive System

Organoids are 3D multicellular *in vitro* constructs that recapitulate morphological and functional features of tissues and organs *ex vivo*. Organoids are derived from tissues containing tissue-specific adult progenitor cells or from induced pluripotent stem cells (iPSC) that self-organise into 3D structures in a supportive hydrogel droplet, replacing the tissue ECM. Organoids require specific growth media, designed to mimic the tissue-specific signalling pathways and recapitulate the niche environment (Kim et al.,

2020), with most models using a core set of factors to support proliferation, renewal and differentiation (Alzamil et al., 2021, Kretzschmar and Clevers, 2016). Many human organoid systems from different tissues of origin have been created including brain (Lancaster et al., 2013), retina, (Nakano et al., 2012), intestine (Sato et al., 2009) and kidney (Takasato et al., 2014).

The cultivation of organoids from human female reproductive tissues provides the opportunity to gain insight into understudied tissues (Fig. 1.5). For the female reproductive tract, protocols for ovarian cancer (Kopper et al., 2019, Maenhoudt et al., 2020), fallopian tube (Kessler et al., 2015), endometrium (Turco et al., 2017, Boretto et al., 2017), cervix (Chumduri et al., 2018, Maru et al., 2020), and trophoblast organoids (Haider et al., 2018, Turco et al., 2018) have been described. These organoids are all generated from adult tissue, and mostly retain functional and morphological features. Interestingly, organoid work has even expanded to the formation of embryo-like organoids, using stem cells to self-assemble into 3D structures capable of recapitulating post-implantation human epiblast and amnion formation (Zheng et al., 2019, Ojosnegros et al., 2021).

1.4.2.1 Endometrial gland organoids

Long-term chemically defined endometrial gland organoids were established from the human endometrium, based on approaches taken in other tissues (Turco et al., 2017, Boretto et al., 2017). After digesting endometrial tissue enzymatically to separate out the epithelial glands, the dissociated EpC or glandular fragments were embedded in either 70% or 95% Matrigel droplets, respectively. To induce cell proliferation and maintain and enable stem cells to expand, activators of the canonical WNT/β catenin signalling (R-spondin-1 and WNT3A (Wnt family member 3a)) and growth factors including those derived from the stroma (EGF, fibroblast growth factor 10 (FGF10) and hepatocyte growth factor (HGF)) were included in the organoid media from both protocols (Table 1.3). To prevent cell differentiation, A83-01 was used to inhibit transforming growth factor (TGF)-β signalling pathway and Noggin to inhibit bone morphogenetic protein (BMP) signalling pathway. Nicotinamide addition was also found to be important for establishing organoids. A p38 inhibitor (SB202190) and low concentrations of E_2 were also included in one of the protocols (Boretto et al., 2017).

From progenitor cells, these organoids are capable of self-organising into structures similar to their *in vivo* counterparts and have been successfully produced from non-pregnant endometrium and decidua (Turco et al., 2017, Boretto et al., 2017). The

establishment of these organoids have solved previous issues faced with monolayers (Fig. 1.6). Endometrial organoids are composed of a single EpC layer, which forms a spheroidal structure with a central lumen. These organoids are genetically stable, have clonogenic capacity as well as cellular heterogeneity and can recapitulate molecular and histological features of the glands *in vivo* (Turco et al., 2017, Boretto et al., 2017). E_2 treatment induces proliferation of the cells with an increase in Ki67+ cell (Boretto et al., 2017) as well as simulating ciliogenesis (Haider et al., 2019) and when combined with P_4, secretion of histotroph products such as glycodelin is observed. Pregnancy phenotype of the decidua glands can also be produced with the addition of pregnancy signals of the stroma (cAMP and PRL) and trophoblast (hCG and hPL) to the organoid media (Turco et al., 2017). A recent metabolomic analysis of the gland organoid's secretome demonstrated that the intra-organoid (apical) fluid and extraorganoid fluid (basolateral) are biochemically distinct from each other, resembling the *in vivo* observation (Simintiras et al., 2021).

Endometrial gland organoids provide a new opportunity to model the glandular epithelium and address unanswered questions related to stem/progenitor cells, development, and functionality of glands. Additionally, these organoids can be used to create patient-specific organoids to understand different disorders such as miscarriage and infertility, and role the glands play towards these phenotypes.

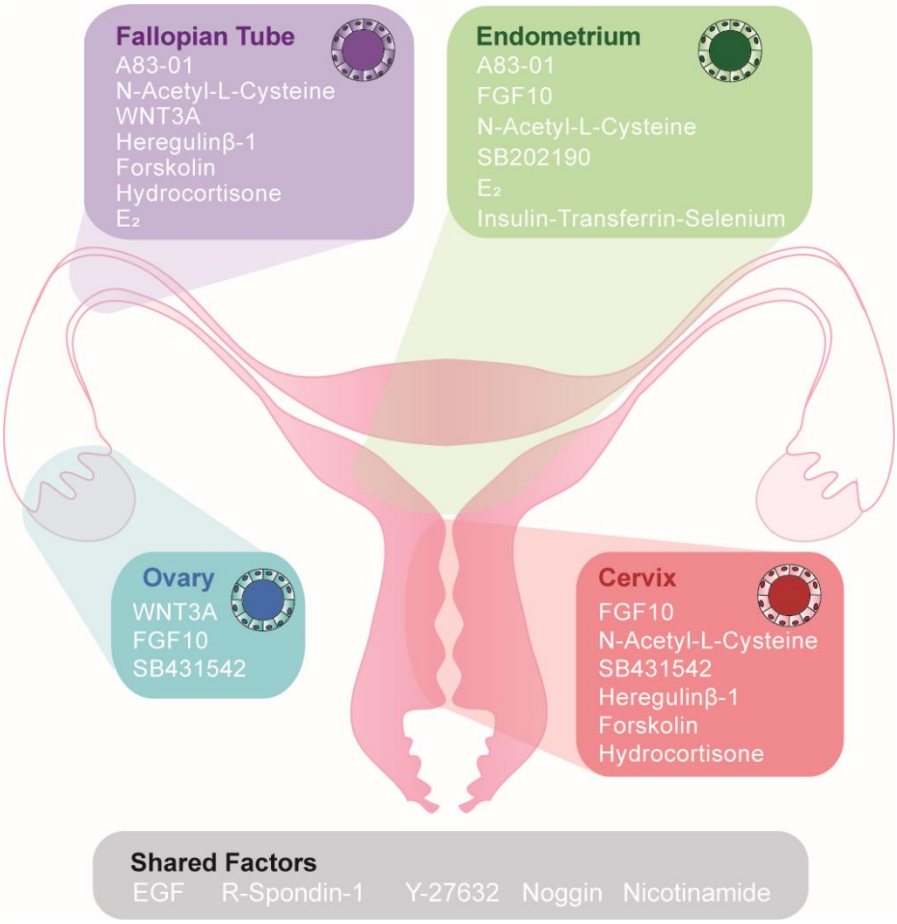

Figure 1.5. ***Female reproductive tract organoids.***

Organoids have been established from the endometrium (Turco et al., 2017, Boretto et al., 2017), fallopian tube (Kessler et al., 2015), cervix (Chumduri et al., 2018, Maru et al., 2020), and ovaries (Kopper et al., 2019, Maenhoudt et al., 2020). A defined, tissue specific combination of growth factors and inhibitors is required to propagate each organoid-system, with shared factors common to many organoids. Reproduced from (Rawlings et al., 2021b).

Table 1.3: A comparison of medium optimised for endometrial gland organoid expansion.

Medium Component	Turco, *et al* (2017)	Boretto, *et al* (2017)	Function
A83-01	✓	✓	A potent inhibitor of TGF-β type I receptor superfamily activin-like kinase ALK4 and ALK7.
Base Medium	Advanced DMEM/F12	DMEM/F12 + Insulin-transferrin-selenium	
Antibiotic	Primocin	Penicillin/ Strptomycin	Prevent infection.
B27 Supplement	✓	✓	Supplement for serum free medium.
E_2	NA	✓	Promotion of growth and expansion.
L-Glutamine	L-Glutamine	Glutamax	Essential amino acid.
N-2 Supplement	✓	✓	Supplement for serum free medium.
N-Acetyl-L-cysteine	✓	✓	Antioxidant.
Nicotinamide	✓	✓	Amide form of niacin and is a precursor for nicotinamide adenine dinucleotide (NAD), which acts as coenzyme in multiple cellular processes.
EGF	✓	✓	Promotes cell growth, proliferation, and differentiation.
FGF10	✓	✓	EnSC derived. Promotes cell growth and proliferation.
HGF	✓	NA	EnSC derived. Promotes cell growth and proliferation.
Noggin	✓	✓	BMP inhibitor.
Wnt activator	R-spondin-1	R-spondin-1 + WNT3A	Promotes canonical WNT/β catenin signalling.
SB202190	NA	✓	p38 inhibitor.

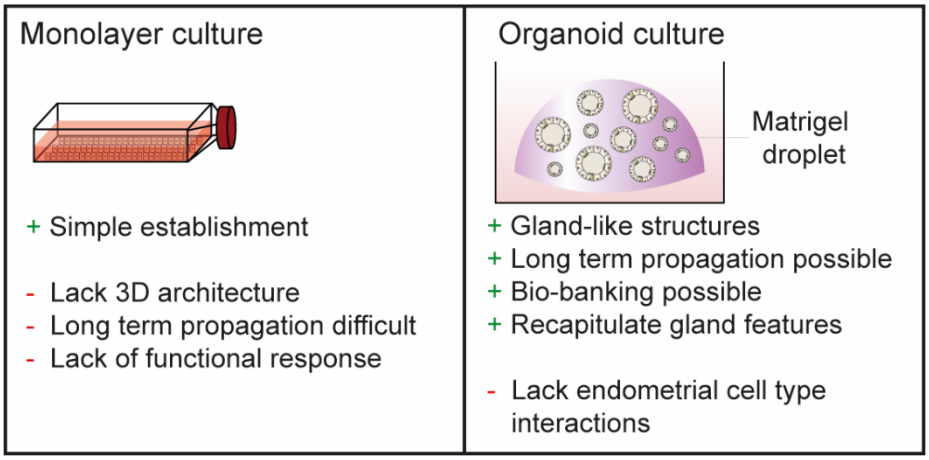

Figure 1.6. ***A comparison of endometrial EpC monolayer and gland organoid cultures.***

Little success was observed with EpC monolayers due to their inability to be propagated long-term and the loss of phenotype. Endometrial gland organoids exhibit morphological and functional features of their *in vivo* counterparts, can be passaged, and cryopreserved for long-term cultures. Modified from (Rawlings et al., 2021b)

1.5 Research Justification and Aims

Uterine epithelial glands are essential for implantation and pregnancy. Glandular defects are hypothesised to play a role in the aetiology of RMM. This study was undertaken to identify the endometrial defects in RMM patients, following the workflow presented in Figure 1.7. A previous study identified altered expression of mitochondria-associated genes in the glands of RMM patients compared with control subjects (Barros, 2017). Therefore, the thesis experimental plan began with the reanalysis of control and RMM endometrial gland RNA-sequencing dataset. Further in-depth computational modelling using Flux Variability and Flux Balance Analysis was undertaken to find the differences in metabolic pathways using this dataset. The focus of the remaining part of the study was to investigate the cause of these differences in RMM.

A reason for altered metabolic gene expression could be due to a mistiming of the endometrium, in particular the glands. Therefore, two approaches were used to address whether there was an out-of-phase response in the glands of RMM patients. First, differentially expressed genes between control and RMM patients were investigated to identify if the genes were temporally regulated. Secondly, a simple timing model using a ratio of two temporal genes was conducted on a larger cohort of endometrial samples. Crosstalk is essential for the function of the different cell types in the endometrium, hence, defects in the endometrial glands may be the results of a poor decidual response or vice versa. Thus, markers of the diverging decidual states were used to identify if RMM was associated with an abnormal decidual response alongside an uNK deficiency.

Glandular function during pregnancy cannot be studied directly in humans for ethical reasons, and animal models do not faithfully recapitulate human implantation and early pregnancy. Due to the technical barriers in growing human endometrial EpC in culture, the ability to advance knowledge of their precise functions has been limited. Development of the endometrial gland organoid model, which recapitulates the *in vivo* structure and function has resolved this problem. Therefore, the second part of the experimental plan was to understand the RMM phenotype further using organoids grown from control and RMM endometrial biopsies, following optimised protocols. RNA-sequencing of these patient organoids highlighted an impaired specification of EpC in RMM. To validate this finding *in vivo*, immunohistochemistry of a senescent marker was conducted on control and RMM endometrial samples. As an abnormal decidual response was found *in vivo* in RMM as well an imbalance of EpC in RMM

organoids, the final part of this study used scRNA-sequencing to explore the impact of the EnSC on subpopulations of RMM EpC using the assembloid model.

Long term, a detailed analysis of glandular defects associated with RMM may lead to the discovery of new therapeutic targets for this debilitating condition.

Thesis aims

1. To characterise the luteal endometrium in RMM patients compared to control subjects.
2. To investigate glandular defects associated with RMM by establishing patient-derived gland organoids.
3. To model the impact of EnSC on RMM gland organoids and investigate the epithelial subpopulations.

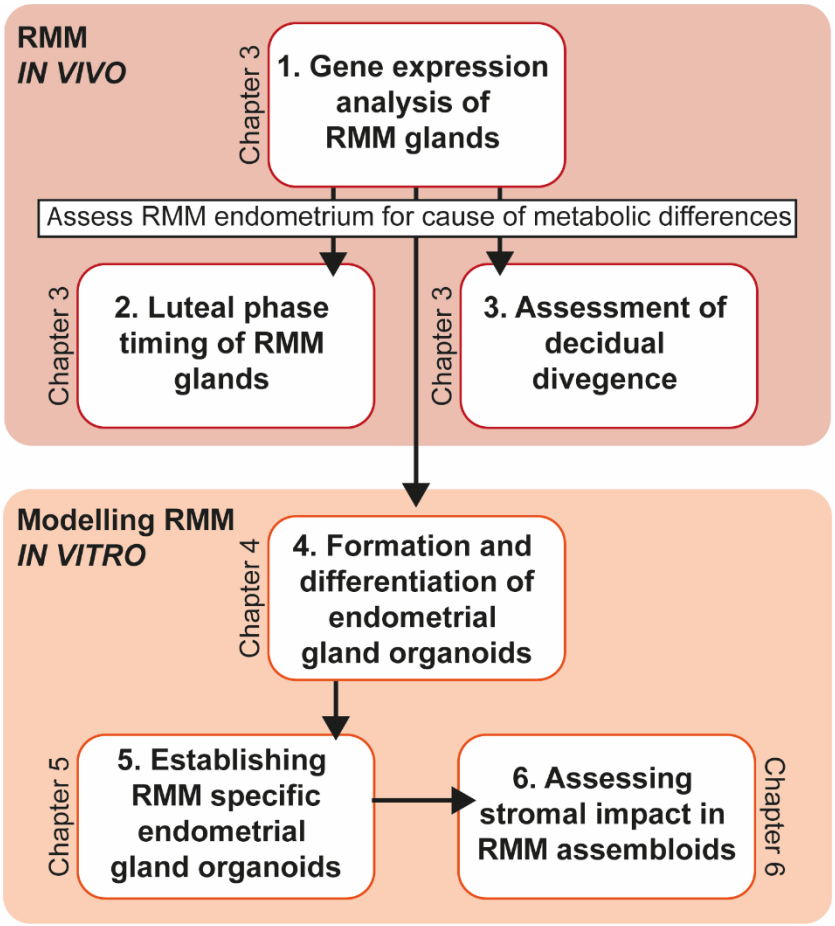

Figure 1.7. ***Workflow of thesis masterplan.***

The workplan for this thesis was conducted in two parts: *in vivo* and *in vitro* work. The experimental plan began with the reanalysis of the LCM RNA-seq of the glands from RMM and control endometrial biopsies (Chapter 3). The following experiments were undertaken to assess RMM endometrium for the cause of differences found between the patient groups. Next, the endometrial timing and decidual response were investigated to identify if the aberrant glandular defects were impacted by these responses (Chapter 3). For a more in-depth exploration of the RMM phenotype both at preconception and pregnancy, patient specific endometrial organoids were generated (Chapter 5), using optimised protocols (Chapter 4). The RMM model was further enhanced by using endometrial assembloids to investigate the impact of EnSC on the different EpC subpopulations.

Chapter 2:
Materials and Methods

2.1 Materials

2.1.1 Cell Culture

Table 2.1. *General cell culture materials and reagents.*

Materials	Manufacturer
40 µm cell strainer	Fisher Scientific
Antibiotic-Antimycotic (100×)	Gibco
Charcoal	Merck
Collagenase type IA	Merck
Corning Cell Recovery solution	Corning
Corning Cryogenic vials (2ml)	Corning
Deoxyribonuclease I (DNase I)	Roche
Dextran	Fisher Scientific
Dulbecco's Modified Eagle Medium (DMEM)/F12 (1:1) with L-Glutamine, phenol free	Gibco
Dulbecco's Modified Eagle Medium (DMEM)/F12 (1:1) with L-Glutamine with phenol red	Gibco
Foetal bovine serum (FBS) heat inactivated	Gibco
Recombinant Human Insulin	Merck
L-Glutamine	Gibco
Mr. Frosty™ Freezing container	Fisher Scientific
Plastic-ware	VWR
RNA-later	Merck
TrypLE™ Express Enzyme (1×), no phenol red	Gibco
TrypLE™ Select Enzyme (10×), no phenol red	Gibco
Trypsin-EDTA solution	Gibco

2.1.2 Organoid Culture

Table 2.2. *Expansion medium components.*

Reagent	Source	Purity/ Composition	Final Concentration	Manufacturer
A83-01	Synthetic	≥ 98% (HPLC)	500 nM	Merck
Advanced DMEM/F12			1×	Gibco
Antibiotic-Antimycotic (100×)		10,000 units/ml of Penicillin, 10,000 units/ml of Streptomycin,	1×	

		25 µg/ml of Fungizone™		
B27 Supplement minus vitamin A 50×	Synthetic	Biotin, DL Alpha Tocopherol Acetate, DL Alpha-Tocopherol, BSA (fatty acid free Fraction V), Catalase, Human Recombinant Insulin, Human Transferrin, Superoxide Dismutase, Corticosteron, D-Galactose, Ethanolamine HCl, Linoleic Acid, Linolenic Acid, P_4, Putrescine 2HCl, Sodium Selenite, T3 (triodo-l-thyronine) *Concentrations are confidential.*	1×	Gibco
L-Glutamine	Synthetic	200 nM L-Glutamine	2 mM	Gibco
N-2 Supplement 100×	Synthetic	Human transferrin 10 mg/ml, Insulin Recombinant Full Chain 500 ng/ml, Selenite 520 pg/ml, Putrescine 1.6 mg/ml, P_4 630 pg/ml	1×	Gibco
N-Acetyl-L-cysteine	Synthetic	≥ 99% (TLC)	1.25 mM	Merck
Nicotinamide	Synthetic	≥ 98% (HPLC)	10 nM	Merck

Recombinant Human EGF	*Escherichia coli* (*E.coli*)	≥ 98% by SDS-PAGE gel and HPLC analyses	50 ng/ml	Peprotech
Recombinant Human FGF10	*E.coli*	≥ 95% by SDS-PAGE gel and HPLC analyses	100 ng/ml	Peprotech
Recombinant Human HGF	BTI-Tn-5B1-4) Hi-5 Insect cells	≥ 98% by SDS-PAGE gel and HPLC analyses	50 ng/ml	Peprotech
Recombinant Human Noggin	HEK293 cells	≥ 95% by SDS-PAGE gel and HPLC analyses	100 ng/ml	Peprotech
Recombinant Human R-spondin-1	CHO cells	≥ 95% by SDS-PAGE gel and HPLC analyses	500 ng/ml	Peprotech

Table 2.3. *Organoid gels.*

Reagent	**Source**	**Composition**	**Manufacturer**
Matrigel™ Matrix Basement Membrane (Growth Factor Reduced)	Engelbreth-Holm Swarm mouse sarcoma	Extracted basement membrane contains extracellular proteins such as Laminin (~60%), Collagen IV (~30%), entactin (~8%) and heparan sulphate proteoglycans and several growth factors. Growth factor concentrations in GFR Matrigel: - 5 ng/ml IGF-1 - 1.7 ng/ml TGF-β - < 0.5 ng/ml EGF - < 5 pg/ml Platelet-derived Growth Factor - N/A Basic FGF - < 0.2 ng/ml Nerve Growth Factor - 1-1.5 ng/ml VEGF	Corning
PureCol® EZ Gel Solution	Bovine Skin	Gel contains ~5mg/ml (0.5 %) purified Type 1 bovine collagen, DMEM/F-12 medium and a mixture of L-Glutamine	Merck

		and dipeptide (L-Alanine-L-Glutamine)	

2.1.3 Cell Culture Treatments

Table 2.4. *Hormones and reagents used as treatments in cell culture.*

Reagent	Concentration	Manufacturer
8-bromoadenosine-3', 5'-cyclic monophosphate (8-bromo-cAMP)	0.5 mM	Merck
E_2	1 nM/10 nM (stated)	Merck
hCG	1 µg/ml	Merck
hPL	20 ng/ml	R&D systems
Medroxyprogesterone acetate (MPA)	1 µM	Merck
P_4	1 µM	Merck
PRL	20 ng/ml	Peprotech
Y-27632	10 µM	Abcam

2.1.4 Chemical Reagents

Table 2.5. *Chemical reagents.*

Reagent	Manufacturer
2× PrecisionPlus SYBR Green Master mix	Primer Design
Agarose powder	Fisher Scientific
Bovine Serum albumin (BSA)	Merck
Chloroform	AnalaR
Haematoxylin	Leica BioSystems
Diastase	Merck
Dimethyl sulphoxyde (DMSO)	Merck
EcoMount (Mounting Media)	Biocare Medical
Ethanol	Fisher Scientific
Ethidium Bromide	Merck
Formalin	VWR
Nuclease Free Water	Life Technologies
ProLong® Gold Antifade Reagent with DAPI	Cell Signalling Technology
QuantiFast SYBR Green PCR Master mix	QIAGEN
RNase ZAP	Fisher Scientific
Triton ×-100	Merck
TRIzol Reagent	Invitrogen
Trypan Blue stain solution	Gibco
Tween 20	Merck
Xylene	Honeywell Research Chemicals

2.1.5 Buffer Compositions

Table 2.6. *Buffer recipes.*

Buffer	Recipe
pH 6 antigen retrieval – Sodium citrate buffer	10 mM sodium citrate 0.05% Tween-20
pH 9 antigen retrieval – Tris-EDTA buffer	10 mM Tris base 1 mM Ethylenediaminetetraacetic acid (EDTA) solution 0.05% Tween 20
TBE (10×), pH 8.3	1.3 M Tris 450 mM Boric acid 25 mM EDTA pH 8
Tris-buffered saline (TBS) (10×), pH 7.6	130 mM NaCl 20 mM Tris
Tris-buffered saline-Tween 20 (TBS-T)	0.1% Tween-20 in 1×TBS

2.1.6 Antibodies

Table 2.7. *Primary antibodies.*

Primary Antibodies	Host	Antigen Retrieval Buffer	Dilution	Manufacturer
CD56	Mouse	pH 9	1:200	Leica
Cytokeratin-18	Rabbit	pH 6	1:200	ABCAM
E-cadherin	Rabbit	pH 6	1:200	Cell Signalling Technology
EpCAM	Rabbit	pH 6	1:200	Cell Signalling Technology
Glycodelin	Rabbit	pH 9	1:100	ABCAM
Osteopontin	Rabbit	pH 6	1:200	ABCAM
p16	Mouse	pH 9	1:5	Roche
PGR	Mouse	pH 6	1:50	Agilent Dako
Vimentin	Mouse	pH 6	1:200	Cell Signalling Technology

Table 2.8. *Secondary antibodies.*

Secondary Antibodies	Dilution	
Goat anti-Mouse IgG (H+L) Cross-Adsorbed Secondary Antibody, Alex Fluor 594	1:500	Invitrogen

Goat anti-Rabbit IgG (H+L) Cross-Adsorbed Secondary Antibody, Alexa Fluor 488	1:500	Invitrogen

2.1.7 Molecular Biology Kits

Table 2.9. *Molecular kits.*

Kit	Manufacturer
AllPrep DNA/RNA Micro Kit	QIAGEN
RNase-Free DNase Set	QIAGEN
RNeasy Plus Micro Kit	QIAGEN
QIAquick Gel Extraction Kit	QIAGEN
QuantiTect Reverse Transcription Kit	QIAGEN

2.1.8 Primers

Table 2.10. *Primer pair sequences and their efficiencies. All primers were purchased from Merck.*

Primer	Sequence (5'-3')	Efficiency
L19 Forward	GCG GAA GGG TAC AGC CAA T	1.98
L19 Reverse	GCA GCC GGC GCA AA	
ACADSB Forward	TCA AAG ATG TGG ATC AGC AGT G	1.92
ACADSB Reverse	AAG GAG GTA ATT CCC TTA TAT CCA A	
DIO2 Forward	ACT CGG TCA TTC TGC TCA A	2.06
DIO2 Reverse	TTC CAG ACG CAG CGC AGT	
FGF19 Forward	TGG AGA TCA AGG CAG TCG C	1.93
FGF19 Reverse	TCG AAA GCA CAG TCT TCC TCC	
GPX3 Forward	GGG GAC AAG AGA AGT CGA AGA	1.87
GPX3 Reverse	GCC AGC ATA CTG CTT GAA GG	
LGR5 Forward	CCC TTC ATT CAG TGC AGT GTT	2.00
LGR5 Reverse	ATT CTG ATC AGC CAG CCA TC	
PAEP Forward	GAG CAT GAT GTG CCA GTA CC	1.91
PAEP Reverse	CCT GAA AGC CCT GAT GAA TCC	
POU5F1 Forward	GGT ATT CAG CCA AAC GAC C	2.00
POU5F1 Reverse	CTC CTG AAG ATT TTC ATT GTT GT	
SCARA5 Forward	CAT GCG TGG GTT CAA AGG TG	1.97
SCARA5 Reverse	CCA TTC ACC AGG CGG ATC AT	

SLC15A2 Forward	AGG AGG CAT CAA ACC CTG T	2.00
SLC15A2 Reverse	CTA GTC CGT TCC TCT GCA TG	
SPP1 Forward	TGC AGC CTT CTC AGC CAA A	1.95
SPP1 Reverse	GGA GGC AAA AGC AAA TCA CTG	

2.1.9 Single-cell RNA-sequencing material

Table 2.11. *Single-cell RNA-sequencing consumables and reagents from Dolomite Bio for the Nadia Instrument.*

Material	**Manufacturer**
0.2 ml PCR tubes	Greiner Bio-One
1× PBS pH 7.4 sterile	Gibco
10× PBS pH 7.4 sterile	Gibco
1 M Tris pH 7.5	Merck
5 µM Überstrainer set	Pluriselect
10 % Tween 20	Fisher Scientific
20 % SDS	Fisher Scientific
20x SSC	Merck
40 % PEG	Merck
70 µm cell strainer	Fisher Scientific
AMPure beads	Agencourt
Barcoded beads in storage buffer (20-40 µm, pre-filtered)	ChemGenes Corporation
dNTPs	Thermo Fisher Scientific
DTT	Merck
EDTA	Fisher Scientific
Exonuclease I	New England Biolabs
Exonuclease I buffer	New England Biolabs
Ficoll PM-400	Merck
Haemocytometer plastic disposable C-Chip	Nano-EnTek
KAPA HiFi HotStart ReaadyMix Kit	Roche
Maxima 5x RT Buffer	Fisher Scientific
Maxima H-Re transcriptase	Fisher Scientific
Nadia Cartridge for scRNA-seq and sNuc-seq – 8 Runs	Dolomite Bio
Nextera XT DNA library Preparation Kit	Illumina
Polyethylene glycol 40 % (w/w) in H_2O	Merck
Qubit dsDNA HS assay kit	Thermo Fisher
RNase inhibitor	Lucigen
Sarkosyl	Merck
Tris (1M) pH 8.0	Fisher Scientific
Tris-EDTA pH 8.0 100× concentrate	Merck
QX200™ Droplet Generation Oil for EvaGreen	BioRad

Table 2.12. *Single-cell RNA-sequencing primers from Dolomite Bio for the Nadia Instrument.*

Primers	**Primer sequence (5'-3')**
Macosko template switch oligo (TSO)	AAGCAGTGGTATCAACGCAGAGTGAAT rGrGrG [1]
SMART PCR Primer (cDNA library amplification)	AAGCAGTGGTATCAACGCAGAGT
New-P5-SMART PCR hybrid oligo (Nextera tagmentation amplification)	AATGATACGGCGACCACCGAGATCTAC ACGCCTGTCCGCGGAAGCAGTGGTATCA ACGCAGAGT*A*C [2]
Nextera N7XX indexing primers	CAAGCAGAAGACGGCATACGAGATTCG CCTTAGTCTCGTGGGCTCGG
Read1CustomSeqB (Sequencing)	GCCTGTCCGCGGAAGCAGTGGTATCAA CGCAGAGTAC

[1] rG stands for ribonucleotide G

[2] The stars denote a base modification called phosphonothioate.

2.1.10 Miscellaneous Materials

Table 2.13. *Miscellaneous materials.*

Material	**Manufacturer**
Coverslips	Fisher Scientific
FrameStar® 384-Well Skirted PCR Plate	4titude
ImmEdge® Hydrophobic Barrier PAP Pen	Vector Laboratories
MicroAmp® Fast Optical 96-Well Reaction Plate with Barcode (0.1ml)	Applied Biosystems
MicroAmp® Optical 96-Well Reaction Plate with Barcode (0.1ml)	Applied Biosystems
MicroAmp® Optical Adhesive Film	Applied Biosystems
Microscopy Slides	Leica BioSystems
RNAse free tubes	Life Technologies
Surgipath Formula 'R' paraffin	Leica BioSystems

2.2 Methods

2.2.1 Human Endometrial Biopsies

Endometrial biopsies were obtained from patients attending the Implantation Clinic at University Hospitals Coventry and Warwickshire NHS Trust, Coventry UK. The use of these samples for research was approved by the NHS National Research Ethics-Hammersmith and Queen Charlotte's & Chelsea Research Ethics Committee (1997/5065) and Tommy's Reproductive Health Biobank (Project TSR19-002E, REC Reference: 18/WA/0356). All samples were taken from patients who had given informed written consent in accordance with the guidelines of the Declaration of Helsinki, 2000. Biopsies were taken from patients who were between 5-13 days post LH surge, according to home ovulation kits. Samples were obtained using a Wallach Endocell® endometrial sampler under ultrasound guidance. The device was inserted into the uterus until the uterine fundus could be felt before being withdrawn to create a negative pressure and rotated 360 °, moving out from the fundus to cervical ostium. Tissue was dissected into four portions and treated as follows: one part fixed in 10% formalin, one part for immediate isolation of endometrial cells stored in 5 ml 10% dextran-coated charcoal treated foetal bovine serum (DCC-FBS) supplemented in DMEM-F12, one part immediately stored in RNAlater and one part snap-frozen in liquid nitrogen and then stored at -80 °C.

2.2.2 Cell Culture

Preparation of dextran-coated charcoal treated stripped foetal calf serum

FBS was stripped of various small molecules including endogenous hormones using dextran charcoal treatment. FBS (500 ml) was treated with 1.25 g of charcoal and 125 mg of dextran and incubated at 57 °C for 2 hours with intermittent mixing. After a 30-minute centrifugation at 400 *g*, supernatant (DCC-FBS) was collected, sterile filtered, aliquoted, and stored at -20 °C for future use.

Isolation of human endometrial stromal and epithelial cells

EnSC and EpC were isolated from fresh endometrial biopsies described by (Barros et al., 2016). Briefly, biopsies were washed in 10% DCC-DMEM media (DMEM/F12 with phenol red, 10% DCC-FBS, 10 µM L-glutamine, 1× antibiotic antimycotic, 1 nM E_2 and 2 µg/ml recombinant human insulin) and minced finely using a scalpel in a

Petri dish. Minced tissue was digested for 1 hour at 37 °C with collagenase type IA (0.5 mg/ml) and deoxyribonuclease type 1 (DNase I) (0.1 mg/ml) in phenol red-free DMEM/F12 (additive-free) medium, with vigorous shaking every 20 minutes. Digested tissue was filtered through a 40 µm cell strainer and rinsed through with 5 ml 10 % DCC medium to wash cells. EnSC and other cells (blood cells, immune cells, endothelial cells, and single EpC) passed through the strainer, whereas epithelial gland isolates were retained. For the isolation of EpC, the strainer was inverted over a 50 ml Falcon tube and backwashed with 10% DCC medium. Both cell types were centrifuged at 280 *g* for 5 minutes and cell pellets were either used immediately or cryopreserved in 10% Dimethyl sulphoxyde (DMSO) in DCC-FBS.

Cell thawing

Cryovials were removed from liquid nitrogen and placed in dry ice. EnSC and EpC were thawed 2-3 minutes at 37 °C in a water bath before they were added to 8 ml of pre-heated 10% DCC or additive free medium, respectively. The cell solution was centrifuged at 280 × *g* for 5 minutes. EnSC plated as monolayer cultures, and EpC were used for gland organoid cultures.

Primary cell culture

All cell culture was conducted in a class II microbiological safety cabinet. EnSC and EpC were managed under standard cell culture conditions using a carbon dioxide (CO_2) incubator maintained at 37 °C, which provided a humid atmosphere with 5% v/v CO_2.

2.2.3 Endometrial Gland Organoid Culture

Endometrial gland organoid culture

Endometrial gland organoids were cultured using a protocol adapted from (Turco et al., 2017). Fresh or frozen EpC pellets were resuspended in additive-free medium. The cell suspensions were pelleted at 600 *g* for 6 minutes in 1.5 ml microcentrifuge tubes. Medium was aspirated and the pellet was resuspended in neat ice-cold Matrigel at a ratio of 1:20 (v:v). Samples in Matrigel were kept on ice until plating. Using ice-cold pipette tips, the Matrigel/cell suspension was plated in 20 µl droplets per well, in a 48-well plate. Droplets were polymerised at 37° C for 15 minutes in a cell culture incubator, then overlaid with Expansion Medium (ExM) (Turco et al., 2017)

(Table 2.2) and maintained at 37 °C in a CO_2 incubator. Medium was replaced every 2-3 days and samples were cultured for 7 days.

Organoid passage

After 7 days of growth, organoids were passaged using an adapted protocol from (Turco et al., 2017). Matrigel droplets were scraped off the plate into a 1.5 ml microcentrifuge along with the culture medium. Multiple droplets (4-5) were pooled per tube and were centrifuged at 600 *g* for 6 minutes. The supernatant was aspirated, and the pellet was resuspended in 150 µl additive-free medium. Repeated pipetting (~300) times was used to dissociate the gel and organoids before 1 ml of cold additive-free medium was added. The suspension was centrifuged at 600 *g* for 6 minutes. The supernatant was removed, and the pellet was resuspended in 150 µl additive-free medium. With moderate force, the organoids were broken down further by pipetting 80 times and 1 ml of additive-free medium was added and centrifuged at 600 *g* for 6 minutes. The supernatant was removed, and the cell pellet resuspended in ice-cold Matrigel. Samples were plated as described above. Medium was replaced every 2-3 days. After 7 days, the organoids were passaged again.

Cyclical versus serial passaging differentiation

Three frozen independent EpC samples were thawed and set up for organoid culture. The organoids either went through 1 to 4 cycles of differentiation without being passaged, or underwent differentiation at passage 0 (P0), passage 1 (P1), passage 2 (P2) and passage 3 (P3). To differentiate the organoids, organoids were first left to grow for 4 days. On the fourth day, organoids for differentiation were primed with 10 nM E_2. After 48 hours, the organoids were treated with 10 nM E_2, 0.5mM 8-Bromoadenosine 3', 5' cyclic monophosphate (8-bromo-cAMP) and 1 µM P_4. In parallel, undifferentiated organoids were maintained in ExM for the 4 days. After another 48 hours, the organoids were harvested from the Matrigel using Corning Cell Recovery Solution at 4 °C. After 1 hour incubation and complete removal of the organoids from the gel, the organoids were centrifuged, washed with cold phosphate buffered saline (PBS) twice and pelleted. The organoids were then snap-frozen and kept at -80 °C for RNA extraction.

Organoid forming efficiency assay and differentiation

Frozen EpC samples from 45 endometrial biopsies were thawed and resuspended in additive-free media, depending on the sample size. A portion of the cell suspension

was used to culture organoids to P2, which were differentiated and harvested for RNA extraction as described previously.

The remaining EpC solution was centrifuged, and the pellet was resuspended in 0.25 % Trypsin-EDTA for 10 minutes at 37 °C. Cells were washed with 10% DCC-DMEM to deactivate the enzyme, centrifuged, resuspended, and counted. EpC were resuspended in ice-cold Matrigel to either 100 or 1000 cells per 5 µl of Matrigel and plated per well in a 96-well plate and incubated at 37 °C for 15 minutes to polymerise the Matrigel. A minimum of three wells per sample were plated. Afterwards, 100 µl of ExM supplemented with 10 µM Y-27632 was added to each well for the first 3 days. Medium was replaced every 2-3 days. Brightfield images were taken at ×2 magnification using the EVOS FL Auto Imaging System Instrument on day 0 and 10. The number of organoids for each day were manually counted for each sample and were averaged. Organoid forming efficiency (OFE) was calculated using the formula:

$$\text{OFE (\%)} = \frac{number\ of\ organoids}{number\ of\ seeded\ cells} \times 100$$

Control vs RMM - Organoid forming efficiency assay

Frozen EpC samples of 10 control and 10 RMM patients were used for an OFE assay as described by (Turco et al., 2017). Samples were grown to P2. Organoids from 4/5 droplets were removed using Cell Recovery Solution at 4 °C. After 1 hour, the organoids were centrifuged at 600 *g* for 6 minutes. The Cell Recovery Solution was removed from the pellet, resuspended in PBS, and centrifuged again. The pellet was resuspended in 150 µl additive-free media, pipetted several hundred times to disassociate the organoids before 1 ml of media was added. Samples were centrifuged and 500 µl TrypLE Express Enzyme (1×) was added. Tubes were placed in shaking water batch for 10 minutes. Enzyme was diluted with additive-free media and cell suspension was passed through a 40 µM strainer and centrifuged. Pellet was resuspended in appropriate volume of medium. Cells were counted using haemocytometer and trypan blue was used to account for dead cells in the samples. Cells were resuspended in ice-cold Matrigel to have 100 cells per 5 µl droplet. The samples were plated, imaged and OFE was calculated as described above.

Control vs RMM – Pregnancy assay

P2 organoids from control and RMM endometrial biopsies were left to grow for 4 days in ExM. On the fourth day, organoids were either left untreated in ExM or treated with ExM containing 10 nM E_2, 0.5mM 8-Bromo cAMP, 1 µM P_4, 1 µg/ml hCG, 20 ng/ml

hPL and 20 ng/ml PRL. Media was changed every 3 days. Brightfield images were captured of the organoids on the EVOS FL Auto Imaging System Instrument. After 6 days, the organoids were harvested using Corning Cell Recovery Solution as described previously. The organoids were then snap-frozen and kept at -80 °C for RNA.

2.2.4 Endometrial Stromal Cell Culture

Fresh or frozen EnSC pellets were resuspended in 5 or 10 ml of 10% DCC-DMEM medium, depending on the pellet size. The cell solution was seeded into an appropriately sized cell culture flask and incubated at 37 °C and 5 % CO_2. Medium was changed the next day to remove any suspension cells (blood, immune cells, and dead cells) and after every 2-3 days. Once EnSC had grown to confluent monolayers, the medium was removed. Cells were washed with PBS and were incubated in 0.5/1 ml 0.25 % Trypsin-EDTA for 5 minutes at 37 °C, depending on the size of the flask. Flask sides were tapped to help dislodge any remaining attached cells. Cell detachment was inspected under a microscope. Enzyme activity was stopped by addition of 4.5/9 ml 10% DCC-DMEM medium and cell suspension was centrifuged at 280 *g* for 5 minutes. Cells were resuspended in 10% DCC-DMEM medium to split into a ratio of 1 in 2 or 1 in 3 in new flasks.

2.2.5 Assembloid Culture

Assembloid formation and differentiation

Both P1 EnSC and endometrial gland organoids were passaged with their respective passaging protocols as described. At 1:1 (v/v) ratio, single cell suspension of 5×10^4 EnSC were combined with epithelial organoids passaged at a ratio of 1:2 per assembloid culture. The EnSC and gland organoid mixture was resuspended in ice-cold PureCol® EZ Gel Solution at ratio of 1:20 (v:v) and kept on ice until plating. Droplets of 20 µl gel/cell suspension were plated per well in a 48-well plate with ice-cold pipette tips and cured at 37 °C for 90 minutes in a cell culture incubator. Assembloids were cultured for 4 days in ExM containing 10 nM E_2 to allow for the samples to grow and expand. On the fourth day, if a forward time-course was used samples were harvested or treated using a differentiation media containing ExM, 1nM E_2, 0.5 mM 8-bromo-cAMP and 1 µM MPA for another four days. If a reverse time course was used, assembloids were left to grow in ExM + E_2 as a control or treated using the differentiation media above unless otherwise stated for another four days.

Establishment of a defined assembloid minimal differentiation medium

Three independent biopsies were used to create both organoid and assembloid cultures at P2. Duplicates wells were plated out for each DM composition in a 48 well-plate. All samples were cultured for 4 days in ExM with 10 nM E_2, and on day 4 each sample was subjected to different DM composition. Each sample also had a control which continued to grow in ExM with E_2. After 4 days, all samples were harvested for RNA. Organoid samples were harvested using Cell Recovery Solution as described elsewhere. For assembloids samples, supernatant was removed, washed with PBS before 200 µl of collagenase type IA (0.5 mg/ml) was added to each well. Droplets were scrapped off and with the enzyme solution, duplicate wells were added to 1.5 ml tubes, which were placed in a water bath for 10 minutes at 37 °C, shaken every 5 minutes. Samples were centrifuged, washed with PBS, and pelleted. The assembloids pellets were snap-frozen and kept at -80 °C for RNA extraction.

Control vs RMM assembloids – frozen stromal cells

Three RMM and three control cryopreserved endometrial biopsies were set up for gland organoid culture and EnSC were propagated as monolayers. At P2, EnSC and gland organoid pellets were combined to generate assembloids for each sample. A minimum of 12 wells were plated out for each sample in a 48-well plate. All samples were cultured for 4 days in ExM with 10 nM E_2, and the medium was refreshed every 48 hours. Assembloids were then either harvested for single-cell RNA-seq (scRNA-seq) as day 0 samples or differentiated using the following media: base media (Advanced DMEM/F12, N-2 supplement, B12 supplement, antibiotic/antimycotic and L-glutamine), N-Acetyl-L-cysteine (NAC), 1 nM E_2, 0.5mM 8-bromo-cAMP and 1 µM MPA. Medium was again refreshed every 48 hours and on day 4 of differentiation, assembloids were harvested for scRNA-seq.

Control vs RMM assembloids – fresh stromal cells

Three RMM and two control cryopreserved EpC samples were set up for gland organoid culture. In parallel, freshly isolated EnSC from a control endometrial biopsy were cultured as monolayers. At P2, all five gland organoid cultures were mixed individually with P3 EnSC from the single biopsy to establish assembloids. A minimum of 12 wells were plated out for each assembloid culture in 48-well plate. All samples were cultured for 4 days in ExM with E_2, and the medium was refreshed every 48 hours. Assembloids were then either harvested for scRNA-seq as day 0 samples or

differentiated using the same differentiation media as above. Medium was again refreshed every 48 hours and on day 4 of differentiation, assembloids were harvested for scRNA-seq.

2.2.6 Imaging of Organoids, Assembloids and Whole Tissue

Organoid, assembloid and endometrial tissue embedding and sectioning

Undifferentiated and differentiated samples for both organoids and assembloid cultures were grown in PureCol® EZ Gel Solution, using a forward time-course (*See: Assembloid formation and differentiation*). Media was removed from organoids and assembloids and PBS was added. Collagen gel droplets were peeled off the well plate gently with tweezers to ensure the droplet remained in one piece and placed into a bijoux tube with the PBS. PBS was removed and samples were stained with haematoxylin for 5 minutes to identify the droplet in later steps. Samples were washed and fixed with 10% formalin for 20 minutes. Samples were washed twice in PBS and stored at 4 °C for maximum a week. Before embedding, samples were dehydrated by immersion in increasing concentrations of ethanol for 1 hour at 70% and 90% and 90 minutes at 100%. Samples were transferred to a glass vial and incubated in xylene for 1 hour.

Fixed droplets and endometrial biopsies that had been fixed overnight at 4 °C were then embedded in Surgipath Formula ‘R’ paraffin wax using the Shandon Excelsior ES Tissue processor. Paraffin embedded biopsies and organoid/assembloid samples were sectioned into 3 µm or 5 µm slices, respectively, with a microtome and mounted onto microscope slides. To adhere the samples onto the slides, samples were incubated for an hour or overnight at 60 °C. Slides were stained or stored at 4 °C.

Immunofluorescence of organoids and assembloids

For immunofluorescence of organoids and assembloids, sections were subjected to a series of deparaffinisation and hydration steps of three xylene washes for 5 minutes each, two 100% isopropanol washes, one 70% isopropanol wash and one distilled water wash for 2 minutes each. Antigen retrieval of the sections was undertaken by submerging the sections in a pH buffer that was dependent on the antibody (Table 2.8) and placed in a Pickcell pressure cooker for 2 hours, which included time for the slides to cool. Slides were removed from the buffer and placed into a dark moisture chamber, washed with distilled water and a border was created around each section using a hydrophobic pen (PAP).

For immunolabelling for extracellular markers, samples were washed with Tris-buffered saline-Tween 20 (TBS-T) for 2 minutes and blocked in 2% bovine serum albumin (BSA)/TBS-T for 20 minutes. Primary antibodies were diluted in TBS-T (Table 2.8) and kept overnight 4 °C. Sections were washed three times in TBS-T before either secondary rabbit or mouse antibodies conjugated to Alexa Fluor 488 or 594, respectively, diluted 1:500 in TBS-T were added and kept at room temperature for 2 hours. Sections were then washed in TBS-T three times and mounted in ProLong® Gold Antifade Reagent with DAPI for nuclear counterstain.

For immunolabelling for intracellular markers, samples were washed with PBS for 2 minutes and permeabilised by 0.1% Triton ×-100 in PBS for 30 minutes. Samples were washed three times with PBS and blocked in 1% BSA/PBS for 30 minutes. Primary antibodies were diluted (Table 2.8) in 0.05% Triton ×-100/1% BSA/PBS and kept overnight at 4 °C. Samples were washed three times in PBS before either secondary rabbit or mouse antibodies conjugated to Alexa Fluor 488 or 594, respectively, diluted 1:500 in PBS were added and kept at room temperature for 2 hours. Samples were then washed in PBS three times and nuclear counterstained as mentioned above.

Sections were visualised using the EVOS FL Auto Imaging system using the GFP, TxRed and DAPI cubes to visualise Alexa Fluor 488 and 594, and DAPI, respectively. Images of individual channel data were saved as .TIF images and using the 'Merge Channel' tool in ImageJ software, images were merged into single colour images and saved as jpeg files. Images that were being compared to each other, brightness and contrast were enhanced to each other to the same degree.

Immunohistochemistry of endometrial tissue

Endometrial tissue from control and RMM patients were stained for uNK and $p16^{+}$ cells as described in (Brighton et al., 2017). Briefly, the Lecia BondMax autostainer was used, which fully automated: deparaffinization, pH 6 antigen retrieval, antibody staining of uNK-specific cell surface antigen, CD56 or p16 (Table 2.8), haematoxylin counter stain and DAB colour development. After the autostainer, the slides were dehydrated, cleared and cover-slipped using DPX coverslip mountant in a Tissue-Tek Prisma Automated Slide stainer. Brightfield images were obtained of the stained tissue on a Mirax Midi slide scanner using a ×20 objective lens. Case Viewer (3D Histec) was used to view images and for analysis.

For all patient samples, CD56 positive cells were quantified in compartments directly under the luminal epithelium to avoid inconsistencies that reflect reduced uNK cell densities at greater depth. Three regions were randomly selected for each patient within Panoramic Viewer before analysing in ImageJ software. Luminal and glandular EpC were removed manually before colour deconvolution into $CD56^+$ staining of constituent brown and the blue haematoxylin staining of the EnSC. Area of positive staining above a manually determined background threshold was used to quantify staining intensity. The uNK percentage from each area was calculated as CD56/EnSC × 100, and the average of all three images was taken. uNK scores and percentile values were calculated, using R software.

Separate quantification of the luminal epithelium, glandular epithelium, and stromal compartment was conducted for $p16^+$ cells. Each compartment was manually isolated and the colours deconvolved into constituent brown ($p16^+$ cells) and blue (haematoxylin stain). $P16^+$ quantification was performed as described as above.

2.2.7 RNA Extraction

To minimise RNA degradation, all RNA extraction procedures used RNase-free plastic-ware and nuclease free water. Also, all surfaces and pipettes were cleaned with RNase ZAP.

RNA extraction of organoids, assembloids and endometrial tissue

Total RNA extraction of the organoid and assembloids pellets was performed using either RNeasy Micro Kit (QIAGEN), or AllPrep RNA/DNA kit with on-column RNase-Free DNase I digestion, following manufacturer's protocol and eluted in 14 µl.

For total RNA extractions of endometrial tissue which had been stored in RNAlater and then stored at -80 °C, TRIzol Reagent was used according to manufacturer's instructions, with a rotor-stator homogenisation. Sample was placed into a nuclease free tube and 1 ml of TRIzol was added. Samples were homogenised using a mechanical probe and left to stand on the bench for 1 minute. Samples were snap frozen and stored at -80 °C.

Homogenised tissue samples were thawed on ice to proceed with the remaining RNA extraction. First, 20% of the volume of chloroform was added to TRIzol/homogenised tissue solution and vortexed. Samples were centrifuged at 16 000 × *g* for 20 minutes at 4 °C to separate the sample into an aqueous and an organic phase. RNA remained in the colourless upper aqueous layer and was carefully transferred into another

nuclease free tube, containing half the original volume of isopropanol and vortexed. Samples were centrifuged at 16 000 × *g* for 15 minutes at 4 °C to precipitate the RNA to form a pellet at the bottom. Supernatant was discarded, RNA pellets were washed with 1 ml of 70% ethanol and centrifuged at 16 000 × *g* for 20 minutes at 4 °C. Wash step was repeated. Supernatant was discarded, and the pellets were air-dried to remove any remaining ethanol. The RNA pellets were dissolved in 30 µl of nuclease free water.

RNA concentration and purity were assessed by a Nanodrop Spectrophotometer. Values deemed suitable for downstream analysis were those of ≥ 1.80 on the 260/280 absorbance scale, indicating pure RNA without contamination of protein. Samples were stored at -80 °C.

2.2.8 Gene Expression Analysis by Reverse Transcription Quantitative Polymerase Chain Reaction

cDNA Synthesis

For cDNA (complementary DNA) synthesis, extracted RNA was reverse transcribed using QuantiTect Reverse Transcription Kit, following manufacturer's instructions. RNA samples and the reagents were thawed on ice. To prevent any concentration gradients, the reagents were briefly vortexed and centrifuged. Then, 2 µl of 7× gDNA Wipeout buffer was added to 1 µg of endometrial tissue RNA. However, for organoid and assembloid samples 1 µg was not possible. Instead, for all samples, the lowest concentration of RNA across all the samples was used. The template RNA was made up with a total volume of 14 µl with RNase-free water. The samples were incubated for at 42 °C for 2 minutes for any traces of genomic DNA to be removed. After, samples were immediately placed on ice. A reverse-transcription master mix was prepared. For each sample, 1 µl of Quantiscript Reverse Transcriptase (RT), 4 µl 5× Quantiscript RT buffer and 1 µl RT Primer Mix was added to the template RNA, mixed, and stored on ice. A RT negative control was also prepared that replaced the RT with nuclease free water. All other stages were identical. Reactions were incubated at 42 °C for 30 minutes and then inactivated by incubation at 95 °C for 3 minutes. Endometrial tissue cDNA was diluted with 180 µl of nuclease free water to give a final volume of 200 µl.

Primer design

Primers were designed from Universal ProbeLibrary Assay Design Center (https://lifescience.roche.com/en_gb/brands/universal-probe-library.html#assay-design-center). Primers were designed with the following requirements:

a. Melting temperature (Tm) is calculated with the formula Tm = 69.3 + (41(GC/L)) – (650/L), where GC is the number of G and C bases in the primer and L is the number of nucleotides in the primer. Tm of the primer should be between 58 °C and 59.9 °C.
b. Total amplicon length should be between 75-125 base pairs.
c. Tm should not differ from the forward and reverse primer by greater than 1 °C
d. At the 3' end of the primer, the last five bases should include 3 bases which could be either G or C.
e. There should be no more than 4 of the same bases consecutively.
f. Primer length should be between 18-24 bases.
g. To distinguish between cDNA and gDNA, primers are required to be exon spanning.
h. Amplicon Tm is calculated by the following = 64.9+(0.41*(((C+G)/L)*100))-(500/L).

To confirm specificity, primer sequences were submitted to Primer Blast (https://www.ncbi.nlm.nih.gov/tools/primer-blast/). Primer sequences are presented in Table 2.10.

Primer testing and efficiency calculations

Primers were optimised to determine no non-specific product was being amplified and to determine efficiencies. Forward and reverse primers were used at 20 µM in a total volume of 19 µl in SYBR Green master mix and loaded onto a 96-well plate. For each primer pair, 1 µl of pooled cDNA from organoids was added to four wells each or 1 µl of nuclease free water was added to two wells each. Genes were amplified in 7500 Fast Real-Time PCR System (Applied Biosystems). The amplified product of the four wells was combined, mixed with the loading dye, and first, loaded on a 3% agarose gel. Agarose gel was made by adding agarose powder to 1× TBE in a conical flask and microwaving to dissolve gel. For 50 ml of gel, 1 µl of ethidium bromide was added. Gel was poured into a plate with a comb and left to set for 30 minutes before loading.

Gels were run in 1× TBE buffer at 100 V until the dye had run a quarter of the length of the gel. Using a UV transilluminator, the gel was imaged to check that for each primer pair only one product was amplified and of the correct size. If the primer pair fit these criteria, then a 1.8% agarose gel was run with the remaining amplified product/loading dye. After, the gel was finished running, the purified product was excised from the gel, using QIAGEN QIAquick Gel Extraction Kit, following the manufacturer's instructions. The DNA was quantified by Nanodrop Spectrometer.

To examine primer efficiencies, purified products were serially diluted between 100 pg/µl to 10 ag/µl in 1/10 dilution factor, providing 8 dilutions. Using the appropriate primers and a SYBR Green Master mix, the serial dilutions were amplified in triplicates, and cycle threshold (Ct) values measured. The log of the concentration of cDNA was plotted against average Ct values. The following calculation was used to calculate primer efficiencies:

$$Primer\ Efficiency = 10^{\frac{-1}{Gradient\ of\ the\ line}}$$

All primer efficiencies calculated are plotted in Figure 2.1. All other primer efficiencies were calculated by Brosens group.

Reverse Transcription Quantitative Polymerase Chain Reaction

Reverse Transcription Quantitative Polymerase Chain Reaction (RT-qPCR) was used to determine relative mRNA abundance of genes of interest. SYBR Green detection reagents (2× PrecisionPlus SYBR Green Master mix or QuantiFast SYBR Green PCR Master mix) were used to amplify genes of interest. Reactions were either carried out in a 96- or 384-well plate in total volume of 20 µl or 10 µl, respectively. Each reaction in a 96-well plate contained 10 µl of SYBR Green PCR Master mix, 0.3 µl of forward primer (20 µM), 0.3 µl of reverse primer (20 µM), and 8.4 µl nuclease free water. Each reaction in a 384-well plate contained 5 µl of SYBR Green detection reagent, 0.15 µl of forward primer (20 µM), 0.15 µl of reverse primer (20 µM), and 3.7 µl nuclease free water. In both sized reactions, 1 µl cDNA template or RT negative control was added to each well and set up either in duplicate or triplicate for technical replication. Non-template controls were used in which the cDNA was replaced with nuclease free water. Plates were sealed with optical cover, briefly centrifuged to remove air bubbles and placed in either 7500 Fast Real-Time PCR System (96-well Block) or QuantiStudio® 5 Real-Time PCR Instrument (384-well Block).

Thermocycling conditions for when 2× PrecisionPlus SYBR Green Master mix was used were as follows: 95 °C for 2 minutes at the hold stage and then 95 °C for 15 seconds and 60 °C for 1 minute for 40 cycles at the PCR stage.

Thermocycling conditions for when QuantiFast SYBR Green PCR Master mix was used were as follows: 95 °C for 5 minutes at the hold stage and then 95 °C for 10 seconds and 60 °C for 30 seconds for 40 cycles at the PCR stage.

Melt curves were ran at the end to ensure that the amplified products were specific and the SYBR Green fluorescence was a direct measurement of accumulation of product of interest.

RT-qPCR Analysis

Analysis of endometrial tissue was carried out using the Delta Delta Ct method to compare between the Ct values of samples of interest, using one sample as a calibrator. The Ct values of the samples were adjusted to the housekeeping gene, *L19*. A fold change value was calculated to indicate the relative fold change between the calibrator and the other samples.

Ct values from organoid and assembloids samples were also normalised to housekeeping gene, *L19*, and instead used the Pffafl method to account for variable primer efficiencies (*See: Table 2.10 Primers*). An untreated sample was used to compare to the normalised data to identify the relative fold change of expression between the treatment and control samples.

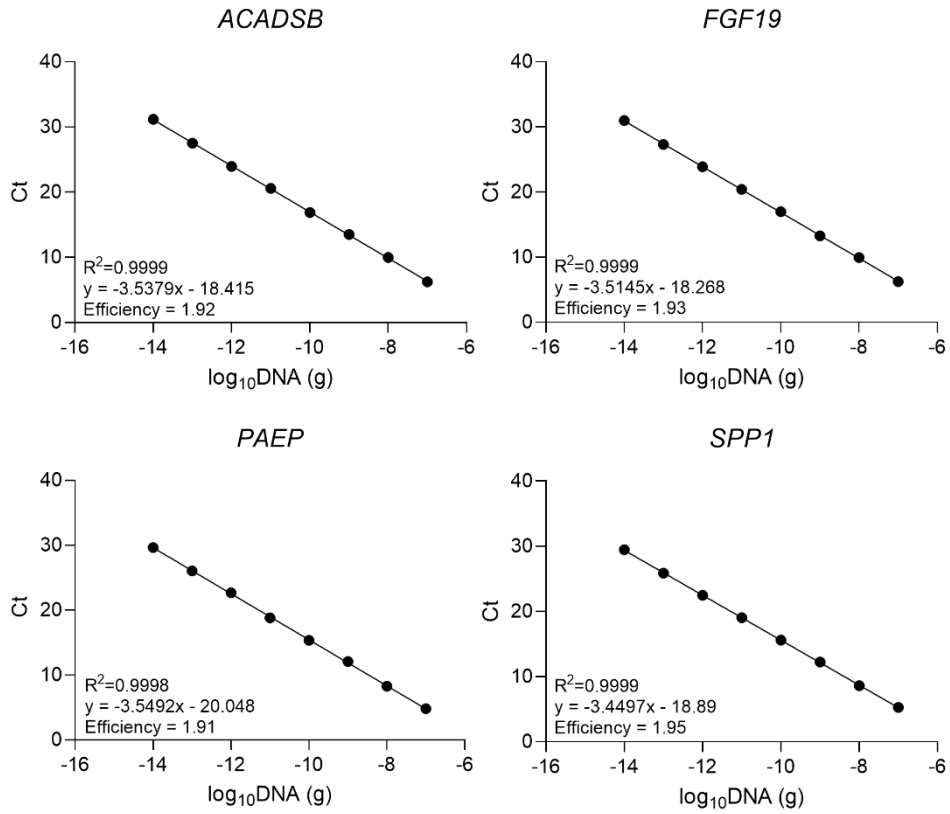

Figure 2.1. ***Primer optimisation of endometrial gland organoid genes.***

Designed primers were tested using pooled cDNA samples. Amplified products were checked for single, specific product, purified, and serially diluted to amplify with appropriate primers and a SYBR Green Master mix. Ct values were measured to calculate the primer efficiencies.

2.2.9 RNA-Sequencing

Data Mining

Endometrial gland laser capture microdissection (LCM) RNA-sequencing (RNA-seq) data (control vs RMM) from Flavio Barros's thesis: 'Characterization of human endometrial glandular epithelium *in vitro* and *in vivo*' (2017) and the dataset 'Changes in human endometrial gland transcriptome over the window of implantation: GSE84169 from Gene Expression Omnibus (GEO) repository was reanalysed to identify differences between control and RMM samples and glandular timing. Dataset 'Endometrium through the menstrual cycle: GDS2052' from the GEO repository was data mined for gene expression in Chapter 3. scRNA-seq data from 'Single-cell RNA Sequencing of Endometrial Assembloid Cultures: GSE168405' was mined for cell markers of EpC subpopulations of assembloid cultures in Chapter 5 and 6 and SASP related genes in Chapter 6.

Bioinformatics analysis of LCM RNA-sequencing data

LCM RNA-seq data was processed using DESeq2 package in R software and transcripts per million (TPM) were calculated as described by (Wagner et al., 2012). Rld function of DESeq2 tool was used to create regularised-logarithm transformed data for principal component analysis (PCA). Differential gene expression analysis was conducted for both datasets, separately and transcripts that had expression read count value < 20 in all samples combined were removed. For LCM control vs RMM data, differential expression analysis was performed in RMM with references to the controls. In the gland temporal dataset, differential gene expression analysis was performed in LH+8 with references to LH+5, LH+11 with references to LH+8, and LH+11 with references to LH+5. Differentially expressed genes (DEGs) were identified using two thresholds: $P < 0.01$ and FDR corrected $P < 0.05$ and these genes were used to perform gene ontology (GO) analysis using the Gene Ontology consortium database (Consortium, 2019).

Metabolic modelling of control vs RMM gland LCM RNA-sequencing data

To examine metabolic differences in RMM glands compared to the control glands, the human metabolic reconstruction (recon3D) was used. All model simulations were performed using cobra toolbox in Matlab. First, the average gene expression value (regularised-logarithm transformed) from RMM and control glands were mapped to the human metabolic network to assign expression value to reactions following

mapExpressionToReactions function from cobra toolbox. Briefly, to calculate the expression value for a reaction, 'or' and 'and' logic in Gene-Protein-Reaction relation was replaced by max and min, respectively. The expression ratio (RMM vs control) was calculated for each reaction. By setting the reaction flux lower bound to zero, all Exchange, Sink and DM reactions were made irreversible. BIOMASS maintenance reaction was set as the model objective and simulations were performed using HAM media constraints with unlimited oxygen uptake. Histidine was added in the theoretical media as it was necessary for growth.

Flux variability analysis was performed. This analysis method predicts the flux range of each reaction in the defined media condition to achieve the maximum growth. The predicted flux range was considered for control. To calculate the flux range in RMM condition, the minimum and maximum flux of control condition were multiplied with the expression ratio. Finally, these flux ranges were set as reactions constrain and flux balance analysis was performed to predict the reaction flux in both RMM and control conditions.

RNA-sequencing of organoids

Four control and four RMM endometrial glands were cultured as organoids and at P2 were treated with the pregnancy media *(See: Control vs RMM – Pregnancy assay).* The RNA extracted from the untreated and treated samples for all eight samples underwent RNA-seq.

RNA quality was analysed on an Agilent 2100 Bioanalyzer (Agilent Technologies) using a nano Bioanalyzer chip according to the manufacturer's instructions by Genomics Facility at University of Warwick. RNA integrity number (RIN) score for all samples was ≥ 6. Libraries were prepared using TruSeq RNA V2 kit (Illumina) and sequenced using Illumina NextSeq platform using a high output 75 cycle kit (v2.5) (75 bp single read).

Transcriptomic maps of single-end reads were generated using bowtie-2.2.6, samtools-1.2, and tophat-2.1.0 against the hg19 human genome assembly. Transcript counts were assessed with HTSeq-0.6.1 against the gencode.v19 transcript annotation using the strand reverse setting and intersection-non-empty mode.

Bioinformatics analysis of gland organoid RNA-sequencing data

Organoid RNA-seq data was processed using DESeq2 package in R software and TPMs were calculated as described by (Wagner et al., 2012). Rld function of DESeq2 tool was used to create regularised-logarithm transformed data for PCA analysis. To identify batch effects, removeBatchEffect function from the limma package in R was used. The function was performed on treatment effect, patient effect, and batch effect. For the organoid data, RMM with references to control organoids and treated with references to untreated were performed for differential gene expression analysis. DEGs were identified using a stringent threshold (fold change 2 and FDR corrected $P < 0.05$) and were used to perform GO analysis using the Gene Ontology consortium database (Consortium, 2019). Heatmaps of relative expression (Z-scores) of genes in patient groups and treatments were generated in RStudio (v 1.4.1106).

2.2.10 Single-cell RNA-sequencing

Assembloid harvest, single-cell capture, library preparation

Supernatant from assembloids was removed, washed with PBS before 200 µl of collagenase type IA (0.5 mg/ml) with DNase I (0.1 mg/ml) in additive-free medium was added to each well. Droplets were scrapped off and with the enzyme solution were added to a 1.5 ml tube. Tubes with the droplets/enzyme solution were placed in a water bath for 10 minutes at 37 °C and shaken every 5 minutes. Samples were centrifuged, supernatant removed and replaced with 500 µl 5× TrypLE ™ Select Enzyme diluted in additive-free medium with DNase I (0.1 mg/ml). Tubes were placed in water bath for 10 minutes and then pellets were dissociated further by repeat pipetting (~300×). Samples were centrifuged, washed in PBS, and spun again. Cell pellets were resuspended in 400 µl of 0.1% BSA in PBS per sample. To achieve a single cell suspension, 100 µl of cell buffer was first added to coat 35 µm cell sieve before the sample was added. Cells were counted using haemocytometer and trypan blue was used to account for dead cells in the samples. Samples were diluted or concentrated to 300 000 cells per ml.

Droplet generation was performed using a Nadia Instrument (Dolomite Bio, Cambridge, UK), according to the manufacturer's guidelines, using reagents described by (Macosko et al., 2015) and the scRNA-seq v1.8 protocol (Dolomite Bio). The pooled beads were processed as described previously for assembloids (Rawlings et al., 2021a) and sequenced using a NextSeq 500 with high output 75

cycle cartridge (Illumina, Cambridge, UK) by the Genomics Facility at University of Warwick.

Bioinformatics analysis of assembloid single-cell RNA-sequencing

Assembloid scRNA-seq data processing was performed using Drop-Seq_tools-2.3.0 (DropseqAlignmentCookbook_v2Sept2018, http://mccarrolllab.com/dropseq) and as described previously (Rawlings et al., 2021a). To ensure high-quality data for analysis, cells with at least 200 genes detected and genes that were detected in at least 3 cells were included. To eliminate doublets and poor-quality cells, cells with more than 2000 genes and more than 5% mitochondrial gene transcripts were excluded from the analysis. Seurat v3 standard workflow (Stuart et al., 2019) was used to integrate samples based on the patient of origin. This workflow was also used for label transfer to identify population according to marker curation performed in our previous work (Rawlings et al., 2021a). GO analysis was performed on DEGs ($P < 0.05$, and FDR corrected $P < 0.05$) between control and RMM subpopulations using the GO consortium database (Consortium, 2019). Dot plots of significantly enriched GO terms (FDR corrected $P < 0.05$) and heatmaps of relative expression (Z-scores) of genes in subpopulations were generated in RStudio (v 1.4.1106).

2.2.11 Statistical analysis

Data were analysed using the statistical package GraphPad Prism (version 9). Data were tested for normal distribution, using Shapiro-Wilk test for data with ≤ 50 samples and the Kolmogorov-Smirnov test for experiments with > 50 samples.

The following tests were performed for comparison of two data sets: Welch's *t*-test for unpaired, parametric data; Wilcoxon test for paired, non-parametric data, or Mann-Whitney test for unpaired, non-parametric data.

The following tests were performed for multiple row comparisons of paired data: Multiple paired *t*-test for parametric data or Multiple Wilcoxon test for non-parametric. Whereas the following tests were performed for multiple row comparisons of unpaired data: multiple unpaired *t*-test for parametric data and Multiple Mann Whitney test for non-parametric data.

For paired, non-parametric data significance was tested between several groups using Friedman test and Dunn's multiple comparisons post hoc test. Spearman's rank test was utilised for correlative analysis test of non-parametric data. Only values of $P < 0.05$ were considered statistically significant.

Chapter 3:
Analysis of the Luteal Endometrium in Recurrent Missed Miscarriage

3.1 Introduction

Endometrial glands secrete a rich product, histotoph, comprising of numerous components including ions, carbohydrates (glycogen), amino acids, lipids and proteins (Kelleher et al., 2019), which are phagocytosed by trophoblast cells and transferred to the growing embryo (Burton et al., 2002, Hempstock et al., 2004). Endometrial histotroph sustains pregnancy by nourishing the conceptus until the onset of placental perfusion at the end of the first trimester (Burton et al., 2002).

A common feature of RMM patients is early onset of fetal growth restriction, suggesting a lack of histotrophic nutrition maybe a plausible cause of RMM. Dr Flavio Barros, a former student in the Brosens lab used laser-capture microdissection (LCM) to isolate the glands from mid-luteal endometrial biopsy tissue of RMM patients and control subjects for RNA-sequencing (RNA-seq) (Barros, 2017). This allowed the investigation of transcriptomic differences in the glands from these patients with minimal contamination of other cell types. An aberrant mitochondrial gene signature was revealed in RMM glands prior to conception and was predicted to lead to metabolic stress during early pregnancy (Barros, 2017).

Tight spatiotemporal regulation of endometrial function is critical to synchronise growth, differentiation and remodelling of the endometrium with oocyte maturation, fertilization and embryo implantation (Suhorutshenko et al., 2018, Critchley et al., 2020). Endometrial function requires effective crosstalk between the glands and EnSC. Glands secrete paracrine-acting factors such as peptide hormones, prostanoids, cytokines and growth factors that promote or enhance stromal decidualisation (Kelleher et al., 2019). The endometrium or a compartment thereof, being out-of-phase can lead to reproductive disorders such as implantation failure and miscarriage (Salker et al., 2012, Ruiz-Alonso et al., 2013). The predicted metabolic defect identified in RMM could be a result of an out-of-phase gland differentiation response. This in turn could impact the stromal decidualisation and result in dysregulation of the processes mentioned above, including pregnancy.

In this chapter, I aimed to characterise the luteal endometrium in RMM patients. First, the RNA-seq of control and RMM LCM glands was reanalysed in order to further characterise metabolic differences. To address whether endometrial glands are out-of-phase, temporally regulated genes and a molecular timing model were used to study gland timing in RMM patients. Additionally, the decidual pathway in RMM patients was investigated.

3.2 Results

3.2.1 The transcriptome of mid-luteal endometrial glands in RMM

LCM was used by Dr Flavio Barros, a former student, to isolate endometrial glands in mid-luteal, snap-frozen biopsies from 8 RMM and 8 control subjects (Barros, 2017) (Fig. 3.1). All samples were obtained 7 to 10 days following the pre-ovulatory LH surge (LH+7 to LH+10). Appendix table 1.1 shows the demographic characteristics of 16 samples used in the original RNA-seq experiment. Total RNA was extracted from the isolated glands and subjected to RNA-seq. The initial analysis revealed upregulation of several mitochondrial genes in the RMM glands, suggesting a potential bioenergetic defect (Barros, 2017). This finding was broadly in keeping with the original hypothesis that endometrial glands in RMM are subjected to metabolic stress in early gestation, leading to gradual failure in histotrophic nutrition. With support of Dr Tauqeer Alam, a bioinformatician, I re-analysed the RNA-seq data with a view to gain more in-depth insights into the metabolic changes in endometrial glands from the RMM patients (Fig. 3.1).

First, principal component analysis (PCA) was performed. No separation of the control and patient groups was observed in PC1 or PC2 (Fig. 3.2a). However, the gland transcriptome of control subjects and RMM patients separated, albeit imperfectly, by PC4 and PC5, accounting for 8% and 6% of variance in gene expression, respectively (Fig. 3.2b). These observations suggest relative discrete differences in like-for-like gene expression between the case and control groups.

A heatmap of the differentially expressed genes (DEGs) was generated (Fig. 3.3). Based on $P < 0.01$, 373 genes were upregulated in RMM glands, and 145 genes were downregulated when compared to controls. Following multiple testing correction, only 31 genes were upregulated in RMM patients and 3 were downregulated (FDR-corrected P value < 0.05). RMM glands were characterised by upregulation of genes involved in the electron transport chain, including genes that encode for subunits of complex IV (*COX5B* and *COX8A*) (Elurbe and Huynen, 2016, Rotko et al., 2021), a component of a regulator of complex IV assembly (*SURF1*) (Pecina et al., 2004), subunits of complex I *(NDUFA1* and *NDUFS5*) (Scheffler and Yadava, 2001, Elurbe and Huynen, 2016), and a component of complex III (*UQCR11*) (Guo et al., 2018). In addition, two mitochondrial ribosomal (*MRPL41* and *43*) (Sylvester et al., 2004) and protein (*GLRX5*) genes were also upregulated (Banci et al., 2014).

Genes upregulated in RMM glands were subjected to gene ontology (GO) analysis using the Gene Ontology Consortium database (Consortium, 2019). Notably, GO analysis of both the larger (n= 373) and the more stringent (n=31) gene sets identified oxidative phosphorylation and associated processes, such as 'ATP metabolic processes', 'energy derivation by oxidation of organic compounds,' and 'generation of precursor metabolites,' as enriched in RMM glands (Fig. 3.4a and 3.5). Using the larger gene set, several additional processes were identified including 'Cellular component biogenesis,' 'Organelle organisation' and 'Monosaccharide metabolic process.' For completion, the 145 genes downregulated in RMM glands ($P < 0.01$) were also subjected to GO analysis (Fig. 3.4b). Only 3 GO categories related to extracellular processes were downregulated in RMM patients.

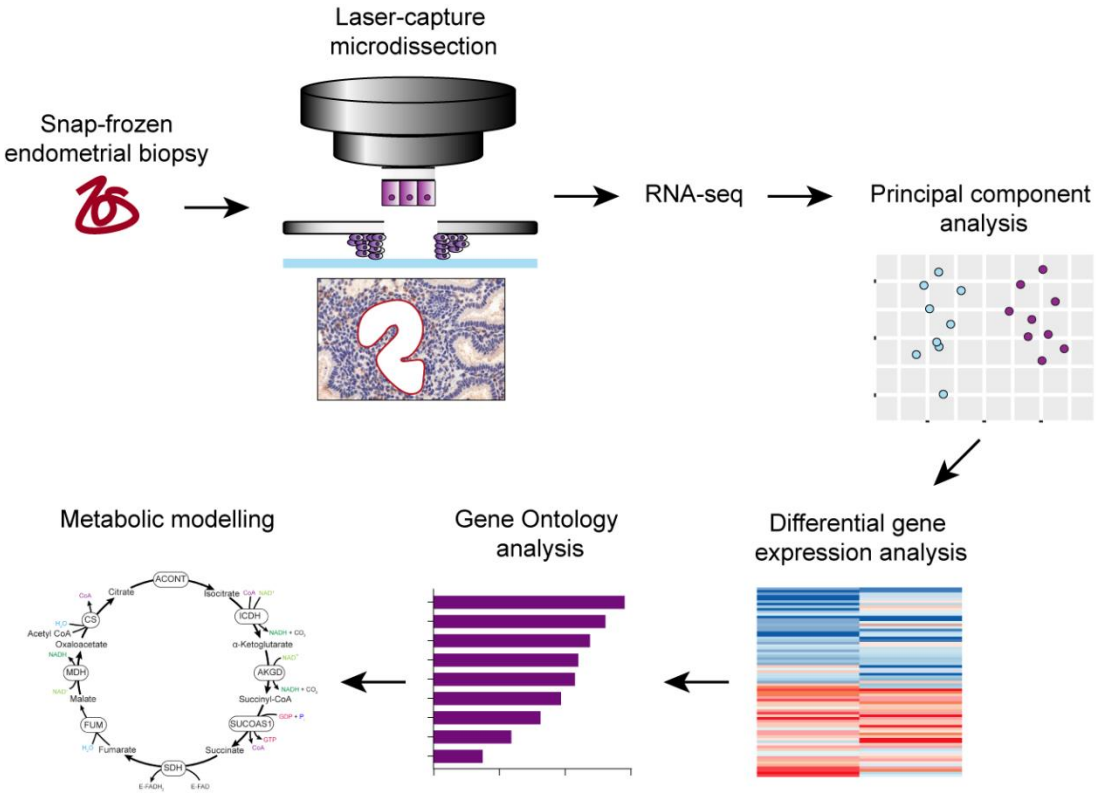

Figure 3.1. ***LCM glands RNA-seq and analyses workflow.***

Schematic representation of LCM of endometrial glands for RNA-seq and analyses workflow. Snap-frozen endometrial biopsies were sectioned with a cryostat and mounted on polyethylene naphthalate membrane slides. The sections were stained with cresyl-violet and eosin-Y and overlaid with glass slides. Glands of interest were identified microscopically and dissected with a UV laser (red line represents laser trace around gland), using a LCM unit. Isolated glands were retrieved using diffuser caps and stored in lysis solution before RNA extraction and sequencing. The following analyses was undertaken of the RNA-seq data: PCA, differential gene expression analysis, GO analysis and metabolic modelling using FVA and FBA.

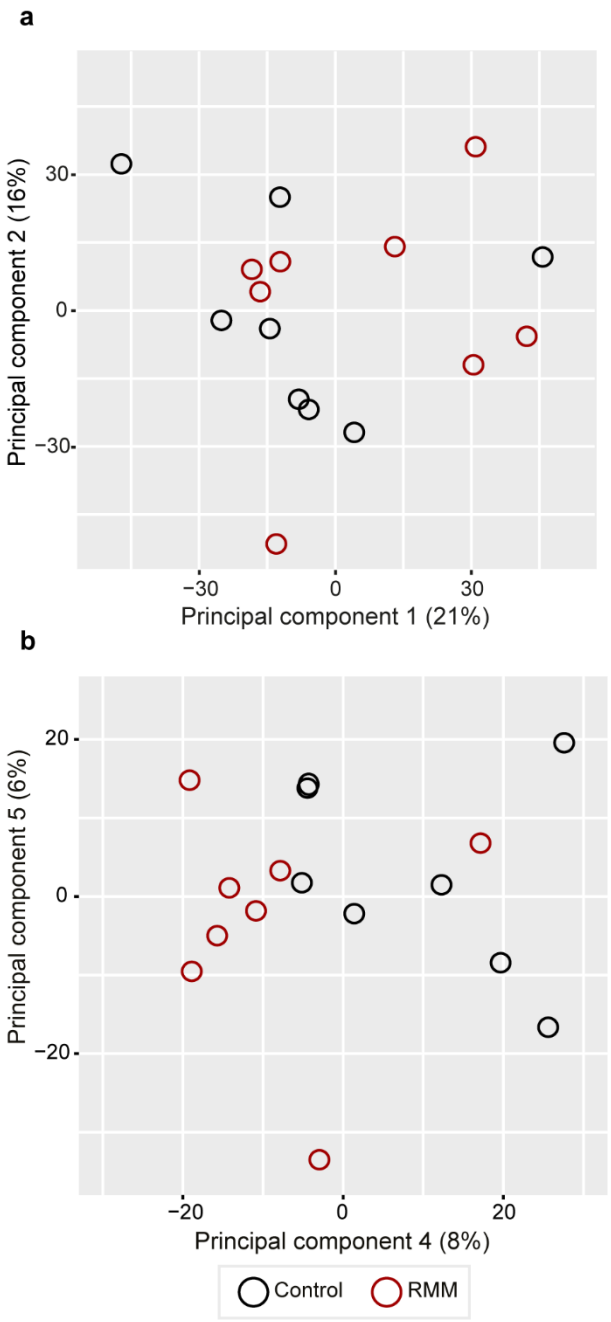

Figure 3.2. ***Control and RMM endometrial glands group based on similar gene expressions*****.**

PCAs of RNA-seq data from laser-captured endometrial glands from mid-luteal control (black) and RMM (red) endometrial biopsies (n=8 per group).

a) Grouping shown based on PC1 and PC2.

b) Grouping shown based on PC4 and PC5.

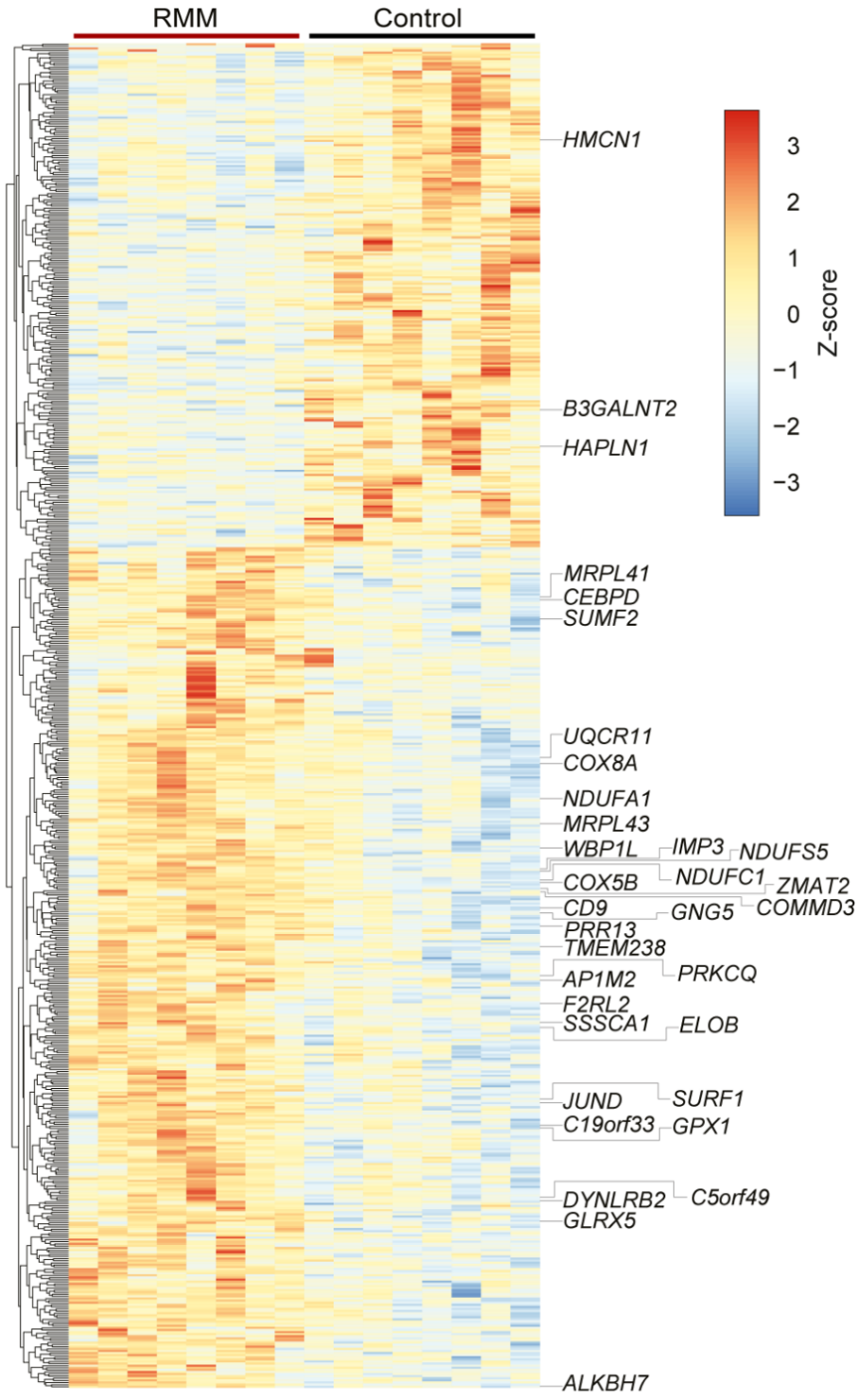

Figure 3.3. ***Heatmap of DEGs between control and RMM endometrial glands.*** Heatmap of RNA-seq data showing regularised-logarithm transformed expression (Z-scores) of DEGs between control and RMM endometrial glands ($P < 0.01$). Highlighted genes remained significantly differentially expressed following FDR correction (Benjamini-Hochberg, FDR-corrected $P < 0.05$).

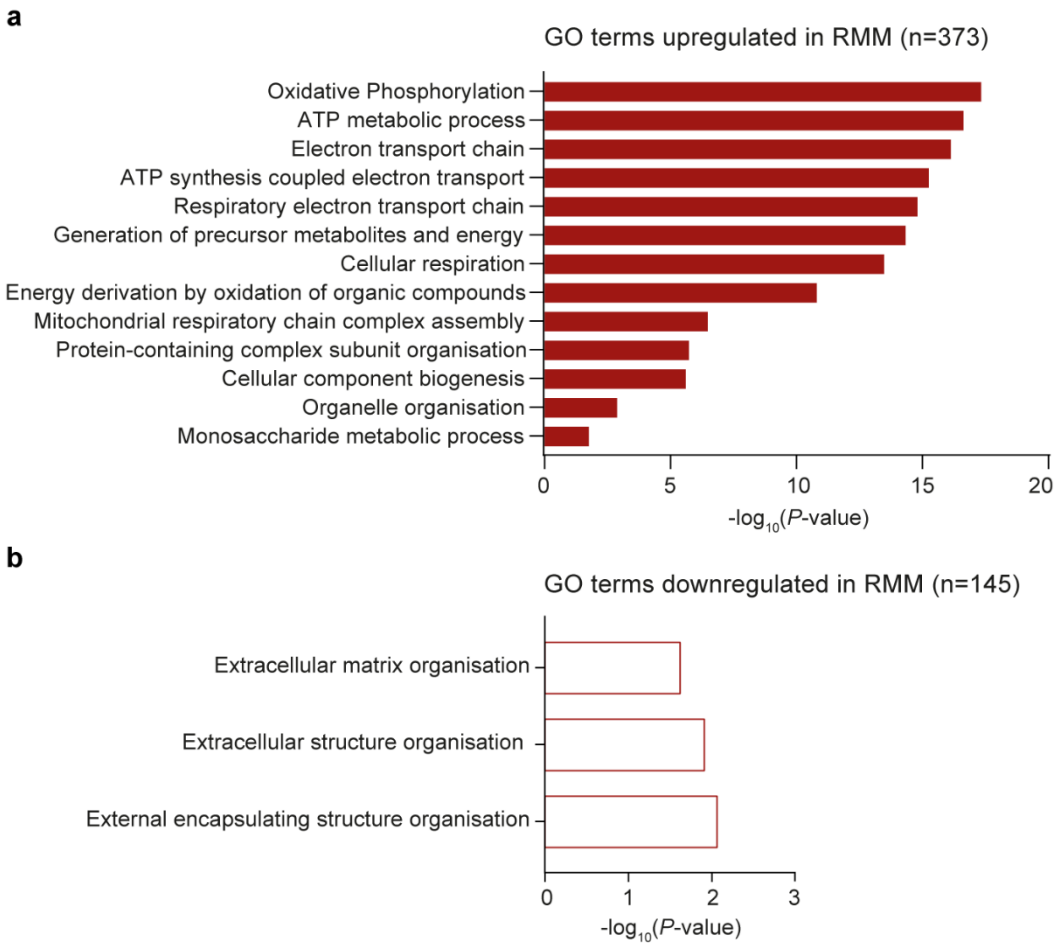

Figure 3.4. ***GO analysis of DEGs upregulated and downregulated in RMM glands.***

Bar plots showing significantly enriched GO terms (FDR-corrected $P < 0.05$) related to biological processes in RMM glands. DEGs with $P < 0.01$ were used as input for the analysis (number of genes in brackets).

a) GO terms upregulated in RMM compared to controls.

b) GO terms downregulated in RMM compared to controls.

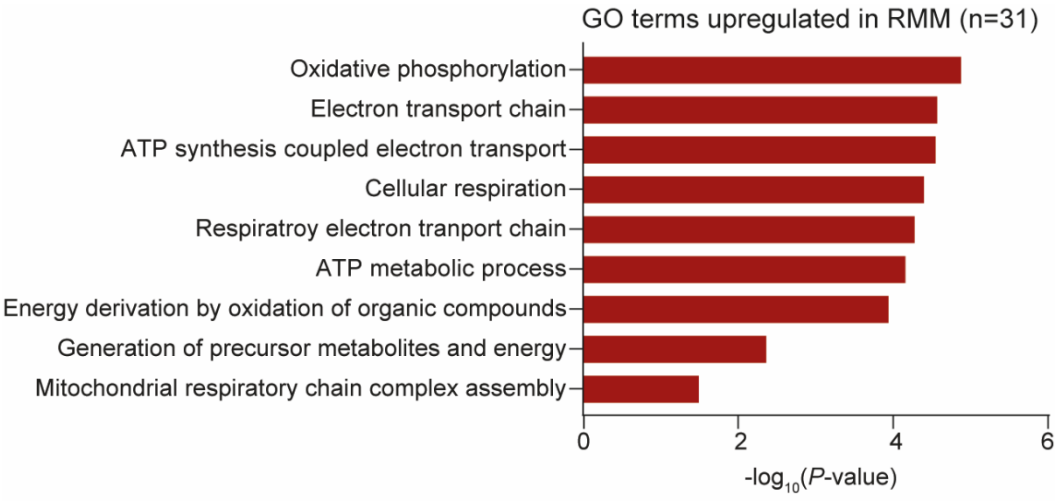

Figure 3.5. ***Oxidative phosphorylation and related processes upregulated in RMM glands.***

Significant GO terms (FDR-corrected $P < 0.05$) related to biological processes upregulated in RMM glands compared to controls. DEGs (n=31) with FDR-corrected $P < 0.05$ were used as input for the analysis.

3.2.2 Computationally efficient flux variability and flux balance analysis

In-depth metabolic modelling was undertaken to evaluate the flux of enzymatic reactions in metabolic pathways of interest. Metabolic flux denotes rate of turnover of molecules in a given enzymatic reaction. Flux variability analysis (FVA) is a computational tool for assessing the minimum and maximum of each reaction flux (Gudmundsson and Thiele, 2010). FVA is used alongside flux balance analysis (FBA) to predict the optimal flow of metabolites through the metabolic network (Orth et al., 2010). The constraints calculated by FVA highlight reactions with more importance under the biological objective, in this case maximum growth to predict the flux range.

Human metabolic reconstruction (recon3D) was used to examine the metabolic differences in RMM patients compared to controls subjects (Brunk et al., 2018). FVA was used to predict the optimal flux for control and RMM glands (Fig. 3.6). Briefly, the average expression values for genes encoding relevant enzymes in RMM and control glands were mapped to the human metabolic network. A ratio of RMM vs control gene expression was calculated for each reaction. For FVA, the predicted flux range was modelled for control glands and the reaction flux range for RMM glands was then calculated by multiplying the control ranges with the expression ratio. These ranges were then set as constraints. To predict the reaction flux in both groups, FBA was performed.

Five pathways were explored: the tricarboxylic acid (TCA) cycle, oxidative phosphorylation, glycolysis, fatty acid oxidation (FAO) and the pentose phosphate pathway (PPP). The results of these analyses are depicted in Figures 3.7-3.10. The width of the arrows in the figures correspond to flux values in control glands whereas the reaction flux changes (%) in RMM glands are highlighted by the colour of the arrows.

As oxidative phosphorylation was found to be upregulated in RMM glands, I began my analysis by modelling the TCA cycle. The TCA cycle releases stored energy through the oxidation of acetyl coenzyme A (acetyl-CoA) derived from carbohydrates, fats, and proteins (Akram, 2014). Starting with citrate synthase (CS), which catalyses the synthesis of citrate from oxaloacetate and acetyl-CoA, the reaction fluxes in control glands become progressively larger as the TCA cycle unfolds and continue to increase through oxidative phosphorylation (Fig. 3.7 and Appendix Table 2.1). As anticipated, the majority of the reaction fluxes were upregulated in RMM glands with predicted flux changes ranging between 1.2 to 100% (Fig 3.7). Only isocitrate

dehydrogenase (ICDx) had a flux of zero in control glands, giving rise to a flux change of 100% in RMM glands (grey arrow in Fig 3.7).

Next, I focussed on the glycolysis pathway, which amongst other functions, produces acetyl-CoA for the TCA cycle under aerobic settings. FVA was used to investigate flux changes in glycolysis reactions in RMM compared to controls glands (Fig. 3.8 and Appendix Table 2.2). There are two phases in glycolysis: the preparatory phase and the payoff phase (Ganapathy-Kanniappan and Geschwind, 2013). The preparatory phase reactions were upregulated in RMM with flux changes between 0-15.8%. However, the payoff phase reactions were downregulated with a decrease in flux ranging from 0.5-19%. Most prominent was the downregulation of the reaction that produces pyruvate, which results in reduced acetyl-CoA production. (Fig 3.8) Under hypoxic or stress conditions, pyruvate is broken down for anaerobic respiration by lactate dehydrogenase (Bolaños et al., 2010). The reaction flux for anaerobic respiration was also reduced in RMM.

FAO is the breakdown of fatty acids in the mitochondria to generate acetyl-CoA, which enter the TCA cycle, thus producing more NADH (reduced form of nicotinamide adenine dinucleotide) and $FADH_2$ (reduced form of flavin adenine dinucleotide) for oxidative phosphorylation (Houten et al., 2016). Therefore, this pathway may be the cause of the upregulation in oxidative phosphorylation. The modelling was limited to the transport and breakdown of three fatty acids (Fig. 3.9 and Appendix Table 2.3). The FVA revealed palmitoyl transfer through inner mitochondrial membrane and complete breakdown into eight acetyl-CoA molecules was downregulated in RMM (0.22% and 100% flux change, respectively) (Fig. 3.9a). However, the breakdown of palmitoyl to octanoyl, as well as the complete breakdown of octanoyl, (a short chain fatty acid that does not require a transfer) were both upregulated in RMM (100% and 53.7% flux change, respectively) (Fig. 3.9a). Additionally, the transfer of cervonyl and its breakdown into timnodnyl and acetyl-CoA reaction flux was increased in RMM (197% and 197% flux change, respectively) (Fig. 3.9b).

The PPP branches from the preparatory phase of glycolysis to produce nicotinamide adenine dinucleotide phosphate (NADPH - reduced form), which is crucial for fatty acid synthesis, scavenging of reactive oxygen species (ROS) and ribonucleotides production (Patra and Hay, 2014). Hence, the efficacy of histotrophic nutrition may rely on this pathway. In mid-luteal RMM glands, FVA revealed modest downregulation of all reaction fluxes (1.8-7.8% flux change) (Fig. 3.10 and Appendix Table 2.4). No flux change data were obtained for transaldolase (TAD), which catalyses

glyceraldehyde 3-phosphate and sedoheptulose 7-phosphate into fructose 6-phosphate and erythrose 4-phosphate.

In summary, FVA indicated that the metabolic perturbations in RMM glands may be more pronounced than inferred by standard RNA-seq analysis. Specifically, increased flux through the TCA cycle and heightened oxidative phosphorylation was associated with decreased flux through the PPP and payoff phase of the glycolysis pathway. Moreover, upregulation of oxidative phosphorylation may be a consequence of increased FAO.

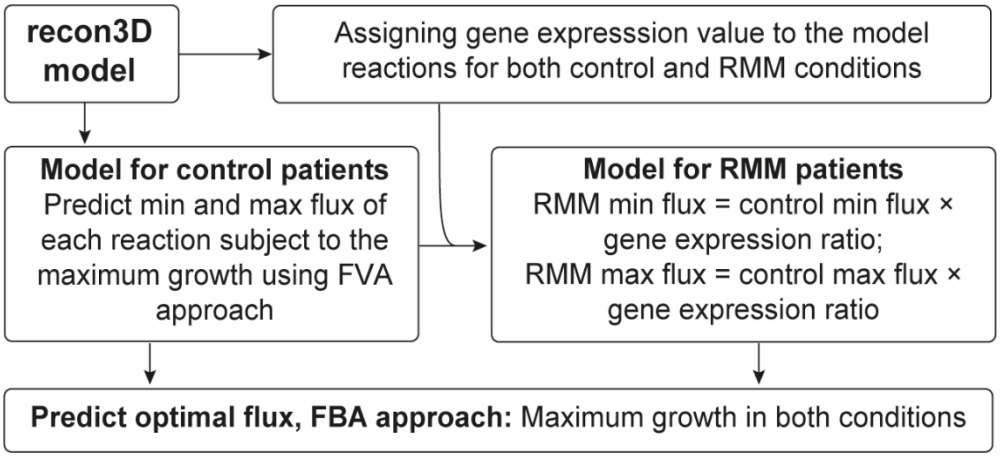

Figure 3.6. ***Metabolic modelling of control and RMM glands.***

Schematic for metabolic modelling to predict optimal flux for control and RMM groups using the RNA-seq data. The human metabolic reconstruction (recon3D) was used to examine the metabolic differences (Brunk et al., 2018). Average gene expression value from RMM and control glands were mapped to the human metabolic network to assign expression value to reactions. The expression ratio of genes encoding relevant enzymes in RMM vs control glands was calculated for each reaction. Next, FVA was undertaken, and the predicted flux range was modelled for the control glands. For the modelling of the RMM group, the minimum (min) and maximum (max) flux of each reaction of the control conditions were multiplied with the expression ratio. Finally, these ranges were set as constraints and to predict the reaction flux in both groups, FBA was performed under maximum growth.

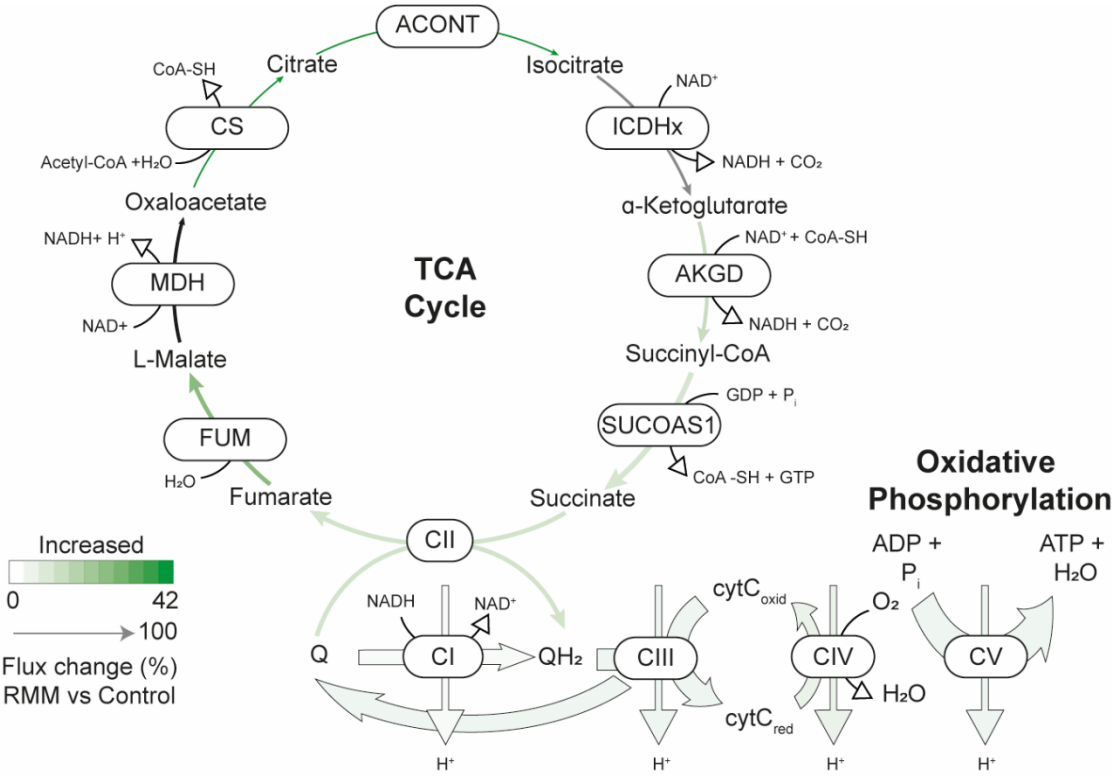

Figure 3.7. ***Upregulation of metabolic flux in TCA cycle and oxidative phosphorylation pathways in RMM glands compared to control.***

Diagram showing changes in the predicted metabolic flux of the TCA cycle and oxidative phosphorylation pathway in RMM compared to controls glands based on modelling LCM RNA-seq data. The width of the reaction (line width) indicates the flux value in the control samples and the colour represent flux change (%) in RMM. Green shades represent an increase in flux change in RMM glands. The grey arrow represents a flux change of 100, indicating a flux of 0 in control. No data for malate dehydrogenase (MDH) forward reaction was produced (black arrow) but the reverse reaction was downregulated. ACONT – aconitase, ICDHx – isocitrate dehydrogenase, AKGD – α-ketoglutarate dehydrogenase, SUCOAS1 – succinyl CoA synthetase, SDH – succinate dehydrogenase, FUM – fumarase, CS – citrate synthase, CI – complex I, CII – complex II, CIII - complex III, CIV – complex IV, CV – complex V, CoA-SH – coenzyme A, H_2O – water, NAD^+/NADH - nicotinamide adenine dinucleotide oxidised/reduced, CO_2 – carbon dioxide, GDP – guanosine diphosphate, GTP - guanosine triphosphate, P_i – phosphate, Q – ubiquinone, QH_2 – ubiquinol, $cytC_{oxid}$ – cytochrome c (oxidised), $cyctC_{red}$ – cytochrome (reduced), H^+ - hydrogen ion, ATP – adenosine triphosphate, ADP – adenosine diphosphate.

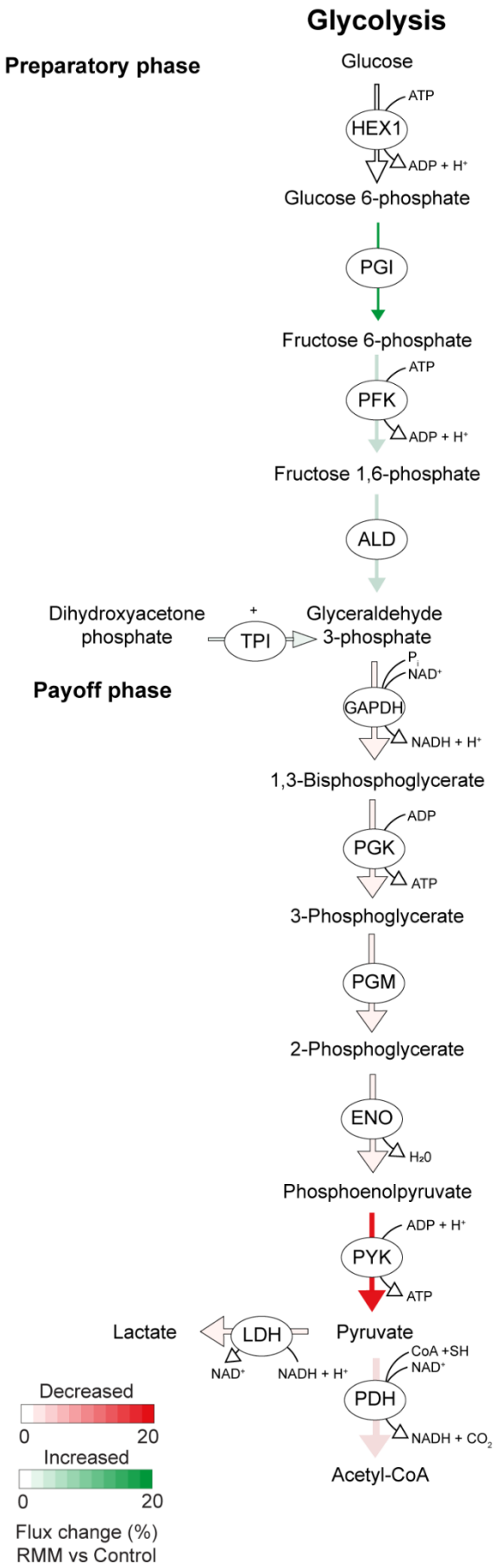
Glycolysis
Preparatory phase
Glucose
ATP
HEX1
ADP + H+
Glucose 6-phosphate
PGI
Fructose 6-phosphate
ATP
PFK
ADP + H+
Fructose 1,6-phosphate
ALD
Dihydroxyacetone phosphate
TPI
Glyceraldehyde 3-phosphate
Payoff phase
Pi
NAD+
GAPDH
NADH + H+
1,3-Bisphosphoglycerate
ADP
PGK
ATP
3-Phosphoglycerate
PGM
2-Phosphoglycerate
ENO
H20
Phosphoenolpyruvate
ADP + H+
PYK
ATP
Lactate
LDH
Pyruvate
NAD+
NADH + H+
CoA +SH
NAD+
PDH
NADH + CO2
Acetyl-CoA
Decreased
0
20
Increased
0
20
Flux change (%)
RMM vs Control

Figure 3.8. ***Glycolysis metabolic flux in RMM glands compared to controls.***
Diagram showing changes in the predicted metabolic flux in glycolysis in RMM glands compared to controls using LCM RNA-Seq data. The width of the reaction (line width) indicates the flux value in the control and colour represents the flux change (%) in RMM. Green shades represent an increase in flux change in RMM glands and red shades represent a decrease in flux change. HEX1 – hexokinase, PGI – phosphohexose isomerase, PFK – phospho-fructokinase-1, ALD – aldolase, TPI – triose phosphate isomerase, GAPD – glyceraldehyde 3-phosphate dehydrogenase, PGK – phosphoglycerate kinase, PGM – phosphoglycerate mutase, ENO – enolase, PYK – pyruvate kinase, PDH – pyruvate dehydrogenase, LDH – lactate dehydrogenase, ATP – adenosine triphosphate, ADP – adenosine diphosphate, H^+ - hydrogen ion, NAD^+/NADH - nicotinamide adenine dinucleotide oxidised/reduced, P_i – phosphate, H_2O – water, CoA-SH – coenzyme A, CO_2 – carbon dioxide.

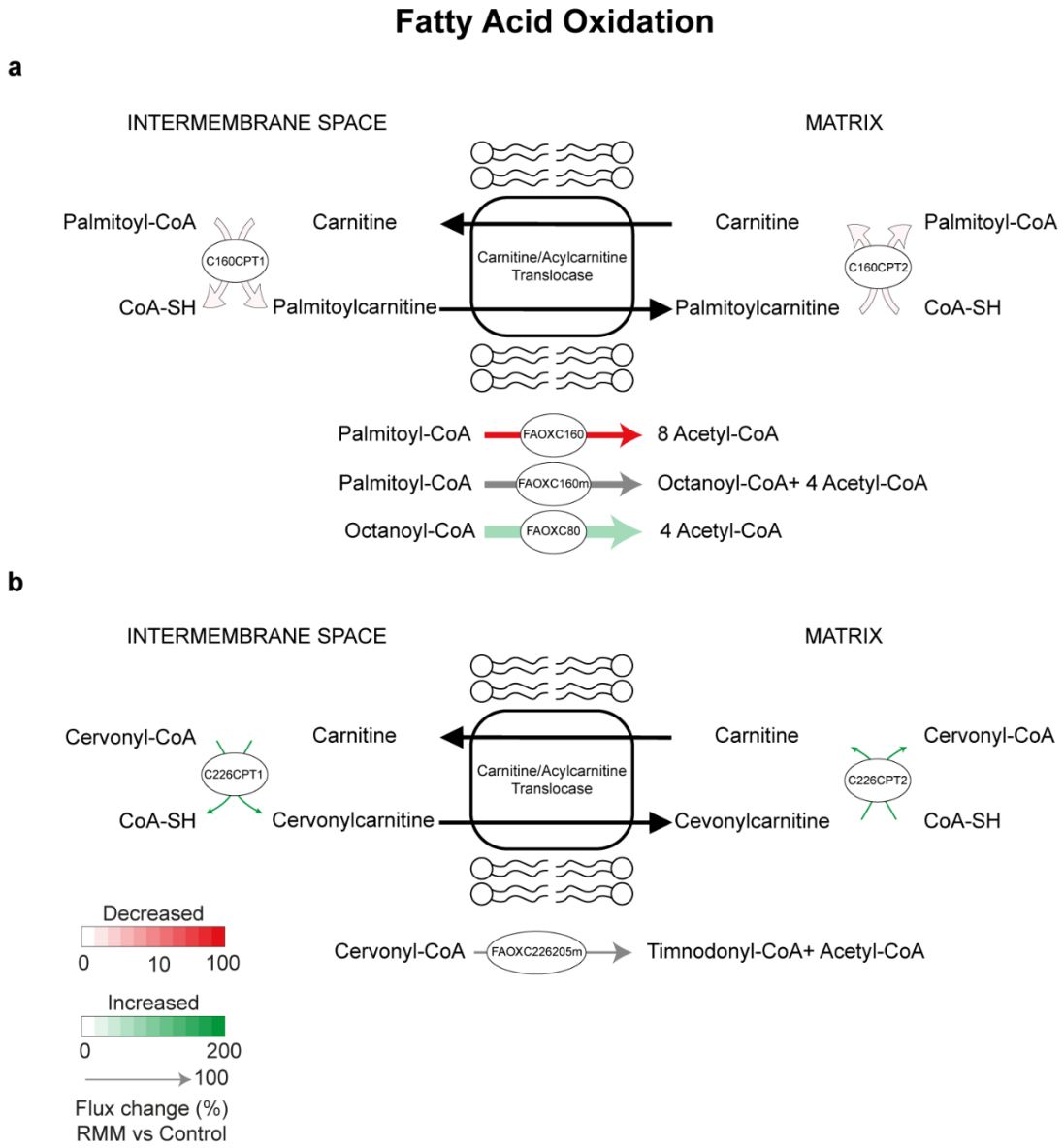

Figure 3.9. ***FAO metabolic flux in RMM glands compared to controls.***

Schematic of predicted metabolic flux of FAO of three fatty acids in RMM and control glands using FVA and FBA of LCM RNA-Seq data. The width of the reaction (line width) indicates the flux value in the control samples and the colour represent flux change (%) in RMM. Green shades represent an increase in flux change in RMM glands and red shades represent a decrease in flux change. The grey arrow represents a flux change of a 100, indicating a flux of 0 in control. C160CPT1 - Carnitine O-palmitoyltransferase, C160CPT2 - C160 transport into the mitochondria, C226CPT1 - Carnitine C22:6 transferase, C226CPT2 - C226 transport into the mitochondria, FAOXCx - Fatty acid oxidation (carbon chain), CoA-SH – coenzyme A.

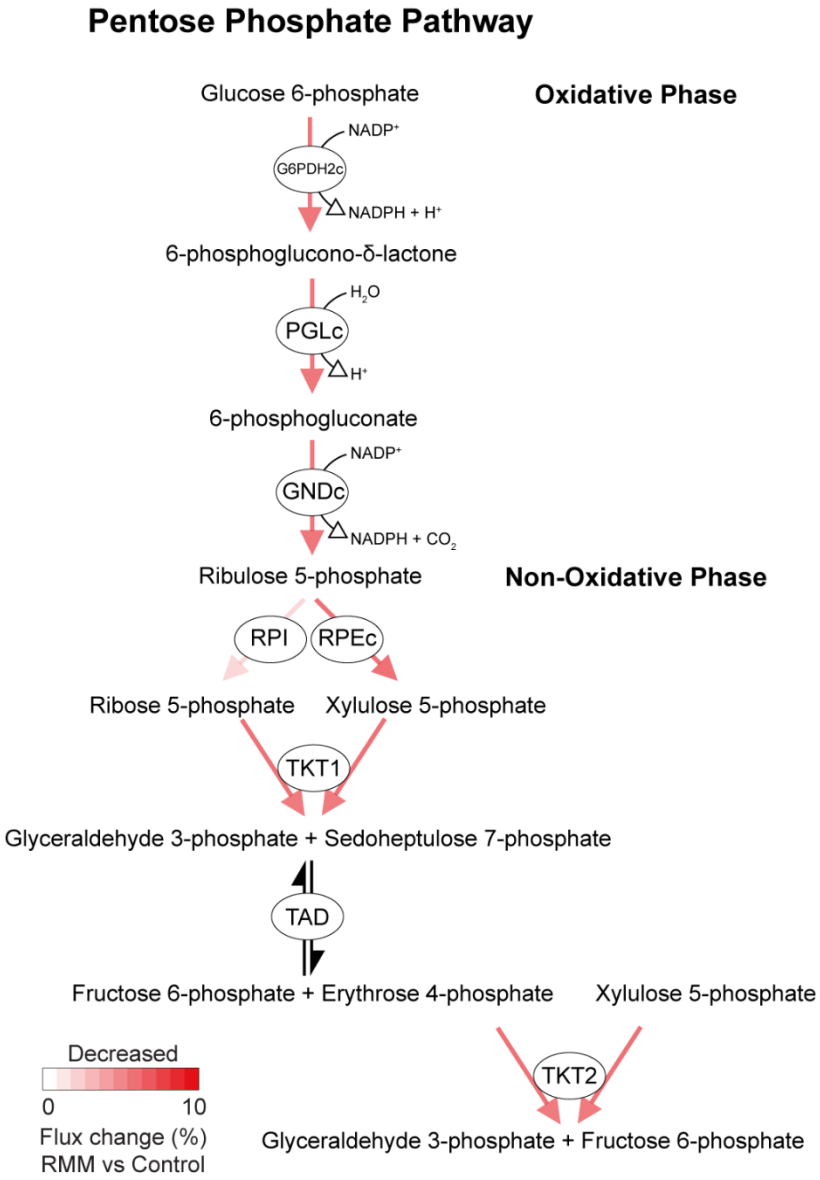

Figure 3.10. ***Downregulation of metabolic flux in the PPP in RMM glands compared to controls.***

Schematic of PPP showing decrease in the predicted metabolic flux in RMM glands compared to controls using FVA and FBA of LCM RNA-Seq data. The width of the reaction (line width) indicates the flux value in the control and colour represents the flux change (%) in RMM. Red shades represent a decrease in flux change. No data for transaldolase (TAD) reaction (black arrow). G6PDH2 – glucose 6-phosphate dehydrogenase, PGL – 6-phosphogluconolactonase, GND – 6-phosphogluconate dehydrogenase, RPI – ribose 5-phosphate isomerase, RPE – ribulose 5-phosphate 3 – epimerase, TKT- transketolase, $NADP^+$/NADPH - Nicotinamide adenine dinucleotide phosphate oxidised/reduced, H^+ - hydrogen ion, H_2O – water, CO_2 – carbon dioxide.

3.2.3 Timing of RMM glands

The endometrium is a highly dynamic tissue, characterised by coordinated changes in gene expression that vary from day to day (Ruiz-Alonso et al., 2012). Although all endometrial biopsies from control and RMM patients were timed relative to the LH surge as measured by home ovulation kits, it is possible that mistiming of the biopsy accounts for the differences in glandular gene expression between the control and case group. Mistiming may reflect variation in accuracy of commercially available home ovulation kits, user error, variation in the time between the LH surge and ovulation and altered kinetics of progesterone production by the corpus luteum (Brosens et al., 1978). Alternatively, the responsiveness of the endometrial glands to steroid hormone signalling and local cues may be altered in RMM resulting in a differentiation response that either lags behind or is accelerated when compared to control tissues.

To investigate if glandular defects in RMM are due to an out-of-phase response, I took two complementary approaches. First, I analysed the transcriptome of LCM endometrial glands obtained in the early-, mid-, and late-luteal phase and examined the temporal regulation of genes differentially regulated between control and RMM patients. Second, in section 3.2.4, I developed a simple glandular timing model that enables rapid assessment of a much larger cohort of samples.

The bioinformatic approach started with re-analysis of 9 RNA-seq libraries, representing the transcriptomes of LCM endometrial glands obtained on LH+5 (n=3), LH+8 (n=3), and LH+11 (n=3); representing early-, mid-, and late-luteal endometrium, respectively. Appendix Table 1.2 shows the demographic details. The data were deposited in Gene Expression Omnibus (GEO), accession number GSE84169. The early- and mid-luteal glands grouped together on PC 1 and PC 2, accounting for 38% and 21% variance, respectively (Fig. 3.11). Late luteal samples (LH+11) were more variable with one biopsy being a suspected outlier. Transition of endometrial glands from early- to mid-luteal phase, i.e., coinciding with the putative window of implantation, was associated with a marked transcriptional response, characterised by induction and repression of 1141 and 879 genes, respectively (FDR-corrected $P < 0.05$). Subsequent progression from mid- to late-luteal phase involved up- and downregulation of 209 and 163 genes, respectively. Taken together, a total of 2392 temporally expressed genes were identified in endometrial glands across the luteal phase of the cycle.

The Venn diagrams in Figure 3.12 show the intersection between temporally regulated genes and genes that are differentially expressed between control subjects and RMM patients. Out of the core set of 34 DEGs (FDR-corrected $P < 0.05$) associated with RMM, only 4 (*C19orf33*, *GPX1*, *CEBPD*, *PRKCQ*) exhibited a temporal expression profile (Fig 3.12a and 13). Out of the less stringent set of 518 putative DEGs ($P < 0.01$), 34 were temporally regulated genes (Fig 3.12a). Thus, this analysis indicates that the RMM-associated gene signature cannot be explained by out-of-phase endometrial glands or mistiming of endometrial biopsies

Temporally regulated glandular genes were subjected to GO analysis. As expected, upregulated genes upon transition from early- to mid-luteal phase were highly enriched GO categories such as 'Secretion by cell' (FDR-corrected $P < 0.0001$) and 'ECM organisation' (FDR-corrected $P < 0.001$) (Fig. 3.14a). Other enriched categories indicated that acquisition of a receptive glandular phenotype involves an acute inflammatory response (e.g., 'Regulation of response to stress' and 'Acute inflammatory response'). Conversely, acquisition of a secretory phenotype during the mid-luteal phase coincided with down-regulation of cell cycle genes (Fig. 3.14b). Enrichment of GO terms related to cellular stress responses was even more pronounced upon comparison of genes upregulated in the late-luteal phase compared to the early-luteal phase (Fig. 3.14c).

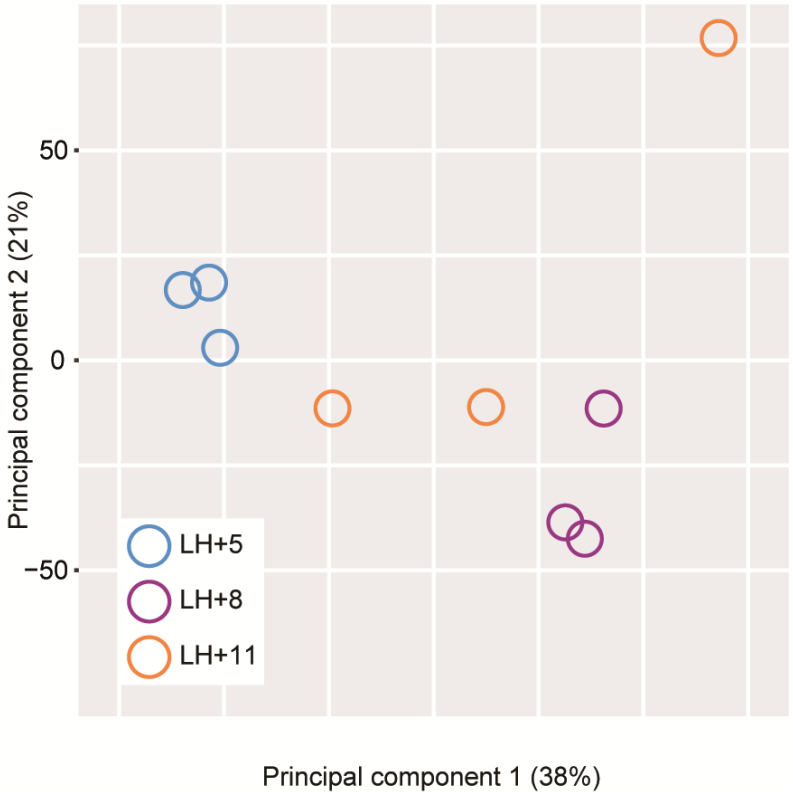

Figure 3.11. ***PCA of LCM endometrial glands across the luteal phase.***
PCA of RNA-seq data from LCM endometrial glands from early- (LH+5, blue), mid- (LH+8, purple) and late-luteal phase (LH+11, orange) of the menstrual cycle (n=3 per timepoint). Grouping shown are based on PC1 and PC2.

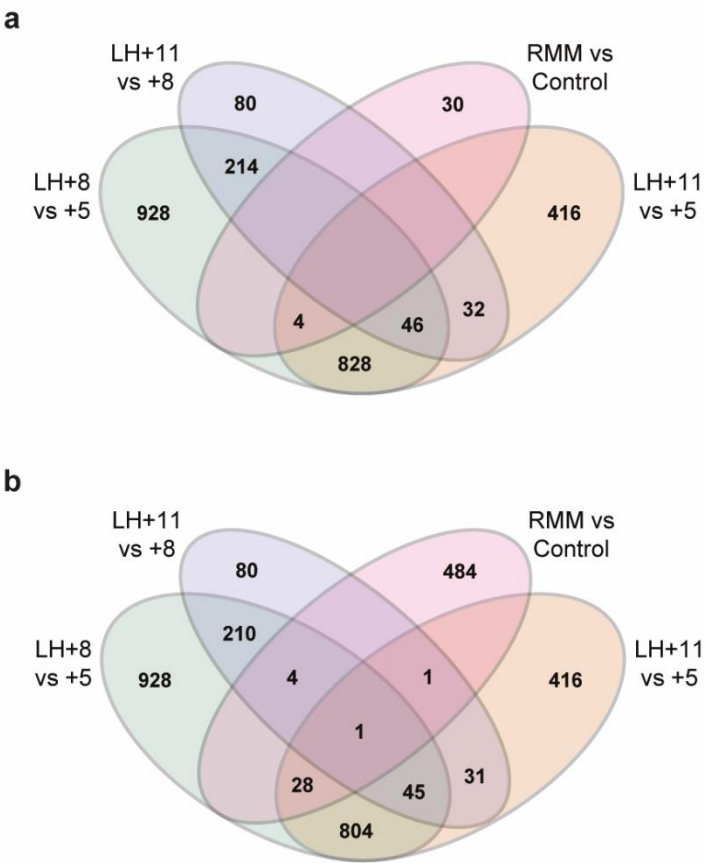

Figure 3.12. ***Venn diagrams depicting intersections of DEGs in endometrial glands across the luteal phase and between control subjects and RMM patients.***
a) Venn diagram depicting intersection of 34 core RMM genes (FDR-corrected $P < 0.05$) and temporally regulated glandular genes across the luteal phase. Only 4 out of 34 (12%) RMM genes were temporally regulated.
b) Venn diagram depicting intersection of 518 RMM genes ($P < 0.01$) and temporally regulated glandular genes across the luteal phase. Only 34 out 518 (6.6%) RMM genes were also temporally regulated.

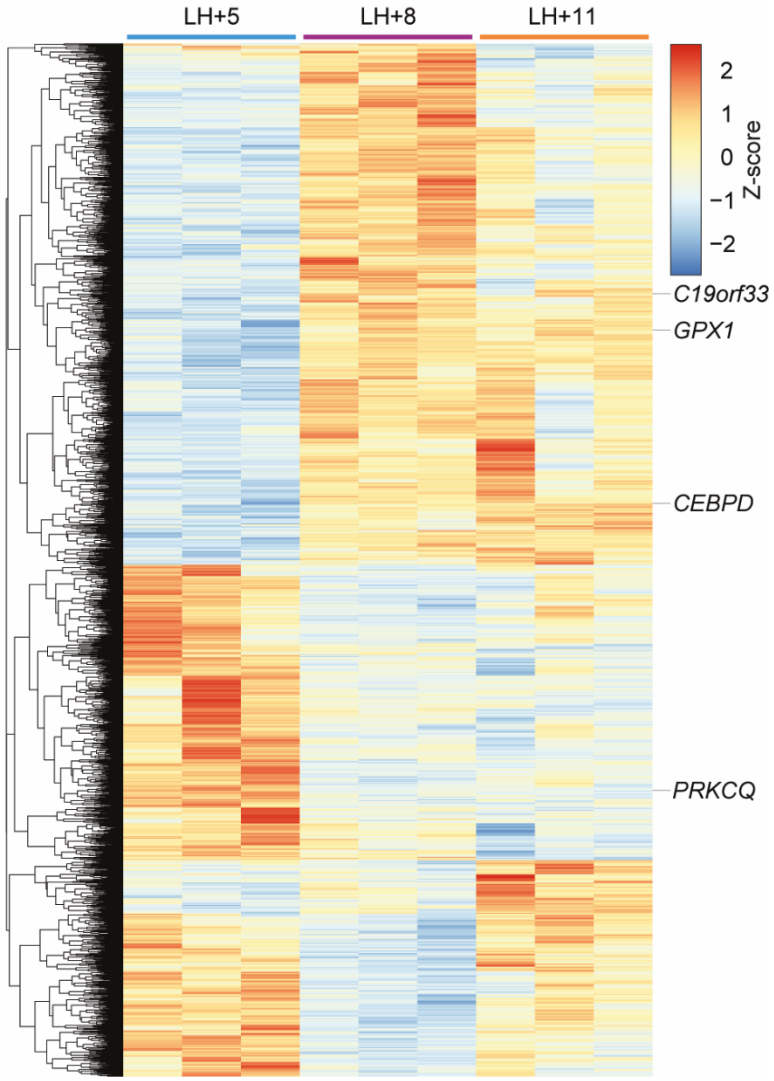

Figure 3.13. ***Heatmap depicting temporally regulated glandular genes across the luteal phase.***

Heatmap showing regularised-logarithm transformed expression (Z-scores) of RNA-seq data for DEGs either between LH+5 vs +8, LH+5 vs +11, or LH+8 vs +11 (FDR-corrected $P < 0.05$). Genes highlighted were also differentially expressed between control and RMM glands.

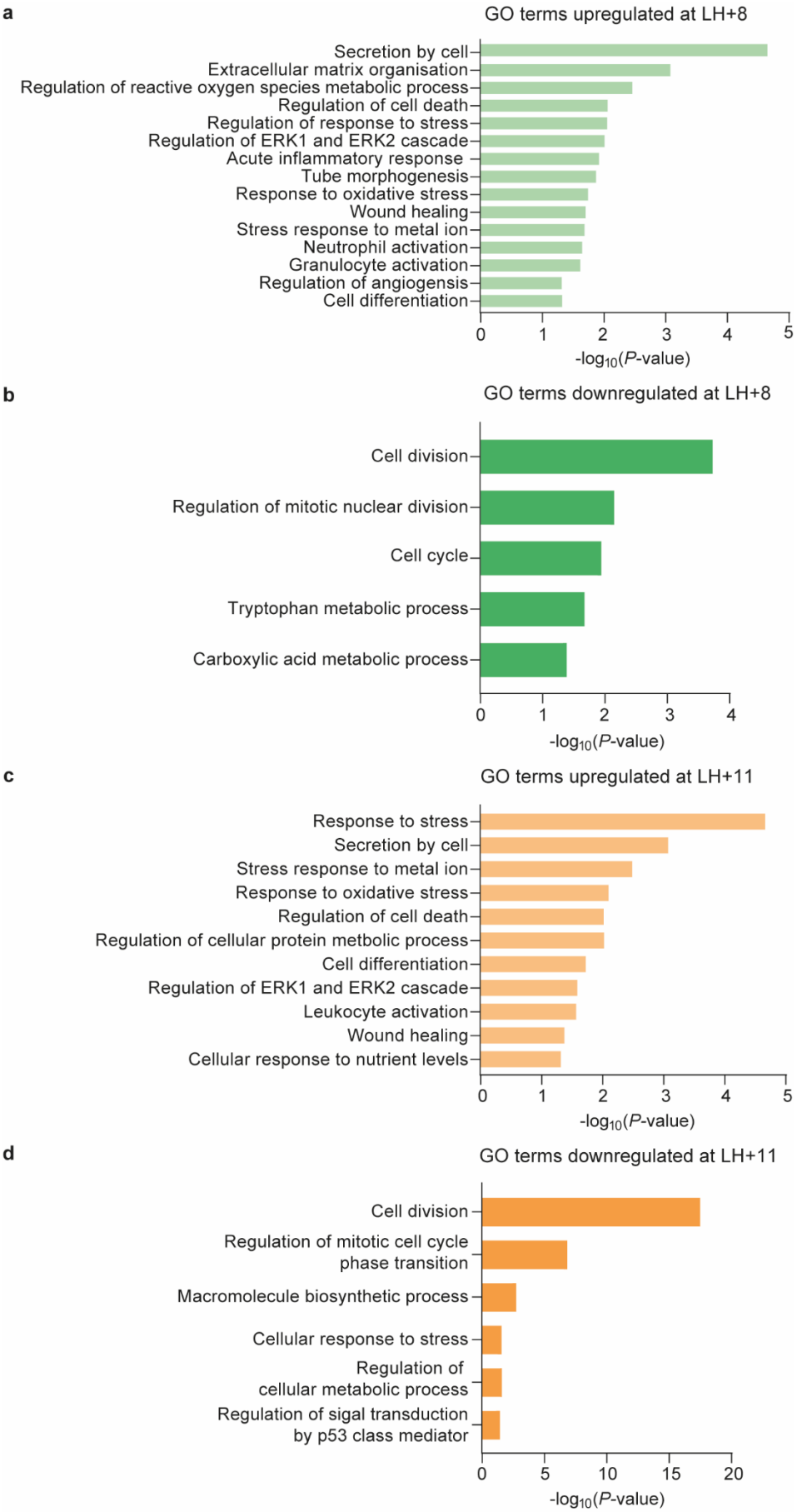
a
GO terms upregulated at LH+8
Secretion by cell
Extracellular matrix organisation
Regulation of reactive oxygen species metabolic process
Regulation of cell death
Regulation of response to stress
Regulation of ERK1 and ERK2 cascade
Acute inflammatory response
Tube morphogenesis
Response to oxidative stress
Wound healing
Stress response to metal ion
Neutrophil activation
Granulocyte activation
Regulation of angiogensis
Cell differentiation
0 1 2 3 4 5
-log10(P-value)
b
GO terms downregulated at LH+8
Cell division
Regulation of mitotic nuclear division
Cell cycle
Tryptophan metabolic process
Carboxylic acid metabolic process
0 1 2 3 4
-log10(P-value)
c
GO terms upregulated at LH+11
Response to stress
Secretion by cell
Stress response to metal ion
Response to oxidative stress
Regulation of cell death
Regulation of cellular protein metbolic process
Cell differentiation
Regulation of ERK1 and ERK2 cascade
Leukocyte activation
Wound healing
Cellular response to nutrient levels
0 1 2 3 4 5
-log10(P-value)
d
GO terms downregulated at LH+11
Cell division
Regulation of mitotic cell cycle phase transition
Macromolecule biosynthetic process
Cellular response to stress
Regulation of cellular metabolic process
Regulation of sigal transduction by p53 class mediator
0 5 10 15 20
-log10(P-value)

Figure 3.14. ***GO analysis of temporally regulated glandular genes.***

Bar plots showing significantly enriched GO terms (FDR-corrected $P < 0.05$) related to biological processes across the luteal phase. DEGs with FDR-corrected $P < 0.05$ were used as input for the analysis.

a) GO terms upregulated on LH+8 compared to LH+5.

b) GO terms downregulated on LH+8 compared to LH+5.

a) GO terms upregulated on LH+11 compared to LH+5.

a) GO terms downregulated on LH+11 compared to LH+5.

3.2.4 Molecular timing model

Many endometrial timing models have been created to distinguish receptive from non-receptive endometrium, especially in the context of assisted reproductive technology to optimise embryo transfer [e.g. Endometrial Receptivity Analysis (ERA) (Ruiz-Alonso et al., 2013), ERPeak^{SM} (CooperSurgical)]. However, most - if not all - models do not use cell-specific marker genes nor account for variability in cellular composition between tissue samples (Suhorutshenko et al., 2018). Therefore, a gland specific molecular timing model was developed based on two epithelial cell-specific genes with opposing temporal expression patterns across the luteal phase of the cycle. By calculating the ratio of these two epithelial cell-specific genes, variation in the number of glands between endometrial biopsies is negated.

Single-cell RNA-seq (scRNA-seq) data from luteal phase endometrial biopsies were mined to identify epithelial cell-specific genes with opposing temporal expression profiles (Lucas et al., 2020), *GPX3* (encodes glutathione peroxidase 3) and *SLC15A2* (encodes solute carrier family 15 member 2, a proton coupled peptide transporter). Cross-referencing against a publicly available microarray dataset of endometrial biopsies obtained across the menstrual cycle (GEO: GDS2052) confirmed that *GPX3* expression increases dramatically upon transition from the early- to mid-luteal phase of the cycle (Talbi et al., 2006). Expression remains high in some but not all late-luteal phase samples, likely reflecting declining circulating progesterone levels (Fig. 3.15). By contrast, *SLC15A2* expression peaks during the early-luteal phase of the cycle, after which expression first declines rapidly and then more modestly upon transition from the mid- to late-luteal phase of the cycle (Fig. 3.15).

The transcript levels of *GPX3* and *SLC15A2* were measured by RT-qPCR in 263 endometrial biopsies obtained between LH+5 to LH+11 (Fig. 3.16a). Demographic details of this sample set are shown in Appendix Table 1.3. The RT-qPCR data were then used to create distribution graphs of expression on each day (Fig. 3.16b). The expression pattern of both *GPX3* and *SLC15A2* closely matched the microarray data (GEO: GDS2052). Next, the *GPX3*/*SLC15A2* mRNA ratio was calculated for each sample (Fig. 3.16c) and a distribution graph was generated (Fig. 3.16d). As anticipated, the ratio value increased over a broad range throughout the luteal phase of the cycle.

Next, I used this approach to test if endometrial gland responses are out-of-phase in RMM. Transcript levels of *GPX3* and *SLC15A2* were measured by RT-qPCR in endometrial biopsies obtained from 93 control subjects and 75 RMM patients and the

molecular timing ratio was calculated. Demographic characteristics of this sample set are shown in Appendix Table 1.4. Biopsies were obtained between LH+5 to LH+11 and the temporal patterns for both genes plotted in both groups (Fig. 3.17a and c). *GPX3* and *SLC15A2* mRNA expression did not differ between RMM and control endometrium (Fig. 3.17a and c) nor did the *GPX3/SLC15A2* ratio (Fig. 3.17e). Percentile values were calculated for the two genes (Fig. 3.17b and d) and for the *GPX3*/*SLC15A2* ratios (Fig 3.17f). Again, no differences were identified between control and RMM glands, supporting previous analysis that the RMM glands are not out-of-phase.

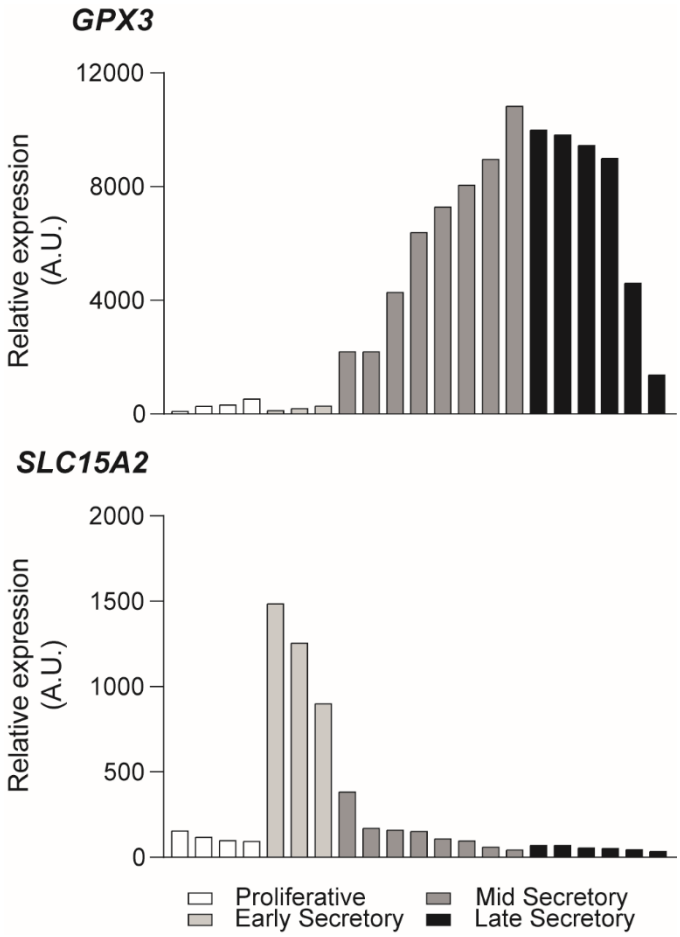

Figure 3.15. ***Glandular genes*** **GPX3** ***and*** **SLC15A2** ***expression across the menstrual cycle.***

Expression of glandular genes *GPX3* and *SLC15A2* across the proliferative phase, and early-, mid-, and late-secretory phase as indicated by the grey-scale key. Microarray data was mined from data deposited in the Gene Expression Omnibus (GEO Profiles, GDS2052). Each bar plotted represents an individual endometrial biopsy.

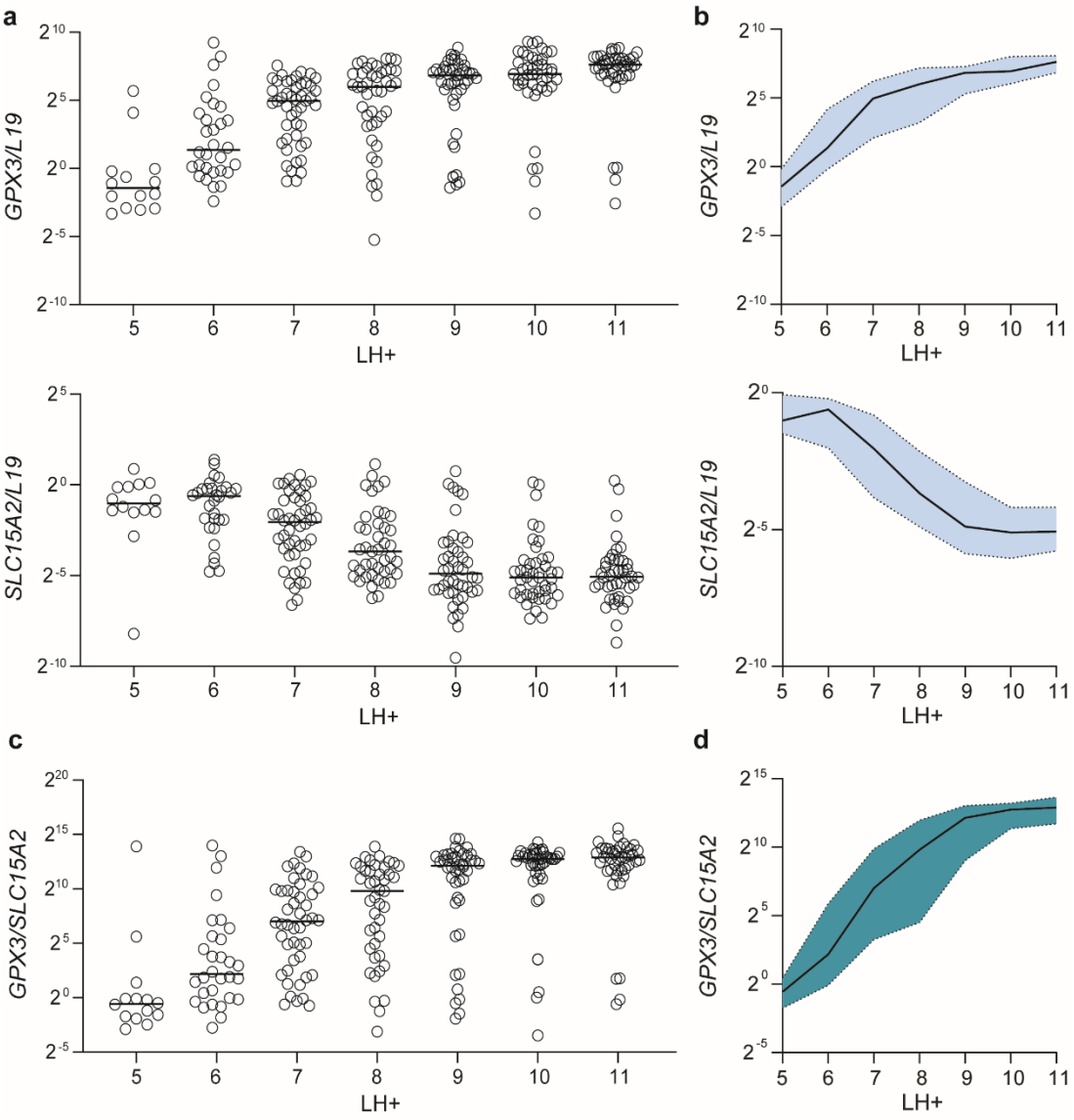

Figure 3.16. ***Glandular timing ratio of GPX3/SLC15A2 in endometrial biopsies.***

a) *GPX3* and *SLC15A2* transcript levels were quantified by RT-qPCR analysis in 263 endometrial biopsies obtained between LH+5 and LH+11. Each circle represents an individual biopsy, and a line marks the median for each day. The median number of samples for each day was 43 (range: 14-46).

b) Distribution of *GPX3* and *SLC15A2* expression for each day was plotted as the 95% confidence interval.

c) Timing ratio (*GPX3/SCL15A2*) was calculated using *GPX3* and *SLC15A2* transcript levels of 263 endometrial biopsies obtained between LH+5 and LH+11. Each circle represents an individual biopsy, and a line marks the median for each day.

d) Distribution of *GPX3/SCL15A2* ratio for each day was plotted as the 95% confidence interval.

Data collected in collaboration with Dr Joanne Muter.

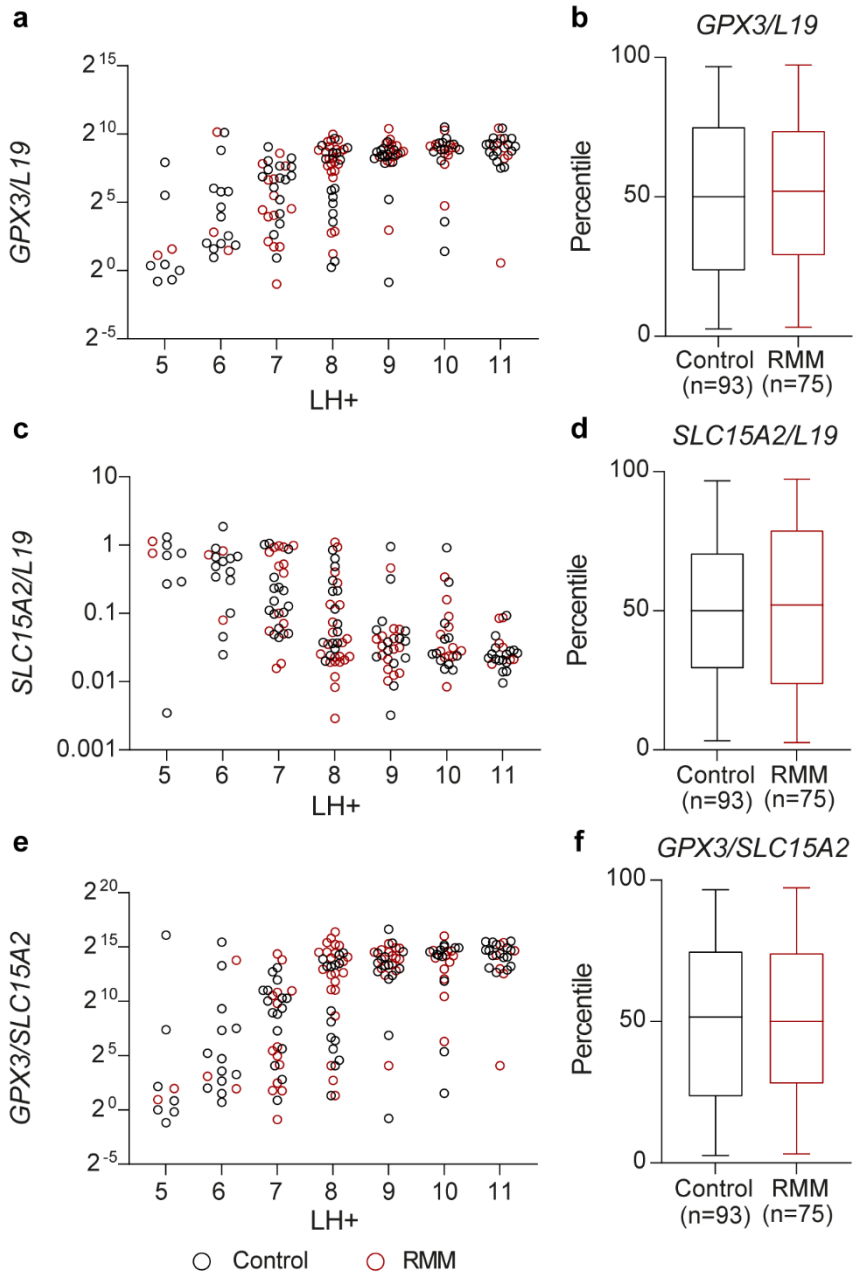

Figure 3.17. *RMM glands are not out-of-phase.*

GPX3 and *SLC15A2* transcript levels and timing ratio (*GPX3/SCL15A2*) of control subject (n= 93, black) and RMM patient (n=75, red) endometrial biopsies obtained between LH+5 and LH+11 and calculated percentile distributions presented as boxplots. Each circle represents an individual biopsy. Median number of samples for each day for control was 14 (range: 7-16) and RMM patients was 12 (range: 2-22). Patient groups were tested for significance either using Welch's *t*-test or Mann Whitney test after testing for normal distribution using Shapiro-Wilk or Kolmogorov-Smirnov tests.

a) *GPX3* transcript levels were quantified by RT-qPCR analysis of endometrial biopsies of control and RMM patients.

b) Distribution of *GPX3* percentiles in endometrial biopsies of control subjects and RMM patients. Percentiles calculated based on delta CT (dCt) of *GPX3* expression using Excel.

c) *SLC15A2* transcript levels were quantified by RT-qPCR analysis of endometrial biopsies of control and RMM patients.

d) Distribution of *SLC15A2* percentiles in endometrial biopsies of control subjects and RMM patients. Percentiles calculated based on dCt of *SLC15A2* expression using Excel.

e) Timing ratio (*GPX3/SCL15A2*) was calculated using *GPX3* and *SLC15A2* transcript levels of control and RMM endometrial biopsies.

f) Distribution of timing ratio percentiles in endometrial biopsies of control subjects and RMM patients. Percentiles calculated based on dCt of *GPX3/SLC15A2* using Excel.

3.2.5 Decidualisation in RMM

Crosstalk between the glands and EnSC is pivotal for their function. Glands produce and secrete factors that impact stromal decidualisation such as PGE_2, LIF and relaxin (Kelleher et al., 2019). Equally, decidual EnSC secrete a variety of factors, including PRL, during pregnancy, that may impact glandular function and histotrophic nutrition (Burton et al., 2007). Consequently, glandular defects may have secondary effects on decidualisation or vice versa. RPL has been associated with a lack of decidual precursor cells, pro-senescent decidual response and uNK cell deficiency (Lucas et al., 2016, Lucas et al., 2020, Tewary et al., 2020). A pro-senescent decidual response is thought to create an endometrial environment that is easy to invade but also prone to breakdown in early pregnancy. While bleeding commonly precedes pregnancy loss in RPL, this is not the case in RMM.

SCARA5 and *DIO2* are highly selective marker genes of diverging decidual states (Lucas et al., 2020). *SCARA5,* encoding scavenger receptor class A member 5, is a progesterone-dependent marker of decidual cells (Lucas et al., 2020). *DIO2* (encodes Type II iodothyronine deiodinase), which catalyses the conversion of prohormone thyroxine (3,5,3',5'-tetraiodothyronine, T4) to the bioactive thyroid hormone (3,5,3'-triiodothyronine, T3) is a gene repressed by progesterone in endometrial EnSC. However, upon acquisition of progesterone resistance in senescent decidual cells, *DIO2* becomes re-expressed (Lucas et al., 2020).

To examine if RMM is associated with an abnormal decidual response, LH-timed endometrial biopsies from 93 control subjects and 73 RMM patients were processed for RT-qPCR and immunohistochemistry (IHC). Demographic details of this sample set are shown in Appendix Table 1.5. Transcript levels of *SCARA5* and *DIO2* were measured, and temporal expression profiles plotted for both control and RMM samples (Fig. 3.18a and c). For each gene, percentiles were calculated to normalise for the day of the biopsy in the cycle as described previously (Lucas et al., 2020). In addition, the abundance of uNK cell underlying the luminal epithelium were quantified by a validated and standardised IHC approach (Lash et al., 2016). Percentiles were calculated to normalise for the day of the biopsy in cycle using an existing percentile graph based on analysis of 1997 LH-timed biopsies (Brighton et al., 2017). Quantification of uNK cells in this samples set was performed with assistance of Dr Katherine Fishwick.

SCARA5 mRNA expression increased progressively from the early- to mid-luteal phase in control whereas expression in RMM appeared blunted across the luteal

phase (Fig. 3.18a). In agreement, *SCARA5* percentiles in RMM samples were significantly lower when compared to control samples ($P < 0.01$, Welch's *t*-test, Fig. 3.18b). On the other hand, *DIO2* expression in control subjects decreased from early- to mid-luteal phase before plateauing, a pattern largely recapitulated in RMM samples (Fig. 3.18c). *DIO2* percentiles did not differ between control and RMM samples ($P > 0.05$, Mann Whitney) (Fig. 3.18d). The abundance of uNK cells in stroma underlying the luminal epithelium increased as the luteal phase progressed, although this response appeared blunted in RMM biopsies, at least in the mid-luteal phase (Fig. 3.18e). In agreement, uNK cell percentiles were significantly lower in RMM compared to control biopsies ($P < 0.05$ Welch's *t*-test) (Fig. 3.18f). Taken together, my analysis revealed that RMM is associated with impaired decidualisation and relative uNK cell deficiency when compared to control samples.

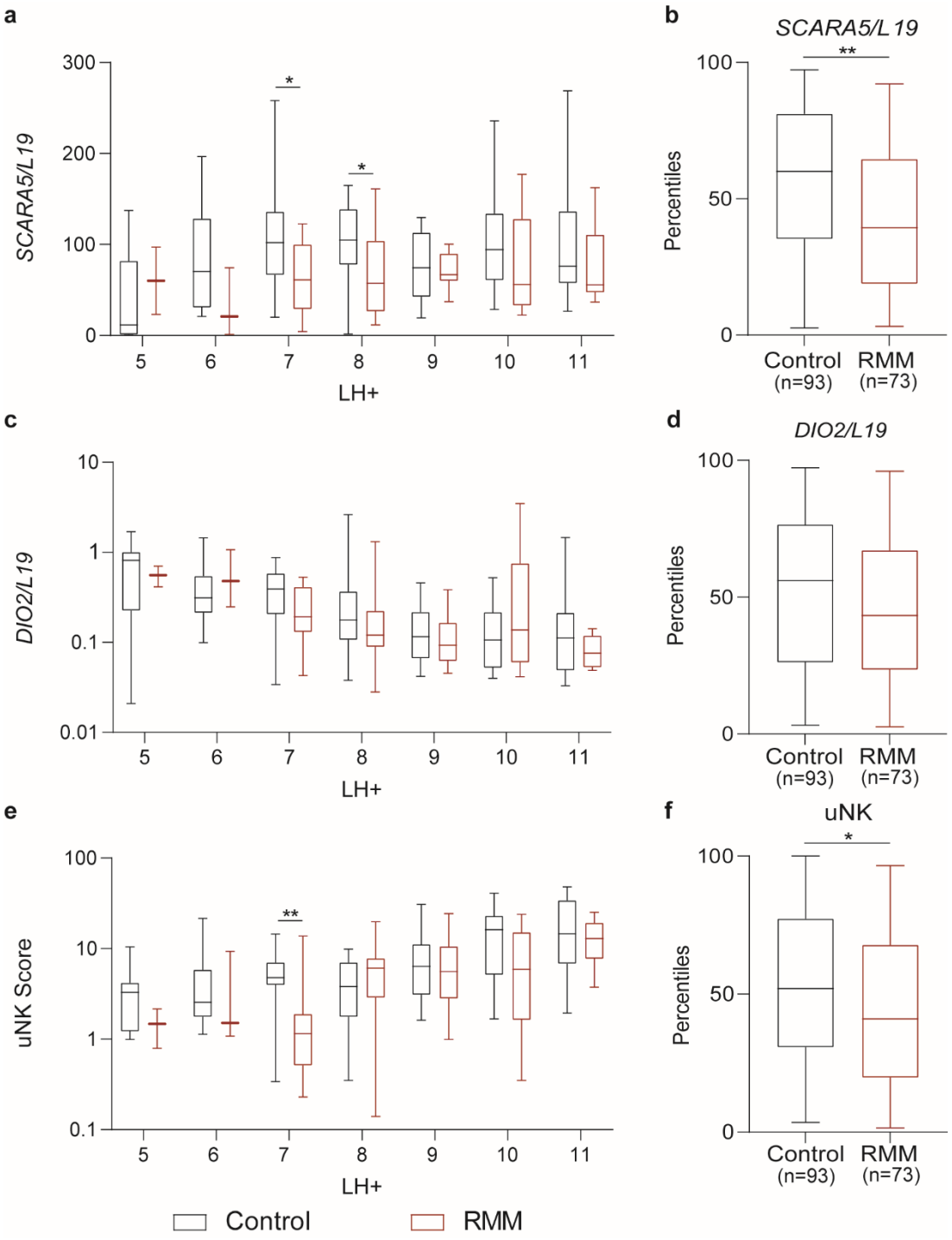

Figure 3.18. ***Stromal and uNK defects in RMM endometrium***.

Transcript levels and uNK scores of control subject (n=93, black) and RMM patient (n=73, red) endometrial biopsies obtained between LH+5 and LH+11 and calculated percentiles distributions presented as boxplots. Median number of samples for each day for control was 14 (range: 7-16) and RMM patients was 12 (range: 2-21). Patient groups were tested for significance either using Welch's *t*-test or Mann Whitney test after testing for normal distribution using Shapiro-Wilk or Kolmogorov-Smirnov tests.

a) *SCARA5* transcript levels were quantified by RT-qPCR analysis of timed endometrial biopsies of control and RMM patients. * indicates $P < 0.05$ obtained by Welch's *t*-test.

b) Distribution of *SCARA5* percentiles in endometrial biopsies of control subjects and RMM patients. Percentiles calculated based on dCt of *SCARA5* expression using Excel. ** indicates $P < 0.01$ obtained by Welch's *t*-test.

c) *DIO2* transcript levels were quantified by RT-qPCR analysis of timed endometrial biopsies of control and RMM.

d) Distribution of *DIO2* percentiles in endometrial biopsies of control subjects and RMM patients. Percentiles calculated based on dCt of *DIO2* expression using Excel.

e) Timed endometrial tissue of control and RMM was stained for uNK cells (CD56) and counted. ** indicates $P < 0.01$ obtained by Mann Whitney test.

f) Distribution of uNK in endometrial biopsies of control subjects (n=93) and RMM patients (n=73). Percentiles calculated based on uNK cell scores using R software. * indicates $P < 0.05$ obtained by Welch's *t*-test.

3.3 Discussion

Currently, there is very little understanding of RMM, and studies are scarce. Other than the outcome of multiple miscarriages, RMM and RPL present with different phenotypes. Therefore, it is plausible the underlying pathologies are not the same. One feature of RMM is the early onset of fetal growth restriction, which could be the result of glandular defects that are detrimental to histotrophic nutrition. To test this hypothesis, I aimed to identify defects in the glands of RMM patients using RNA-seq data. Additionally, I determined whether the glandular defects in RMM were due to an out-of-phase response and if an aberrant decidual response occurred in RMM patients.

As anticipated, the TCA cycle and oxidative phosphorylation were upregulated in RMM glands. Pregnancy requires a large secretory output from the glands. Initially, it was postulated that the upregulation of mitochondrial-related genes in RMM glands, leads to excessive secretion prior to conception, and eventually to early secretory exhaustion (Barros, 2017). However, the metabolic modelling indicated pronounced perturbations in metabolic pathways in RMM glands that may consequently reduce the composition of glandular secretion for histotrophic nutrition.

Interestingly, the reaction catalysed by pyruvate kinase was the most downregulated reaction of glycolysis. Reduced levels of pyruvate results in less acetyl-CoA conversion for oxidative phosphorylation. However, to meet the demand of the glands, a compensatory method of using FAO may be implemented by the glands. FAO also produces acetyl-CoA molecules, which can be fed into the TCA cycle for oxidative phosphorylation (Houten et al., 2016). Despite, only a limited number of fatty acid degradations, the modelling data suggests an upregulation of FAO in RMM glands. Increased FAO could explain the upregulation of oxidative phosphorylation in RMM as the breakdown of fatty acids produces the highest yield of ATP compared to any other macromolecule. Additionally, lipids are an important part of histotrophic nutrition (Kelleher et al., 2019). The PPP is important in producing NADPH for fatty acid synthesis as well as nucleotide biosynthesis. Both biosynthesis pathways are crucial for the secretory phenotype of the glands in early pregnancy. A downregulation of the PPP was observed in RMM glands. A reduction in fatty acid synthesis due to depleted NADPH levels and upregulation of FAO could result in a deficit in the glands at pregnancy.

It was speculated whether the glandular defects in RMM were a consequence of an out-of-phase endometrium, specifically out-of-phase glands. Many models have been created to distinguish receptive from non-receptive endometrium (Noyes et al., 1950, Haouzi et al., 2009, Díaz-Gimeno et al., 2011). However, the endometrium is a heterogenous tissue and these models ignore the variability in cellular composition between each sample. Not considering cellular heterogeneity in whole-tissue analysis could result in misinterpretation of the results (Shen-Orr and Gaujoux, 2013). In addition, the ability to measure phenotypic changes between patients at the cellular level is critical for obtaining a detailed understanding.

Therefore, two epithelial specific timing methods were performed to time the endometrium. Both methods concluded the glands were not out-of-phase in RMM. Hence, the gland defects in RMM patients are not due to glandular asynchrony. Notably, RMM are able to conceive, likely due to the endometrium being correctly timed for implantation. It is plausible that the defects in RMM do not impact implantation, instead cause issues in pregnancy, leading to a missed miscarriage.

The endometrium is a heterogenous tissue and more than one cell type may be dysfunctional in a disorder. In this study, RMM was found to be associated with uNK cell deficiency and impaired decidualisation. After ovulation, uNK cell numbers rise substantially and have a role in clearing the acute senescent decidual cells to allow for embryo implantation (Brighton et al., 2017). Furthermore, during pregnancy uNK cells are implicated in the remodelling of spiral arteries before and during trophoblast invasion (Chazara et al., 2011, Xiong et al., 2013, Salker et al., 2012). Decidual cells secretions of interleukins are implicated in activation and proliferation of uNK cells (Ashkar et al., 2003, Ain et al., 2004). Thus, a poor decidual response is likely to impact the recruitment of uNK cells in RMM patients.

Notably, RPL has been linked also to uNK cell deficiency (Lucas et al., 2020). However, a striking difference between these pathological states is the lack of excessive decidual senescence in RMM. Excessive decidual senescence is characterised by constitutive expression of inflammatory mediators and ECM proteins and proteinases (Lucas et al., 2020), which are likely to promote breakdown of the emerging maternal-fetal interface in early gestation. By contrast, the decidual response appears less advanced in RMM samples, which arguably could be caused by glandular dysfunction or, conversely, impact glandular differentiation responses. Without excessive decidual senescence, the RMM endometrium is more robust and unlike RPL, does not lead to breakdown of the maternal-fetal interface and prominent

bleeding. Decidualisation and uNK cell recruitment is regulated by glandular secretions such as PGE_2 (Smith and Kelly, 1988), and cytokine and chemokine (C-X-C motif) ligand 14 (CXCL14) (Mokhtar et al., 2009), respectively. An impaired decidual response may be caused by the glandular dysfunction observed in RMM.

Overall, these detailed findings exhibit an atypical gland and decidual response in the endometrium of RMM patients, unique from RPL. However, these biopsies are from pre-conception endometrium, and *in vivo* samples only provide a single snapshot in time of what is taking place. An *in vitro* model allows for functional testing of a patient phenotype, further dissection of the pathways as well pharmacologically testing. To investigate the RMM phenotype further an *in vitro* system is required.

Chapter 4:
Formation Efficacy and Differentiation Capacity of Endometrial Gland Organoids

4.1 Introduction

Modelling defects of the endometrial glands requires a suitable *in vitro* model. However, until recently studying the glands was challenging due to the failure of primary endometrial EpC to propagate in culture, especially when isolated from luteal-phase biopsies (Barros, 2017). The cells lose their structural characteristics as well as the ability to proliferate and differentiate (Classen-Linke et al., 1996, Hombach-Klonisch et al., 2005). Endometrial EpC grown as monolayers also lack the physiological and architectural state of glands *in vivo*.

Following the development of adult stem cell derived organoid cultures from other tissues (Lancaster and Knoblich, 2014, Simian and Bissell, 2017, Rossi et al., 2018, Kim et al., 2020), gland organoids were established from the human endometrium (Turco et al., 2017, Boretto et al., 2017) (Fig. 4.1). Similar to other organoids, endometrial epithelial stem/progenitor cells self-organise into 3D gland-like structures in the presence of a chemically defined medium termed expansion medium (ExM), containing growth factors, supplements and signal transduction pathway modulators (Turco et al., 2017, Boretto et al., 2017). Endometrial gland organoids can be passaged for up to 6 months and cryopreserved while remaining genetically stable (Turco et al., 2017, Boretto et al., 2017). The organoids recapitulate the structural features of the glands found *in vivo*, respond to hormonal signals, and secrete components found in glandular secretions, such as glycodelin (Turco et al., 2017).

During the proliferative phase, endometrial EpC proliferate rapidly in response to rising oestrogen to form the glands of the functional layer (Ferenczy and Bergeron, 1991). Regeneration of the endometrial glands following menstruation, pregnancy loss, parturition or iatrogenic destruction (e.g., curettage) is mediated by adult stem/progenitor cells residing in the basal layer (Tempest et al., 2018b). Endometrial glands are clonal, meaning that single stem/progenitor cells produce all descendant cells within individual glands (Tanaka et al., 2003, Moore et al., 2020), although there is evidence that some glands are regenerated by more than one epithelial stem/progenitor cell (Tempest et al., 2020). Epithelial stem/progenitor cells have been identified in the basal endometrial layer of hysterectomy specimens and are capable of self-renewal, exhibit high proliferative potential and differentiate into 3D gland-like structures in a defined chemical medium (Gargett et al., 2009, Valentijn et al., 2013, Nguyen et al., 2017, Tempest et al., 2020).

Endometrial gland organoids can also be established from pipelle biopsies, indicating the presence of multipotent progenitor cells in the functional layer (Turco et al., 2017). Like their native counterparts, gland organoids are clonal, and form from cells seeded at single-cell density, enabling quantification of the abundance of endometrial epithelial stem/progenitor cells in a biopsy sample. This assay has been termed the organoid forming efficiency (OFE) assay (Turco et al., 2017). Endometrial gland organoids express a gene signature that include epithelial stem cells markers, such as *LRIG1*, *PROM1*, *AXIN2* and *SOX9 (Turco et al., 2017)*. *SOX9* is highly expressed in the glandular portion that resides in the basal endometrial layer (Valentijn et al., 2013). Consequently, it has been postulated that expansion of $SOX9^{+}$ cells drive organoid formation *in vitro* (Turco et al., 2017).

In this chapter, I exploited the ability to generate endometrial gland organoids to assess different differentiation protocols and to determine the clinical variables that may impact on the differentiation and OFE of gland organoids.

4.2 Results

4.2.1. Cyclical vs passage differentiation of endometrial organoids

Endometrial gland organoids are established from endometrial biopsies (Fig. 4.1). After mechanical and enzymatical digestion, the endometrial samples are passed through a strainer to collect the gland isolates. The isolates are resuspended in a gelatinous protein mixture, Matrigel, that provides the matrix for the organoids to grow. The cured gland/matrigel droplets are then grown in ExM. To recapitulate the hormone-dependent changes in gland function across the menstrual cycle, Turco *et al* (2017) used the following differentiation: a 4-day growth period in ExM followed by 2 days priming in ExM with E_2 and then 2 days in ExM supplemented with E_2, 8-Bromoadenosine-3',5'-cyclic monophosphate (8-bromo-cAMP) and P_4 (Fig. 4.2a). It was not reported if gland organoids require passaging to elicit a robust differentiation response nor was the impact of cyclical differentiation on gland organoid responses evaluated (Turco et al., 2017).

I began with investigating the effect of passaging on gland organoid differentiation. For organoid passage, a mechanical rather than enzymatic approach was taken to ensure organoid breakdown into single-cell suspensions. Recovery of the organoids from the Matrigel followed by mechanical digestion requires approximately 380 repeat pipetting of the samples (Turco et al., 2017). Passaging allows for re-expansion of the cultures but arguably does not recapitulate physiological regeneration of the endometrium. As the endometrium is exposed to iterative cycles of growth and differentiation, I also evaluated the impact on gland organoids of repeated cycles of differentiation without additional passaging.

As depicted in Figure 4.2, three independent gland organoid cultures were set up to evaluate the impact of repeated passaging or cyclical differentiation using the original Turco differentiation protocol outlined above (Fig. 4.2a). In both experimental designs, undifferentiated gland organoids maintained in ExM for 8 days were used as control cultures. For cyclical differentiation, organoids were set up at passage 0 (P0) and then were subjected to the first cycle of differentiation. Organoids were recovered for RNA extraction after undergoing 1 to 4 cycles (C1-C4) of differentiation (Fig. 4.2b). To assess the impact of passaging, organoids were set up at P0 and either differentiated or maintained in ExM. The undifferentiated glands organoids were then passaged, and the experiment repeated. Total RNA was extracted from

undifferentiated and differentiated gland organoids at P0, passage 1 (P1), passage 2 (P2), and passage 3 (P3) (Fig. 4.2b).

Endometrial gland organoids are spheroids consisting of an epithelial layer surrounding a central lumen (Turco et al., 2017, Boretto et al., 2017). Glandular structures were difficult to discern at P0 but became apparent at P1 (Fig. 4.3). Organoids subjected to cyclical differentiation without passaging also began as tissue isolates but gland-like structures become apparent by C2. Notably, with additional cycles of differentiation the organoids darkened and appeared to collapse (Fig. 4.3). The Matrigel droplets also reduced in size, a sign of progressive gel disintegration. With little space to expand into, these gland-like structures were observably smaller than their passaged counterparts.

PAEP (encodes for progestagen-associated endometrial protein, also known as glycodelin) is a commonly used marker of glandular differentiation (Turco et al., 2017, Boretto et al., 2017). *PAEP* expression is low during the proliferative phase but increases markedly in response to progesterone signalling during the luteal phase (Seppälä et al., 2002). Hence, induction of *PAEP* was quantified by RT-qPCR to measure differentiation capacity of gland organoids following serial passaging or cyclical differentiation. Relative expression of *PAEP* normalised to *L19*, a housekeeping gene encoding ribosomal protein L19, were plotted to highlight the intrinsic variability between organoid cultures from different patient samples (Fig 4.4a). *PAEP* transcript levels in undifferentiated organoids decreased from C3 and P2 onwards (Fig 4.4b), resulting in a robust induction upon treatment with E_2, 8-bromo-cAMP and P_4 (Fig 4.4c).

Based on organoid morphology and the improved differentiation response, P2 was selected for all future differentiation experiments. The responsiveness of P2 gland organoids to differentiation signals was validated by IHC in independent cultures (Fig. 4.5). Organoids were stained for structural markers cytokeratin, E-cadherin (epithelial cadherin) and EpCAM. Morphologically, undifferentiated organoids consisted of a single EpC layer but upon differentiation became enlarged and multi-layered. Glycodelin accumulated in the lumen of the differentiated organoids in parallel with loss of PGR, hallmarks of glandular differentiation *in vivo* (Wang et al., 1998).

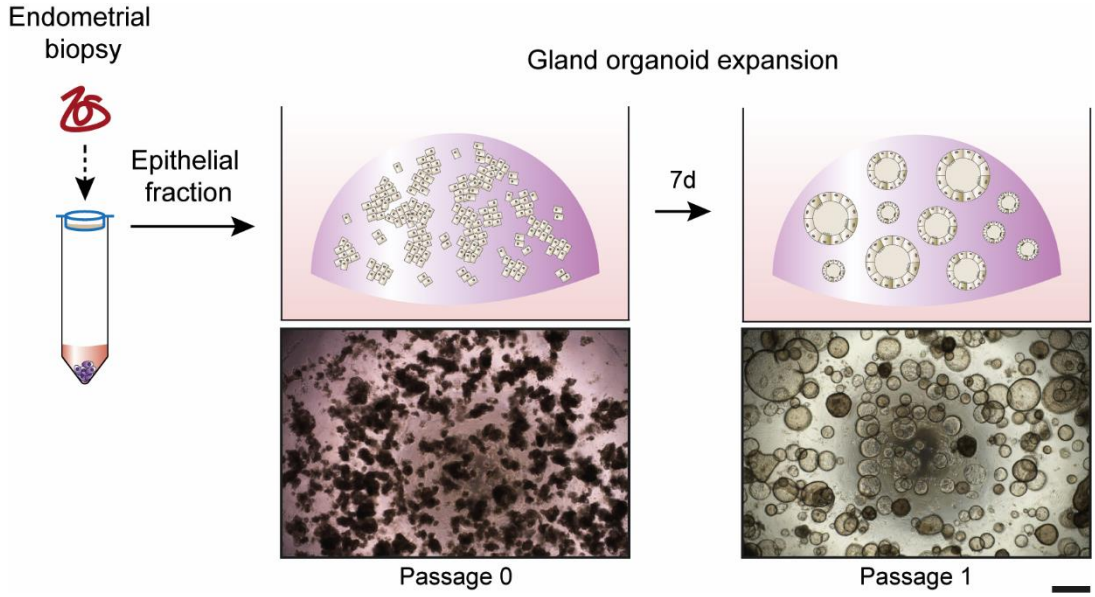

Figure 4.1. ***Endometrial gland organoid expansion.***

Schematic representation of endometrial gland organoid expansion. Endometrial biopsies were mechanically and enzymatically digested. The epithelial fraction of tissue isolates was collected in the strainer and resuspended in Matrigel. Droplets of gland isolates/Matrigel (20 µl) were plated in a 48-well plate and cured at 37 °C before ExM was added (Passage 0). Over the next 7 days, organoids form from progenitor cells, but many gland isolates remain. The culture was then mechanically passaged to remove the cells from the Matrigel and to break down the tissue and organoids. The cell pellet was replated in fresh Matrigel (Passage 1) and grown for another seven days to form organoids. Scale bar = 500 µm. Protocol adapted from (Turco et al., 2017).

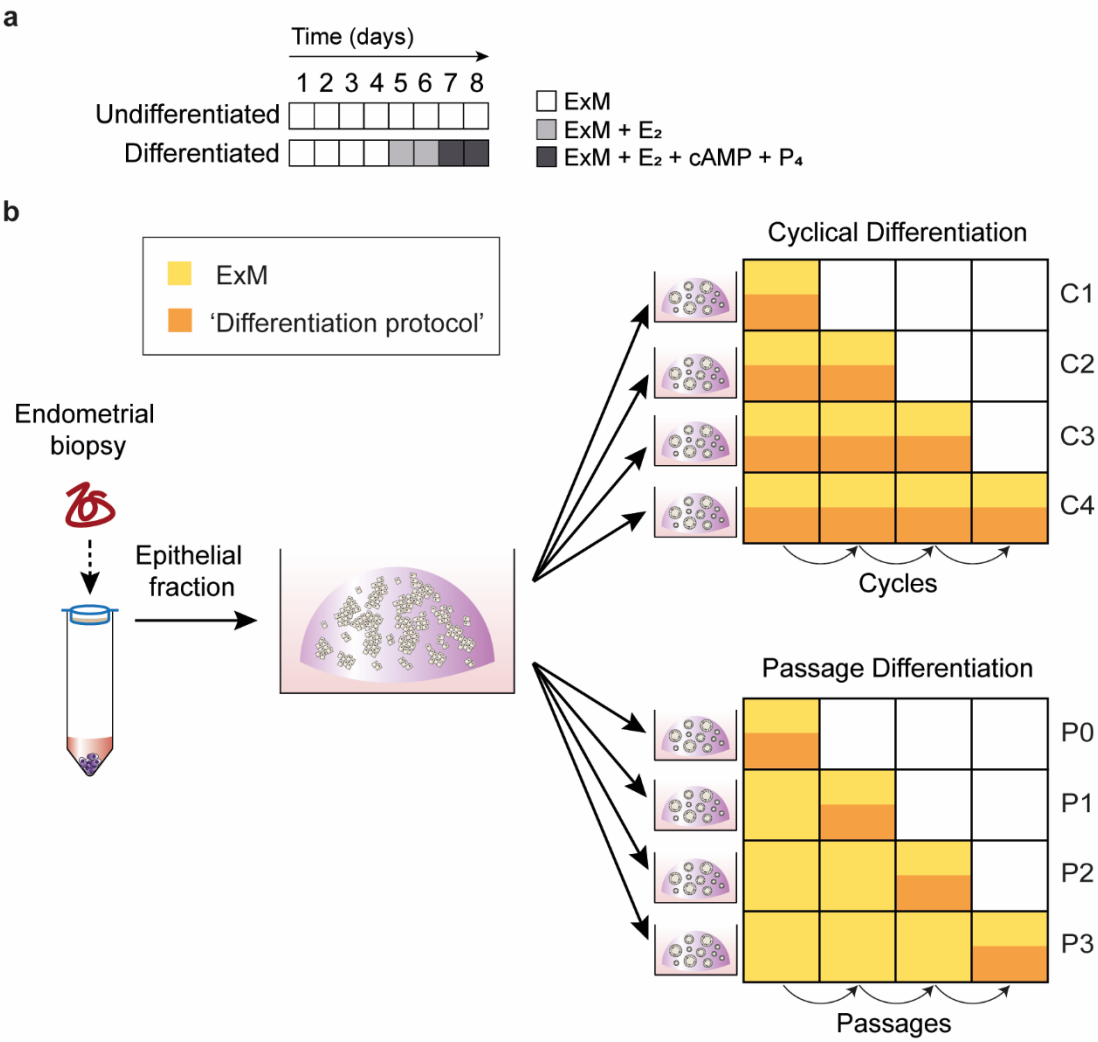

Figure 4.2. ***Cyclical and passage differentiation protocol.***

a) Schematic summary of differentiation protocol. Samples were either left undifferentiated for 8 days in ExM or grown for 4 days, primed with E_2 for 2 days and then differentiated with E_2, cAMP and P_4.

b) Schematic summary of cyclical and passage differentiation protocol. Epithelial fraction was separated from a digested endometrial biopsy. Samples were resuspended in Matrigel, plated, cured, and ExM was added. The sample was used in parallel for two differentiation protocols. For cyclical differentiation, at C1 the samples were either left undifferentiated in ExM for 8 days or differentiated. Gland organoids were then harvested for RNA or went through another cycle of differentiation. Organoids underwent 1 to 4 cycles of differentiation. For passage differentiation, samples were differentiated as above at each passage before harvesting for RNA. Organoids underwent 0 to 3 passages.

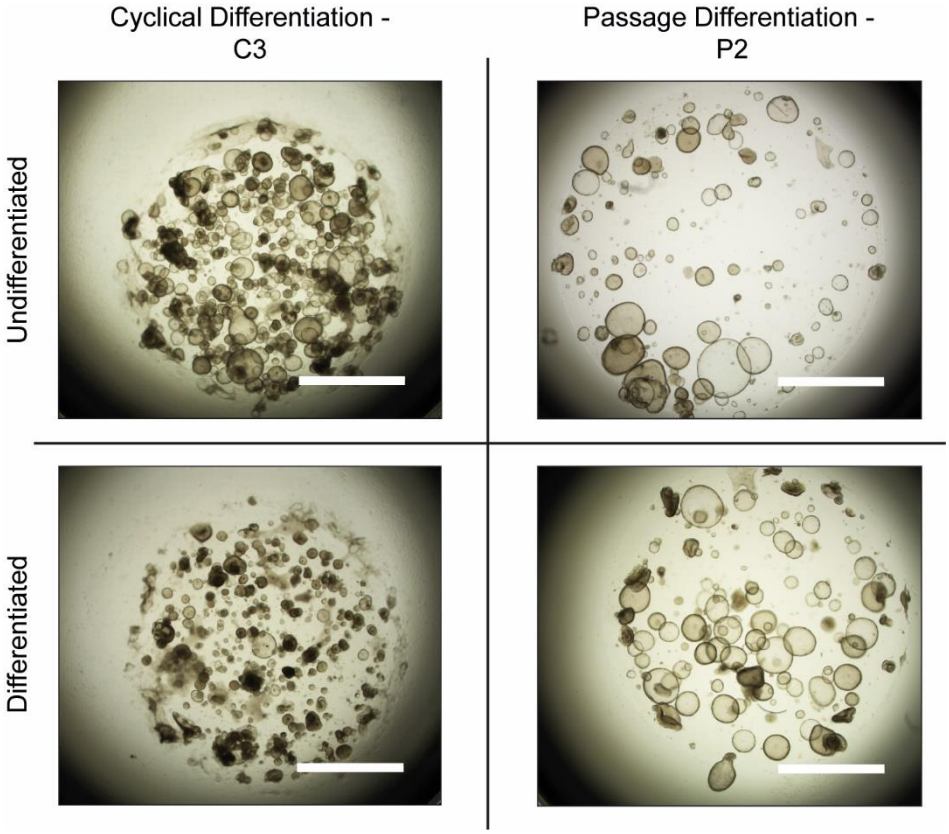

Figure 4.3. ***Representative images of cyclical and passage differentiation of gland organoids.***

Representative images of undifferentiated and differentiated organoids from the same endometrial biopsy at C3 of cyclical differentiation and at P2 of passage differentiation. Scale bar = 2 mm.

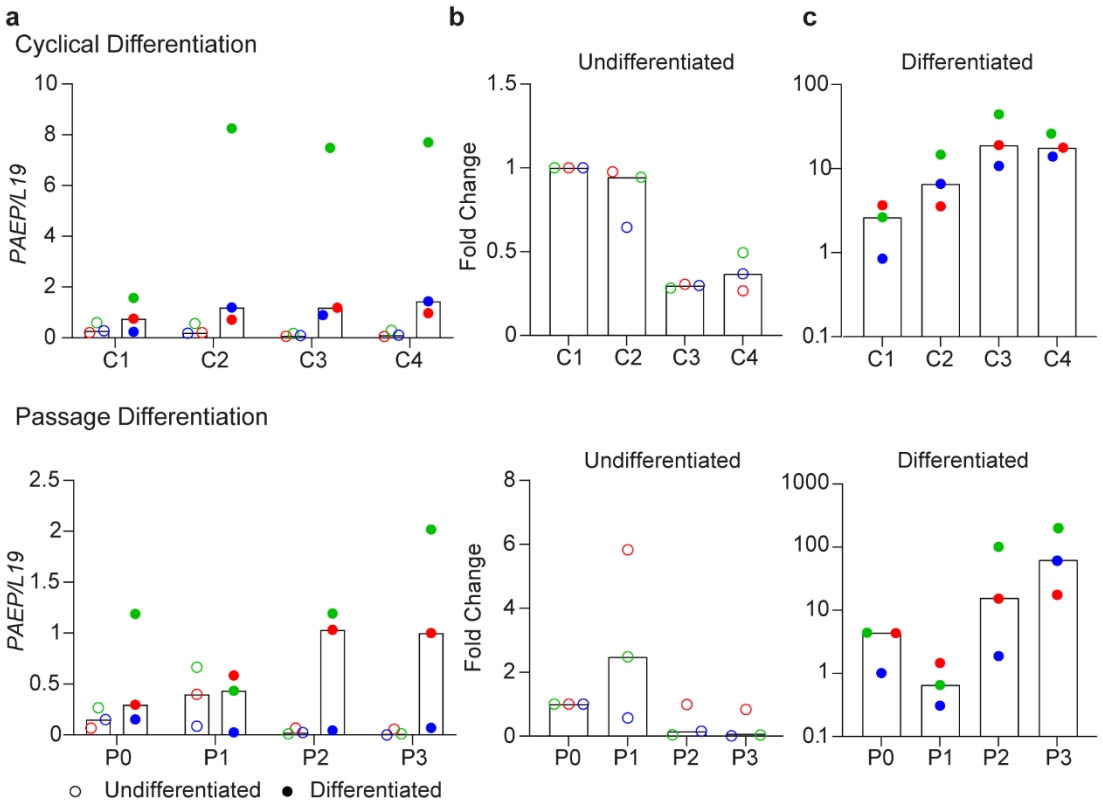

Figure 4.4. ***Differentiation response improves in gland organoids with increased number of cycles and passages.***

PAEP expression in organoids of undifferentiated (open dot) and differentiated samples (closed dot) (n=3) at each cycle or passage. Data points are coloured to represent expression in gland organoids established from independent endometrial biopsies. Bars show median.

a) Bar plot showing relative expression of *PAEP* normalised to *L19* expression of cyclical and passage differentiation.

b) Bar plot showing induction of *PAEP* expression in undifferentiated organoids. Expression values are presented as fold change relative to expression levels in undifferentiated gland organoids at C1/P0.

c) Bar plot showing induction of *PAEP* expression in differentiated organoids. Expression values are presented as fold-change relative to expression levels of undifferentiated gland organoids at the same cycle/passage.

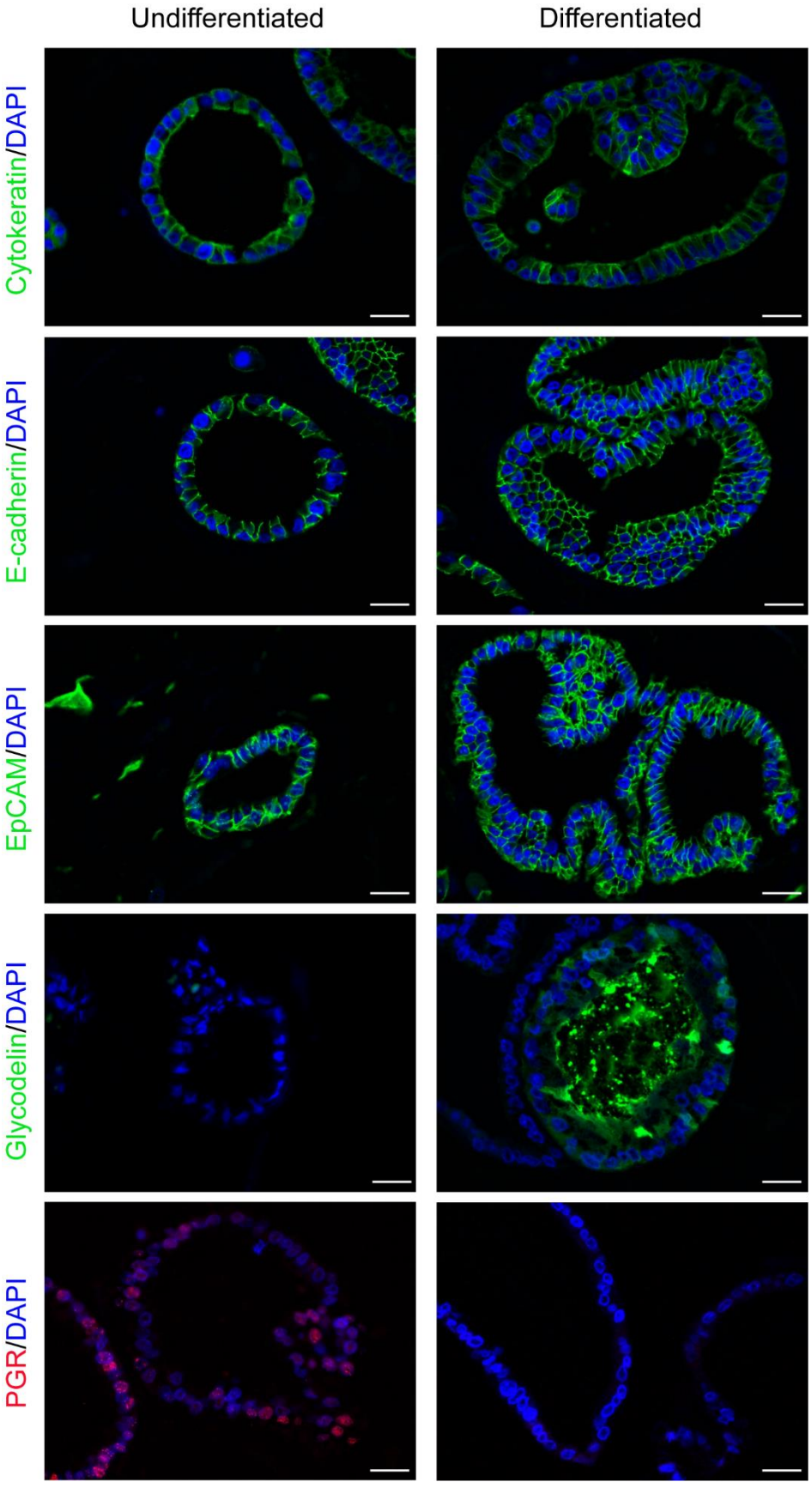
Undifferentiated
Differentiated
Cytokeratin/DAPI
E-cadherin/DAPI
EpCAM/DAPI
Glycodelin/DAPI
PGR/DAPI

Figure 4.5. ***Immunofluorescence microscopy of undifferentiated and differentiated organoids.***

Representative immunofluorescence labelling of structural markers (cytokeratin-18, E-cadherin and EpCAM) and differential markers (glycodelin and PGR) in undifferentiated and differentiated organoids grown in collagen gel using a forward time-course. Nuclei were counterstained with DAPI. Samples were visualised by epifluorescence microscopy. Scale bar = 25 µM.

4.2.2 Organoid formation efficacy

Organoid formation relies on the premise that single adult stem cells expand into 3D structures when cultured in a chemically defined medium (Lancaster and Knoblich, 2014). As such, organoid formation can be used to measure the abundance of adult stem cells in a tissue by seeding cells at low density. For example, Turco *et al*. (2017) reported an efficiency of 2-4% when 100 endometrial EpC were seeded in 5 µl Matrigel droplets (n=3). To investigate the epithelial stem/progenitor cell population in clinical samples, the epithelial fractions of 45 endometrial biopsies were digested into single cells immediately following sample collection (Fig. 4.6). Either 100 or 1000 cells from each biopsy were seeded in 5 µl Matrigel droplets and left to grow for 10 days in ExM. The total number of organoids were counted and the OFE (% organoids formed) calculated.

A strong correlation was observed between OFE between the two seeding densities ($P < 0.0001$, $r = 0.8536$, Spearman correlation) (Fig. 4.7a). A significant increase was found in OFE between the two seeding densities (Fig. 4.7b). Seeding 1000 endometrial EpC increased the OFE by 37% when compared to 100 seeded cells [average (standard deviation (SD)) OFE = 7.10% (5.95) versus 5.64% (5.12), respectively] ($P < 0.01$, Wilcoxon test). As expected, a ~12-fold increase in organoid formation was observed when 1000 endometrial EpC were seeded compared to 100 [average (SD) number of organoids = 70.99 (59.52) versus 5.64 (5.12), respectively] ($P < 0.0001$, Wilcoxon test) (Fig. 4.7c).

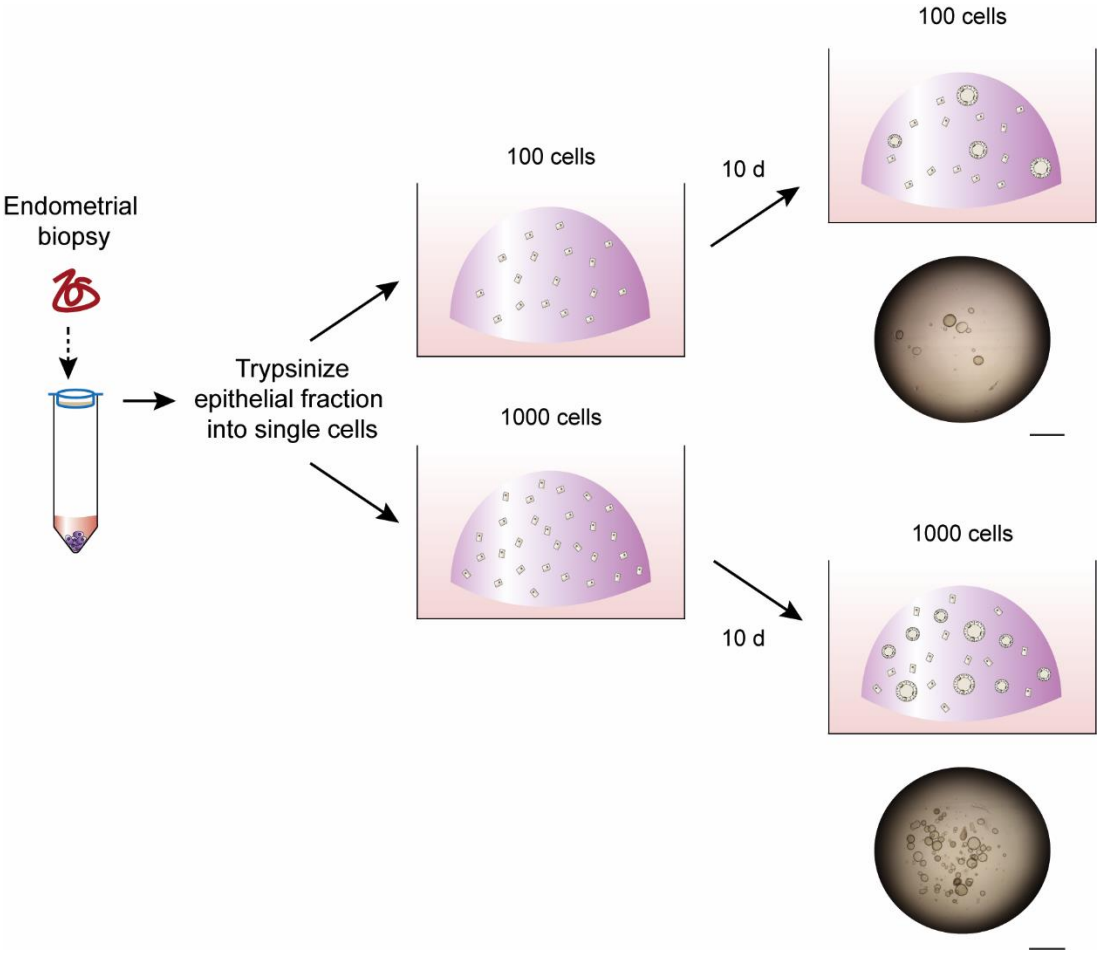

Figure 4.6. ***OFE assay at P0.***

Schematic representation of OFE assay at P0. Endometrial biopsies were mechanically and enzymatically digested. Epithelial fraction of gland isolates was collected in the strainer and were digested further into single cells using Trypsin. EpC were counted and resuspended at a density of 100 cells and 1000 cells per 5 µl of Matrigel. The droplets were plated. Organoids were grown for 10 days in ExM and imaged. Organoids were counted and efficiency was calculated. Scale bar = 1 mm.

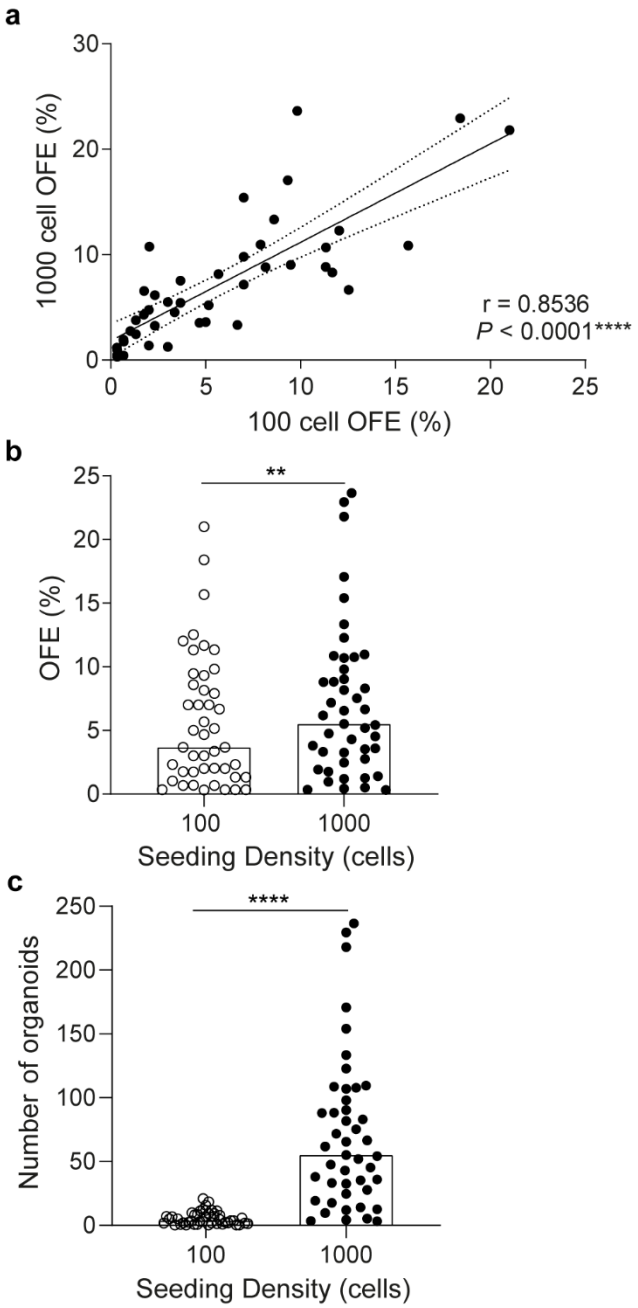

Figure 4.7. *Seeding density does not change OFE.*

a) Spearman correlation (*r*) between OFE of 100 cells and 1000 cells in 45 subjects. Graph shows best-fit line and 95% confidence intervals.

b) OFE (%) of 100 (open dot) and 1000 (closed dot) cells per droplet of Matrigel of 45 endometrial biopsies. Bars show median. Each dot represents individual patients. ** indicates $P < 0.01$ (Wilcoxon test; normal distribution tested with Shapiro-Wilk test).

c) Number of organoids formed from 100 (open dot) and 1000 (closed dot) cells per droplet of 45 endometrial biopsies. Bars show median. Each dot represents individual patients. **** indicates $P < 0.0001$ (Wilcoxon test; normal distribution tested with Shapiro-Wilk test).

4.2.3 Impact of demographic factors on OFE and organoid differentiation

I mined the data obtained from the 45 biopsies to examine if OFE varies according to demographic characteristics. However, no correlation was found between OFE and the age of the donor, body mass index (BMI), day of the biopsy relatively to the pre-ovulatory LH surge (home ovulation tests), or number of previous miscarriages (Fig. 4.8).

I further examined the responsiveness of gland organoids to differentiation signals in a cohort of 35 samples, using the differentiation protocol outlined in Figure 4.2a. *PAEP* expression at P2 was quantified by RT-qPCR in undifferentiated organoids and organoids differentiated with E_2, 8-bromo-cAMP and P_4 (Fig. 4.9a). A significant increase in *PAEP* expression was observed in P2 glands organoids exposed to the differentiation signal for 2 days ($P < 0.001$, Wilcoxon test). The presence of more naïve cells could plausibly result in a blunted glandular differentiation response. However, no significant correlation was found between OFE and induction of *PAEP* mRNA expression ($P < 0.05$, $r = -0.03097$, Spearman correlation) (Fig. 4.9b). Additionally, no correlation was found between *PAEP* induction and age of the donor, BMI, day of the biopsy relatively to the pre-ovulatory LH surge, or number of previous miscarriages (Fig 4.10).

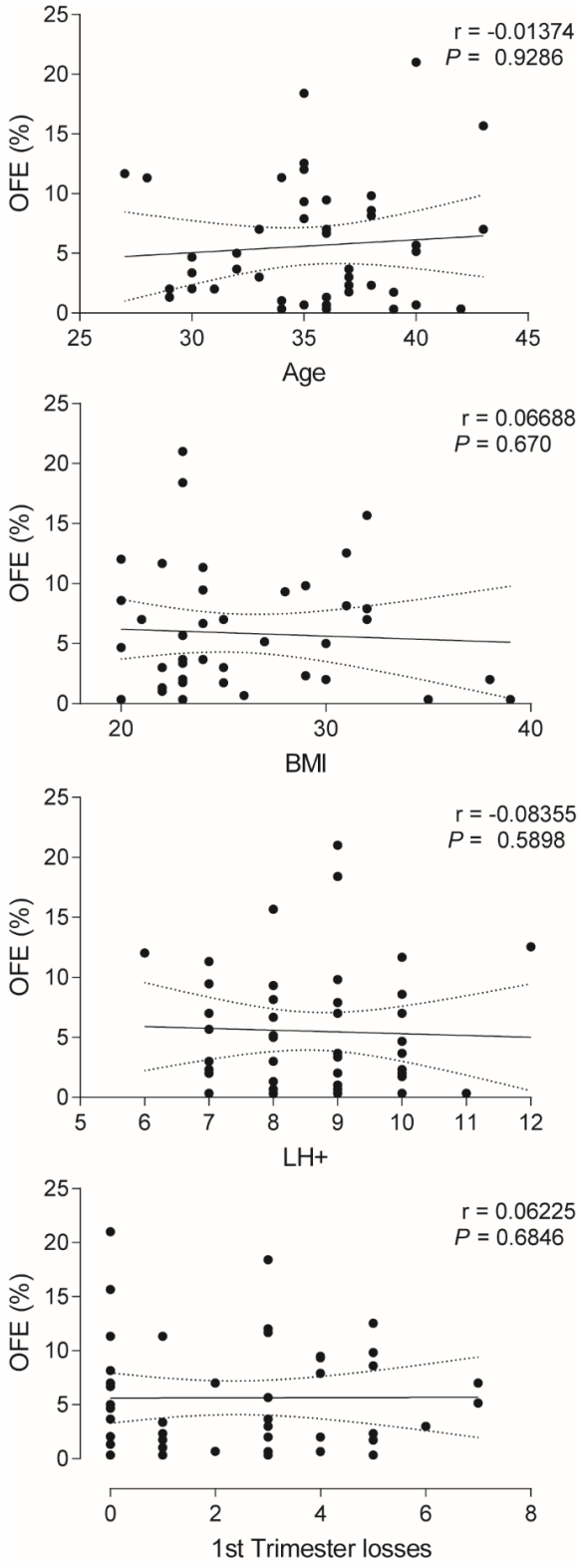

Figure 4.8. ***Correlation between OFE and clinical variables.***

Spearman correlation (*r*) graphs showing best-fit line and 95% intervals between OFE and age (n=45), BMI (n=43), timing of the biopsy relatively to pre-ovulatory LH surge (n=44), and number of previous 1st trimester losses (n=45).

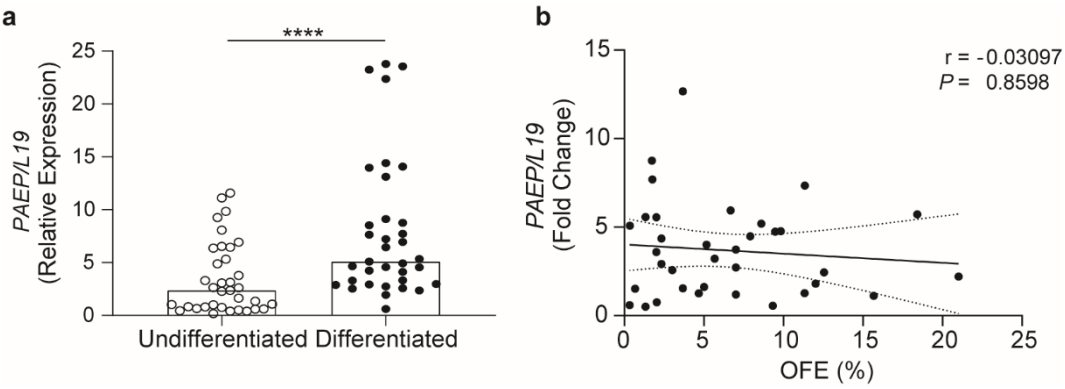

Figure 4.9. PAEP *expression increases with differentiation in gland organoids but does not correlate with OFE.*

a) Induction of *PAEP* expression in undifferentiated (open dot) and differentiated (closed dot) gland organoids from 35 endometrial biopsies. Data are presented as relative expression compared to expression levels in undifferentiated endometrial gland organoids. Bars show median. **** indicates $P < 0.0001$ (Wilcoxon test; normal distribution tested with Shapiro-Wilk test).

b) Spearman correlation (*r*) between OFE and induction of *PAEP* mRNA expression in endometrial gland organoids established from 35 endometrial biopsies. Expression values are presented as fold change relative to expression levels in matching undifferentiated glands organoids. Graph shows best-fit line and 95% confidence intervals.

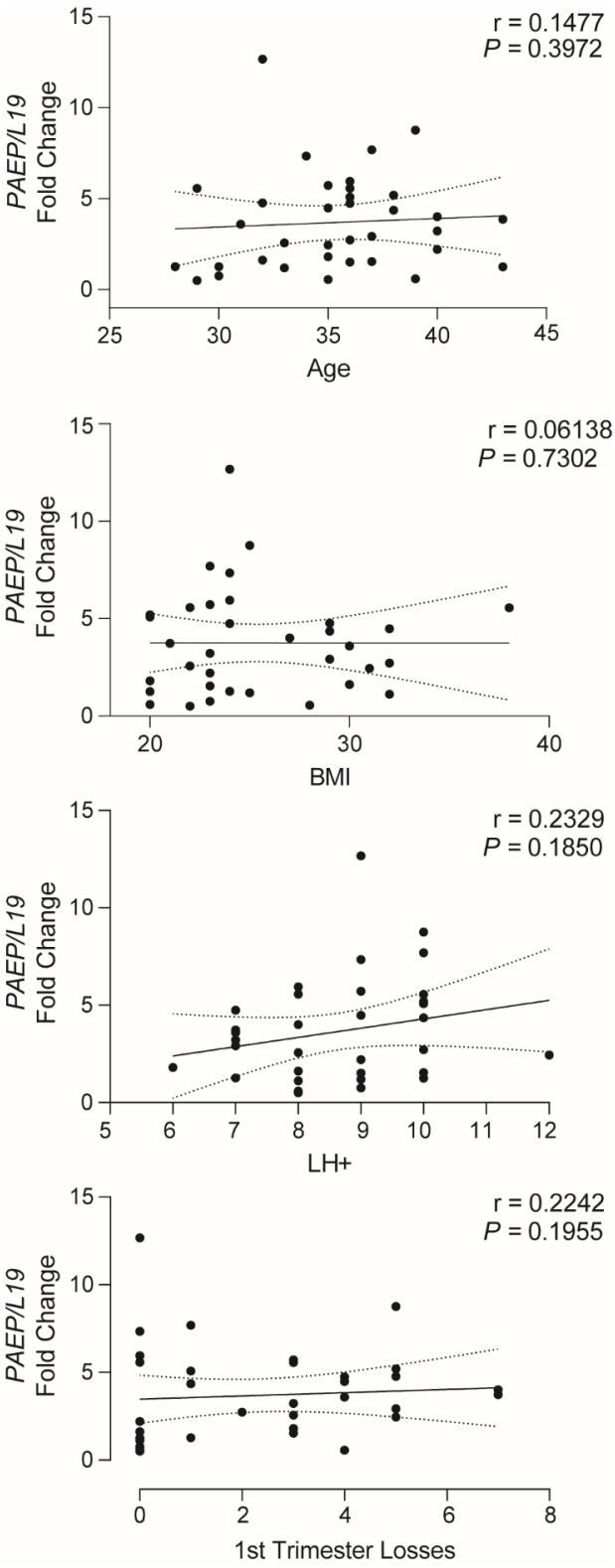

Figure 4.10. PAEP *expression does not depend on clinical variables.*

Spearman correlation (*r*) graphs show best-fit line and 95% confidence intervals between induction of *PAEP* expression upon organoid differentiation and age (n=35), BMI (n=34), timing of the biopsy relatively to pre-ovulatory LH surge (n=34), and number of previous 1st trimester losses (n=35).

4.3 Discussion

Past challenges of studying endometrial glands have been overcome by the establishment of the endometrial gland organoids from non-pregnant endometrium and the decidua (Turco et al., 2017, Boretto et al., 2017). Organoids can be cultured for up to 6 months, but whether passaging was required to elicit a robust differentiation response had not been reported. Culture of primary EnSC has demonstrated a reduction in cell subpopulations with increased culture time, which can reflect emerging replicative exhaustion (Brighton et al., 2017). Organoid differentiation after passaging was evaluated and in parallel the impact of repeated cycles of differentiation.

After a few passages, a robust differentiation response was observed in gland organoids, as a result of a lower baseline expression of *PAEP*. It is plausible the remnant effects of progesterone signalling *in vivo* may continue until P2. Additionally, the culture consisted of mainly gland organoids, morphologically similar to organoids observed in the literature (Turco et al., 2017) whereas in earlier passages, gland isolates remained. Despite a similar induction of *PAEP* in cyclically differentiated organoids, morphologically the organoid cultures were different. Regardless of being set up from P0, majority of the culture grew into organoids. With limited space to expand, the organoids darkened, and the gel began to breakdown at the edges. At the end of the luteal phase, if implantation does not take place, the functional layer is broken down and shed. As there was no breakdown after differentiation, the organoids could not regrow. By the end of C3, the organoids had been cultured for 24 days but Matrigel is reported to be stable for only 14 days. Therefore, P2 was chosen for all future differentiation experiments.

Immunofluorescence of P2 organoids further demonstrated that organoids behaved as endometrial glands. Epithelial specific structural markers E-cadherin and EpCAM labelled positively along the plasma membrane of the organoids and cytokeratin labelled the cytoskeleton inside the cell. These markers highlighted the changes in structure of the organoids with differentiation. Similarly, the glands in the endometrium change from a simple tubular structure to a spiral, coiled shape (Garry et al., 2010, Tempest et al., 2020). The secretory transformation of the glands was also demonstrated in the organoids by secretion of glycodelin into the lumen. PGR is downregulated in the mid-secretory phase of the cycle (Wang et al., 1998) and this was observed with differentiation in the organoids.

Gland EpC are descendants of a single stem/progenitor cells (Tanaka et al., 2003, Tempest et al., 2020). Likewise, the organoids form from one progenitor cell. Therefore, the clonal capacity of the glands can be studied using OFE assay. Patient characteristics including number of 1st trimester losses did not correlate with number of progenitor cells or with the responsiveness of organoids to differentiation signals. Interestingly, RPL is associated with a deficiency in mesenchymal stem cells and an aberrant decidual response (Lucas et al., 2016). These observations suggest glandular responses in miscarriage are different to that of the EnSC.

In summary, my analysis has identified a robust differentiation method for future experiments of gland organoids and a further understanding of epithelial stem/progenitor cell's role in patient characteristics. These protocols can now be used to create RMM specific organoids to study glandular defects.

Chapter 5:
Endometrial Gland Organoids as a Model for Recurrent Missed Miscarriage

5.1 Introduction

Organoids established from adult-stem cells have great potential in modelling human disease (Kim et al., 2020). Organoids can mimic pathologies at the organ level, making them more advantageous to investigate mechanisms of disease than traditional cell culture methods (Rossi et al., 2018). Further, patient-specific organoids can be used for drug testing and personalised medicine. So far, organoids from different tissues have been used to study infectious diseases, heritable genetic disorders, and many cancers (Kim et al., 2020).

Recently, endometrial disorders have been successfully modelled in patient-derived gland organoids. Using the same organoid culturing conditions optimised for healthy endometrium (Boretto et al., 2017), endometriosis organoids from ectopic implants at different sites and clinical stages were generated, in parallel with patient-matched eutopic endometrial gland organoids (Boretto et al., 2019). In comparison to eutopic endometrial gland organoids, altered signalling pathways were discovered in the endometriosis organoids. Also, endometrial cancer organoids have been derived from precancerous and tumour tissue (Turco et al., 2017, Boretto et al., 2019). Several challenges were encountered while trying to capture the phenotype of endometrial cancer of different grades, including lower OFE and limited organoid expansion as the non-malignant cells tend to outcompete cancer cells in culture (Boretto et al., 2019). These hurdles were addressed by adapting the culture medium for cancer organoids, enabling the recapitulation of the mutational landscape and histological features of primary tumours *in vitro* (Boretto et al., 2019). Notably, the grade and the phenotype of cancers were maintained upon injection of cells derived from organoids into the uterine horn of mice. Moreover, endometrial organoids were found to replicate patient-specific drug responses, and therefore amenable to drug screening (Boretto et al., 2019).

The primary function of endometrial glands is to provide histotrophic nutrition for the developing conceptus prior to the onset of placental perfusion at the end of the first trimester of pregnancy (Kelleher et al., 2019). In Chapter 3, I provided evidence that midluteal endometrial glands may differ between control subjects and RMM patients. In the subsequent chapter, I optimised endometrial gland organoid cultures but found no obvious differences in OFE or differentiation capacity between endometrial gland organoids established from control or RPL patients. In this chapter, I explore if

endometrial gland organoids can be used to model *in vivo* glandular defects associated with RMM and to dissect potential drivers and mechanisms of disease.

5.2 Results

5.2.1 Epithelial progenitor cell population in RMM

The transcriptomic analysis presented in Chapter 3 suggested that RMM is associated with metabolic perturbations in endometrial glands prior to conception, characterised foremost by increased oxidative phosphorylation, potentially a consequence of increased FAO. Increased oxidative phosphorylation, reflecting metabolic dependence on FAO, is a hallmark of quiescent adult stem cells, including in skeletal muscle and brain (Ryall et al., 2015, Knobloch et al., 2017). As described in Chapter 4, patient-specific organoids can be used to quantify the endometrial epithelial stem/progenitor cell population in patient samples.

To examine if RMM glands have more stem/progenitor cells, OFE assays were performed on gland organoids established from 10 control and 10 RMM biopsies. Patient demographics listed in Appendix Table 1.6. Organoids were grown to P1, recovered from the Matrigel, and enzymatically and mechanically dissociated into single cells as described previously (Turco et al., 2017). From each sample, 100 endometrial EpC were seeded in 5 µl Matrigel droplets and cultured for 10 days (Fig 5.1 and 2). The total number of organoids were counted and OFE calculated. The OFE of RMM samples was 64% higher when compared to control samples (Fig. 5.3a). The average [SD] OFE in RMM compared to control samples was 8.54% [3.42] versus 5.22% [2.57], respectively; $P < 0.05$, Welch's *t* test. Thus, the oxidative phosphorylation gene signature associated with RMM glands could potentially be accounted for by a significantly higher abundance of epithelial stem/progenitor cells.

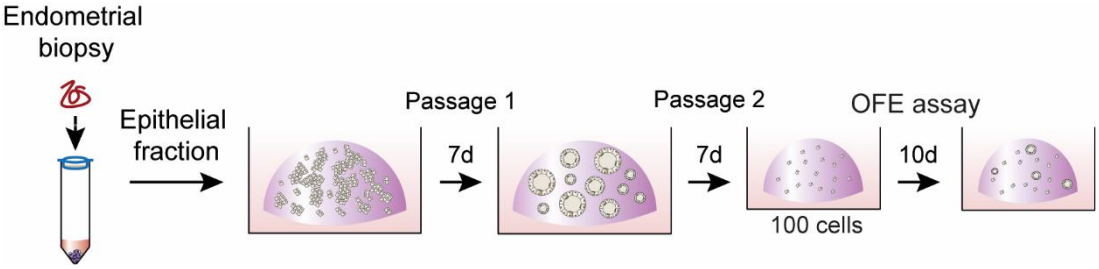

Figure 5.1. ***OFE assay at P2.***

Schematic representation of OFE assay at P2. Endometrial biopsies were mechanically and enzymatically digested, and the epithelial fraction was collected in the strainer. Organoids were grown then to P2 and harvested from Matrigel using Cell Recovery solution and broken down mechanically and enzymatically with TrypLE Select. Cells were counted and resuspended at a density of 100 cells per 5 µl Matrigel droplets. Organoids were grown for 10 days in ExM and then imaged, counted and OFE calculated.

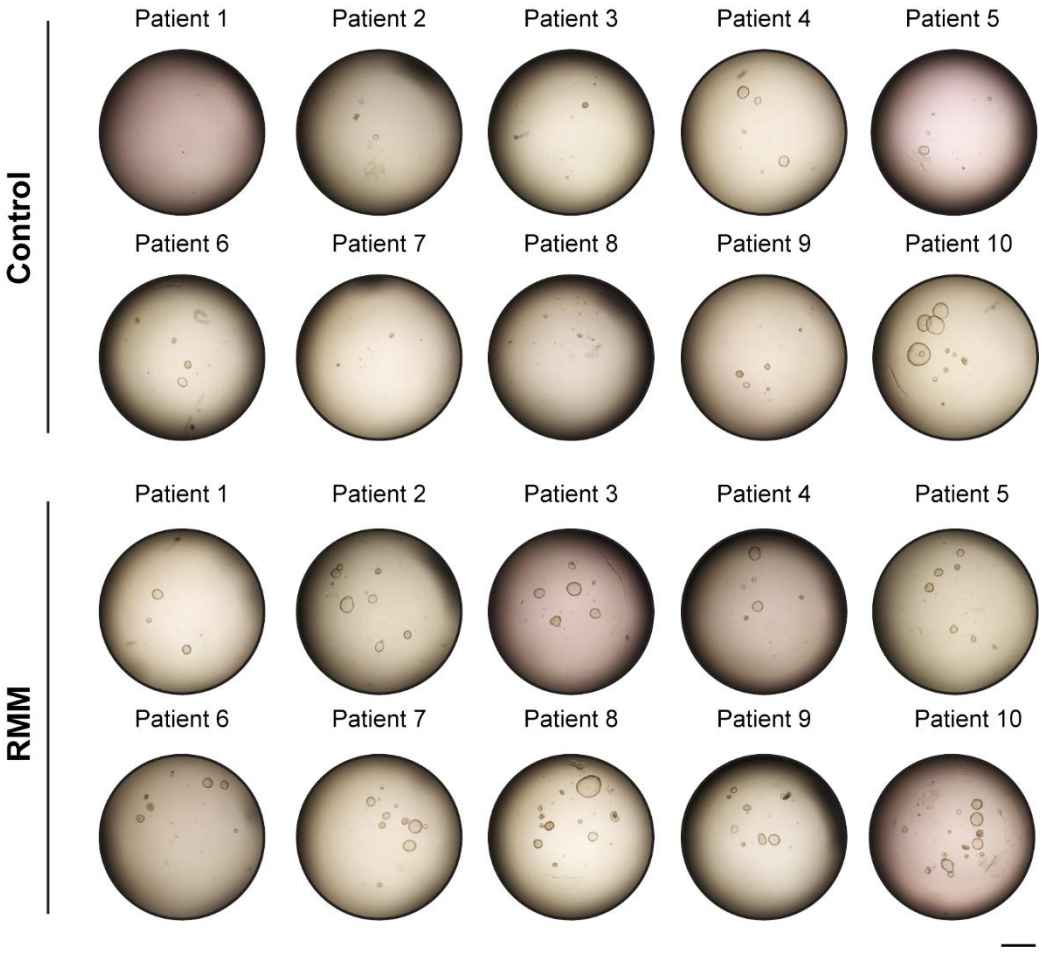

Figure 5.2. ***OFE assay of control and RMM endometrial gland organoids.*** Representative images of OFE assay at day 10 in cultures established from 10 control and 10 RMM endometrial biopsies. Scale bar = 1 mm.

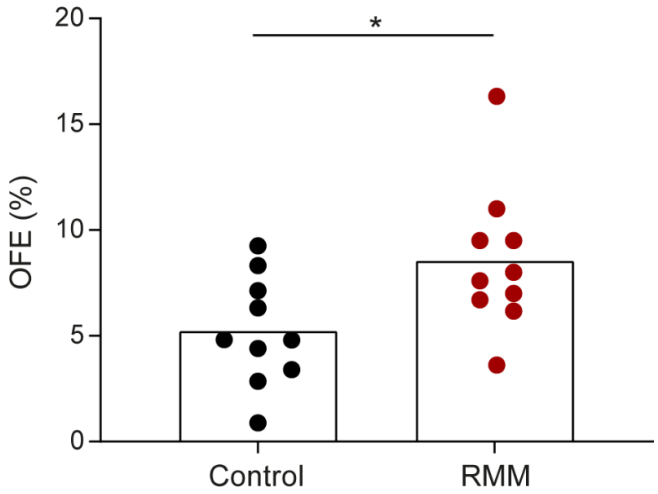

Figure 5.3. ***RMM endometrial glands harbour more epithelial stem/progenitor cells.***

OFE (%) at P2 of control subjects (n=10, black dot) and RMM patients (n=10, red dot), using a seeding density of 100 cells per 5 µl Matrigel droplet. Dots represent OFE from different patient biopsies. Bars show mean. * indicates $P < 0.05$ (Welch's *t* test, normal distribution tested with Shapiro-Wilk test).

5.2.2 The transcriptome of control and RMM organoids

To test the hypothesis that endometrial glands are intrinsically different in RMM, RNA-seq was performed on undifferentiated and differentiated organoid cultures. To mimic the endocrine environment of pregnancy, the same differentiation protocol was used as described by Turco *et al* (2017). Briefly, gland organoids were established from mid-luteal endometrial biopsies from control subjects (n=4) and RMM patients (n=4). Patient demographics are listed in Appendix Table 1.7. Gland organoids at P2 were first grown in ExM for 4 days, followed by differentiation for 6 days in 'pregnancy medium' consisting of ExM supplemented with E_2, 8-bromo-cAMP, P_4, hCG, hPL and PRL (Fig. 5.4 and 5). In parallel, undifferentiated gland organoids were maintained in ExM for 10 days as control cultures. Total RNA was extracted and sequenced. The data were analysed in collaboration with Dr Tauqeer Alam, a bioinformatician.

The transcriptomic profiles of gland organoids were subjected to PCA to examine clustering of samples by patient group and treatment. This analysis showed good separation of samples in PC1, accounting for 38% of variance, by treatment but not patient group (Fig. 5.6a). We speculated that separation of samples by patient group could be masked by an underlying confounding factor. To explore this possibility, the treatment effect was first removed using the removeBatchEffect function from the limma package in R. PCA now showed pairwise grouping of undifferentiated and differentiated organoids but no apparent separation between control and RMM organoids (Fig. 5.6b). Next, the patient group effect was removed from the data and PCA repeated. As expected, the samples now separated unequivocally by treatment, captured by PC1 with 39% variance (Fig. 5.6c). Moreover, we identified an unknown factor, captured by PC2 with 26% variance, which separated our cohort of samples into two distinct groups, each consisting of gland organoids from control subjects and RMM patients (Fig. 5.6c). The batch effect that caused separation of the gland organoids into two groups, independently of treatment or patient group, did not appear to be related to the age of the women, cycle day of the biopsies, number of previous miscarriages, or days of organoids in culture (Appendix Table 1.6). Importantly, removal of this unexplained batch effect from the data yielded a PCA plot showing very clear grouping of samples by treatment (PC1 with 44% variance) and patient group (PC2 with 15% variance) (Fig. 5.6d).

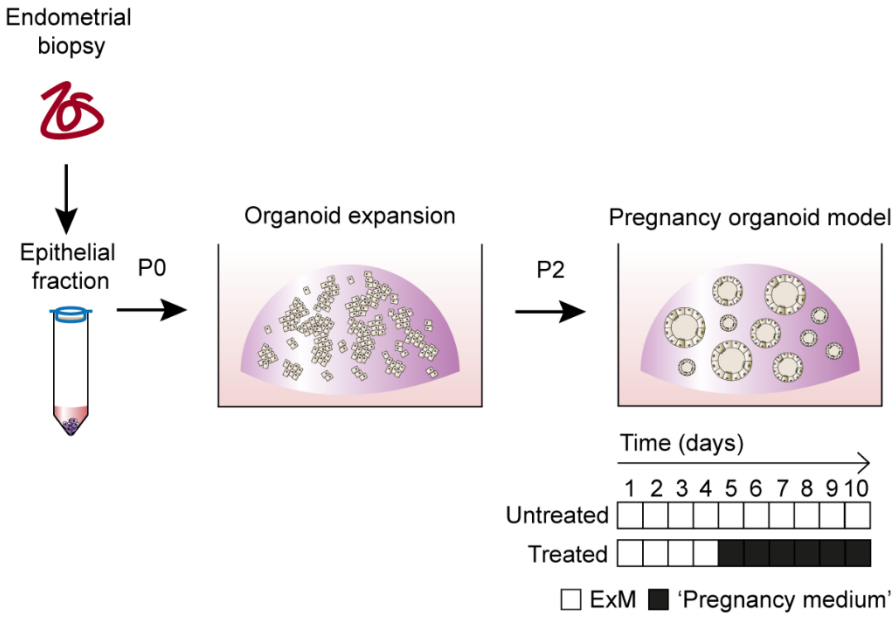

Figure 5.4. ***Schematic representation of the pregnancy assay.***

Schematic representation of organoid culture from endometrial biopsies for a pregnancy assay time-course. Endometrial gland organoids were grown to passage 2 and either left untreated (ExM) for 10 days or grown for 4 days in ExM and then treated for 6 days with a 'pregnancy medium,' containing ExM supplemented with E_2, 8-bromo-cAMP, P_4, hCG, hPL and PRL.

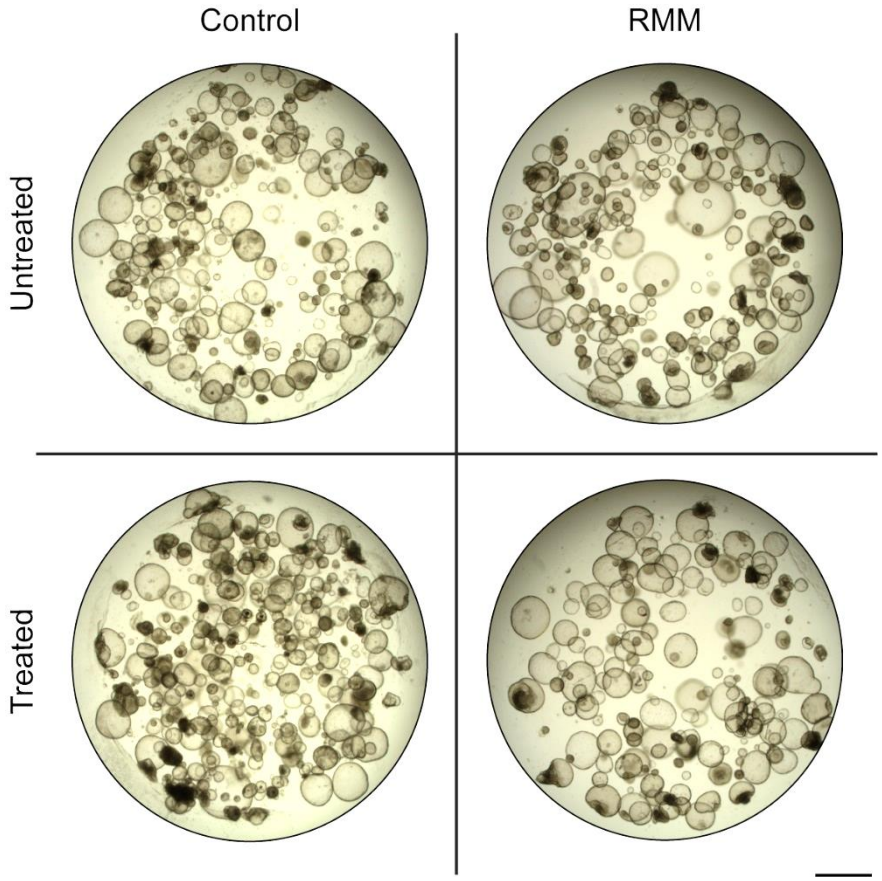

Figure 5.5. ***Representative images of control and RMM pregnancy assay organoids.***

Representative images of untreated and treated gland organoids of control and RMM endometrial biopsies. Scale bar = 1 mm

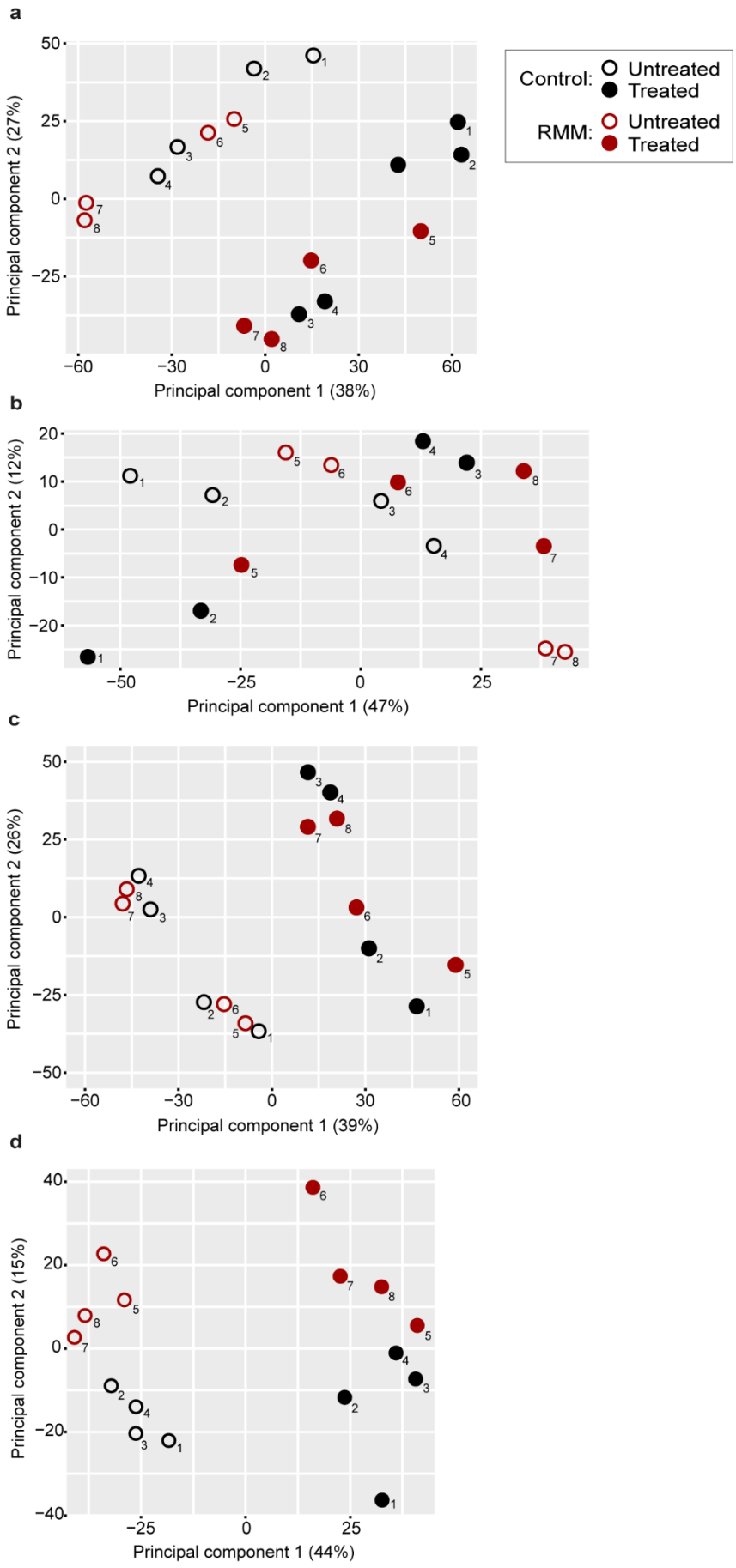
a
Control: Untreated
Treated
RMM: Untreated
Treated
Principal component 2 (27%)
Principal component 1 (38%)
b
Principal component 2 (12%)
Principal component 1 (47%)
c
Principal component 2 (26%)
Principal component 1 (39%)
d
Principal component 2 (15%)
Principal component 1 (44%)

Figure 5.6. ***RMM gland organoids group based on patient group and treatment.***
PCAs of RNA-seq data from untreated (open dot) and treated (closed dot) organoids of control (black dot; 1-4) and RMM (red dot; 5-8) endometrial biopsies (n=4 per group).

a) Grouping shown based on PC1 and PC2.

b) Grouping shown based on PC1 and PC2 after removal of treatment effect.

c) Grouping shown based on PC1 and PC2 after removal of patient effect.

d) Grouping shown based on PC1 and PC2 after correcting for batch effect.

Next, differential gene expression analyses (fold-change > 2 and FDR-corrected $P < 0.05$) were performed on undifferentiated and differentiated glands. Using these stringent criteria, 1905 genes were found to be differentially expressed upon differentiation with 1135 (59.6%) and 770 (40.4%) up- and down-regulated, respectively (Fig. 5.7). Amongst the genes downregulated upon differentiation were several encoding secretory signalling proteins, including including WNT ligands (*WNT4*, *WNT6*, *WNT7B* and *WNT10A*), members of the FGF family (*FGFR3*, *FGF9*, *FGF18*, and *FGF19*) and TGF-β superfamily (*TGFB2*, *TGFB3*, *BMP3*, *BMP4*, and *BMP7*). In addition, several genes implicated in the Notch signalling pathway were also downregulated, including mastermind like transcriptional coactivator 2 and 3 (MAML2 and MAML3) and SOX9 (Sinha et al., 2021). Notably, SOX9 is a key transcription factor implicated in the regulation of proliferation and differentiation of epithelial stem/progenitor cell populations in several tissues, including the endometrium (Cousins et al., 2021). Another striking observation was the loss of multiple genes involved in cell-cell interactions, including 17 genes encoding protocadherins. Not surprisingly, downregulated genes were enriched in GO categories such as 'cell-cell adhesion', 'cell communication' and 'cell morphogenesis' as well GO terms related to stem cells (e.g. 'stem cell differentiation'), cell cycle (e.g. 'regulation of cell population proliferation') and signalling (e.g. 'canonical Wnt signalling', 'response to growth factor' and 'Notch signalling pathway') (Fig. 5.8a).

Several genes induced upon gland organoid differentiation encoded transcription factors implicated in endometrial differentiation [e.g. *ATF3* (Cheng et al., 2017), *FOXO1 (*Nakamura *et al., 2013)*, *FOSL2*, *POU5F1* (OCT4), *PPARG* (Chi et al., 2020) and *ZBTB16* (PLZF) (Fahnenstich et al., 2003)], cyclin dependent kinase inhibitors (*CDKN1C*, *CDKN2B* and *CDKN2D*), stress/senescent-associated inflammatory mediators [(e.g. *IL1A*, *IL6*, *CXCL8, GDF15* (Rawlings et al., 2021a)], and canonical markers of glandular differentiation [e.g. *PAEP* (Seppälä et al., 2002), *CXCL14* (Mokhtar et al., 2009), *SPP1* (Singh and Aplin, 2009), and *HBEGF* (Leach et al., 1999)] or endometrial receptivity [e.g. *LIF* (Stewart et al., 1992), *ARG2* (Altmäe et al., 2017) and *MT1F* (Hu et al., 2014)]. Further, 35 members of the solute carrier family, which regulate membrane transport, were also induced upon gland organoid differentiation. GO analysis of induced genes showed enrichment of 'Epithelial cell differentiation', 'Response to corticosteriods', 'Response to cAMP', 'Response to stress', 'Inflammatory response', 'Female pregnancy', 'Cilium movement' and 'Negative regulation of growth' (Fig. 5.8b). This expression profile suggests that gland organoids, like their *in vivo* counterparts, mount an acute stress response following

cell cycle arrest, which in turn drives epithelial differentiation and senescence. In agreement, 257 genes upregulated upon gland organoid differentiation were also induced in endometrial glands upon progression of the early- to late-luteal phase of the cycle (FDR-corrected $P < 0.05$; Fig. 5.9). GO analysis of this network of genes revealed enrichment of terms such as 'Negative regulation of growth,' 'Cell differentiation,' 'Response to stress' (Fig. 5.10). As shown in Figure 5.9, most of the genes induced upon glandular differentiation *in vitro* and *in vivo* peak in expression during the midluteal phase of the cycle (LH+8), although a subset of genes are maximally expressed in late secretory endometrium (LH+11). I also identified 83 genes repressed upon gland organoid differentiation as well as endometrial glands upon progression of the luteal phase (Fig. 5.9). However, this gene set was not enriched in any GO category.

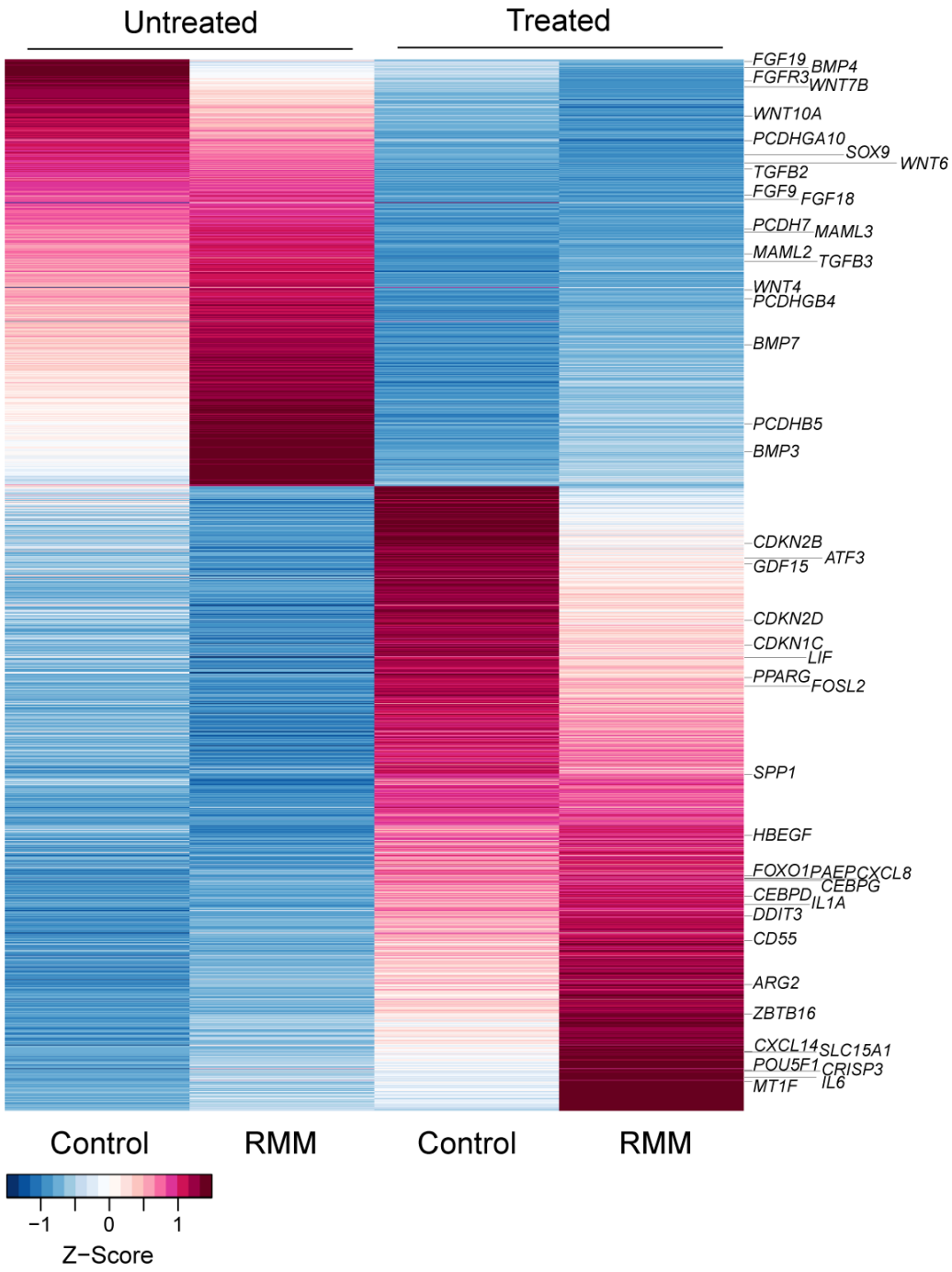

Figure 5.7. ***Heatmap of DEGs between untreated and treated organoids.***
Heatmap of RNA-seq data showing DEGs (Z-scores) between treatment after FDR correction (Fold-change > 2 and Benjamini-Hochberg, FDR-corrected $P < 0.05$).

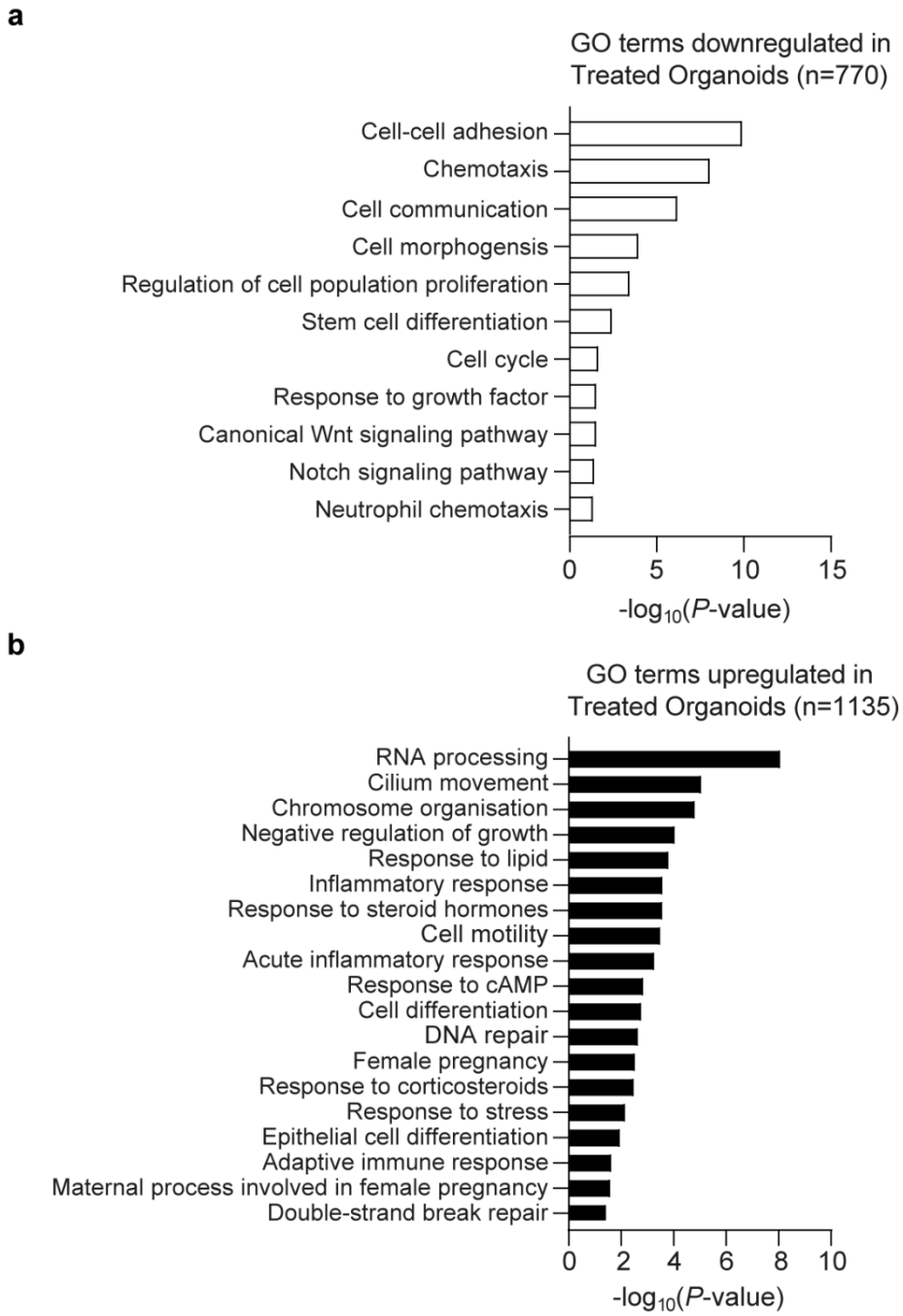

Figure 5.8. ***GO analysis of DEGs upregulated and downregulated in treated gland organoids.***

Bar plots showing significantly enriched GO terms (FDR-corrected $P < 0.05$) related to biological processes in treated gland organoids. DEGs with FDR-corrected $P < 0.05$ were used as input for the analysis (number of genes in brackets).

a) GO terms downregulated in treated gland organoids compared to untreated.

b) GO terms upregulated in treated gland organoids compared to untreated.

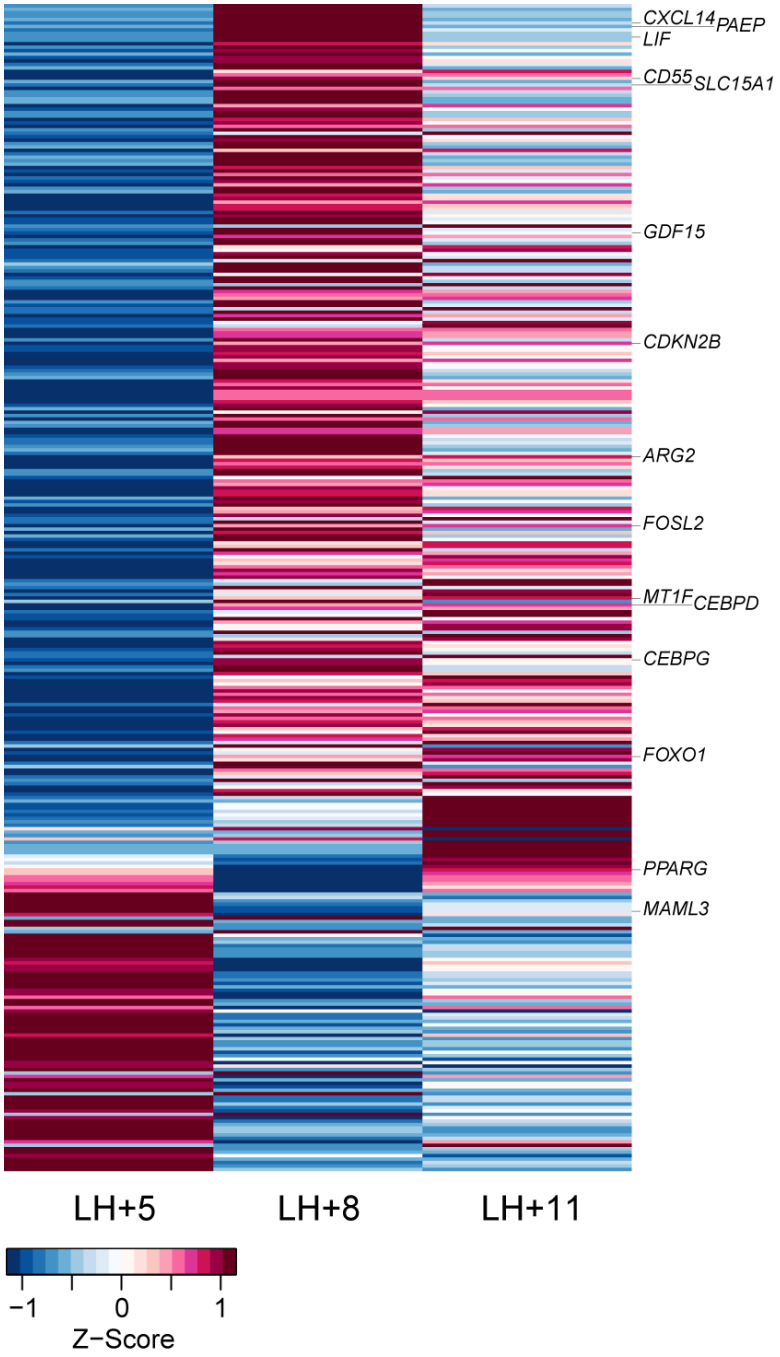

Figure 5.9. ***Genes induced upon differentiation of gland organoids are temporally regulated during the luteal phase*** **in vivo*****.***

Heatmap showing relative expression (Z-scores) of treatment induced genes of gland organoids that are significantly regulated during the luteal phase of the cycle in endometrial glands (FDR-corrected $P < 0.05$).

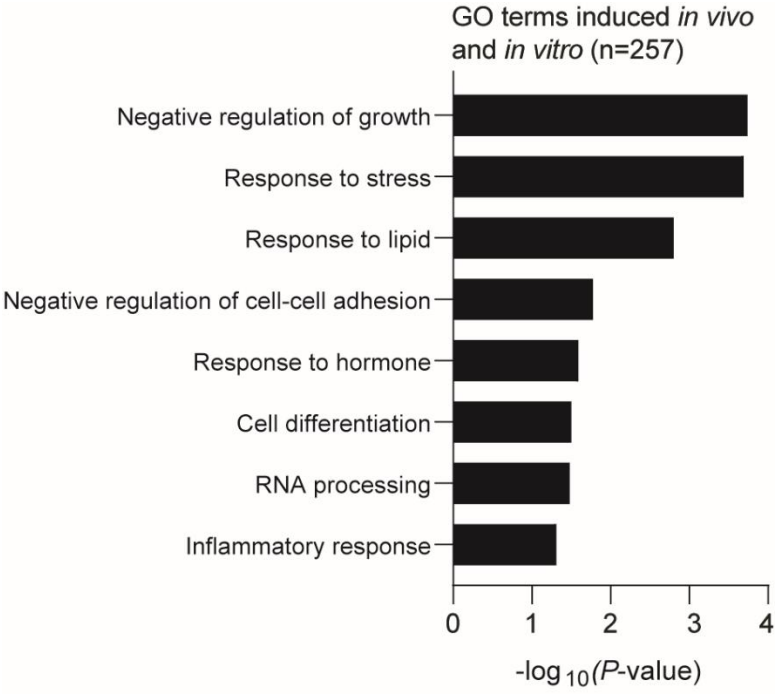

Figure 5.10. ***GO analysis of temporally regulated glandular genes induced upon organoid differentiation.***

Bar plots showing significantly enriched GO terms (FDR-corrected $P < 0.05$) related to biological processes induced across the luteal phase of the cycle in glands and in treated gland organoids. DEGs (n=257) with FDR-corrected $P < 0.05$ were used as input for the analysis.

Next, I mined for genes that were differentially expressed between control and RMM organoids. Using the same stringent criteria (fold-change > 2 and FDR-corrected $P < 0.05$), 444 genes were found to be differentially expressed between control and RMM gland organoids with 221 (49.8%) and 223 (50.2%) genes up- and down-regulated, respectively (Fig. 5.11). Out of these 444 DEGs, 186 (41.9%) were also regulated upon differentiation of gland organoids. GO analysis of genes upregulated in RMM organoids did not reveal informative biological categories. However, notable genes enriched in RMM gland organoids included *LGR5*, *POU5F1*, and *PPARGC1A*. *LGR5* encodes a receptor for R-spondins that potentiates the canonical Wnt signalling pathway and acts as an epithelial stem cell marker in multiple tissues (Xu et al., 2019). Further, $LGR5^+$ stem/progenitor cells are indispensable for uterine gland development in mice (Seishima et al., 2019). *POU5F1* encodes OCT4, a transcription factor critical for embryonic stem cell pluripotency (Zeineddine et al., 2014). In gland organoids, *POU5F1* is upregulated upon differentiation, although there is no evidence that expression of this transcription factor changes in endometrial glands across the menstrual cycle. *PPARGC1A* (coding PPARG coactivator 1 alpha) is a key metabolic gene. PPARGC1A is a transcriptional co-activator for nuclear receptors with essential roles in adaptive thermogenesis, and regulation of glucose and fatty acid metabolism (Liang and Ward, 2006).

In contrast to genes upregulated in RMM organoids, downregulated genes were enriched in multiple GO categories, including ‘cell differentiation’, ‘epithelial development’, and ‘epithelial-mesenchymal cell signalling’ (Fig. 5.12). Genes repressed in RMM gland organoids included cell cycle inhibitors (*CDKN1A* and *CDKN2B*) and multiple transcription factors involved in development and differentiation [e.g. *FOXA1* (Friedman and Kaestner, 2006), *FOXC1* (Han et al., 2017), *LEF1* (Shelton et al., 2012), *ID3* (Sikder et al., 2003), *HES5* (Ohtsuka et al., 1999), and *NR2F1* (Sosa et al., 2015)]. Downregulation of LEF1 (coding lymphoid enhancer binding factor 1) points towards perturbed Wnt signalling (Shelton et al., 2012) whereas loss of *HES5* (Hes family bHLH transcription factor 5) is indicative of an altered Notch pathway (Ohtsuka et al., 1999). Additional notable downregulated genes include *WNT7A, LIFR* (LIF receptor subunit alpha), and *BMP4*. Wnt7a is critical regulator of postnatal uterine gland morphogenesis and function in mice (Dunlap et al., 2011). Out of the 223 genes repressed in RMM, 88 (39.5%) were significantly regulated upon differentiation of gland organoids.

Finally, undifferentiated and differentiated organoids were established from eight RMM patients (n=8) and control subjects (n=8) for RT-qPCR validation of the RNA-seq analysis (Fig. 5.13). Patient demographics are presented in Appendix Table 1.8. The RNA-seq analysis indicated that *FGF19* and *POU5F1* are differentially expressed between the patient groups and in response to treatment. In agreement, *FGF19* transcript levels were significantly lower in RMM organoids when compared to control organoids, irrespective of differentiation status (FDR-corrected $P < 0.05$, multiple Mann Whitney test). Further, *FGF19* was significantly downregulated in differentiated control organoids (FDR-corrected $P < 0.05$, multiple Wilcoxon test) but not RMM cultures (Fig. 5.13a). As expected, *POU5F1* was upregulated in differentiated organoids (FDR-corrected $P < 0.05$, multiple Wilcoxon test), but the magnitude of induction was significantly higher in RMM compared to control organoids (FDR-corrected $P < 0.01$, multiple Mann Whitney test) (Fig. 5.13b). *ACADSB* encodes for short/branched chain specific acyl-CoA dehydrogenase and was induced upon differentiation as observed in the RNA-seq data (FDR-corrected $P < 0.01$, multiple paired *t* test) and like, *POU5F1* the level of induction was significantly more pronounced in RMM organoids (FDR-corrected $P < 0.05$, multiple unpaired *t* test) (Fig. 5.13c). However, *LGR5* expression pattern was found not to be different in undifferentiated or differentiated organoids established from control subjects and RMM patients upon validation (Fig. 13d). RNA-seq analysis indicated higher expression of this gene in RMM gland organoids.

Taken together, the data suggests that RMM is associated with intrinsic defects in the endometrial epithelial stem/progenitor cell population, which impact on the stemness, metabolism, cell cycle regulation and differentiation potential of its progeny.

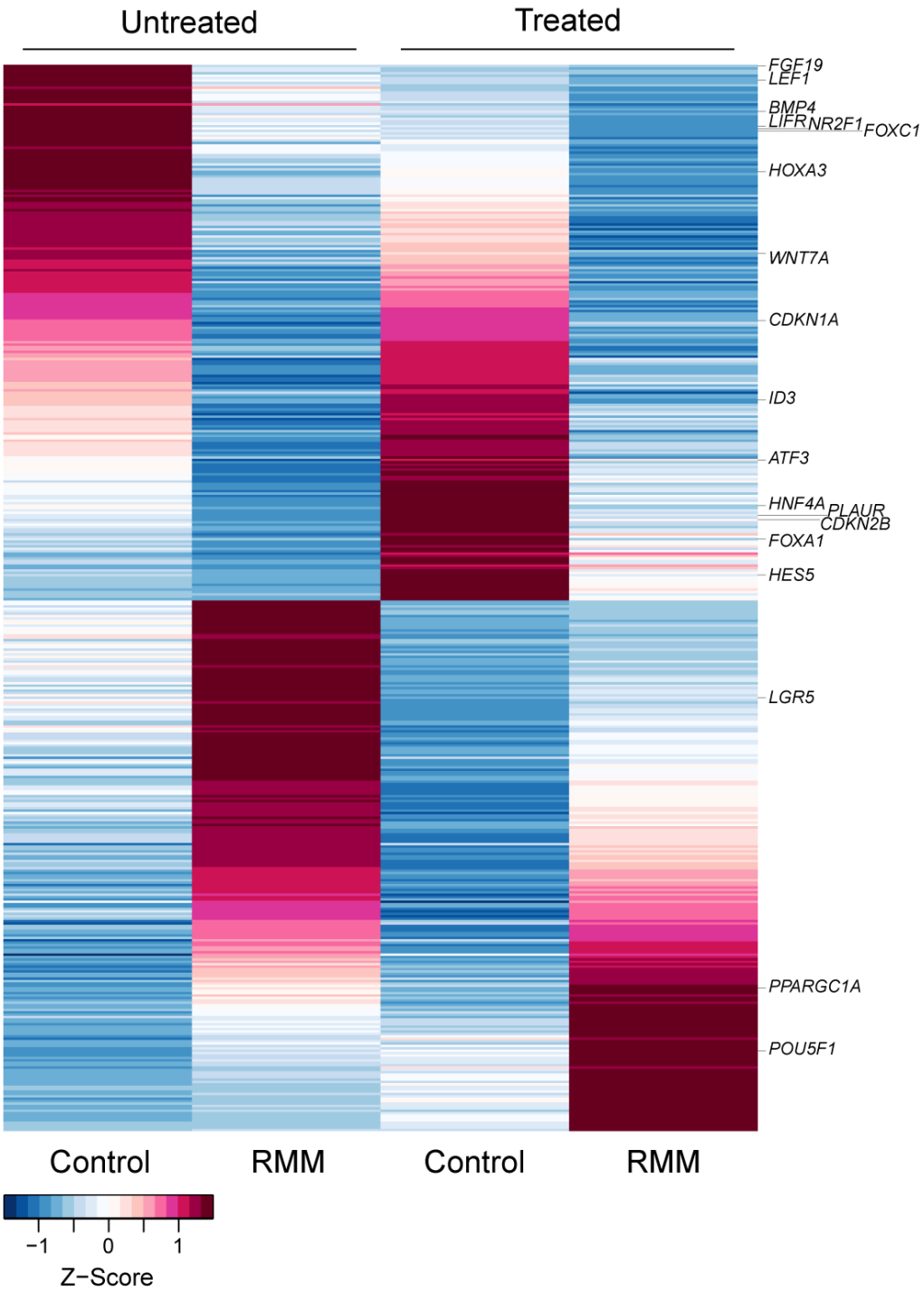

Figure 5.11. ***Heatmap of DEGs between control and RMM organoids.***

Heatmap of RNA-seq data showing DEGs (Z-scores) between patient group after FDR correction (Fold-change > 2 and Benjamini-Hochberg, FDR-corrected $P < 0.05$).

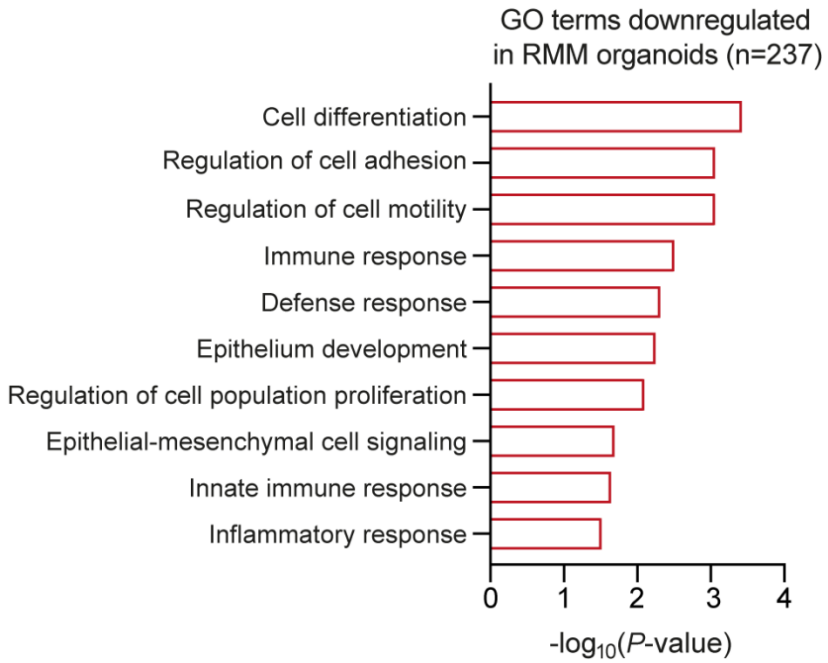

Figure 5.12 ***GO analysis of DEGs downregulated in RMM gland organoids.***
Bar plots showing significantly enriched GO terms (FDR-corrected $P < 0.05$) related to biological processes repressed in RMM gland organoids. DEGs (n=237) with FDR-corrected $P < 0.05$ were used as input for the analysis.

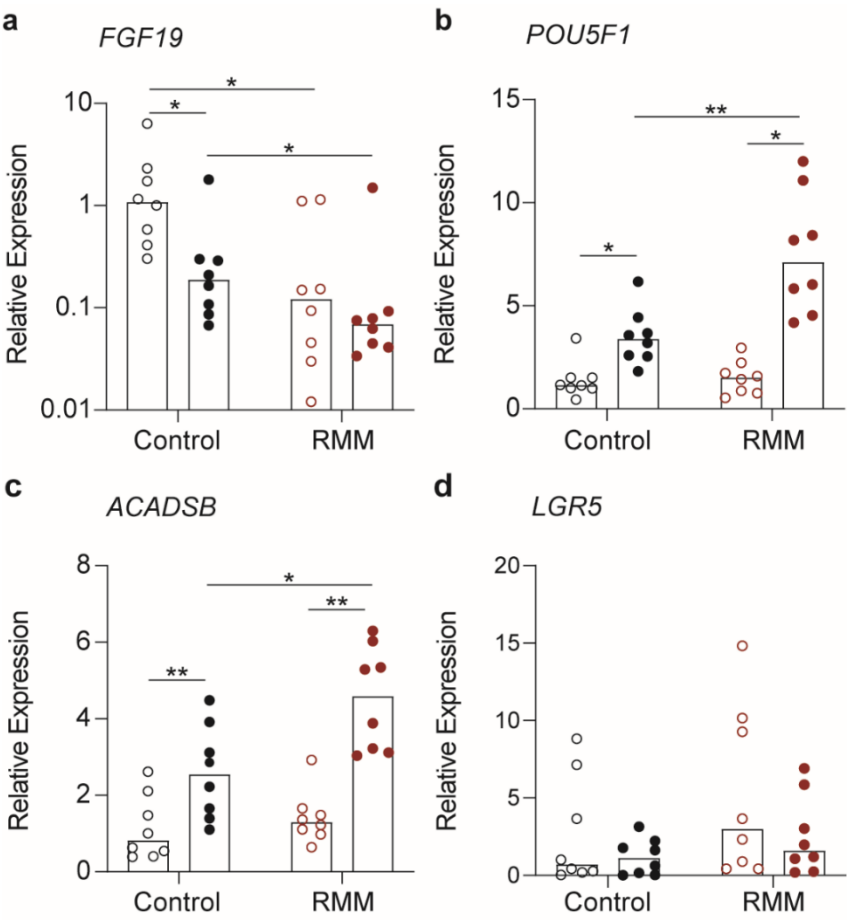

Figure 5.13. ***Validation of gland organoid RNA-seq.***

Four DEGs transcript levels were quantified by RT-qPCR in untreated (open dot) and treated (closed dot) organoids from control (black) and RMM (red) endometrial biopsies. Dot represents individual patients (n=8 per group and treatment). Bars show median. Normal distribution was tested with Shapiro-Wilk test

a) Transcript levels of *FGF19.* * indicates FDR-corrected $P < 0.05$. Multiple Wilcoxon test was used for treatment comparison and Multiple Mann Whitney test used for patient group comparison.

b) Transcript levels of *POU5F1.* * and ** indicates FDR-corrected $P < 0.05$ and $P < 0.01$, respectively. Multiple Wilcoxon test was used for treatment comparison and Multiple Mann Whitney test used for patient group comparison.

c) Transcript levels of *ACADSB.* * and ** indicates FDR-corrected $P < 0.05$ and $P < 0.01$, respectively. Multiple paired *t*-test was used for treatment comparison and Multiple unpaired *t*-test used for patient group comparison

d) Transcript levels of *LGR5.*

5.2.3 The RMM gland gene signature is maintained in organoid cultures

Although the transcriptomic analysis of gland organoids revealed that RMM is associated with much more pronounced cellular perturbations than expected, the *in vivo* gene signature was not recapitulated when using stringent criteria to identify DEGs. However, Figure 5.14 shows a heatmap of the Z-scores of the core gene signature identified by RNA-seq of laser-captured glands in organoids. Out of the 30 core genes, 19 (63.3%) were upregulated in RMM organoids, suggesting the disease signature is partly conserved in the gland organoids. The majority of these genes (n=17) were upregulated in the undifferentiated RMM gland organoids, with only 2 core genes induced upon treatment. Notably, 8 out of the 10 genes relating to oxidative phosphorylation were upregulated in the RMM compared to control organoids.

Based on metabolic modelling, I postulated that oxidative phosphorylation and FAO are upregulated in RMM glands (Chapter 3). Hence, I investigated the relative expression of FAO genes and genes encoding complex I proteins in the electron transport chain in control and RMM organoids (Fig. 5.15). As is the case *in vivo* (Fig. 5.15a), a majority of complex I genes were upregulated in RMM organoids, independently of differentiation status. Likewise, genes involved in FAO were unambiguously upregulated in RMM organoids, even more so than that *in vivo* (Fig. 5.15b). Importantly, the relative expression of *CPT1A* and *CPT1B*, encoding for the rate-limiting enzymes in FAO (Zammit, 2008), is higher in both organoids and endometrial glands *in vivo* (Fig. 5.15b).

Figure 5.14. ***RMM gland gene signature in RMM gland organoids.***

Heatmap of organoid RNA-seq data showing relative expression (Z-scores) of upregulated DEGs in RMM glands. * indicates genes involved in the electron transport chain and mitochondrial proteins.

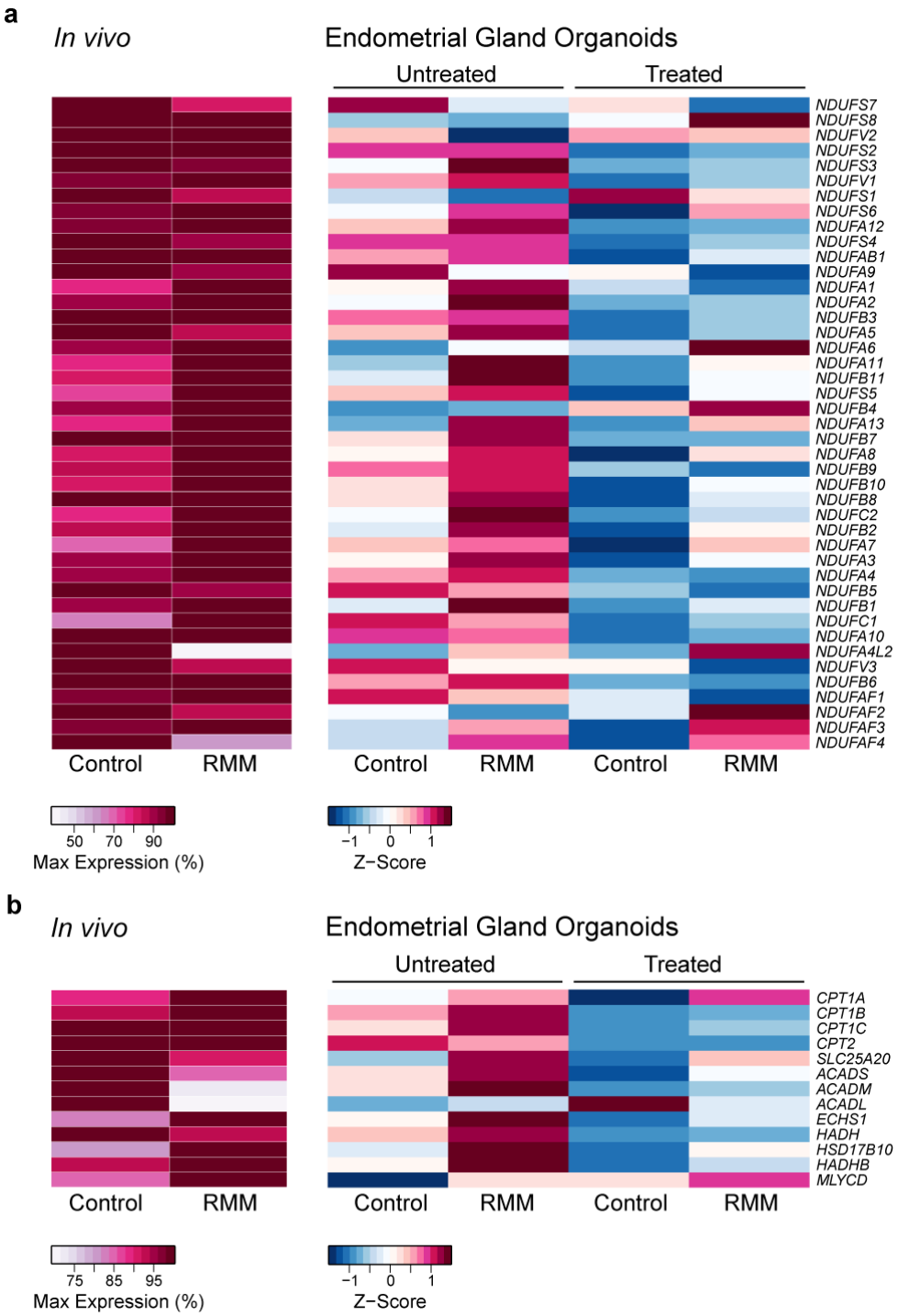

Figure 5.15. ***Heatmaps of complex I and FAO gene expression.***

a) Heatmaps showing relative expression of complex I genes in gland *in vivo* (max Expression (%)) and in untreated and treated gland organoids (Z-scores) from control and RMM endometrial biopsies.

b) Heatmaps showing relative expression of FAO genes in gland *in vivo* (max Expression (%)) and in untreated and treated gland organoids (Z-scores) from control and RMM endometrial biopsies.

5.2.4 Marker genes of epithelial cell states in control and RMM organoids

I extended the mining of organoid transcriptomic profiles to include marker genes of different EpC states identified first in endometrial assembloids (Rawlings et al., 2021a). Endometrial assembloids, consisting of gland organoids and primary EnSC were established in our lab to mimic the mid-luteal implantation window. Although it is well established that gland organoids harbour specialist ciliated EpC (Turco et al., 2017, Fitzgerald et al., 2019, Haider et al., 2019), single cell transcriptomics of assembloids revealed that non-ciliated EpC give rise to two distinct subpopulations upon differentiation, termed 'differentiated' and 'senescent' EpC (Rawlings et al., 2021a). Further, cross referencing with genome-wide expression profiles of the endometrium across the cycle showed that marker genes of differentiated EpC transiently peak during the mid-luteal phase of the cycle. In parallel, multiple senescent EpC marker genes are induced but their expression continues to rise during the late-secretory phase (Rawlings et al., 2021a). In addition to marker genes of different subpopulations (ciliated, differentiated, and senescent cells), I also mined the transcriptome data for putative epithelial stem/progenitor cell markers genes reported in the literature (Valentijn et al., 2013, Turco et al., 2017, Tempest et al., 2020, Cousins et al., 2021).

The heatmap presented in Figure 5.16 revealed coordinated dysregulation of marker genes in differentiated RMM organoids. The pattern suggests that differentiation of RMM organoids results in relative deficiency in ciliated and senescent epithelial subpopulations when compared to control organoids and excess of differentiated.

In agreement with the OFE assay (Fig. 5.2), the relative expression of six putative stem/progenitor cell markers was higher in the RMM organoids, four in undifferentiated cultures (*AXIN2, PROM1, LRIG1 and LRG5*) and two upon differentiation (*FUT4* and *POU5F1*). Prominin 1 (encoded by *PROM1*, also known as CD133) is a transmembrane glycoprotein widely expressed on adult stem cells, where it is thought to function in maintaining stem cell properties by supressing differentiation (Li, 2013). LRIG1 (leucine rich repeats and immunoglobulin like domains 1) is a negative regulator of receptor tyrosine kinase signalling (Laederich et al., 2004). This protein has been described as gatekeeper to exit from quiescence in adult stem cells (Marqués-Torrejón et al., 2021). In the brain, it marks quiescent stem cells that are poised for cell cycle re-entry and subsequent transition into activated and proliferative adult neural stem cells. *PROM1* and *LRIG1* are expressed in

endometrial gland organoids (Turco et al., 2017), but no functional studies have been conducted to validate them as an epithelial endometrial stem/progenitor cell marker.

Taken together, the coordinated differences in the expression of these marker genes in patient-specific organoids reinforce my observation that RMM is associated with more naïve or quiescent epithelial stem cells. Further, differences in the state of epithelial stem/progenitor cells in the endometrium profoundly impact on subsequent specification of glandular EpC into functionally distinct subpopulations upon differentiation.

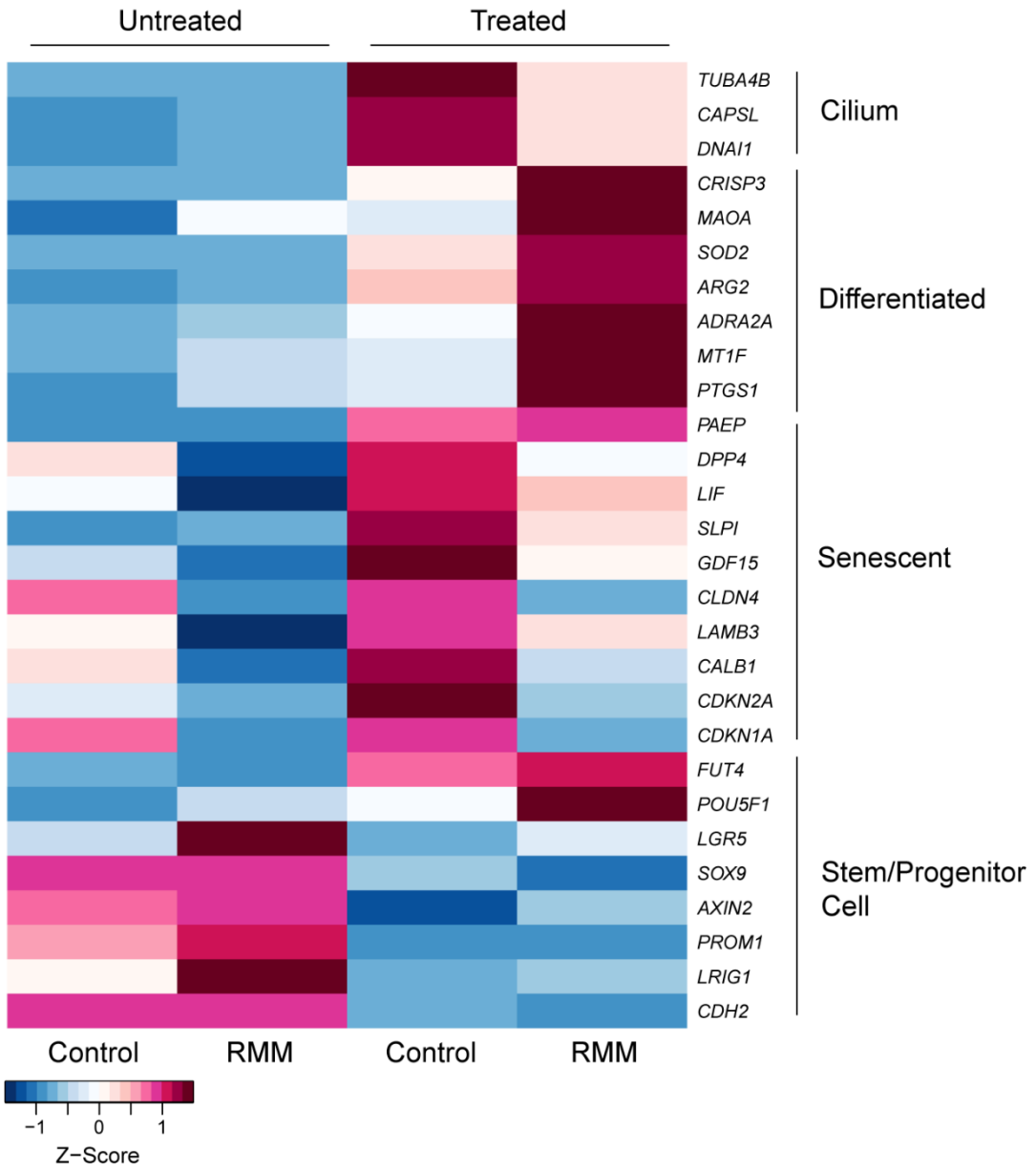

Figure 5.16. ***Relative expression of marker genes of epithelial subpopulations in RMM organoids.***

Heatmap of organoid RNA-seq data showing relative expression (Z-scores) of EpC marker genes of ciliated, differentiated, and senescent cell populations and endometrial epithelial stem/progenitor cell markers. Assembloid marker genes were deposited in the Gene Expression Omnibus (GEO Profiles, GSE168405).

5.2.5 Analysis of $p16^+$ cells in mid-luteal endometrium from control and RMM patients

Based on immunohistochemical analysis of 308 timed biopsies, luteal phase endometrium was shown to harbour highly dynamic populations of $p16^{INK4a}$-positive cells (Brighton et al., 2017). $P16^{INK4a}$ (p16, encoded by *CDKN2A*) is a canonical marker of cellular senescence (Li et al., 2011). In luteal-phase endometrium, $p16^+$ cells were shown to be scattered throughout the stroma, glandular epithelium and most prominently, luminal epithelium. Further, the abundance of $p16^+$ cells was shown to peak in glandular and luminal epithelium upon transition from mid- to late-luteal phase of the cycle (Brighton et al., 2017).

Gene expression profiling of differentiated gland organoids indicated that the emergence of senescent EpC is blunted in RMM (Fig 5.16). To validate this observation, the abundance of $p16^+$ cells was examined by IHC in 93 controls and 48 RMM formalin-fixed endometrial biopsies obtained between LH+5 to LH+11 (Fig 5.17). Patient demographics are presented in Appendix Table 1.9. The ratio of $p16^+$ and $p16^-$ cells was calculated separately for glandular epithelium, luminal epithelium, and stroma. Percentiles were calculated to normalise for the day of cycle using an existing percentile graph based on analysis of 308 LH-timed biopsies (Brighton et al., 2017). This study was performed with assistance from Dr Katherine Fishwick.

Representative images of $p16^+$ cells in the endometrium are shown in Figure 5.17. No significant differences in the abundance of $p16^+$ cells were observed in either the stroma or luminal epithelium when normalised to the days of the biopsy in the cycle (Fig. 5.18a and b). However, the abundance of $p16^+$ cells was significantly lower in RMM glands ($P < 0.05$, Mann Whitney test), exemplified by the markedly lower interquartile range in the percentile graph (Fig. 5.18b). This observation not only corroborates the gland organoid RNA-seq data, but it also suggests that lack of senescent EpC in peri-implantation endometrial glands may impact on histotroph production, or the ability of invading trophoblast to access the histotroph in pregnancy. or both.

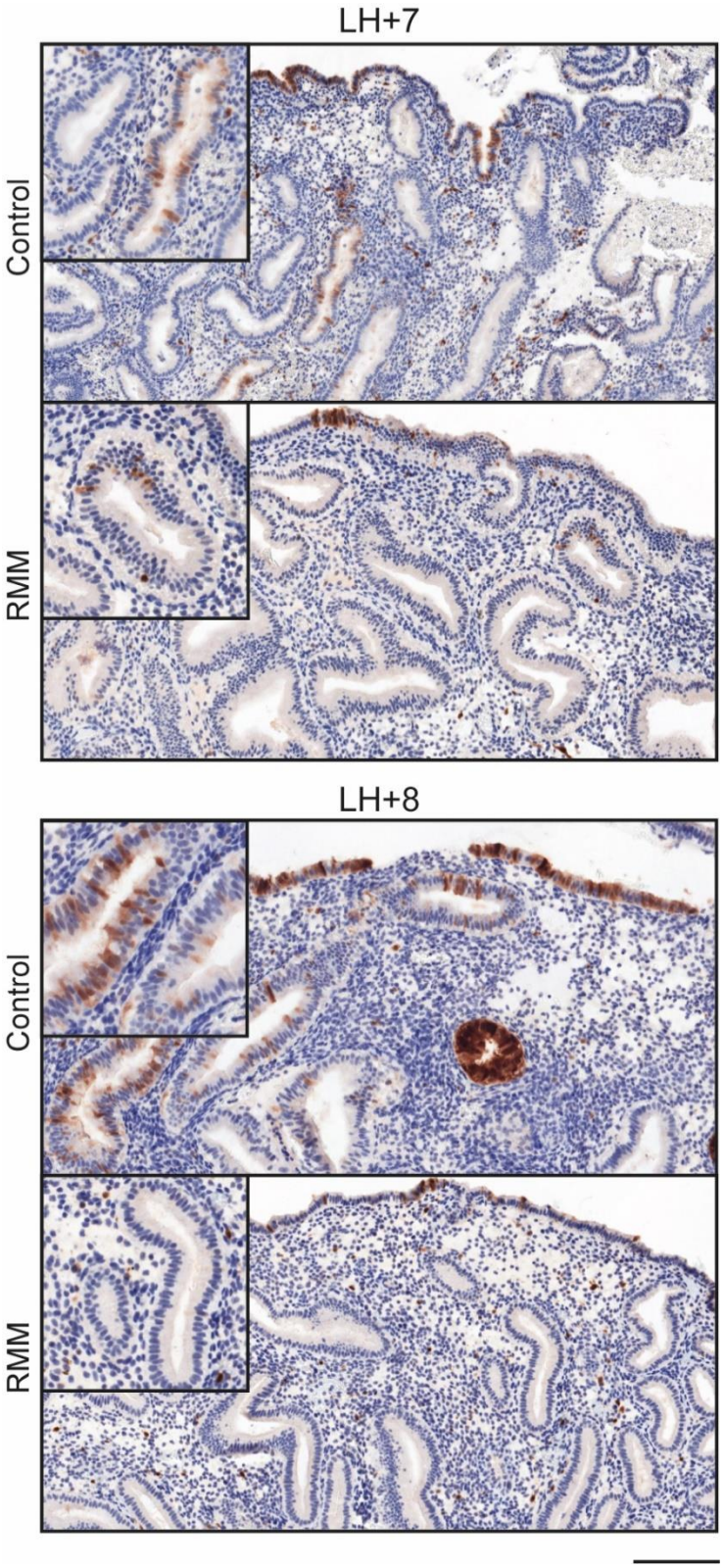

Figure 5.17. ***Immunohistochemistry of p16⁺ cells in control and RMM endometrium.***

Representative images of immunohistochemistry of $p16^+$ cells distribution in control and RMM endometrium at LH+7 and +8. Scale bar = 200 µm.

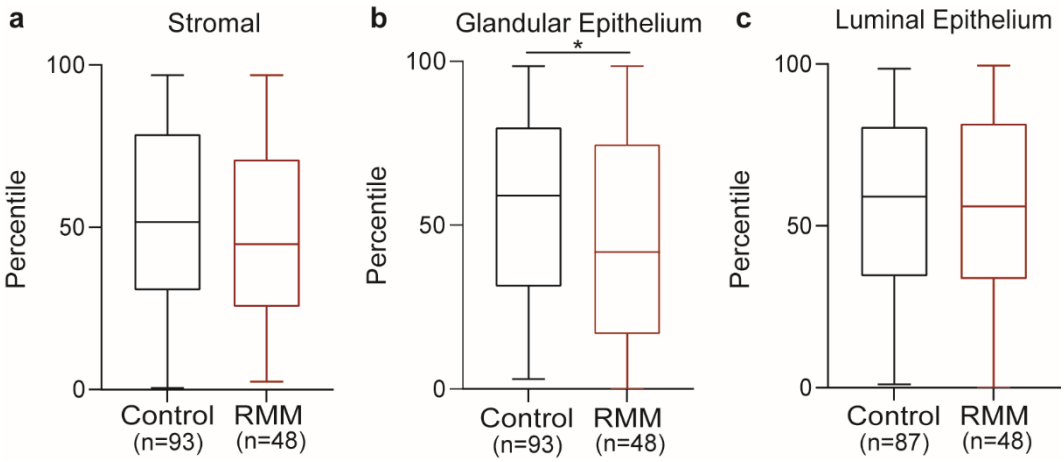

Figure 5.18. ***Decreased levels of p16⁺ cells in RMM glands.***

The abundance of p16⁺ cells between LH+5 and LH+11 in the stroma, glandular epithelium, and luminal epithelium were assessed by colour deconvolution using control and RMM endometrial biopsies. Percentiles calculated based on p16⁺ cells scores using R software and were presented as boxplots. Normal distribution was tested with Shapiro-Wilk test.

a) Distribution of p16⁺ in the stromal compartment of control subjects (n=93) and RMM patients (n=48).

b) Distribution of p16⁺ in the glandular epithelium of control subjects (n=93) and RMM patients (n=48). * indicates $P < 0.05$ obtained by Mann Whitney test.

c) Distribution of p16⁺ in the luminal epithelium of control subjects (n=87) and RMM patients (n=48).

5.3 Discussion

Studying endometrial disorders *in vivo* using biopsy tissue is limited to just a snapshot in time, that can only be observed and not manipulated. The establishment of endometrial gland organoid cultures allows for the modelling of glands from different endometrial disorders. Subtle transcriptomic differences and metabolic perturbations were identified in RMM glands in Chapter 3. Using optimised protocols described in Chapter 4, patient specific RMM gland organoids were established.

My results demonstrate that RMM, but not RPL, is associated with an increased abundance of epithelial progenitor cells. An excess of progenitor cells is predicted to impact on differentiation of tissues (Zakrzewski et al., 2019). Pathways used to generate energy for cellular processes are highly dependent on whether the cells are quiescent, proliferating, or differentiated (Vander Heiden et al., 2009). Like other stem cells, my results indicate that endometrial epithelial progenitor cells are likely to favour FAO during their quiescent state, resulting in increased oxidative phosphorylation, as inferred in Chapter 3.

Importantly, I established and validated a model for studying this phenotype using RMM patient-specific glands organoids. The transcriptomic signature found in the RMM glands *in vivo* was recapitulated, at least in part, in the RMM organoids and characterised by similar metabolic defects. Based on gene expression profiling, FAO was highly upregulated in undifferentiated organoids but dependence on FAO continued after differentiation. During the regeneration of a healthy endometrium, a rise in glycolytic enzymes is observed in the glands (Ferenczy and Bergeron, 1991). It is likely a switch from FAO to glycolysis occurs as stem/progenitor cells transition from a quiescent to proliferative state as seen in other tissues (Ryall et al., 2015, Tümpel and Rudolph, 2019). Metabolic reprogramming is a common phenomenon that takes place in cancer and immune cells that induces a metabolic switch from one pathway to another determining their phenotype (Yoshida, 2015, Pålsson-McDermott and O'Neill, 2020). A defect in RMM stem/progenitor cells may occur that reprograms these cells such that their progeny continue to rely on FAO even after differentiation.

In keeping with organoid formation efficiency, the RNA-seq revealed an upregulation of stem cell marker genes implicated in maintenance of quiescence in RMM. Unfortunately, apart from *AXIN2*, the other markers have not been validated as endometrial gland stem/progenitor cell markers (Cousins et al., 2021). *LGR5* is a controversial stem/progenitor cell marker in the endometrium, with the highest

expression localised to the luminal epithelium (Tempest et al., 2018a, Cousins et al., 2021). Although gland organoids are generated from endometrial biopsies of the functional layer that do contain both luminal and glandular epithelium, the majority of isolated cells come from the latter compartment. Currently, it is not known if luminal EpC can establish organoids. As *LGR5* is co-expressed with several epithelial stem/progenitor cell markers, it can be concluded that there are more progenitor cells in RMM.

An abundance of stem/progenitor cells which continue to be present during the secretory phase contribute to poor development and differentiation of the glands in RMM. Two signalling pathways, Wnt and Notch, were perturbed in RMM. Wnt signalling is critical for gland development, maintenance of stem cells, endometrial repair and essential for implantation and pregnancy (Nusse et al., 2008, Fan et al., 2012, Goad et al., 2017). Interestingly, progesterone-mediated inhibition of Wnt signalling occurs in the secretory phase, which is important for EpC to differentiate into secretory cells (Wang et al., 2009, Garcia-Alonso et al., 2021). Notch signalling is critical for fetal-maternal communication during implantation and placentation (Cuman et al., 2014). Despite Notch signalling found to be upregulated in the undifferentiated organoids, in the menstrual cycle, expression of Notch proteins and ligands increases in the secretory phase in the glands (Cobellis et al., 2008, Cuman et al., 2014). However, in undifferentiated organoids Notch signalling may have role in the maintenance of stem cells (Siebel and Lendahl, 2017). In the differentiated RMM gland organoids, the RNA-seq data suggests altered Notch signalling that could have a negative impact on the processes previously mentioned. Taken together, the dysregulation of these pathways alongside the loss of other key transcription factors is evidence of abnormal development and differentiation response in the glands of these patients.

Gland EpC diverge into differentiated and senescent subpopulations upon differentiation and were distinguished in control and RMM organoids using previously identified marker genes (Rawlings et al., 2021a). A deficiency in senescent and ciliated EpC was observed in RMM organoids, suggesting a lack of specification in differentiated EpC. This finding was validated by IHC of *in vivo* glands using the canonical senescence marker, p16. A recent IHC study found the percentage of $p16^{+}$ cells in the glands and lumen were significantly lower in women who went on to have a miscarriage in comparison to those who had a live birth (Parvanov et al., 2021). The findings were even more significant in those women suffering with RPL (Parvanov et

al., 2021). It was suggested that an unfavourable environment for implantation may be caused by the decrease in senescent $p16^+$ cells. However, in the present study no difference was observed in the lumen, making the specific decrease in the glands unique to RMM.

With the rise of oestrogen in the proliferative phase, rapid proliferation of EnSC and gland EpC takes places with the greatest proliferative rates observed in the upper third of the functional layer (Ferenczy et al., 1979). Stromal senescence is believed to be driven by replicative stress encountered during this period (Brighton et al., 2017). Similarly, epithelial senescence occurs in cells susceptible to replicative stress (Rawlings et al., 2021a) and is reflected by the telomerase activity during the menstrual cycle (Hapangama et al., 2017). Telomerase is a reverse transcriptase enzyme, which counteracts telomere shortening in cells due DNA replication that could lead to cellular senescence. In the endometrium, only the EpC express human telomerase reverse transcriptase, which is the catalytic subunit of telomerase and demonstrates telomerase activity (Hapangama et al., 2017). Peak expression of both genes is found in the proliferative phase, which then falls dramatically during the mid-luteal phase, where the telomere lengths are at their shortest (Valentijn et al., 2015). Interestingly, this precedes the rise in $p16^+$, indicating these senescent cells are also progesterone-independent like stromal senescent cells (Brighton et al., 2017).

Epithelial senescent cells secrete implantation specific SASP including implantation and growth factors, such as amphiregulin and epiregulin, which transform the cytotrophoblasts into extravillous trophoblasts (Yu et al., 2019, Cui et al., 2020, Rawlings et al., 2021a). However, the function of these cells during pregnancy is not known. One hypothesis is that secretion of proteinases by epithelial senescent cells may breakdown the surrounding basement membrane, thereby accommodating endoglandular trophoblast invasion for histotrophic nutrition access (Huppertz, 2020, Rawlings et al., 2021a). Interestingly, often absent patches are observed around the circumference of the glands, and the presence or absence of trophoblast cells is not associated with the degeneration (Burton et al., 2020). The cause of these patches is currently unknown, but secretions of proteinases from senescent EpC is a plausible theory. With fewer senescent cells in RMM glands, trophoblast transformation and invasion could be blocked, thus limiting the access for histotrophic nutrition. Limited histotrophic support may reduce the signalling of key mitogenic growth factors from the glands required for trophoblast growth and invasion, leading to a thinner

cytotrophoblastic shell, poor arterial plugging and early onset of maternal circulation as seen in missed miscarriages (Jauniaux et al., 2003b).

In summary, I established and validated RMM patient-specific gland organoids that are distinguishable from control organoids. The findings from the gland organoids have revealed additional defects in RMM glands, which suggest an intrinsic defect in their stem/progenitor cells that drives the metabolic reprogramming and lack of specification in the differentiated cells. However, the RMM gland organoid model could be further developed by the addition of EnSC to provide a more physiological environment and to identity the cell-cell interactions between the two compartments.

Chapter 6:
Endometrial Assembloids as a Model for Recurrent Missed Miscarriage: A preliminary study

6.1 Introduction

Insight into the interactions between EpC and EnSC within the endometrium is essential to understand the endometrial physiology and associated pathologies (Fitzgerald et al., 2021). Currently, most *in vitro* endometrial studies focus on a single cell type, although layered or scaffold co-culture models of EnSC and EpC, or epithelial spheroids have also been developed (Bentin-Ley et al., 1994, Arnold et al., 2001, Wang et al., 2012). One study demonstrated that coculturing of these two cell types on Matrigel resulted in a multi-fold increase in epithelial differentiation, thus, highlighting the potential for studying the paracrine relationship *in vitro* (Arnold et al., 2001). However, these studies also illustrated the challenges of co-cultures, such as lack of matrix stability and impaired molecular and functional responsiveness, and inability to propagate long-term cultures. In another 3D model, EnSC and EpC were allowed to aggregate in agarose moulds into an organoid structure with a stromal centre and outer layer of EpC with the apical side facing away from the EnSC (Wiwatpanit et al., 2020). These cultures were able to replicate aspects of the proliferative phase endometrium of the menstrual cycle, but their responsiveness to differentiation signals remained unexplored. Additionally, the cell-cell interactions were not investigated.

A more physiological model of incorporating primary EnSC with the gland organoid model from Turco *et al* (2017) was established in our group and were termed 'endometrial assembloids' (Rawlings et al., 2021a). The EpC fractions of digested endometrial biopsies were used to establish gland organoids. In parallel, primary EnSC were grown as monolayer cultures (Fig. 6.1a). At P2, EnSC were combined with digested organoid EpC in a 1:1 ratio. As EnSC appeared stressed when cultured in Matrigel (Rawlings, 2020), the assembloid model uses a hydrogel matrix comprising of 97% type I and 3% type III collagens. This ECM composition is akin to mid-luteal endometrium (Aplin et al., 1988, Oefner et al., 2015) and has a predicted elastic modulus similar to non-pregnant endometrium (10^2 Pa) (Abbas et al., 2019). To stimulate EnSC proliferation and expansion within the matrix, ExM was supplemented with E_2 (Rawlings, 2020). Robust secretion of PRL and CXCL14 was observed upon differentiation of the assembloids, indicating coordinated stromal decidualisation and gland organoid differentiation (Rawlings et al., 2021a).

We reasoned that assembloids may no longer require the exogenous growth factors and pathway modulators found in the ExM upon differentiation because of the

presence of the decidualising EnSC. Therefore, in this chapter, I tested this hypothesis and optimised the differentiation medium for assembloids. Using this new differentiation medium, I explored differences in gene expression in different epithelial subpopulations in RMM and control assembloids using scRNA-seq.

6.2 Results

6.2.1 Optimisation of the differentiation medium for endometrial assembloids.

Endometrial assembloids, established from primary endometrial EnSC and gland organoids, represent a novel tool to explore endometrial physiology and pathology. Figure 6.1a provides a schematic overview of the protocol used to establish endometrial assembloids. Briefly, mid-luteal endometrial biopsies were digested and gland organoids established from isolated glands. In parallels, purified EnSC were propagated in standard monolayer cultures. At P2, single cell suspensions of 5×10^4 EnSC were combined with dissociated organoid EpC at 1:1 ratio into a 20 µl hydrogel droplets. For structural characterisation, assembloids were first expanded in ExM plus E_2 for 4 days, and then differentiated in ExM, E_2, 8-bromo-cAMP and medroxyprogesterone acetate, (MPA), a progestin widely used for *in vitro* decidualisation experiments (Gellersen and Brosens, 2014) (Fig. 6.1b). Immunofluorescence microscopy was used to assess the architecture of assembloids as well as their differentiation response.

Alongside the stromal marker, vimentin, assembloids were co-stained with an epithelial marker, i.e. cytokeratin-18, E-cadherin and EpCAM. As shown in Figure 6.2, primary EnSC expanded within the assembloids and created a dense matrix around the gland-like organoids structures. Differentiation resulted in osteopontin expression and glycodelin accumulation in the lumen of the gland organoids, whereas PGR expression was downregulated in both EnSC and EpC, a response akin to luteal phase endometrium (Wang et al., 1998).

ExM contains multiple exogenous growth factors and inhibitors (Table 1.1). The purpose of these factors is to recapitulate the endometrial microenvironment and allow the gland organoids to differentiate in the absence of paracrine signalling from the neighbouring EnSC (Turco et al., 2017). Hence, I hypothesised that once established, assembloids no longer require these exogenous factors as glandular differentiation should be supported by decidualised EnSC (Jones et al., 1998, Filant and Spencer, 2014). To test this hypothesis, two complementary experimental designs were chosen involving either removal of each exogenous factor from the ExM or addback of each factor to the base medium (Advanced DMEM/F12, N-2 supplement, B12 supplement, antibiotic/antimycotic and L-glutamine).

Gland organoids and assembloids were established in parallel from three mid-luteal phase endometrial biopsies and grown for 4 days in ExM with E_2. For the removal experiments, cultures were then differentiated in E_2, 8-bromo-cAMP and MPA for 4 days in either ExM or in ExM with omission of each exogenous factor individually (Table 6.1a). For the add-back experiments, cultures were also differentiated in E_2, 8-bromo-cAMP and MPA for 4 days in either ExM, base medium, or base medium supplemented with a single exogenous factor added individually (Table 6.1b). Undifferentiated cultures were maintained in ExM with E_2 for a further 4 days. Induction of *PAEP* and *SPP1* transcripts were measured by RT-qPCR to assess the glandular differentiation response.

The relative induction of *PAEP* and *SPP1* was consistently higher in gland organoids than in matched assembloids for all differentiation media based on ExM irrespective of systematic removal of individual factors (Fig. 6.3). Notably, removal of A83-01, a TGF-β kinase/activin receptor-like kinase inhibitor (Tojo et al., 2005), significantly enhanced the induction of both genes in gland organoids ($P < 0.05$ and $P < 0.01$, Friedman's test for matched samples). Taken together, the removal of a single exogenous factor was not sufficient to reveal a contribution of decidual signal on glandular differentiation.

However, *L19* was used as a housekeeping gene to normalise mRNA levels between the different samples in both gland organoids and assembloids (Thellin et al., 1999). As assembloids are established using two different cell types, an issue arises when comparing RT-qPCR data of organoids and assembloids. In assembloids, the total RNA originates from gland organoids and EnSC, thus diluting the number of epithelial RNA molecules present and leading to lower amplification of epithelial genes. Due to the contribution of both cell types, *L19* would not be diluted. Hence, when normalising epithelial genes to *L19*, the relative expression would be lower than expected, making it difficult to interpret the data.

On the other hand, the differentiation of the gland organoids in base medium without the exogenous factors resulted in a blunted the induction of *PAEP* and *SPP1* compared to ExM (Fig 6.4). The responsiveness of the gland organoids to differentiation signals could not be restored by add-back of individual factors. However, a robust induction of *PAEP* and *SPP1* assembloids was observed in assembloids with the addition of N-acetyl-L-cysteine (NAC) to the base medium ($P < 0.05$, Friedman's test for matched samples). These findings show that the addition of EnSC renders most ExM components indispensable for differentiation. NAC is a

precursor of L-cysteine and reduced glutathione (Zafarullah et al., 2003). It works as an antioxidant by acting as a scavenger of free radicals such as ROS that have a partial reduction of oxygen. Too many ROS can result in oxidative stress that can lead to intracellular damage and apoptosis (Ray et al., 2012). Hence, for all subsequent differentiation experiments, assembloids were first expanded in ExM supplemented with E_2 and then differentiated in minimal differentiation medium (MDM), consisting of base medium supplemented with NAC, E_2, 8-bromo-cAMP and MPA.

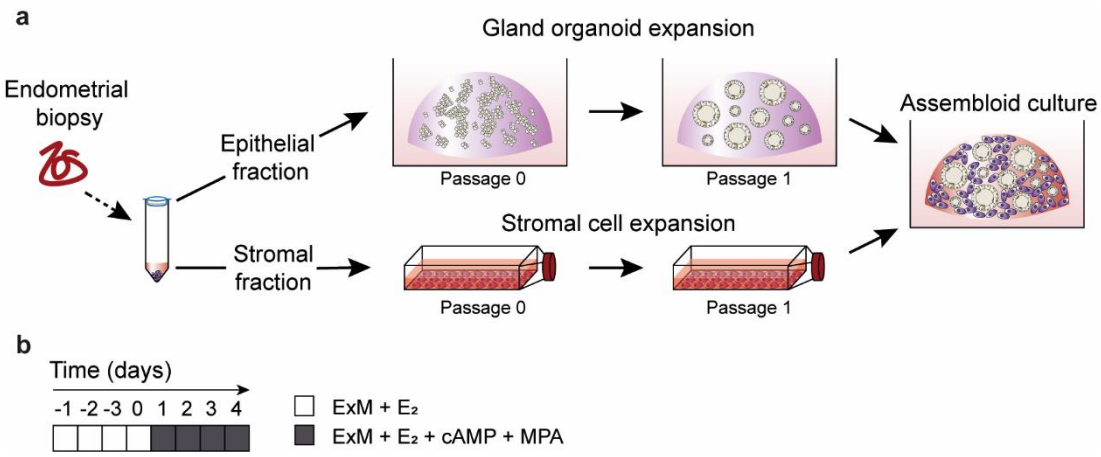

Figure 6.1. ***Establishing endometrial assembloids.***

a) Schematic representation for establishment of endometrial assembloids. Endometrial biopsies were mechanically and enzymatically digested. Epithelial and stromal fractions were separated using a strainer. Stromal fraction was propagated as a monolayer. Epithelial fraction was resuspended in Matrigel for organoid expansion. For P0-1, endometrial gland organoids and EnSC were expanded separately. At P2, dissociated gland organoids and EnSC were mixed in a collagen hydrogel at ratio 1:1 and aliquoted into 20 µl droplets in a 48-well plate and cured at 37 °C for 90 minutes. ExM supplemented with E_2 was added to the assembloids and medium was refreshed every 48 hours.

b) Schematic summary of assembloid differentiation protocol. Samples were grown for 4 days in ExM supplemented with E_2 (growth phase). On day 4, the medium was replaced with differentiation medium, which contains ExM supplemented with E_2, 8-bromo-cAMP and MPA and was refreshed after 48 hours. The assembloids were differentiated for 4 days (differentiation phase) and harvested on day 8 for downstream analyses.

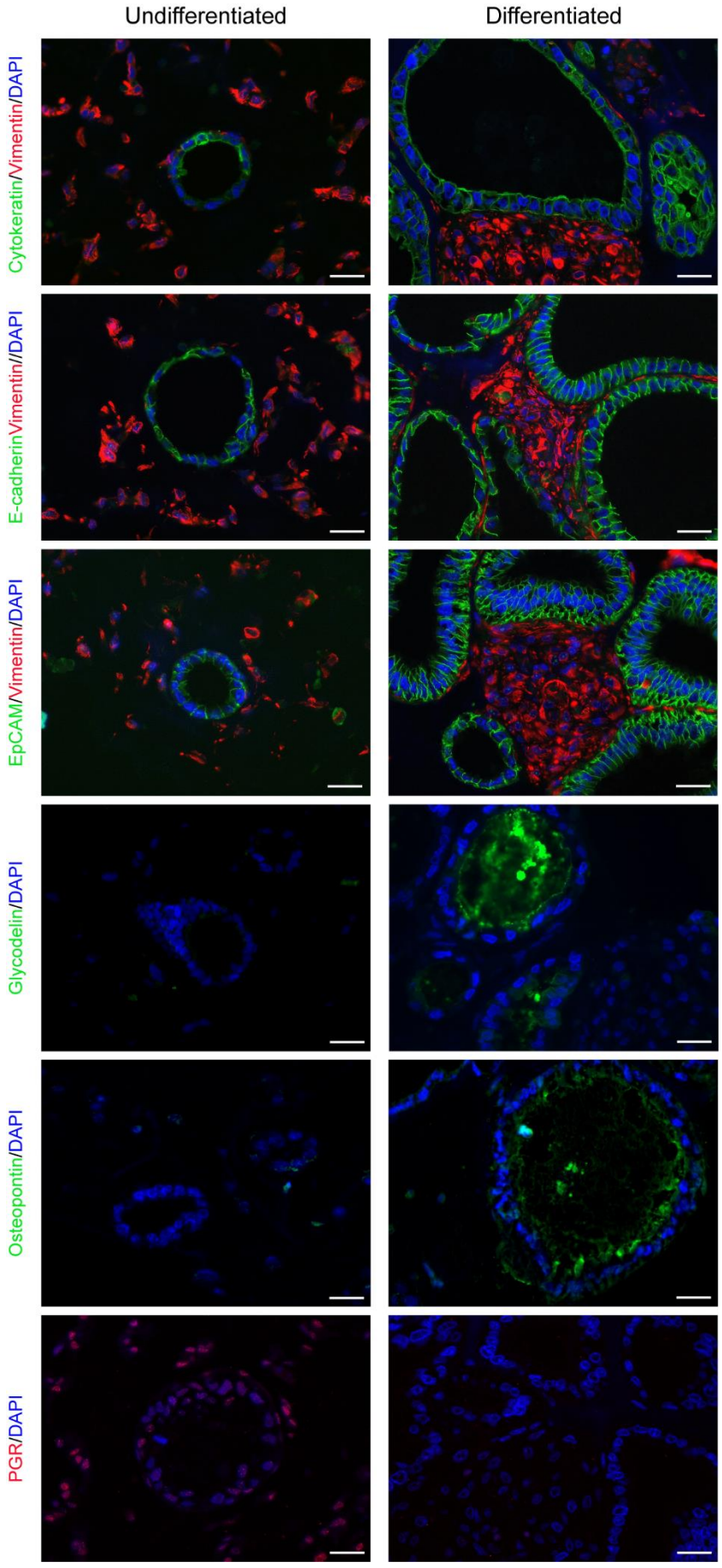
Undifferentiated
Differentiated
Cytokeratin/Vimentin/DAPI
E-cadherinVimentin//DAPI
EpCAM/Vimentin/DAPI
Glycodelin/DAPI
Osteopontin/DAPI
PGR/DAPI

Figure 6.2. ***Immunofluorescence microscopy of undifferentiated and differentiated assembloids.***

Representative dual-immunofluorescence images showing expression of EpC markers (cytokeratin-18, E-cadherin, and EpCAM) and EnSC marker, vimentin, in undifferentiated and differentiated assembloids. To assess differentiation, assembloids were stained for glycodelin, osteopontin and PGR. Nuclei were counterstained with DAPI. Samples were visualised by epifluorescence microscopy. Scale bar = 50 µM. Data collected in collaboration with Dr Thomas Rawlings.

Table 6.1. ***Minimal differentiation media formulation: removal and add-back of ExM components.*** Grey represents medium components included.

a

	Media Formulation: removal of ExM components									
Medium Components	ExM/E_2	ExM/E_2/cAMP/MPA	-NAC	-A83-01	-Nicotinamide	-EGF	-Noggin	-R-spondin-1	-FGF10	-HGF
BM	■	■	■	■	■	■	■	■	■	■
NAC	■	■		■	■	■	■	■	■	■
A83-01	■	■	■		■	■	■	■	■	■
Nicotinamide	■	■	■	■		■	■	■	■	■
EGF	■	■	■	■	■		■	■	■	■
Noggin	■	■	■	■	■	■		■	■	■
R-spondin-1	■	■	■	■	■	■	■		■	■
FGF10	■	■	■	■	■	■	■	■		■
HGF	■	■	■	■	■	■	■	■	■	
E_2 + cAMP + MPA		■	■	■	■	■	■	■	■	■

b

	Media Formulation: add-back of ExM components										
Medium Components	ExM/E_2	ExM/E_2/cAMP/MPA	Base Medium	+NAC	+A83-01	+Nicotinamide	+EGF	+Noggin	+R-spondin-1	+FGF10	+HGF
BM	■	■	■	■	■	■	■	■	■	■	■
NAC	■	■		■							
A83-01	■	■			■						
Nicotinamide	■	■				■					
EGF	■	■					■				
Noggin	■	■						■			
R-spondin-1	■	■							■		
FGF10	■	■								■	
HGF	■	■									■
E_2 + cAMP + MPA		■	■	■	■	■	■	■	■	■	■

***** Base Medium (BM) includes Advanced DMEM/F12, N-2 supplement, B12 supplement, antibiotic/antimycotic and L-glutamine.

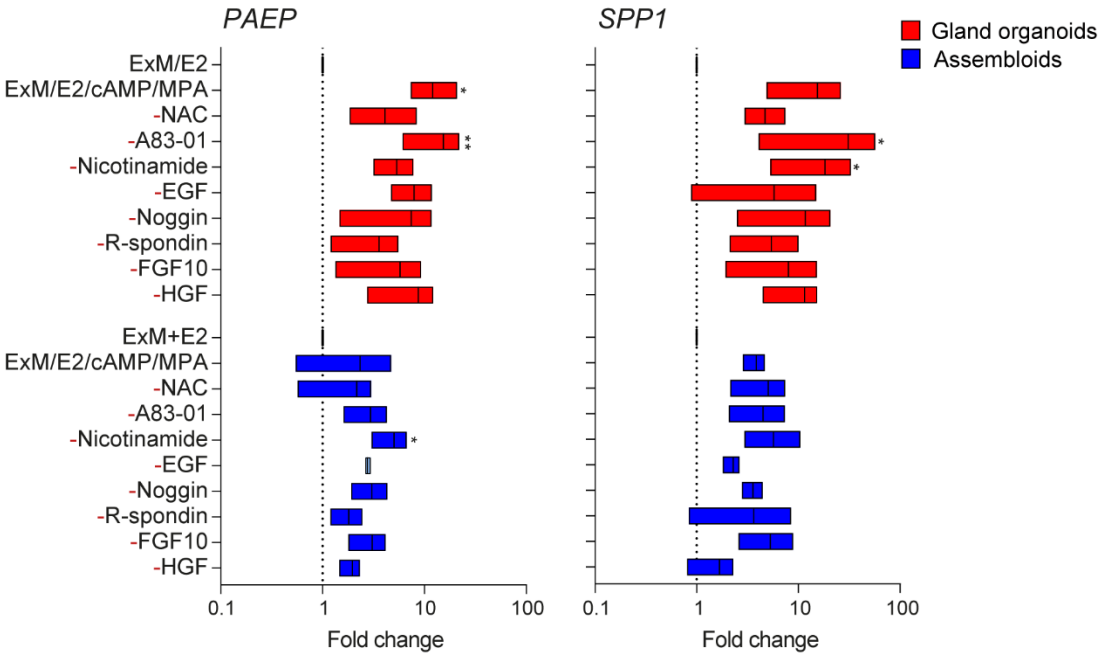

Figure 6.3. ***Optimisation of minimal differentiation medium for endometrial organoids: systematic removal of ExM components.***

Parallel endometrial gland organoids (red) and assembloids (blue) were established from 3 endometrial biopsies and differentiated with cAMP and MPA for 4 days in either ExM, or ExM with each exogeneous factor removed individually (-). Induction of glandular differentiation markers, *PAEP* and *SPP1* were measured by RT-qPCR. Data are presented as fold-change relative to expression levels in undifferentiated gland organoids or assembloids cultured in ExM supplemented with E_2. Bars shows minimal, maximal, and median fold-change. * and ** indicate $P < 0.05$ and $P < 0.01$ (Friedman's test for matched samples). Data collected in collaboration with Dr Thomas Rawlings.

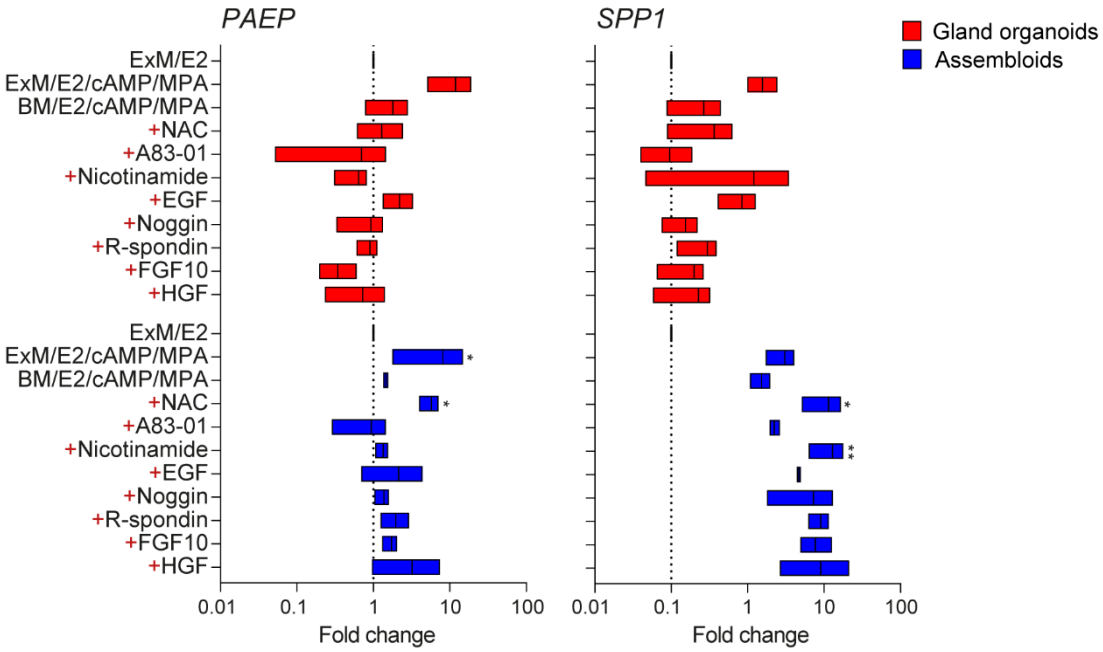

Figure 6.4. ***Optimisation of minimal differentiation medium for endometrial organoids: systematic add-back of ExM components.***

Parallel endometrial gland organoids (red) and assembloids (blue) were established from 3 endometrial biopsies and differentiated with cAMP and MPA for 4 days in either ExM, base medium (BM) or base medium with each exogeneous factor added individually (+). Induction of glandular differentiation markers, *PAEP* and *SPP1* were measured by RT-qPCR. Data are presented as fold-change relative to expression levels in undifferentiated gland organoids or assembloids cultured in ExM supplemented with E_2. Bars shows minimal, maximal, and median fold-change. * and ** indicate $P < 0.05$ and $P < 0.01$ (Friedman's test for matched samples). Data collected in collaboration with Dr Thomas Rawlings.

6.2.2 Single-cell RNA-seq analysis of control and RMM assembloids

Single-cell transcriptomics of endometrial assembloids cultured for 4 days in MDM demonstrated the emergence of distinct differentiated and senescent subpopulations in both glands and stroma. Further, assembloid marker genes for differentiated and senescent EpC and EnSC mapped to mid- and late-luteal phase of the cycle, respectively (Rawlings et al., 2021a) . As shown in Chapter 5, marker genes for differentiated EpC were upregulated in RMM gland organoids whereas marker genes of senescent were downregulated. Additionally, a blunted decidual response in RMM endometrium was identified in Chapter 3, which may contribute to glandular perturbations. Thus, to investigate epithelial subpopulations in RMM and define the contribution of EnSC, I performed scRNA-seq analysis of RMM and control assembloids. I was assisted in these experiments by Dr Emma Lucas.

Primary cryopreserved EpC and EnSC from control (n=3) and RMM (n=3) biopsies were used to establish assembloids (Fig. 6.5a). In parallel, assembloids were generated from control (n=2) and RMM (n=3) gland organoids, using fresh (i.e. not cryopreserved) EnSC isolated from a single biopsy. Thus, the stromal fraction was identical for both RMM and control assembloids (Fig. 6.5b). Patient demographics are presented in Appendix Table 1.10 and 11. The purpose of this experimental design was (i) to test if cryopreservation of EnSC impacts on assembloid formation and (ii) to examine if EnSC from a control biopsy rescue the differences in glandular gene expression between control subjects and RMM.

scRNA-seq was performed on undifferentiated assembloids grown for 4 days in ExM supplemented with E_2 and assembloids differentiated in MDM for 4 additional days (Fig. 6.5 and 6). Unfortunately, cryopreserved EnSC exhibited an excessive stress response when cultured in hydrogels, resulting in contamination of the transcriptomic profiles of both EpC and EnSC by ambient RNA. Therefore, I limited my analysis to control and RMM assembloids established from cryopreserved EpC and fresh EnSC.

Cells were only included in the analysis if they expressed > 200 but < 2000 genes and had < 5% mitochondrial reads to minimise doublets and low-quality cells (broken or damaged cells), respectively (Fig. 6.7a and b). Overall, all samples had low percentage of mitochondrial genes (Fig. 6.7b). Previously, Shared Nearest Neighbour (SNN) and Uniform Manifold Approximation and Projection (UMAP) analysis identified eleven cell clusters in assembloids (Rawlings et al., 2021a). Using the Seurat standard workflow, a label transfer was used to map populations in this dataset

using the marker curation established in previous experiments (Rawlings et al., 2021a). A total of 10 cell clusters were assigned to all 4520 cells in this dataset and graphed computationally by the UMAP algorithm (Fig 6.8). Undifferentiated and differentiated EpC segregated within the UMAP-2 dimension in keeping with previous observations (Rawlings et al., 2021a).

Transcriptomic profiles were obtained from 3,781 EpC but only 739 EnSC. The reason for the low recovery of EnSC is unclear. Although it may be possible to rectify this problem by sequencing more cells, this was not achievable within the timeframe of my studies. Hence, I limited my analysis to EpC.

Based on curated marker genes, five epithelial subsets were mapped to assembloids established from control and RMM patients (Fig. 6.9). The two undifferentiated epithelial subpopulations, EpS1 (n=79) and EpS2 (n=2361) represent actively dividing cells (high expression of cell cycle genes) and cells expressing marker genes of proliferative phase endometrium, respectively. A discrete population of ciliated cells, EpS3 (n=26) was also present in both undifferentiated and differentiated assembloids.

As anticipated, two distinct epithelial populations were identified in differentiated assembloids, consisting of differentiated population, (EpS4, n=799) and, the senescent population, EpS5 (n=194). As described previously (Rawlings et al., 2021a), senescent cells were identified based on expression of genes encoding the cyclin-dependent kinase inhibitors $p16^{INK4a}$ and $p21^{CIP1}$ in parallel with canonical SASP factors which are also implantation factors including DPP4 (Kim et al., 2017), growth differentiation factor 15 (*GDF15*) (Basisty et al., 2020) and insulin growth factor binding protein 3 (*IGFBP3*) (Elzi et al., 2012) (Fig. 6.10). The final population, termed transitional population (TP, n=322), highly expressed long non-coding RNAs (*NEAT1* and *KCNQ1OT1)*, which are implicated in mesenchymal-epithelial and epithelial-mesenchymal transition (MET/EMT) (Chen et al., 2021, Bian et al., 2019).

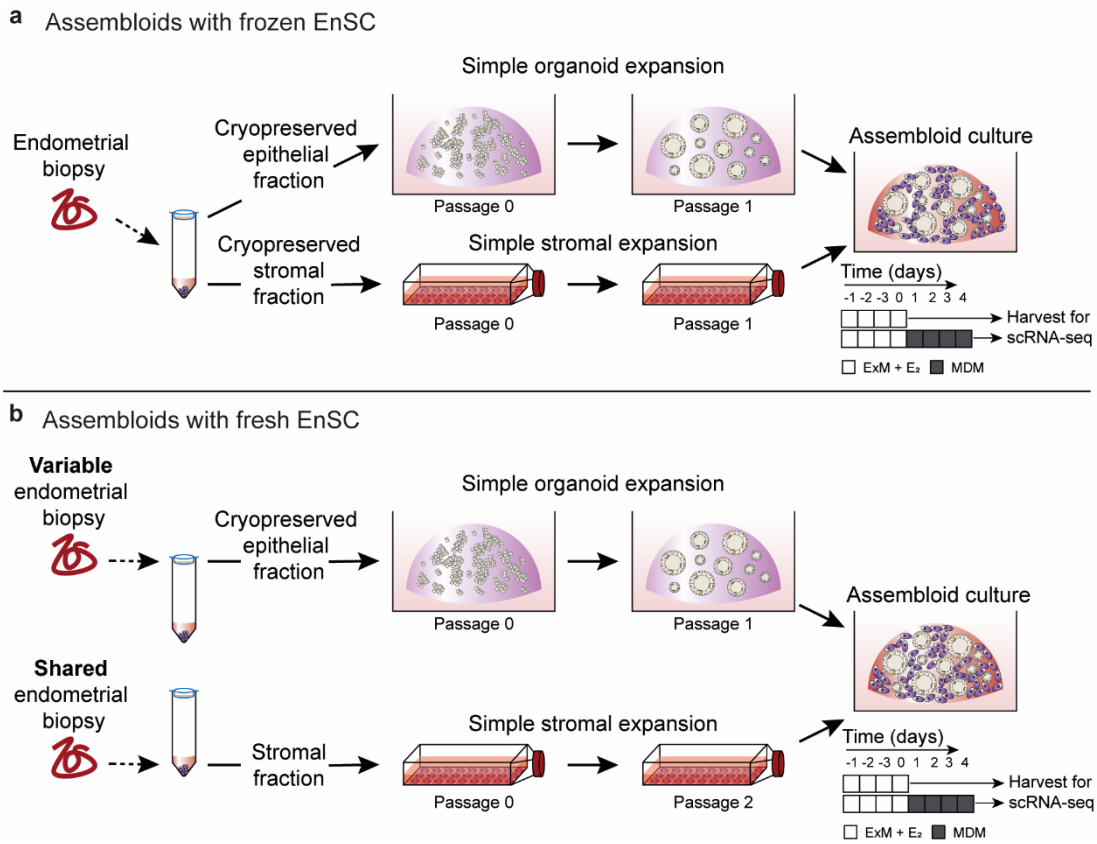

Figure 6.5. ***Experimental design of scRNA-seq of RMM and control assembloids.***

a) Endometrial organoids and EnSC from the same cryopreserved endometrial biopsy were used to establish assembloid cultures. scRNA-seq was performed on undifferentiated assembloids grown for 4 days in ExM supplemented with E_2 and assembloids differentiated in MDM for a further 4 days.

b) Assembloids were set up with endometrial organoids from either cryopreserved epithelial fractions of control or RMM endometrial biopsies. All assembloids had EnSC from one fresh control endometrial biopsy. scRNA-seq was performed on undifferentiated assembloids grown for 4 days in ExM supplemented with E_2 and assembloids differentiated in MDM for a further 4 days.

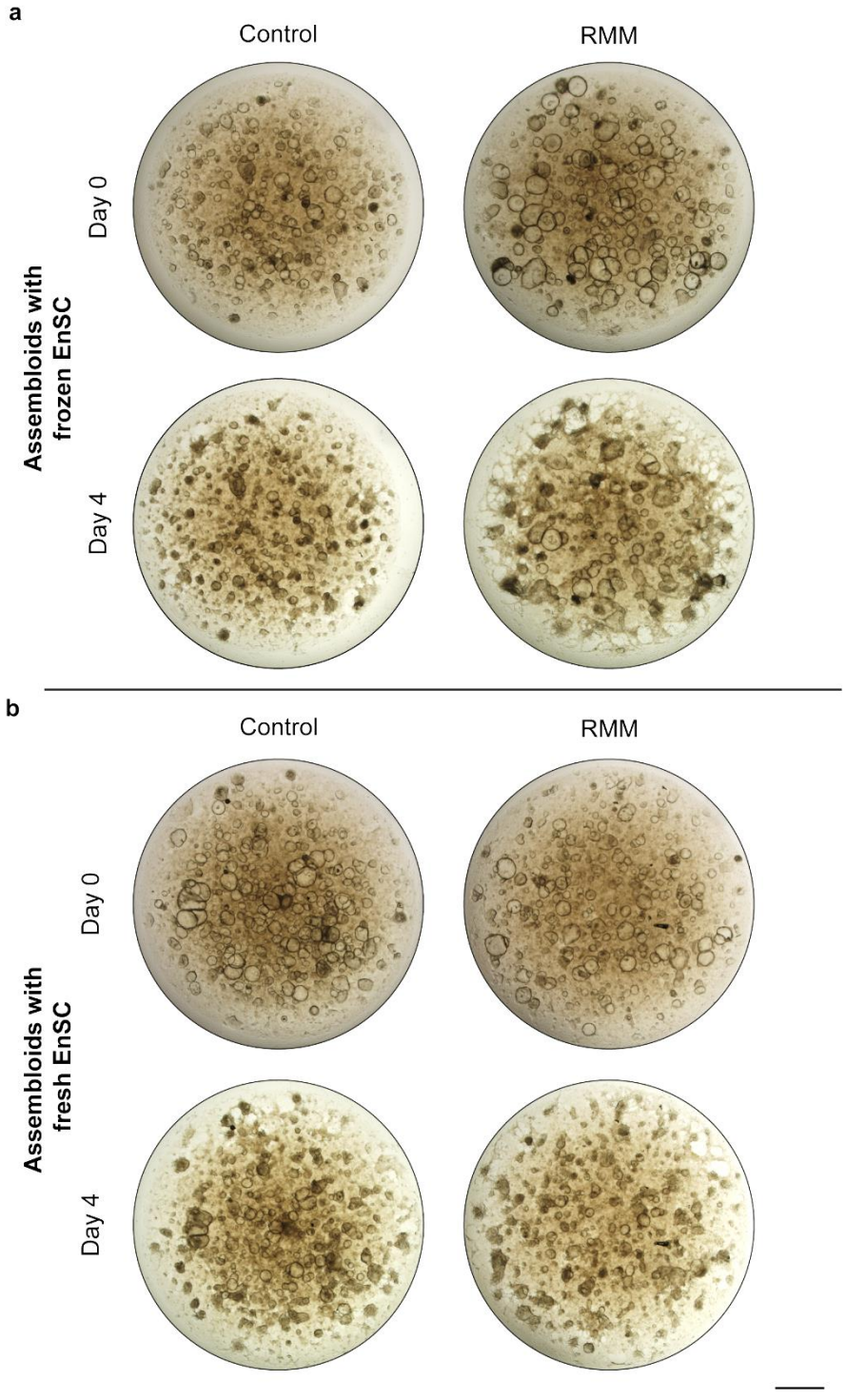

Figure 6.6. ***Representative images of control and RMM assembloids.***

a) Representative images of undifferentiated and differentiated assembloids of control and RMM cryopreserved endometrial biopsies. Scale bar = 1 mm

b) Representative images of undifferentiated and differentiated assembloids of control and RMM cryopreserved gland organoids and fresh control EnSC. Scale bar = 1 mm.

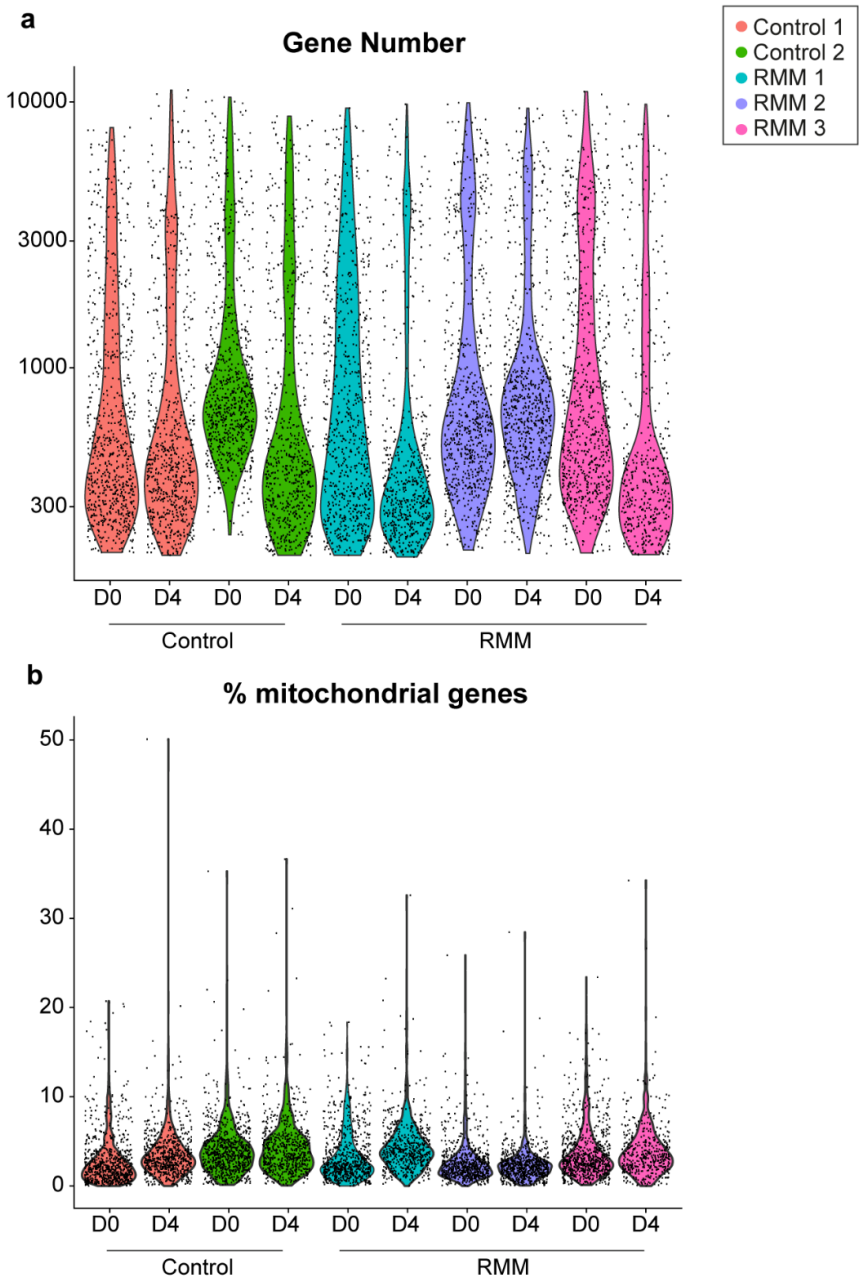

Figure 6.7. ***Quality control of assembloid scRNA-seq data.***

Violin plots representing:

a) the number of genes per cell.

b) the percentage mitochondrial DNA per cell.

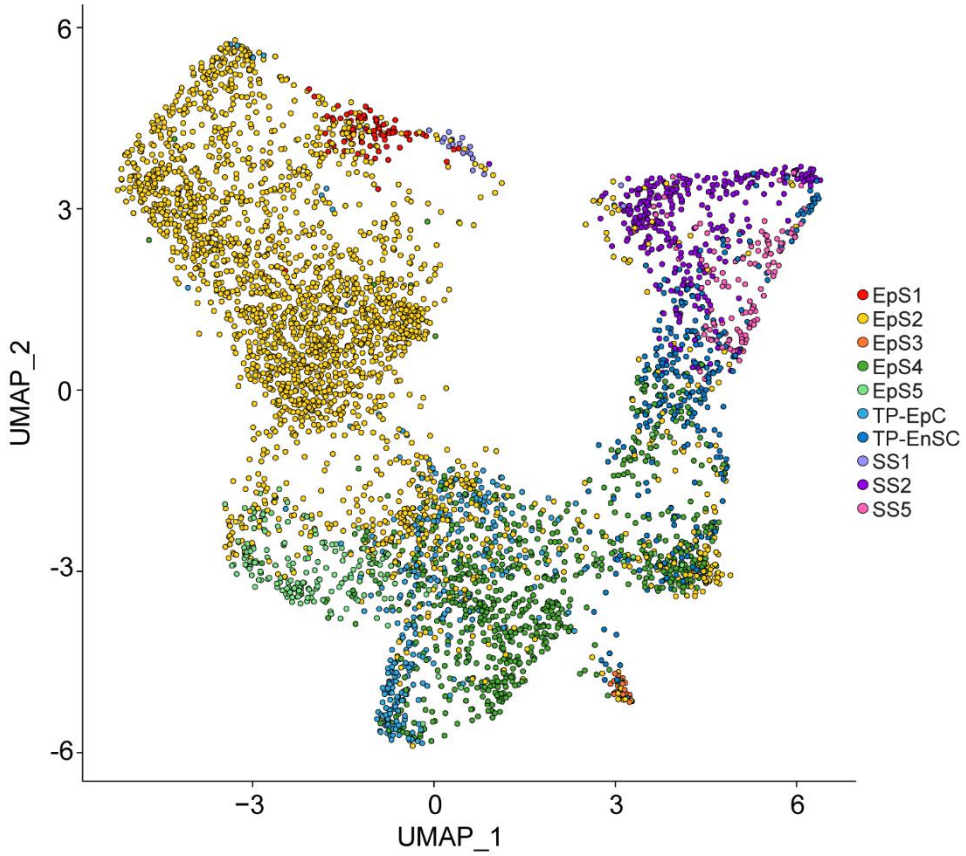

Figure 6.8. ***UMAP of epithelial and stromal subsets in assembloids.***

UMAP visualisation of transcriptome recovered from 5 undifferentiated and differentiated assembloids and, colour-coded for different epithelial and stromal subpopulations (EpS and SS, respectively).

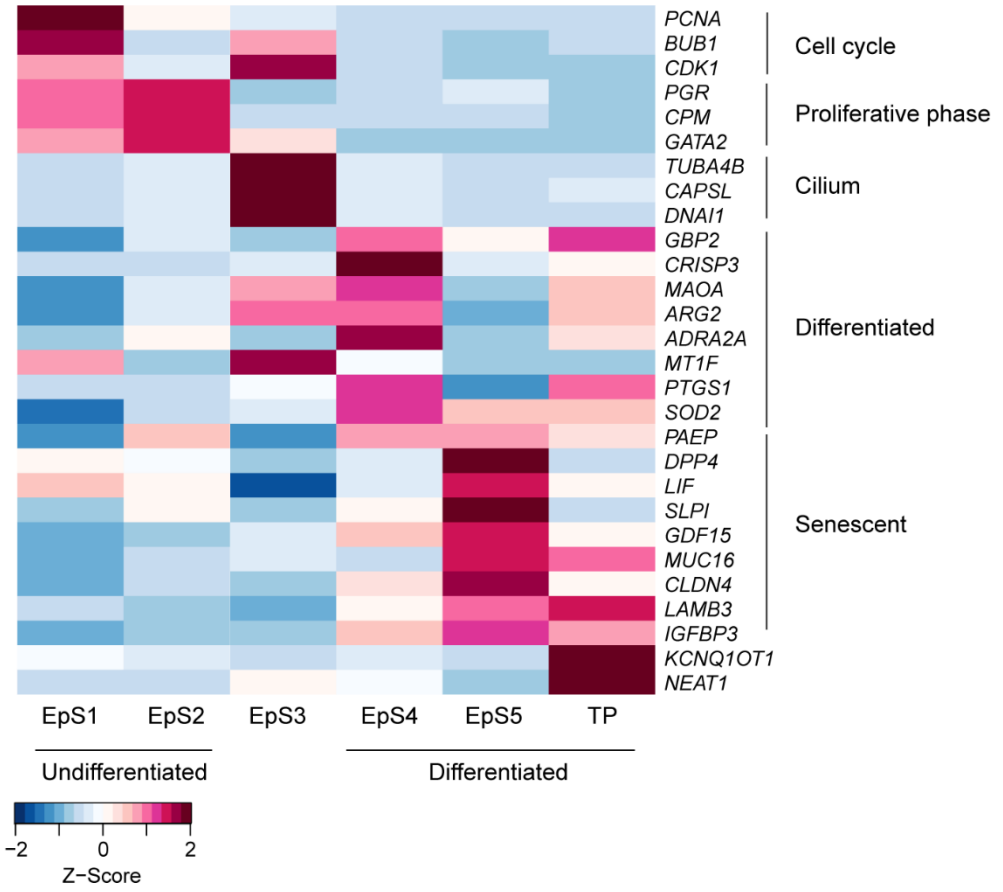

Figure 6.9. ***Heatmap of epithelial marker genes in undifferentiated and differentiated assembloids.***

Heatmap showing relative expression (Z-scores) of epithelial marker genes of epithelial subpopulations (EpS1-5) and TP. Curation of marker genes was based on previous scRNA-seq analysis of endometrial assembloids. The data are publicly available (GEO Profiles, accession number: GSE168405).

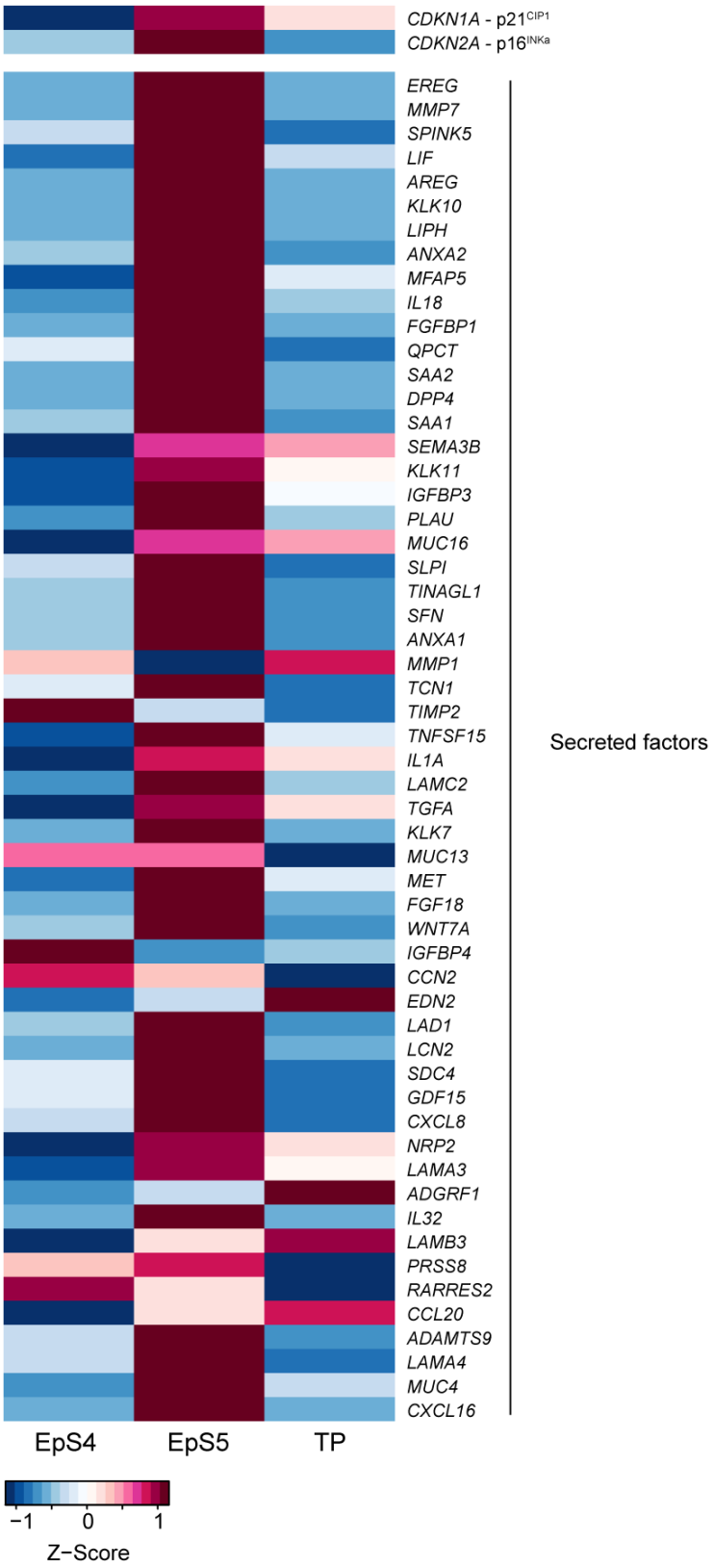

Figure 6.10. ***Heatmap showing relative expression of cyclin-dependent kinase inhibitors and SASP-related genes in differentiated assembloids.***

The heatmap is based on the relative expression (Z-scores) of indicated genes in the EpC subpopulations of differentiated assembloids.

Next, UMAPs were generated for the epithelial subpopulations of control and RMM assembloids (Fig. 6.11). No obvious differences were observed in the grouping of the subpopulations between the two groups. Figure 6.12a depicts the number of DEGs in each of the subpopulations with and without multiple testing correction. Not unexpectedly, FDR correction had a profound impact on the number of the DEGs in the smaller populations, i.e. EpS1, EpS3, EpS5 and TP (Fig. 6.12b).

Based on $P < 0.05$, a total 122 genes were found to be differentially expressed in EpS2 (i.e. proliferative EpC) between control and RMM assembloids (Fig. 6.12a). EpS2 genes repressed in RMM included various glycolytic genes, *TPI1* (encoding triosephophate isomerase), *GAPDH* (glyceraldehyde 3-phosphate dehydrogenase), *PGK1* (Phosphoglycerate kinase 1), *ENO1* (alpha-enolase), *PKM* (pyruvate kinase) (Bolaños et al., 2010). Most of the downregulated glycolytic genes were of the pay-off phase of glycolysis as observed in RMM glands *in vivo* (Fig. 3.8). Other notable repressed metabolic genes in RMM assembloids included *SAT1* (spermidine/spermine N1-acetyltransferase 1), which encodes the rate limiting enzyme in polyamine metabolism (Pegg, 2008), and *SCD* (stearoyl-CoA desaturase), a key enzyme for lipogenesis (Miyazaki et al., 2005). Based on a more stringent criterium (FDR-corrected $P < 0.05$), 40 genes were found to be DEGs with 6 (15%) and 34 (85%) up- and down-regulated, respectively, in RMM glands (Fig. 6.12b). GO analysis revealed no significant enrichment of biological categories from EpS2 genes upregulated in RMM assembloids. By contrast, EpS2 genes downregulated in RMM were enriched in multiple metabolic GO terms for both sets of downregulated genes including, 'Canonical glycolysis,' 'Gluconeogenesis,' and 'Purine nucleotide metabolic process,' irrespective of FDR correction (Fig. 6.13 and 14).

Next, I mined for DEGs in EpS4 (i.e. differentiated EpC) of control and RMM assembloids. Based on $P < 0.05$, 359 DEGs were identified of which 219 (61%) genes were upregulated and 140 (39%) were downregulated in EpS4 of RMM glands (Fig. 6.12a). Strikingly, EpS4 genes upregulated in RMM glands are implicated in oxidative phosphorylation (*NDUFB8*, *UQCR11*, *NDUFB4*, *NDUFA4*, *NDUFB2*, *MT-ND1* and *MT-ATP6*). Other upregulated genes included cytokines and chemokines (*IL1B*, *CXCL1* and *CXCL2)*, thioredoxin (*TXN),* matrix metallopeptidases inhibitors (*TIMP1*, *TIMP2*, *TIMP3*) and seven collagen related proteins. Upregulated EpS4 genes were enriched in GO terms such as 'Oxidative phosphorylation,' 'Extracellular matrix organisation' and 'Oxidative stress' (Fig. 6.13). Further, the only notable GO term enriched in EpS4 genes downregulated in RMM assembloids was 'Regulation of

epithelial cell differentiation'. Following FDR correction ($P < 0.05$), 79 EpS4 genes were differentially expressed with 62 (78.4%) and 17 (21.6%) up- and down-regulated, respectively in RMM assembloids (Fig. 6.12b). Upregulated EpS4 genes were enriched in two GO terms, 'Response to lipid' and 'Response to stress' (Fig. 6.14).

Following FDR correction, none or few genes were found to be differentially expressed in cycling EpS1 (n=0), ciliated EpS3 (n=0), senescent EpS5 (n=4) and TP (n=3) between control and RMM assembloids. While analysis of DEG based on $P < 0.05$ yielded some interesting observations (Fig. 6.13), confidence in these findings is low. Hence, the data generated in this first scRNA-seq analysis of control and RMM assembloids should be considered preliminary due to technical issues of the limited sample size and low recovery rates of cells, especially EnSC. However, two conclusions can be drawn from the limited data presented. First, the presence of EnSC, whether undifferentiated or decidualised, do not rescue glandular perturbations in RMM. Second, while genes involved in glycolysis are downregulated in undifferentiated RMM assembloids, oxidative phosphorylation is upregulated in differentiated RMM assembloids (Fig. 6.15).

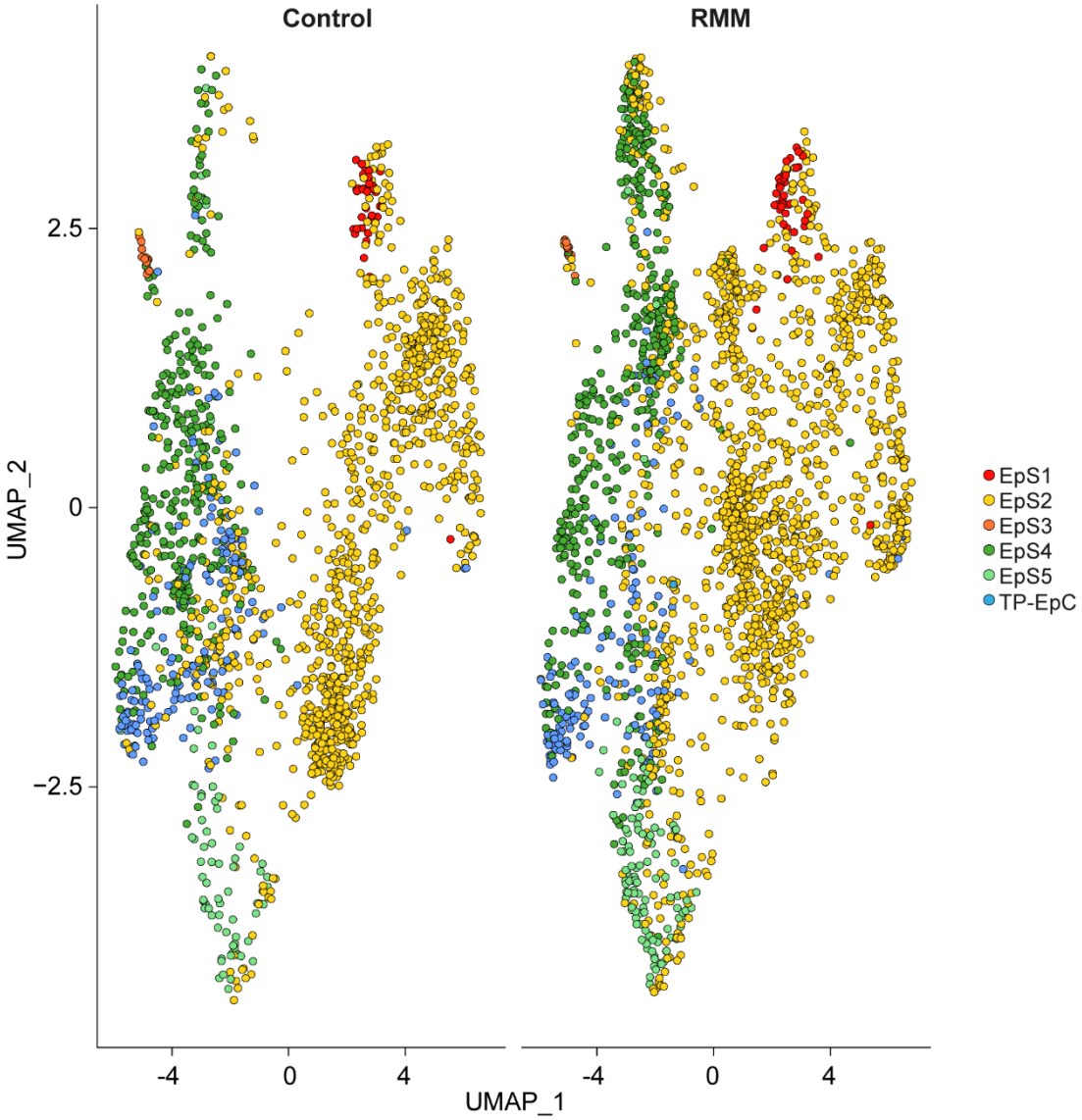

Figure 6.11. ***UMAP of epithelial subsets in control and RMM assembloids.***
UMAP plots of cells from control and RMM assembloids colour-coded for different epithelial subpopulations.

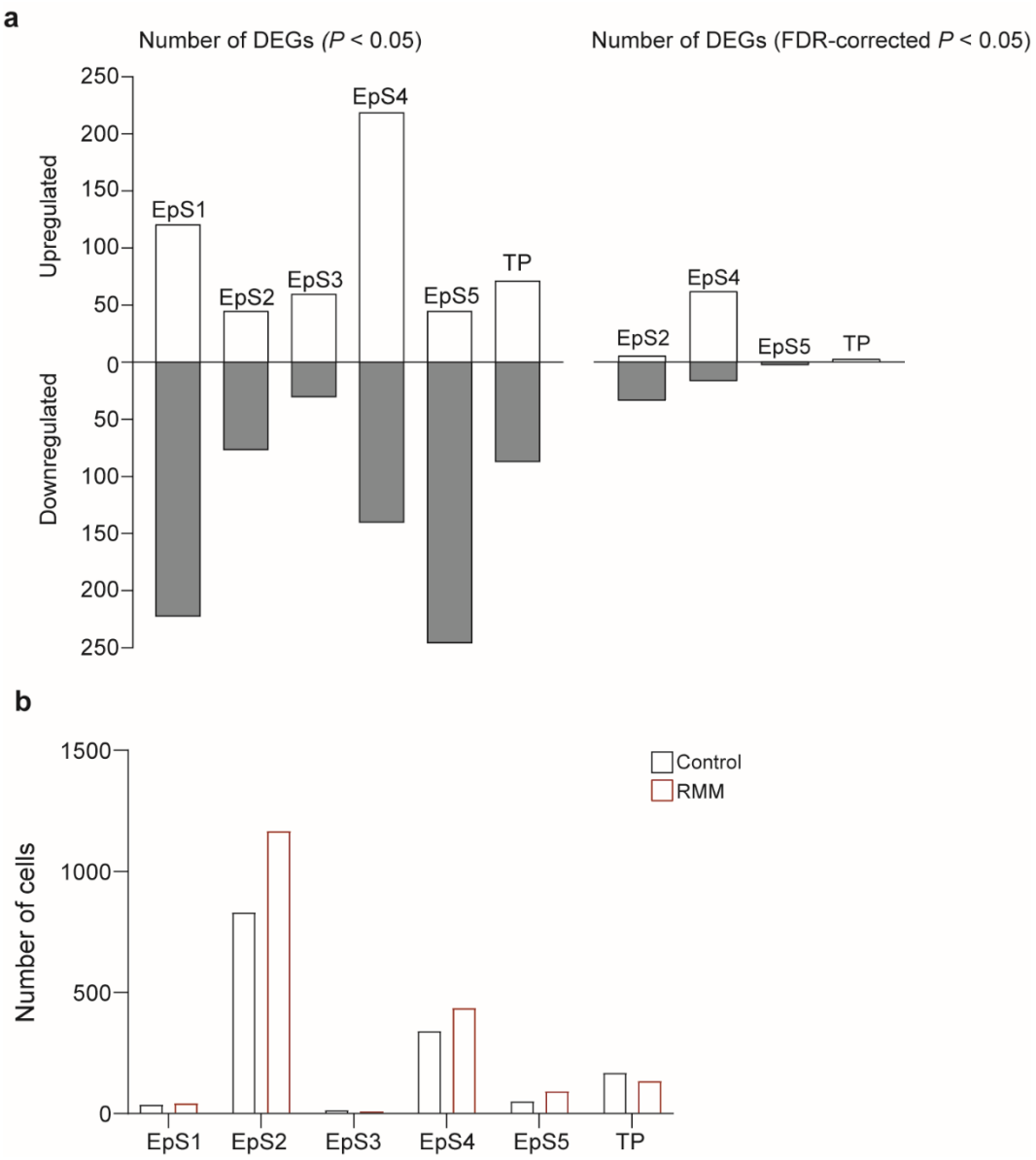

Figure 6.12. ***DEGs in each EpC subpopulation in RMM assembloids.***

Number of DEGs and cells in Day 0 EpS1 and EpS2, Day 4 EpS4 and EpS5 and all EpS3 in RMM assembloids.

a) Bar plot shows the number of DEGs ($P < 0.05$) up- and down-regulated in each epithelial population in RMM assembloids.

b) Bar plot shows the number of DEGs (FDR-corrected $P < 0.05$) up- and down-regulated in each epithelial population in RMM assembloids.

c) Bar plot shows number of cells in each epithelial population in RMM and control assembloids.

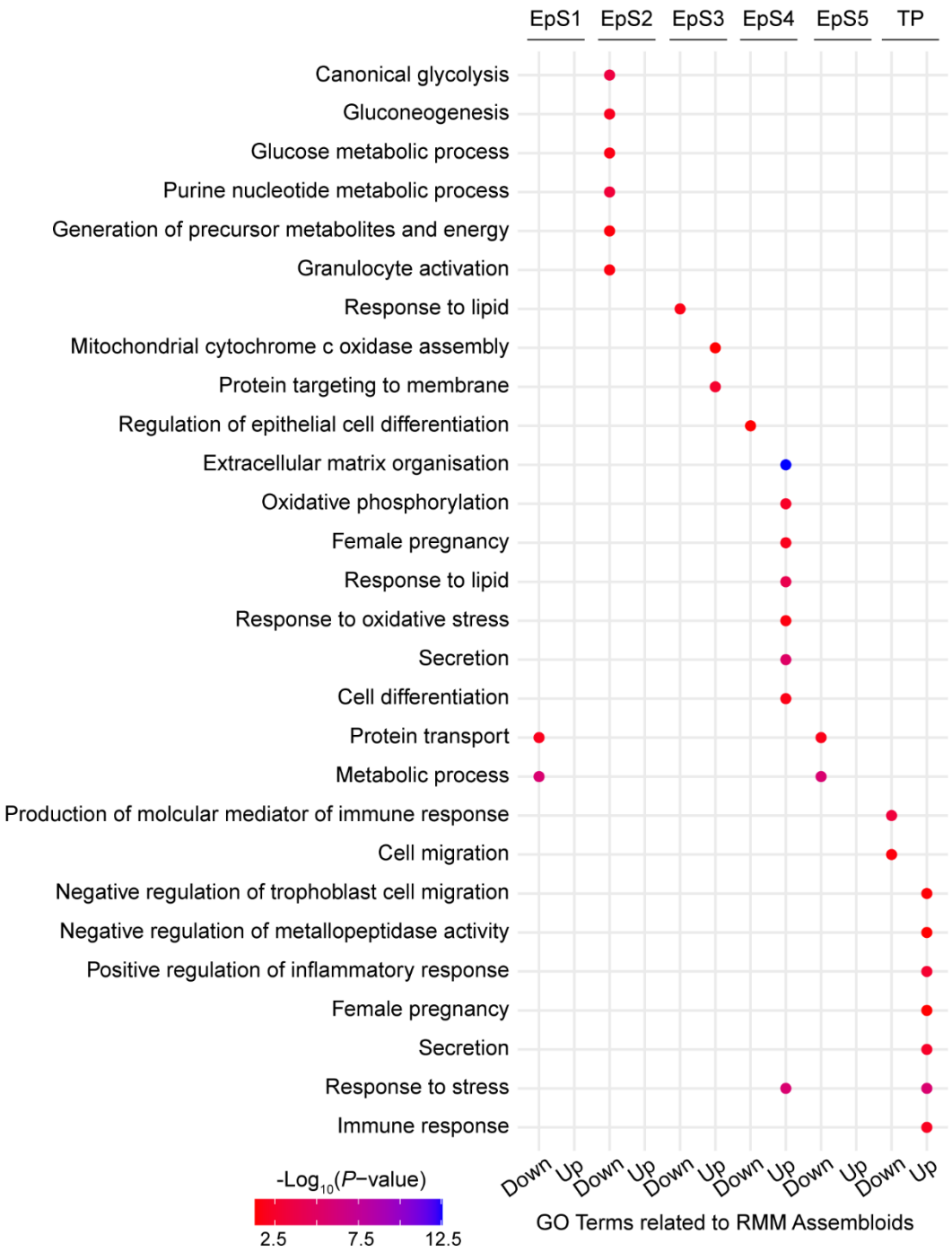

Figure 6.13. ***GO analysis of DEGs upregulated and downregulated RMM assembloids.***

Dot plots showing significantly enriched GO terms (FDR-corrected $P < 0.05$ indicated by the colour) related to biological processes in different epithelial subpopulations in RMM assembloids. DEGs with $P < 0.05$ were used as input for the analysis.

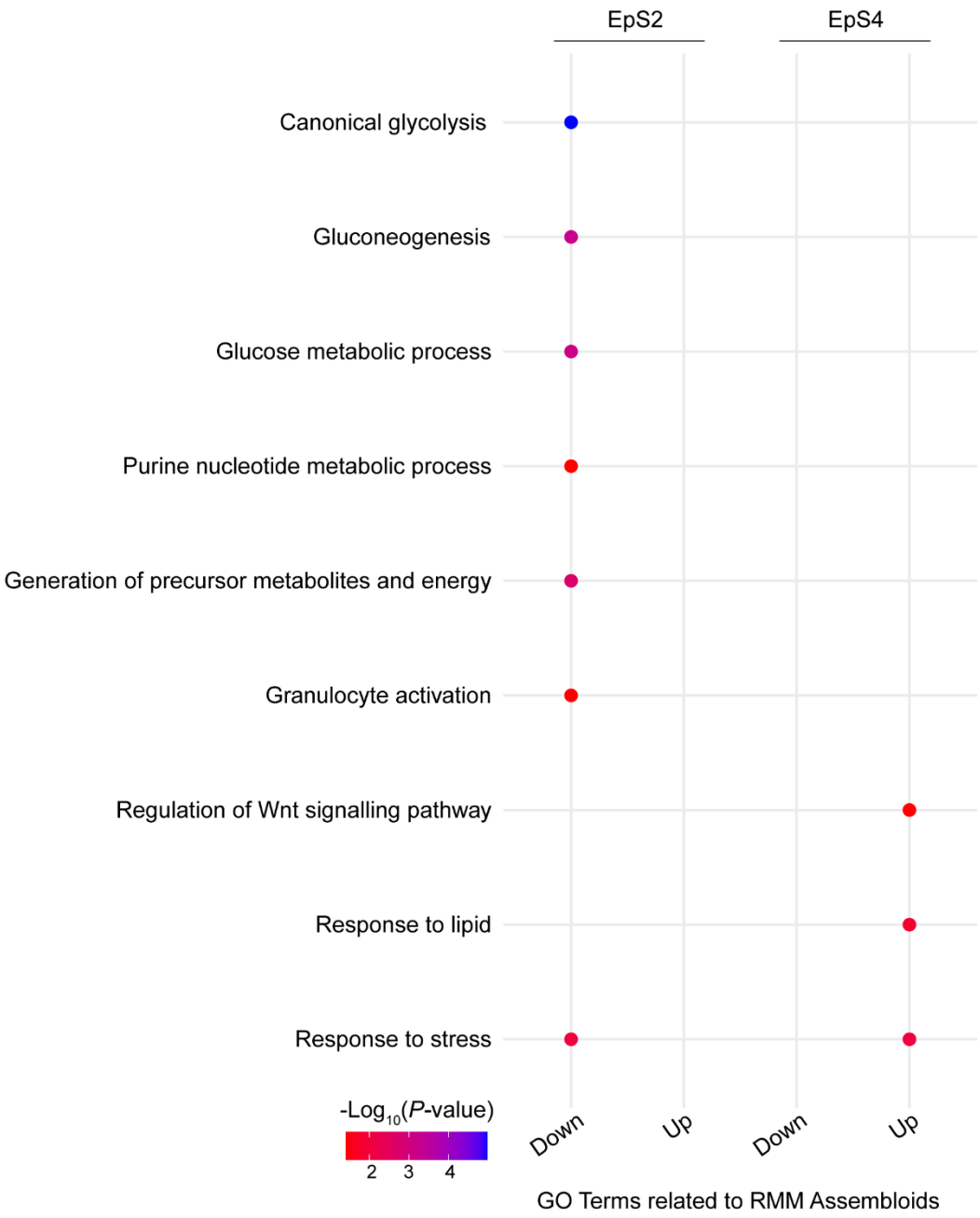

Figure 6.14. ***GO analysis of a stringent set of DEGs upregulated and downregulated RMM assembloids.***

Dot plots showing significantly enriched GO terms (FDR-corrected $P < 0.05$ indicated by the colour) related to biological processes in different epithelial subpopulations in RMM assembloids. DEGs with FDR-corrected *P*-value were used as input for the analysis.

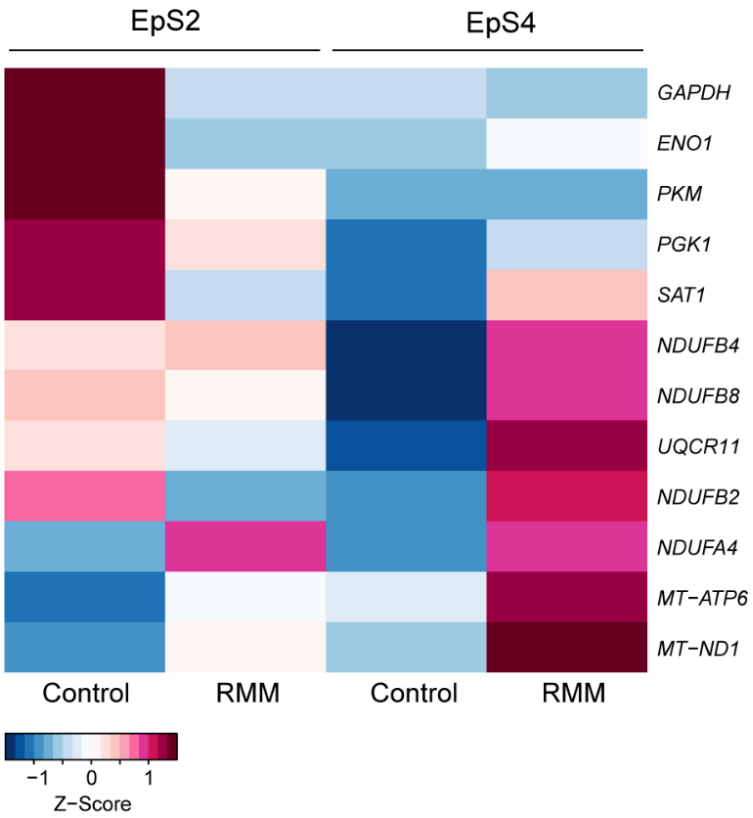

Figure 6.15. Oxidative phosphorylation genes upregulated in RMM assembloids.

Heatmap showing relative expression (Z-scores) of DEGs between control and RMM assembloids in EpS2 and EpS4.

Chapter 7:
General Discussion

7.1 Introduction

RMM is a subset of RPL identified based on a unique pregnancy loss phenotype. Unlike RPL, RMM is characterised by the recurrent pattern of early-onset of fetal growth restriction and a delay in the breakdown of the maternal-fetal interface and bleeding, thus, these miscarriages are frequently detected by ultrasound. Unfortunately, there is limited literature on RMM and consequently, the cause is unknown.

Fetal growth restriction is itself a disorder, defined as birthweight below the third centile, or below the tenth centile with evidence of uteroplacental dysfunction (Aplin et al., 2020). Severe early-onset fetal growth restriction is defined as being below the third growth centile before 32 weeks, whereas less severe cases are when a fetus does not meet the predicted growth trajectory (Aplin et al., 2020). This disorder arises from an insufficient supply of nutrients and oxygen to the fetus due to maternal vascular malperfusion and/or inefficient extraction of substrates by the placenta. However, RMM is a disorder of the first trimester and during this period, histotrophic nutrition is provided by the endometrial glands as the placenta is still developing. Therefore, it is plausible gland defects attributed to a lack of nutrition could be the cause of RMM.

Historically, most of the literature surrounding the endometrial glands has come from animal models, and histology studies due to limited human *in vitro* models. Thus, in humans, endometrial glands are understudied. Recent establishment of endometrial gland organoids has enabled the modelling of the gland epithelium (Turco et al., 2017, Boretto et al., 2017). The establishment of patient-derived gland organoids provides the opportunity to recapitulate the *in vivo* glandular defects and advance the knowledge of the glands in disorders such as RMM.

For the first time, an in-depth study was conducted on RMM with the aim of identifying the endometrial defects that cause RMM. The following objectives were undertaken:

1) First, I analysed the mid-luteal RMM endometrium and identified metabolic defects in endometrial glands and a delayed decidual response in RMM.
2) Next, I optimised gland organoid protocols to establish patient-specific gland organoids that were used to model and dissect the mechanism of the disease.

3) Lastly, I established endometrial assembloids using control and RMM gland organoids for scRNA-seq. The preliminary data highlighted differences in metabolic pathways used by control and RMM EpC subpopulations.

7.2 Endometrial Defects in RMM

7.2.1 Summary of findings

Previously, it was hypothesised that RMM glands are subjected to a metabolic stress in early gestation, leading to gradual failure in histotrophic nutrition. Initial RNA-seq analysis comparison of mid-luteal endometrial glands from control and RMM found an upregulated mitochondrial gene signature in RMM glands, suggesting an increased energy expenditure in keeping with hypothesis (Barros, 2017). To gain more in-depth insights into the RMM glands, I reanalysed the RNA-seq data, using advance metabolic modelling.

As anticipated, oxidative phosphorylation was upregulated in the mid-luteal RMM glands, but FVA and FBA provided the opportunity to explore other metabolic pathways and the impact on each other under maximum growth conditions. TCA was also upregulated but instead of glycolytic products feeding the cycle, fatty acid breakdown was concluded to be the source of acetyl-CoA in RMM glands. FAO yields more NADH and $FADH_2$ than the breakdown of glucose, which in turn results in upregulated oxidative phosphorylation.

Successful establishment of patient-derived endometrial gland organoids from RMM patients and control subjects allowed for the investigation of intrinsic defects in RMM glands. Unlike RPL, RMM endometrial epithelial stem/progenitor cells were found in abundance and during their quiescent state are likely to use FAO as seen in other stem cells (Ryall et al., 2015, Knobloch et al., 2017). Consequently, the data suggests metabolic reprogramming may take place in the progeny of these progenitor cells in RMM. Rather than switching to glycolysis during proliferation, RMM gland EpC remain dependent on FAO, evidenced by the increased expression of FAO genes in undifferentiated RMM organoids. This difference was maintained after differentiation.

RNA-seq of organoid cultures from control and RMM endometrial biopsies also highlighted the atypical signalling pathways in RMM glands, including Wnt and Notch pathways. Both pathways have been demonstrated to be essential for gland development and differentiation (Wang et al., 2009, Cuman et al., 2014, Garcia-Alonso et al., 2021). In RMM, the loss of key transcription factors and ligands highlighted impaired signalling resulting in poor development and differentiation. The poor differentiation response observed in the RMM gland organoids also supports the hypothesis that the EpC population in these samples is more immature, as excessive

progenitor cells are predicted to impact the differentiation of the tissue (Zakrzewski et al., 2019).

In keeping with these findings, a deficiency in epithelial senescent cells is observed in RMM glands. Gland EpC diverge into epithelial differentiated and senescent subpopulations with the latter appearing in the late-luteal phase (Brighton et al., 2017, Rawlings et al., 2021a). Absence of senescence has shown to promote FAO (Ogrodnik et al., 2017, Deleye et al., 2020). Therefore, a lack of specification in differentiation maintains FAO for longer than required in RMM glands. Notably, this acute senescence response in glandular EpC underpins the production of proteinases for the breakdown of the basement membrane of the glands (Rawlings et al., 2021a). This may be an essential process to facilitate endoglandular trophoblast invasion for access to histotrophic nutrition (Huppertz, 2020). A more naïve state results in less advanced differentiation response in RMM glands, resulting in a lack of senescent cells and in turn limited access to the secreted histotroph. Without nutritional support in the first trimester, fetal growth restriction takes place as well as poor development of the cytotrophoblastic shell and arterial plugging, leading to early fetal demise.

RPL patients have excessive decidual senescence which is likely to lead to the breakdown of the maternal-fetal interface in early pregnancy (Lucas et al., 2020). In contrast, RMM endometrium was found to have a blunted decidual response and uNK deficiency. In RMM, no immediate breakdown and bleeding are observed in these patients, unlike in RPL, suggesting the mechanism differs between these two phenotypes. Despite only being a preliminary study, scRNA-seq of endometrial assembloid cultures of RMM organoids with undifferentiated or decidualised EnSC from control subjects did not rescue RMM gland defects. Therefore, it can be concluded the poor differentiation response in the glands drives the delayed decidual response.

7.2.2 Reasons for glandular defects in RMM

7.2.2.1. Somatic mutations

Somatic mutations are random mutations that occur during normal mitotic cell divisions in non-germinal cells and persist in all progenies of mutated cells. In cancer, somatic mutational landscapes have been well characterised (Alexandrov et al., 2013). A recent study described the mutation landscape of the endometrial glands

and found 29 base substitution per gland per year acquired during the adult life and were not related to parity (Moore et al., 2020). As I concluded that intrinsic defects are likely to be present within the epithelial stem/progenitor cell populations in RMM patients, it is plausible a common genetic variation may occur in these cells. Whole-genome sequencing of isolated glands from the endometrium will answer if such mutations occur in the RMM endometrium.

7.2.2.2. Endometrial maturation

Before menarche and early adolescence the endometrium is relatively immature and is not responsive to steroid hormones (Brosens et al., 2015). The endometrium only exhibits a proliferative state after birth and little change in glandular secretions are observed due to intrinsic progesterone resistance (Ober and Bernstein, 1955, Brosens et al., 2015). Therefore, most women will experience the first wave of endometrial regeneration after menarche. However, a few cycles of regeneration are needed to acquire full responsiveness to ovarian hormones for pregnancy known as 'preconditioning' (Brosens et al., 2015). During this period, repeated inflammatory modulations may program stem/progenitor cells such that future senescent progeny rapidly express the inflammatory genes due to their retained inflammatory memory (Niec et al., 2021). An immature uterine environment can impact negatively on pregnancy, as shown by increased risk of preterm birth and small gestational age in teenage mothers (Fraser et al., 1995, Chen et al., 2007). If appropriate preconditioning does not take place and a residual immature environment remains, this may result in the tissue being programmed to induce a poor differentiation response, as observed in RMM.

Developmental models have shown that an adverse intrauterine environment can result in fetal programming of long-term health, believed to be mediated through epigenetic mechanisms (Zhu et al., 2019). Adverse conditions, such as sub-optimal maternal diet, that induce even the smallest of epigenetic changes have long-term effects in fetus, appearing as diseases many years later. In tissue, a similar mechanism of programming may take place in the progenitor cells years before pregnancy. However, when the critical windows of epithelial stem/progenitor cells programming take place is unknown and could occur during uterine adenogenesis, postnatally after the rapid change in hormonal environment, at puberty or during the preconditioning stage. The preconditioning stage is likely a critical window for programming as a lack of inflammatory responses in the first few cycles may impact the epigenetic changes required for inflammatory memory (Niec et al., 2021). A study

into the epigenetics modifications in RMM glands compared to control samples would be required to confirm this hypothesis.

7.2.2.3. High Fat Diet

A high fat diet may contribute to the defects of RMM. Increased presence of fatty acid promotes FAO but can have additional effects on stem/progenitor cells over and above fuel source contribution. In colonocytes of the intestine, butyrate (a short chain fatty acid) was found to suppress intestinal stem cell proliferation by acting as a histone deacetylase inhibitor, which increased access of the transcription factor, FOXO3 (forkhead box O3) (Kaiko et al., 2016). FOXO3 is key in halting cell-cycle progression and maintains quiescence for long-term regenerative potential as seen in hematopoietic stem cells (Tothova et al., 2007). However, in a high fat diet too much butyrate may result in unwanted quiescence and reduced regenerative capacity. A high fat diet may impact the environment of epithelial stem/progenitor cells and is another plausible mechanism of programming an adverse defect in the glands.

7.2.3 Future Developments

7.2.3.1. Single-cell RNA-seq

ScRNA-seq was performed on endometrial assembloids to characterise their EnSC and EpC subpopulations and interactions thereof. Future experiments will require the use of fresh biopsies to rule out the role of cryopreservation and thawing on cellular stress responses. Fresh EnSC- and cryopreserved EpC- generated assembloids did not exhibit overt stress and scRNA-seq analysis revealed metabolic pathways differed in EpC subpopulations in control and RMM endometrial assembloids. Notably, the presence of EnSC from a control patient with RMM gland organoids did not rescue the phenotype. It is likely, therefore, that glands drive the EnSC phenotype in RMM.

Despite interesting preliminary findings, EnSC subpopulations and more than half the EpC subpopulations could not be analysed due to the low cell numbers. The lack of EnSC recovered in the scRNA-seq meant I was not able to observe if a blunted decidual response was created by RMM glands. Hence, more cells will need to be sequenced to successfully compare the subpopulations and strengthen the current observations. With additional cells, cell-cell interactions between EnSC and EpC could also be explored using CellPhoneDB analysis used previously to study cellular

interactions in gland organoid cultures (Fitzgerald et al., 2019, Garcia-Alonso et al., 2021, Rawlings et al., 2021a).

7.2.3.2 Targeting fatty acid oxidation

An intrinsic defect in epithelial stem/progenitor cells reprogrammes RMM glands to be dependent on FAO. To support these findings, validation of FAO upregulation in RMM glands is essential. First, upregulated FAO would result in a reduction of lipids in RMM glands and could be determined both *in vivo* and *in vitro* using lipid staining such BIODPY FL dye or Oil Red O staining. Secondly, to identify if RMM organoids depend on FAO, changes in cellular oxygen consumption (OCR) could be assessed with or without the treatment of the CPT1A inhibitor, etomoxir, in RMM and control gland organoids using a Seahorse Extracellular Flux Analyser. Additionally, within this experiment, the dependence of glycolysis by normal glands can be validated by observing the extracellular acidification rate (ECAR).

In two of the current hypotheses, the cause of RMM is due to defects prior to puberty and can only be diagnosed once the women try to achieve pregnancy. Therefore, even if these hypotheses could be confirmed, it is impossible to prevent these defects. Instead, the perturbations that occur in the menstrual cycle that make the endometrium an unfavourable environment for pregnancy need to be treated. The abundance of stem/progenitor cells leads to a poor differentiation response, which in turn leads to an epithelial senescent cell deficiency. A promising treatment would be to increase epithelial senescent cells. There are several pro-senescence drugs such as CDK4/6 inhibitors Palbociclib and Abemaciclib (Wagner and Gil, 2020). However, the pharmacological approach needs to be specifically targeted for EpC. Moreover, some pro-senescence drugs promote a less favourable outcome of cell death and most importantly are not safe for pregnancy (NICE, 2020, Wagner and Gil, 2020).

An alternative method would be to target FAO. P16 levels have been shown to modulate hepatic FAO such that p16 deficiency elevates FAO gene expression and is associated with enhanced activation of PPARα (Deleye et al., 2020). Another study concluded that mitochondria in senescent hepatocytes cells lose their ability to metabolise fatty acids due to a change in mitochondrial function, leading to lipid accumulation (Ogrodnik et al., 2017). Malonyl-CoA is a naturally occurring inhibitor of FAO, which inhibits CPT1, a rate-limiting mitochondrial enzyme controlling the transfer of fatty acids into the mitochondria and can determine the rates of FAO (Houten and Wanders, 2010). Interestingly, FAO regulates neural stem/progenitor

cells activity and treatment with malonyl-CoA induces cell cycle entry and proliferation (Knobloch et al., 2017). Therefore, malonyl-CoA is an ideal candidate to reduce the abundance of quiescent stem cells by inhibiting FAO, which may increase proliferation, stop metabolic reprogramming and in turn allow for acute senescence in those EpC susceptible to replicative stress. Changes in cellular OCR due to FAO can be assessed with treatment of malonyl-CoA in RMM organoids to confirm a decrease. Senescent markers such as p16 can be used to assess an increase in epithelial senescence. Additionally, an increase in telomerase activity and telomere length can be measured in the glands to confirm the change in senescent levels.

7.2.3.3 CRISPR-Cas9

Several genes and pathways were identified as perturbed in the RMM organoids using RNA-seq. However, there is currently limited knowledge on their exact function as proteins in human endometrial glands. Therefore, these genes and their proteins can be functionally validated using Clustered Regularly Interspaced Short Palindromic Repeats (CRISPR)-Cas9 (CRISPR-associated protein 9). Currently, CRISPR-Cas9 has not been used for genome editing in endometrial organoids. However, CRISPR-Cas9 has successfully been used to knock out various genes in healthy stem cells to generate several types of organoids including brain (Kim et al., 2019), lung (Strikoudis et al., 2019), kidney (Freedman et al., 2015), and intestine (Jung et al., 2019). Optimising this system with the endometrial organoids will give rise to the opportunity to explore proteins and pathway functions and the impact they have on the growth and formation of the control organoids, especially the progenitor/stem cell markers, as well as the differentiation capacity and their secretions. This would improve our understanding of the perturbations in RMM that arise from this altered gene expression. The genes of interest such as the upregulated genes, *LGR5*, *POU5F1* and *PPARGC1A*, and downregulated genes, *HES5* and *LEF1*, can be knocked down in control organoids to identify their function when compared to the wildtype control organoids. Additionally, the loss of *HES5* and *LEF1* will hopefully highlight changes observed in RMM organoids.

7.2.3.4 Endometrial and trophoblast organoids

Recently, trophoblast organoids have been successfully established from first trimester placental tissue using a specific trophoblast organoid medium (Haider et al., 2018, Turco et al., 2018). Fewer epithelial senescent cells were found in the RMM glands both *in vivo* and *in vitro*. It was hypothesised without these cells, access to

histotrophic nutrition would be limited including key factors required for cytotrophoblast growth, transformation, and migration. Hence, a co-culture of RMM endometrial organoids and trophoblast organoids can be generated in the future to model the interactions of these two systems and to validate if the RMM glands have an unfavourable effect on the trophoblast cells. Differentiation of the trophoblast organoids can produce extravillous trophoblast with a specific differentiation medium (Haider et al., 2018, Turco et al., 2018). The presence of the endometrial gland organoids may replace some of these factors in a control sample as previously observed in the endometrial assembloids (Rawlings et al., 2021a). On the other hand, the RMM organoids may limit the invasiveness of these cells. Another recent study established a 3D co-culture of murine embryos and endothelial cells in a microfluidic device that successfully showed interaction of the trophoblast and endothelial cells (Govindasamy et al., 2021). A similar system could be optimised using trophoblast organoids and endothelial cells that would be treated with or without supernatant from RMM organoids. Additionally, a timelapse could be used to visualise if RMM gland organoid secretions would limit the interaction of the two cell types by measuring the invasion of the trophoblast cells.

7.3 Conclusion

In summary, this thesis, for the first time, presents an in-depth study of RMM. Metabolic modelling inferred that the metabolic perturbations in RMM glands were more pronounced than previously perceived and were not due to out-of-phase gland timings. To study RMM glands *in vitro*, I successfully established patient-derived endometrial gland organoids from control and RMM endometrium. Using optimised gland organoid protocols, I found RMM glands have intrinsic defects in the endometrial epithelial stem/progenitor cell population, which impact on the stemness, cell cycle regulation and differentiation potential and leads to a metabolic reprogramming of its progeny. Moreover, a lack of epithelial senescent cells was found in RMM glands that may limit the access of the conceptus to histotrophic nutrition at pregnancy. Preliminary findings from endometrial assembloids supported previous findings that RMM glands use alternative metabolic pathways and the presence of control EnSC is inconsequential to the RMM gland defects. Pharmacologically targeting of FAO to switch from quiescent to proliferative state has promise of reprogramming the metabolic and differential state of RMM glands.

Appendix

1. Demographic Tables

Table 1.1: *Subject demographics of control vs RMM gland RNA-seq*.

	Control (n=8) [a]	**RMM (n=8)** [b]	***P*-value** [c]
Age (years) (median ± IQR)	37 (34-39)	39 (34-40)	0.8591
BMI (median ± IQR)	26 (22-29)	24 (23-25)	0.7809
LH + day (median ± IQR)	9 (8-9)	8 (8)	0.1251
First trimester loss [median (range)]	0 (0-2)	4 (3-8)	0.0002
Live births [median (range)]	1 (0-2)	1 (0-2)	0.8858

[a]Control subjects were awaiting IVF treatment for a number of reasons, including male factor, unexplained, and tubo-ovarian infertility.

[b]RMM were defined as three or more missed miscarriages.

[c]For normally distributed data (age), *P* value was calculated using two-tailed unpaired *t*-test; for non-normally distributed data, (BMI, LH+, first trimester loss and live births) two-tailed Mann Whitney test.

Table 1.2: *Subject demographics of endometrial samples across the luteal phase.*

	LH+5 (n=3)	**LH+8 (n=3)**	**LH+11 (n=3)**
Age (years) [median (range)]	36 (32-40)	38 (34-43)	33 (32-38)
BMI [median (range)]	28 (26-29)	24.4 (23-30)	22.7 (22-23.3)
LH + day [median (range)]	5(5)	8(8)	11(11)
First trimester loss [median (range)]	5(1-15)	0(0-1)	4(2-5)
Live births [median (range)]	0(0)	0(0)	0(0-1)

Table 1.3: *Subject demographics of endometrial samples for the molecular timing model.*

	Endometrial samples
Age (years) (median ± IQR)	36 (33-38)
BMI (median ± IQR)	24 (22-27)
LH + day (median ± IQR)	8 (7-10)
First trimester loss [median (range)]	1 (0-18)
Live births [median (range)]	0 (0-2)

Table 1.4: ***Subject demographics of control and RMM endometrial samples for the molecular timing model.***

	Control (n=93) [a]	**RMM (n=75)** [b]	***P*-value** [c]
Age (years) (median ± IQR)	36 (33-37)	36 (33-39)	0.4451
BMI (median ± IQR)	22 (21-25)	25 (23-28)	<0.0001
LH + day (median ± IQR)	8 (7-10)	8 (8-10)	0.466
First trimester loss [median (range)]	0 (0-2)	5 (3-13)	<0.0001
Live births [median (range)]	0 (0-2)	0 (0-4)	<0.0001

[a]Control subjects were awaiting IVF treatment for a number of reasons, including male factor, unexplained, and tubo-ovarian infertility.

[b]RMM were defined as three or more missed miscarriages.

[c]For non-normally distributed data, (age, BMI, LH+, first trimester loss and live births) *P* value was calculated using two-tailed Mann Whitney test.

Table 1.5: ***Subject demographics of control and RMM endometrial samples for decidual divergence.***

	Control (n=93) [a]	**RMM (n=73)** [b]	***P*-value** [c]
Age (years) (median ± IQR)	36 (33-37)	36 (33-39)	0.4667
BMI (median ± IQR)	22 (21-25)	25 (23-28)	<0.0001
LH + day (median ± IQR)	8 (7-10)	8 (7-9)	0.5312
First trimester loss [median (range)]	0 (0-2)	5 (3-13)	<0.0001
Live births [median (range)]	0 (0-2)	0 (0-4)	0.0002

[a]Control subjects were awaiting IVF treatment for a number of reasons, including male factor, unexplained, and tubo-ovarian infertility.

[b]RMM were defined as three or more missed miscarriages.

[c]For non-normally distributed data, (age, BMI, LH+, first trimester loss and live births) *P* value was calculated using two-tailed Mann Whitney test.

Table 1.6: ***Subject demographics of control and RMM endometrial samples for OFE assay.***

	Control (n=10) [a]	**RMM (n=10)** [b]	***P*-value** [c]
Age (years) (median ± IQR)	37 (34-39)	34 (33-37)	0.1169
BMI (median ± IQR)	22 (21-28)	25 (24-30)	0.2664
LH + day (median ± IQR)	8 (7-9)	10 (8-11)	0.1467
First trimester loss [median (range)]	1 (1-3)	6 (4-7)	0.0002
Live births [median (range)]	0 (0-1)	1 (0-1)	0.6499

[a]Control subjects were awaiting IVF treatment for a number of reasons, including male factor, unexplained, and tubo-ovarian infertility.

[b]RMM were defined as three or more missed miscarriages.

[c]For normally distributed data (age, LH+ and first trimester loss), *P* value was calculated using two-tailed unpaired *t*-test; for non-normally distributed data, (BMI and live births) two-tailed Mann Whitney test.

Table 1.7: ***Subject demographics of control and RMM endometrial samples for organoid RNA-seq.***

	Control (n=4) [a]	**RMM (n=4)** [b]	***P*-value** [c]
Age (years) (median ± IQR)	34 (33)	32 (30-31)	0.2969
BMI (median ± IQR)	21 (20)	24 (24)	0.1033
LH + day (median ± IQR)	9 (9)	10 (8-9)	0.8880
First trimester loss [median (range)]	1(0-2)	5 (3-6)	0.0023
Live births [median (range)]	0 (0-1)	1 (0-1)	>0.9999

[a]Control subjects were awaiting IVF treatment for a number of reasons, including male factor, unexplained, and tubo-ovarian infertility.

[b]RMM were defined as three or more missed miscarriages.

[c]For normally distributed data (age, BMI, LH+ and first trimester loss), *P* value was calculated using two-tailed unpaired *t*-test; for non-normally distributed data, (live births) two-tailed Mann Whitney test.

Table 1.8: ***Subject demographics of control and RMM endometrial samples for organoid RNA-seq validation.***

	Control (n=8) [a]	**RMM (n=8)** [b]	***P*-value** [c]
Age (years) (median ± IQR)	34 (32-36)	35 (33-36)	0.9404
BMI (median ± IQR)	23 (22-28)	24 (22-26)	0.9924
LH + day (median ± IQR)	8 (8-9)	10 (9-11)	0.1198
First trimester loss [median (range)]	1 (0-2)	5 (3-8)	0.0002
Live births [median (range)]	0 (0-1)	1(0-1)	0.2821

[a]Control subjects were awaiting IVF treatment for a number of reasons, including male factor, unexplained, and tubo-ovarian infertility.

[b]RMM were defined as three or more missed miscarriages.

[c]For normally distributed data (age, BMI, and LH+), *P* value was calculated using two-tailed unpaired *t*-test; for non-normally distributed data, (live births and first trimester loss) two-tailed Mann Whitney test.

Table 1.9: ***Subject demographics of control and RMM endometrial samples for p16 immunohistochemistry.***

	Control (n=93) [a]	**RMM (n=48)** [b]	***P*-value** [c]
Age (years) (median ± IQR)	36 (33-37)	36 (33-38)	0.7361
BMI (median ± IQR)	22 (21-25)	25 (23-28)	<0.0001
LH + day (median ± IQR)	8 (7-10)	8 (8-9)	0.5063
First trimester loss [median (range)]	0 (0-2)	5 (3-12)	<0.0001
Live births [median (range)]	0 (0-2)	0 (0-4)	<0.0001

[a]Control subjects were awaiting IVF treatment for a number of reasons, including male factor, unexplained, and tubo-ovarian infertility.

[b]RMM were defined as three or more missed miscarriages.

[c]For normally distributed data (age), *P* value was calculated using two-tailed unpaired *t*-test; for non-normally distributed data, (BMI, LH+, first trimester loss and live births) two-tailed Mann Whitney test.

Table 1.10: ***Subject demographics of control and RMM endometrial samples for assembloid scRNA-seq.***

	Control (n=3) [a]	**RMM (n=3)** [b]	***P*-value** [c]
Age (years) [median (range)]	35 (34-39)	36 (29-38)	>0.9999
BMI [median (range)]	22 (20-28)	22 (20-30)	>0.9999
LH + day [median (range)]	10 (8-10)	10 (7-10)	>0.9999
First trimester loss [median (range)]	0 (0)	7 (3-8)	0.1
Live births [median (range)]	0 (0)	0 (0)	>0.9999

[a]Control subjects were awaiting IVF treatment for a number of reasons, including male factor, unexplained, and tubo-ovarian infertility.

[b]RMM were defined as three or more missed miscarriages.

[c]For non-normally distributed data (age, BMI, LH+, first trimester loss and live births), *P* value was calculated using two-tailed Mann Whitney test.

Table 1.11: ***Subject demographics of control and RMM endometrial samples and fresh control EnSC sample for assembloid scRNA-seq.***

	Control (n=2) [a]	**RMM (n=3)** [b]	***P*-value** [c]
Age (years) [median (range)]	35-39	36 (29-38)	0.8
BMI [median (range)]	20-28)	22 (20-30)	>0.9999
LH + day [median (range)]	8-10	10 (7-10)	>0.9999
First trimester loss [median (range)]	0	7 (3-8)	0.2
Live births [median (range)]	0	0 (0)	>0.9999

	Age	**BMI**	**LH+**	**First trimester loss**	**Live Births**
Fresh EnSC biopsy	35	20	8	0	0

[a]Control subjects were awaiting IVF treatment for a number of reasons, including male factor, unexplained, and tubo-ovarian infertility.

[b]RMM patients defined as three or more missed miscarriages.

[c]For non-normally distributed data (age, BMI, LH+, first trimester loss and live births), *P* value was calculated using two-tailed Mann Whitney test.

2. Flux Variability Analysis Tables

Appendix Table 2.1. The TCA cycle and oxidative phosphorylation reactions for each enzyme, flux in control and RMM samples, and flux change from control to RMM. A negative flux represents the reverse reaction.

Reaction id	Reaction name	List of Reactants	List of Products	Pathways	Flux in Control	Flux in RMM	Flux change (%)
CSm	Citrate synthase	M_accoa_m|M_h2o_m|M_oaa_m	M_cit_m|M_coa_m|M_h_m	Tricarboxylic cycle	1.7864	2.5393	42.1421
ACONTm	Aconitate hydratase	M_cit_m	M_icit_m	Tricarboxylic cycle	1.7864	2.5393	42.1421
ICDHxm	Isocitrate dehydrogenase NAD	M_icit_m|M_nad_m	M_akg_m|M_co2_m|M_nadh_m	Tricarboxylic cycle	0	0.2207	100
AKGDm	2-oxoglutarate dehydrogenase	M_akg_m|M_coa_m|M_nad_m	M_co2_m|M_nadh_m|M_succoa_m	Tricarboxylic cycle	3.5371	4.0196	13.6396
SUCOAS1m	Succinyl-CoA ligase (GDP-forming)	M_coa_m|M_gtp_m|M_succ_m	M_gdp_m|M_pi_m|M_succoa_m	Tricarboxylic cycle	-6.2189	-6.8389	9.9701
r0509 (CII)	Succinate:Ubiquinone Oxidoreductase	M_q10_m|M_succ_m	M_fum_m|M_q10h2_m	Tricarboxylic cycle	4.5371	5.0196	10.6334
FUMm	Fumarase mitochondrial	M_fum_m|M_h2o_m	M_mal__L_m	Tricarboxylic cycle	4.5371	5.7362	26.4271
MDHm	Malatedehydrogenase mitochondrial	M_mal__L_m|M_nad_m	M_h_m|M_nadh_m|M_oaa_m	Tricarboxylic cycle	-25.3516	-24.1154	-4.8761
NADH2_u10mi (CI)	NADH2 u10mi	M_h_m|M_nadh_m|M_q10_m	M_h_i|M_nad_m|M_q10h2_m	Oxidative phosphorylation	28.6547	29.0112	1.2443
CYOR_u10mi (CIII)	CYOR u10mi	M_ficytC_m|M_h_m|M_q10h2_m	M_focytC_m|M_h_i|M_q10_m	Oxidative phosphorylation	36.0058	36.8260	2.2778
CYOOm2i (CIV)	CYOOm2i	M_focytC_m|M_h_m|M_o2_m	M_ficytC_m|M_h2o_m|M_h_i	Oxidative phosphorylation	18.0806	18.6898	3.3695
ATPS4mi (CV)	ATP synthase (four protons for one ATP)	M_adp_m|M_h_i|M_pi_m	M_atp_m|M_h2o_m|M_h_m	Oxidative phosphorylation	82.7411	84.5271	2.1585

Appendix Table 2.2. The glycolysis reactions for each enzyme, flux in control and RMM samples, and flux change from control to RMM.

A negative flux represents the reverse reaction.

Reaction id	Reaction name	List of Reactants	List of Products	Pathways	Flux in Control	Flux in RMM	Flux change (%)
HEX1	Hexokinase (D-glucose:ATP)	M_atp_c|M_glc__D_c	M_adp_c|M_g6p_c|M_h_c	Glycolysis	10	10	0
PGI	Glucose-6-phosphate isomerase	M_g6p_c	M_f6p_c	Glycolysis	2.5330	2.9335	15.8064
PFK	Phosphofructokinase	M_atp_c|M_f6p_c	M_adp_c|M_fdp_c|M_h_c	Glycolysis	4.8607	5.0812	4.5361
FBA	Fructose-bisphosphate aldolase	M_fdp_c	M_dhap_c|M_g3p_c	Glycolysis	4.8607	5.0812	4.5361
TPI	Triose-phosphate isomerase	M_dhap_c	M_g3p_c	Glycolysis	6.7158	6.7564	0.6043
GAPD	Glyceraldehyde-3-phosphate dehydrogenase	M_g3p_c|M_nad_c|M_pi_c	M_13dpg_c|M_h_c|M_nadh_c	Glycolysis	17.2318	17.1331	-0.5729
PGK	Phosphoglycerate kinase	M_3pg_c|M_atp_c	M_13dpg_c|M_adp_c	Glycolysis	-17.2318	-17.1331	-0.5730
PGM	Phosphoglycerate mutase	M_2pg_c	M_3pg_c	Glycolysis	-17.2318	-17.1182	-0.6596
ENO	Enolase	M_2pg_c	M_h2o_c|M_pep_c	Glycolysis	17.2318	17.1181	-0.6596
PYK	Pyruvate kinase	M_adp_c|M_h_c|M_pep_c	M_atp_c|M_pyr_c	Glycolysis	17.0756	13.7157	-19.6768
PDHm	Pyruvate dehydrogenase	M_coa_m|M_nad_m|M_pyr_m	M_accoa_m|M_co2_m|M_nadh_m	Glycolysis	20.8839	20.3150	-2.7243
LDH_L	L-lactate dehydrogenase	M_lac__L_c|M_nad_c	M_h_c|M_nadh_c|M_pyr_c	Glycolysis	-17.9801	-17.7393	-1.3392

Appendix Table 2.3: The FAO reactions for each enzyme, flux in control and RMM samples, and flux change from control to RMM.

Reaction id	Reaction name	List of Reactants	List of Products	Pathways	Flux in Control	Flux in RMM	Flux change %
C160CPT1	Carnitine O-palmitoyltransferase	M_crn_c|M_pmtcoa_c	M_coa_c|M_pmtcrn_c	Fatty acid oxidation	0.2943	0.2937	-0.2205
C160CPT2	C160 transport into the mitochondria	M_coa_m|M_pmtcrn_m	M_crn_m|M_pmtcoa_m	Fatty acid oxidation	0.2943	0.2937	-0.2205
FAOXC160	Beta oxidation of long chain fatty acid	M_coa_m|M_fad_m|M_h2o_m|M_nad_m| M_pmtcoa_m	M_accoa_m|M_fadh2_m|M_h_m|M_nadh_m	Fatty acid oxidation	0.2943	0	-100
FAOXC16080m	Beta oxidation of long chain fatty acid	M_coa_m|M_fad_m|M_h2o_m|M_nad_m| M_pmtcoa_m	M_accoa_m|M_fadh2_m|M_h_m| M_nadh_m|M_occoa_m	Fatty acid oxidation	0	0.2937	100
FAOXC80	Beta oxidation of med/long chain fatty acid	M_coa_m|M_fad_m|M_h2o_m|M_nad_m| M_occoa_m	M_accoa_m|M_fadh2_m|M_h_m|M_nadh_m	Fatty acid oxidation	0.5466	0.8400	53.6714
C226CPT1	Carnitine C22:6 transferase	M_c226coa_c|M_crn_c	M_c226crn_c|M_coa_c	Fatty acid oxidation	0.0013	0.0039	196.8143
C226CPT2	C226 transport into the mitochondria	M_c226crn_m|M_coa_m	M_c226coa_m|M_crn_m	Fatty acid oxidation	0.0013	0.0038	196.8143
FAOXC226205m	Beta oxidation of long chain fatty acid	M_c226coa_m|M_coa_m|M_h2o_m|M_nad_m	M_accoa_m|M_h_m|M_nadh_m| M_tmndnccoa_m	Fatty acid oxidation	0.0013	0.0038	196.8143

Appendix Table 2.4: The pentose phosphate pathway reactions for each enzyme, flux in control and RMM samples, and flux change from control to RMM. A negative flux represents the reverse reaction.

Reaction id	Reaction name	List of Reactants	List of Products	Pathways	Flux in Control	Flux in RMM	Flux change %
G6PDH2c	Glucose 6-Phosphate Dehydrogenase	M_g6p_c|M_nadp_c	M_6pgl_c|M_h_c|M_nadph_c	Pentose phosphate pathway	2.3341	2.2006	-5.7181
PGLc	6-Phosphogluconolactonase	M_6pgl_c|M_h2o_c	M_6pgc_c|M_h_c	Pentose phosphate pathway	2.3341	2.2006	-5.7181
GNDc	Phosphogluconate Dehydrogenase	M_6pgc_c|M_nadp_c	M_co2_c|M_nadph_c|M_ru5p__D_c	Pentose phosphate pathway	2.3341	2.2006	-5.7181
RPI	Ribose-5-phosphate isomerase	M_r5p_c	M_ru5p__D_c	Pentose phosphate pathway	-2.3469	-2.3063	-1.7293
RPEc	Ribulose 5-Phosphate 3-Epimerase	M_ru5p__D_c	M_xu5p__D_c	Pentose phosphate pathway	2.3276	2.1477	-7.7289
TKT1	Transketolase	M_r5p_c|M_xu5p__D_c	M_g3p_c|M_s7p_c	Pentose phosphate pathway	2.3276	2.1477	-7.7289
TKT2	Transketolase	M_e4p_c|M_xu5p__D_c	M_f6p_c|M_g3p_c	Pentose phosphate pathway	2.3276	2.1477	-7.7289

Bibliography

ABBAS, Y., CARNICER-LOMBARTE, A., GARDNER, L., THOMAS, J., BROSENS, J. J., MOFFETT, A., SHARKEY, A. M., FRANZE, K., BURTON, G. J. & OYEN, M. L. 2019. Tissue stiffness at the human maternal–fetal interface. *Human Reproduction,* 34**,** 1999-2008.

AGHAJANOVA, L., STAVREUS-EVERS, A., NIKAS, Y., HOVATTA, O. & LANDGREN, B.-M. 2003. Coexpression of pinopodes and leukemia inhibitory factor, as well as its receptor, in human endometrium. *Fertility and sterility,* 79**,** 808-814.

AIN, R., TRINH, M. L. & SOARES, M. J. 2004. Interleukin-11 signaling is required for the differentiation of natural killer cells at the maternal–fetal interface. *Developmental dynamics: an official publication of the American Association of Anatomists,* 231**,** 700-708.

AKRAM, M. 2014. Citric acid cycle and role of its intermediates in metabolism. *Cell biochemistry and biophysics,* 68**,** 475-478.

AL-SABBAGH, M., FUSI, L., HIGHAM, J., LEE, Y., LEI, K., HANYALOGLU, A. C., LAM, E. W.-F., CHRISTIAN, M. & BROSENS, J. J. 2011. NADPH oxidase-derived reactive oxygen species mediate decidualization of human endometrial stromal cells in response to cyclic AMP signaling. *Endocrinology,* 152**,** 730-740.

ALEXANDROV, L. B., NIK-ZAINAL, S., WEDGE, D. C., APARICIO, S. A., BEHJATI, S., BIANKIN, A. V., BIGNELL, G. R., BOLLI, N., BORG, A., BØRRESEN-DALE, A. L., BOYAULT, S., BURKHARDT, B., BUTLER, A. P., CALDAS, C., DAVIES, H. R., DESMEDT, C., EILS, R., EYFJÖRD, J. E., FOEKENS, J. A., GREAVES, M., HOSODA, F., HUTTER, B., ILICIC, T., IMBEAUD, S., IMIELINSKI, M., JÄGER, N., JONES, D. T., JONES, D., KNAPPSKOG, S., KOOL, M., LAKHANI, S. R., LÓPEZ-OTÍN, C., MARTIN, S., MUNSHI, N. C., NAKAMURA, H., NORTHCOTT, P. A., PAJIC, M., PAPAEMMANUIL, E., PARADISO, A., PEARSON, J. V., PUENTE, X. S., RAINE, K., RAMAKRISHNA, M., RICHARDSON, A. L., RICHTER, J., ROSENSTIEL, P., SCHLESNER, M., SCHUMACHER, T. N., SPAN, P. N., TEAGUE, J. W., TOTOKI, Y., TUTT, A. N., VALDÉS-MAS, R., VAN BUUREN, M. M., VAN 'T VEER, L., VINCENT-SALOMON, A., WADDELL, N., YATES, L. R., ZUCMAN-ROSSI, J., FUTREAL, P. A., MCDERMOTT, U., LICHTER, P., MEYERSON, M., GRIMMOND, S. M., SIEBERT, R., CAMPO, E., SHIBATA, T., PFISTER, S. M., CAMPBELL, P. J. & STRATTON, M. R. 2013. Signatures of mutational processes in human cancer. *Nature,* 500**,** 415-21.

ALTMÄE, S., KOEL, M., VÕSA, U., ADLER, P., SUHORUTŠENKO, M., LAISK-PODAR, T., KUKUSHKINA, V., SAARE, M., VELTHUT-MEIKAS, A., KRJUTŠKOV, K., AGHAJANOVA, L., LALITKUMAR, P. G., GEMZELL-DANIELSSON, K., GIUDICE, L., SIMÓN, C. & SALUMETS, A. 2017. Meta-signature of human endometrial receptivity: a meta-analysis and validation study of transcriptomic biomarkers. *Sci Rep,* 7**,** 10077.

ALZAMIL, L., NIKOLAKOPOULOU, K. & TURCO, M. Y. 2021. Organoid systems to study the human female reproductive tract and pregnancy. *Cell Death & Differentiation,* 28**,** 35-51.

ANDERSEN, A.-M. N., WOHLFAHRT, J., CHRISTENS, P., OLSEN, J. & MELBYE, M. 2000. Maternal age and fetal loss: population based register linkage study. *Bmj,* 320**,** 1708-1712.

APLIN, J., CHARLTON, A. & AYAD, S. 1988. An immunohistochemical study of human endometrial extracellular matrix during the menstrual cycle and first trimester of pregnancy. *Cell and tissue research,* 253**,** 231-240.

APLIN, J. D., HAIGH, T., VICOVAC, L., CHURCH, H. J. & JONES, C. J. 1998. Anchorage in the developing placenta: an overlooked determinant of pregnancy outcome? *Hum Fertil (Camb),* 1**,** 75-79.

APLIN, J. D., MYERS, J. E., TIMMS, K. & WESTWOOD, M. 2020. Tracking placental development in health and disease. *Nature Reviews Endocrinology,* 16**,** 479-494.

ARIAS-STELLA, J. 1954. Atypical endometrial changes associated with the presence of chorionic tissue. *AMA archives of pathology,* 58**,** 112-128.

ARMSTRONG, E. M., MORE, I. A., MCSEVENEY, D. & CARTY, M. 1973. The giant mitochondrion-endoplasmic reticulum unit of the human endometrial glandular cell. *Journal of anatomy,* 116**,** 375.

ARNOLD, J. T., KAUFMAN, D. G., SEPPALA, M. & LESSEY, B. A. 2001. Endometrial stromal cells regulate epithelial cell growth in vitro: a new co-culture model. *Human reproduction,* 16**,** 836-845.

ASHKAR, A. A., BLACK, G. P., WEI, Q., HE, H., LIANG, L., HEAD, J. R. & CROY, B. A. 2003. Assessment of requirements for IL-15 and IFN regulatory factors in uterine NK cell differentiation and function during pregnancy. *The Journal of Immunology,* 171**,** 2937-2944.

BANCI, L., BRANCACCIO, D., CIOFI-BAFFONI, S., DEL CONTE, R., GADEPALLI, R., MIKOLAJCZYK, M., NERI, S., PICCIOLI, M. & WINKELMANN, J. 2014.

[2Fe-2S] cluster transfer in iron–sulfur protein biogenesis. *Proceedings of the National Academy of Sciences,* 111**,** 6203-6208.

BARNHART, K., VAN MELLO, N. M., BOURNE, T., KIRK, E., VAN CALSTER, B., BOTTOMLEY, C., CHUNG, K., CONDOUS, G., GOLDSTEIN, S., HAJENIUS, P. J., MOL, B. W., MOLINARO, T., O'FLYNN O'BRIEN, K. L., HUSICKA, R., SAMMEL, M. & TIMMERMAN, D. 2011. Pregnancy of unknown location: a consensus statement of nomenclature, definitions, and outcome. *Fertil Steril,* 95**,** 857-66.

BARROS, F. S. V. 2017. *Characterization of human endometrial glandular epithelium in vitro and in vivo.* PhD, University of Warwick.

BARROS, F. S. V., BROSENS, J. J. & BRIGHTON, P. J. 2016. Isolation and primary culture of various cell types from whole human endometrial biopsies. *Stem Cells*.

BARTOL, F., WILEY, A., COLEMAN, D., WOLFE, D. & RIDDELL, M. 1988. Ovine uterine morphogenesis: effects of age and progestin administration and withdrawal on neonatal endometrial development and DNA synthesis. *Journal of animal science,* 66**,** 3000-3009.

BASISTY, N., KALE, A., JEON, O. H., KUEHNEMANN, C., PAYNE, T., RAO, C., HOLTZ, A., SHAH, S., SHARMA, V., FERRUCCI, L., CAMPISI, J. & SCHILLING, B. 2020. A proteomic atlas of senescence-associated secretomes for aging biomarker development. *PLoS Biol,* 18**,** e3000599.

BENDER ATIK, R., CHRISTIANSEN, O. B., ELSON, J., KOLTE, A. M., LEWIS, S., MIDDELDORP, S., NELEN, W., PERAMO, B., QUENBY, S., VERMEULEN, N. & GODDIJN, M. 2018. ESHRE guideline: recurrent pregnancy loss. *Hum Reprod Open,* 2018**,** hoy004.

BENTIN-LEY, U., PEDERSEN, B., LINDENBERG, S., LARSEN, J. F., HAMBERGER, L. & HORN, T. 1994. Isolation and culture of human endometrial cells in a three-dimensional culture system. *Reproduction,* 101**,** 327-332.

BERKOWITZ, G. S., SKOVRON, M. L., LAPINSKI, R. H. & BERKOWITZ, R. L. 1990. Delayed childbearing and the outcome of pregnancy. *New England Journal of Medicine,* 322**,** 659-664.

BIAN, Y., GAO, G., ZHANG, Q., QIAN, H., YU, L., YAO, N., QIAN, J., LIU, B. & QIAN, X. 2019. KCNQ1OT1/miR-217/ZEB1 feedback loop facilitates cell migration and epithelial-mesenchymal transition in colorectal cancer. *Cancer biology & therapy,* 20**,** 886-896.

BOLAÑOS, J. P., ALMEIDA, A. & MONCADA, S. 2010. Glycolysis: a bioenergetic or a survival pathway? *Trends in biochemical sciences,* 35**,** 145-149.

BORETTO, M., COX, B., NOBEN, M., HENDRIKS, N., FASSBENDER, A., ROOSE, H., AMANT, F., TIMMERMAN, D., TOMASSETTI, C., VANHIE, A., MEULEMAN, C., FERRANTE, M. & VANKELECOM, H. 2017. Development of organoids from mouse and human endometrium showing endometrial epithelium physiology and long-term expandability. *Development,* 144**,** 1775-1786.

BORETTO, M., MAENHOUDT, N., LUO, X., HENNES, A., BOECKX, B., BUI, B., HEREMANS, R., PERNEEL, L., KOBAYASHI, H., VAN ZUNDERT, I., BREMS, H., COX, B., FERRANTE, M., UJI, I. H., KOH, K. P., D'HOOGHE, T., VANHIE, A., VERGOTE, I., MEULEMAN, C., TOMASSETTI, C., LAMBRECHTS, D., VRIENS, J., TIMMERMAN, D. & VANKELECOM, H. 2019. Patient-derived organoids from endometrial disease capture clinical heterogeneity and are amenable to drug screening. *Nat Cell Biol,* 21**,** 1041-1051.

BRIGHTON, P. J., MARUYAMA, Y., FISHWICK, K., VRLJICAK, P., TEWARY, S., FUJIHARA, R., MUTER, J., LUCAS, E. S., YAMADA, T., WOODS, L., LUCCIOLA, R., LEE, Y. H., TAKEDA, S., OTT, S., HEMBERGER, M., QUENBY, S. & BROSENS, J. J. 2017. Clearance of senescent decidual cells by uterine natural killer cells in cycling human endometrium. *elife,* 6**,** e31274.

BROSENS, I., KONINCKX, P. & CORVELEYN, P. 1978. A STUDY OF PLASMA PROGESTERONE, OESTRADIOL-l7β, PROLACTIN AND LH LEVELS, AND OF THE LUTEAL PHASE APPEARANCE OF THE OVARIES IN PATIENTS WITH ENDOMETRIOSIS AND INFERTILITY. *BJOG: An International Journal of Obstetrics & Gynaecology,* 85**,** 246-250.

BROSENS, I., PIJNENBORG, R., VERCRUYSSE, L. & ROMERO, R. 2011. The "Great Obstetrical Syndromes" are associated with disorders of deep placentation. *Am J Obstet Gynecol,* 204**,** 193-201.

BROSENS, I., ĆURČIĆ, A., VEJNOVIĆ, T., GARGETT, C. E., BROSENS, J. J. & BENAGIANO, G. 2015. The perinatal origins of major reproductive disorders in the adolescent: research avenues. *Placenta,* 36**,** 341-344.

BROSENS, J. J., HAYASHI, N. & WHITE, J. O. 1999. Progesterone receptor regulates decidual prolactin expression in differentiating human endometrial stromal cells. *Endocrinology,* 140**,** 4809-4820.

BROWN, K., HELLER, D. S., ZAMUDIO, S. & ILLSLEY, N. P. 2011. Glucose transporter 3 (GLUT3) protein expression in human placenta across gestation. *Placenta,* 32**,** 1041-1049.

BRUNK, E., SAHOO, S., ZIELINSKI, D. C., ALTUNKAYA, A., DRÄGER, A., MIH, N., GATTO, F., NILSSON, A., PRECIAT GONZALEZ, G. A., AURICH, M. K., PRLIĆ, A., SASTRY, A., DANIELSDOTTIR, A. D., HEINKEN, A., NORONHA, A., ROSE, P. W., BURLEY, S. K., FLEMING, R. M. T., NIELSEN, J., THIELE, I. & PALSSON, B. O. 2018. Recon3D enables a three-dimensional view of gene variation in human metabolism. *Nat Biotechnol,* 36**,** 272-281.

BURTON, G., SCIOSCIA, M. & RADEMACHER, T. 2011. Endometrial secretions: creating a stimulatory microenvironment within the human early placenta and implications for the aetiopathogenesis of preeclampsia. *Journal of reproductive immunology,* 89**,** 118-125.

BURTON, G. J., CINDROVA-DAVIES, T. & TURCO, M. Y. 2020. Histotrophic nutrition and the placental-endometrial dialogue during human early pregnancy. *Placenta*.

BURTON, G. J. & JAUNIAUX, E. 2017. The cytotrophoblastic shell and complications of pregnancy. *Placenta,* 60**,** 134-139.

BURTON, G. J., JAUNIAUX, E. & CHARNOCK-JONES, D. S. 2007. Human early placental development: potential roles of the endometrial glands. *Placenta,* 28**,** S64-S69.

BURTON, G. J., JAUNIAUX, E. & MURRAY, A. J. 2017. Oxygen and placental development; parallels and differences with tumour biology. *Placenta,* 56**,** 14-18.

BURTON, G. J., WATSON, A. L., HEMPSTOCK, J., SKEPPER, J. N. & JAUNIAUX, E. 2002. Uterine glands provide histiotrophic nutrition for the human fetus during the first trimester of pregnancy. *The Journal of Clinical Endocrinology & Metabolism,* 87**,** 2954-2959.

BURTON, G. J., WOODS, A. W., JAUNIAUX, E. & KINGDOM, J. C. 2009. Rheological and physiological consequences of conversion of the maternal spiral arteries for uteroplacental blood flow during human pregnancy. *Placenta,* 30**,** 473-82.

CAPALBO, A., HOFFMANN, E. R., CIMADOMO, D., MARIA UBALDI, F. & RIENZI, L. 2017. Human female meiosis revised: new insights into the mechanisms of chromosome segregation and aneuploidies from advanced genomics and time-lapse imaging. *Human Reproduction Update,* 23**,** 706-722.

CARPENTER, K. D., GRAY, C. A., NOEL, S., GERTLER, A., BAZER, F. W. & SPENCER, T. E. 2003. Prolactin regulation of neonatal ovine uterine gland morphogenesis. *Endocrinology,* 144**,** 110-120.

CARTA, L. & SASSOON, D. 2004. Wnt7a is a suppressor of cell death in the female reproductive tract and is required for postnatal and estrogen-mediated growth. *Biology of reproduction,* 71**,** 444-454.

CHAN, R. W. S., SCHWAB, K. E. & GARGETT, C. E. 2004. Clonogenicity of human endometrial epithelial and stromal cells. *Biology of reproduction,* 70**,** 1738-1750.

CHAUCHEREAU, A., SAVOURET, J.-F. & MILGROM, E. 1992. Control of biosynthesis and post-transcriptional modification of the progesterone receptor. *Biology of reproduction,* 46**,** 174-177.

CHAVEZ-MACGREGOR, M., VAN GILS, C. H., VAN DER SCHOUW, Y. T., MONNINKHOF, E., VAN NOORD, P. A. & PEETERS, P. H. 2008. Lifetime cumulative number of menstrual cycles and serum sex hormone levels in postmenopausal women. *Breast cancer research and treatment,* 108**,** 101-112.

CHAZARA, O., XIONG, S. & MOFFETT, A. 2011. Maternal KIR and fetal HLA-C: a fine balance. *Journal of leukocyte biology,* 90**,** 703-716.

CHEN, H., DENG, X., YANG, Y., SHEN, Y., CHAO, L., WEN, Y. & SUN, Y. 2015. Expression of GRIM-19 in missed abortion and possible pathogenesis. *Fertil Steril,* 103**,** 138-46.e3.

CHEN, X.-K., WEN, S. W., FLEMING, N., DEMISSIE, K., RHOADS, G. G. & WALKER, M. 2007. Teenage pregnancy and adverse birth outcomes: a large population based retrospective cohort study. *International journal of epidemiology,* 36**,** 368-373.

CHEN, Y., LI, J., XIAO, J.-K., XIAO, L., XU, B.-W. & LI, C. 2021. The lncRNA NEAT1 promotes the epithelial-mesenchymal transition and metastasis of osteosarcoma cells by sponging miR-483 to upregulate STAT3 expression. *Cancer Cell International,* 21**,** 1-20.

CHENG, X., LIU, J., SHAN, H., SUN, L., HUANG, C., YAN, Q., JIANG, R., DING, L., JIANG, Y., ZHOU, J., YAN, G. & SUN, H. 2017. Activating transcription factor 3 promotes embryo attachment via up-regulation of leukemia inhibitory factor in vitro. *Reprod Biol Endocrinol,* 15**,** 42.

CHI, R. A., WANG, T., ADAMS, N., WU, S. P., YOUNG, S. L., SPENCER, T. E. & DEMAYO, F. 2020. Human Endometrial Transcriptome and Progesterone

Receptor Cistrome Reveal Important Pathways and Epithelial Regulators. *J Clin Endocrinol Metab,* 105**,** e1419-39.

CHRISTIAN, M., MAK, I., WHITE, J. O. & BROSENS, J. J. 2002. Mechanisms of decidualization. *Reproductive biomedicine online,* 4**,** 24-30.

CHUMDURI, C., GURUMURTHY, R. K., BERGER, H., KOSTER, S., BRINKMANN, V., KLEMM, U., MOLLENKOPF, H.-J., HERBST, H., MANGLER, M. & MEYER, T. F. 2018. Transition of Wnt signaling microenvironment delineates the squamo-columnar junction and emergence of squamous metaplasia of the cervix. *BioRxiv***,** 443770.

CLASSEN-LINKE, I., KUSCHE, M., KNAUTHE, R. & BEIER, H. 1996. Establishment of a human endometrial cell culture system and characterization of its polarized hormone responsive epithelial cells. *Cell and tissue research,* 287**,** 171-185.

COBELLIS, L., CAPRIO, F., TRABUCCO, E., MASTROGIACOMO, A., COPPOLA, G., MANENTE, L., COLACURCI, N., DE FALCO, M. & DE LUCA, A. 2008. The pattern of expression of Notch protein members in normal and pathological endometrium. *Journal of anatomy,* 213**,** 464-472.

CONSORTIUM, G. O. 2019. The gene ontology resource: 20 years and still GOing strong. *Nucleic acids research,* 47**,** D330-D338.

COOKE, P. S., BUCHANAN, D. L., LUBAHN, D. B. & CUNHA, G. R. 1998. Mechanism of estrogen action: lessons from the estrogen receptor-α knockout mouse. *Biology of reproduction,* 59**,** 470-475.

COOMARASAMY, A., DEVALL, A. J., BROSENS, J. J., QUENBY, S., STEPHENSON, M. D., SIERRA, S., CHRISTIANSEN, O. B., SMALL, R., BREWIN, J., ROBERTS, T. E., DHILLON-SMITH, R., HARB, H., NOORDALI, H., PAPADOPOULOU, A., EAPEN, A., PRIOR, M., DI RENZO, G. C., HINSHAW, K., MOL, B. W., LUMSDEN, M. A., KHALAF, Y., SHENNAN, A., GODDIJN, M., VAN WELY, M., AL-MEMAR, M., BENNETT, P., BOURNE, T., RAI, R., REGAN, L. & GALLOS, I. D. 2020. Micronized vaginal progesterone to prevent miscarriage: a critical evaluation of randomized evidence. *Am J Obstet Gynecol,* 223**,** 167-176.

COOMARASAMY, A., DEVALL, A. J., CHEED, V., HARB, H., MIDDLETON, L. J., GALLOS, I. D., WILLIAMS, H., EAPEN, A. K., ROBERTS, T., OGWULU, C. C., GORANITIS, I., DANIELS, J. P., AHMED, A., BENDER-ATIK, R., BHATIA, K., BOTTOMLEY, C., BREWIN, J., CHOUDHARY, M., CROSFILL, F., DEB, S., DUNCAN, W. C., EWER, A., HINSHAW, K., HOLLAND, T., IZZAT, F.,

JOHNS, J., KRIEDT, K., LUMSDEN, M. A., MANDA, P., NORMAN, J. E., NUNES, N., OVERTON, C. E., QUENBY, S., RAO, S., ROSS, J., SHAHID, A., UNDERWOOD, M., VAITHILINGAM, N., WATKINS, L., WYKES, C., HORNE, A. & JURKOVIC, D. 2019. A Randomized Trial of Progesterone in Women with Bleeding in Early Pregnancy. *N Engl J Med,* 380**,** 1815-1824.

COUSINS, F. L., PANDOY, R., JIN, S. & GARGETT, C. E. 2021. The Elusive Endometrial Epithelial Stem/Progenitor Cells. *Frontiers in Cell and Developmental Biology,* 9**,** 868.

CRITCHLEY, H. O., MAYBIN, J. A., ARMSTRONG, G. M. & WILLIAMS, A. R. 2020. Physiology of the endometrium and regulation of menstruation. *Physiological reviews,* 100**,** 1149-1179.

CUI, X., WANG, H., LI, Y., CHEN, T., LIU, S. & YAN, Q. 2020. Epiregulin promotes trophoblast epithelial–mesenchymal transition through poFUT1 and O-fucosylation by poFUT1 on uPA. *Cell proliferation,* 53**,** e12745.

CUMAN, C., MENKHORST, E., WINSHIP, A., VAN SINDEREN, M., OSIANLIS, T., ROMBAUTS, L. J. & DIMITRIADIS, E. 2014. Fetal–maternal communication: the role of Notch signalling in embryo implantation. *Reproduction,* 147**,** R75-R86.

DAVIES, J. E., POLLHEIMER, J., YONG, H. E., KOKKINOS, M. I., KALIONIS, B., KNÖFLER, M. & MURTHI, P. 2016. Epithelial-mesenchymal transition during extravillous trophoblast differentiation. *Cell Adh Migr,* 10**,** 310-21.

DE ZIEGLER, D., BERGERON, C., CORNEL, C., MEDALIE, D., MASSAI, M., MILGROM, E., FRYDMAN, R. & BOUCHARD, P. 1992. Effects of luteal estradiol on the secretory transformation of human endometrium and plasma gonadotropins. *The Journal of Clinical Endocrinology & Metabolism,* 74**,** 322-331.

DELEYE, Y., COTTE, A. K., HANNOU, S. A., HENNUYER, N., BERNARD, L., DERUDAS, B., CARON, S., LEGRY, V., VALLEZ, E., DORCHIES, E., MARTIN, N., LANCEL, S., ANNICOTTE, J. S., BANTUBUNGI, K., POURTIER, A., RAVERDY, V., PATTOU, F., LEFEBVRE, P., ABBADIE, C., STAELS, B., HAAS, J. T. & PAUMELLE, R. 2020. CDKN2A/p16INK4a suppresses hepatic fatty acid oxidation through the AMPKα2-SIRT1-PPARα signaling pathway. *J Biol Chem,* 295**,** 17310-17322.

DEMIR, R., KAYISLI, U., CELIK-OZENCI, C., KORGUN, E., DEMIR-WEUSTEN, A. & ARICI, A. 2002. Structural differentiation of human uterine luminal and

glandular epithelium during early pregnancy: an ultrastructural and immunohistochemical study. *Placenta,* 23**,** 672-684.

DIMITRIADIS, E., MENKHORST, E., SAITO, S., KUTTEH, W. H. & BROSENS, J. J. 2020. Recurrent pregnancy loss. *Nature Reviews Disease Primers,* 6**,** 1-19.

DINIZ-DA-COSTA, M., KONG, C. S., FISHWICK, K. J., RAWLINGS, T., BRIGHTON, P. J., HAWKES, A., ODENDAAL, J., QUENBY, S., OTT, S., LUCAS, E. S., VRLJICAK, P. & BROSENS, J. J. 2021. Characterization of highly proliferative decidual precursor cells during the window of implantation in human endometrium. *Stem Cells*.

DUNLAP, K. A., FILANT, J., HAYASHI, K., RUCKER, E. B., 3RD, SONG, G., DENG, J. M., BEHRINGER, R. R., DEMAYO, F. J., LYDON, J., JEONG, J. W. & SPENCER, T. E. 2011. Postnatal deletion of Wnt7a inhibits uterine gland morphogenesis and compromises adult fertility in mice. *Biol Reprod,* 85**,** 386-96.

DUTTA, E. H., BEHNIA, F., BOLDOGH, I., SAADE, G. R., TAYLOR, B. D., KACEROVSKÝ, M. & MENON, R. 2016. Oxidative stress damage-associated molecular signaling pathways differentiate spontaneous preterm birth and preterm premature rupture of the membranes. *Mol Hum Reprod,* 22**,** 143-57.

DÍAZ-GIMENO, P., HORCAJADAS, J. A., MARTÍNEZ-CONEJERO, J. A., ESTEBAN, F. J., ALAMÁ, P., PELLICER, A. & SIMÓN, C. 2011. A genomic diagnostic tool for human endometrial receptivity based on the transcriptomic signature. *Fertility and sterility,* 95**,** 50-60. e15.

ELURBE, D. M. & HUYNEN, M. A. 2016. The origin of the supernumerary subunits and assembly factors of complex I: A treasure trove of pathway evolution. *Biochimica et Biophysica Acta (BBA)-Bioenergetics,* 1857**,** 971-979.

ELZI, D. J., LAI, Y., SONG, M., HAKALA, K., WEINTRAUB, S. T. & SHIIO, Y. 2012. Plasminogen activator inhibitor 1-insulin-like growth factor binding protein 3 cascade regulates stress-induced senescence. *Proceedings of the National Academy of Sciences,* 109**,** 12052-12057.

ERKENBRACK, E. M., MAZIARZ, J. D., GRIFFITH, O. W., LIANG, C., CHAVAN, A. R., NNAMANI, M. C. & WAGNER, G. P. 2018. The mammalian decidual cell evolved from a cellular stress response. *PLoS biology,* 16**,** e2005594.

FAHNENSTICH, J., NANDY, A., MILDE-LANGOSCH, K., SCHNEIDER-MERCK, T., WALTHER, N. & GELLERSEN, B. 2003. Promyelocytic leukaemia zinc finger protein (PLZF) is a glucocorticoid- and progesterone-induced transcription

factor in human endometrial stromal cells and myometrial smooth muscle cells. *Mol Hum Reprod,* 9**,** 611-23.

FAN, X., KRIEG, S., HWANG, J. Y., DHAL, S., KUO, C. J., LASLEY, B. L., BRENNER, R. M. & NAYAK, N. R. 2012. Dynamic regulation of Wnt7a expression in the primate endometrium: implications for postmenstrual regeneration and secretory transformation. *Endocrinology,* 153**,** 1063-1069.

FERENCZY, A. & BERGERON, C. 1991. Histology of the human endometrium: from birth to senescence. *Annals of the New York Academy of Sciences,* 622**,** 6-27.

FERENCZY, A., BERTRAND, G. & GELFAND, M. M. 1979. Proliferation kinetics of human endometrium during the normal menstrual cycle. *American journal of obstetrics and gynecology,* 133**,** 859-867.

FERENCZY, A. & GURALNICK, M. 1983. Endometrial microstructure: Structure-function relationships throughout the menstrual cycle. *Semin. Reprod. Endocrinol,* 1**,** 205-219.

FERENCZY, A. & MUTTER, G. 2008. The Endometrial Cycle. *Glob. libr. women's med*.

FILANT, J., LYDON, J. P. & SPENCER, T. E. 2014. Integrated chromatin immunoprecipitation sequencing and microarray analysis identifies FOXA2 target genes in the glands of the mouse uterus. *The FASEB Journal,* 28**,** 230-243.

FILANT, J. & SPENCER, T. E. 2013a. Cell-specific transcriptional profiling reveals candidate mechanisms regulating development and function of uterine epithelia in mice. *Biology of reproduction,* 89**,** 86, 1-10.

FILANT, J. & SPENCER, T. E. 2013b. Endometrial glands are essential for blastocyst implantation and decidualization in the mouse uterus. *Biology of reproduction,* 88**,** 93, 1-9.

FILANT, J. & SPENCER, T. E. 2014. Uterine glands: biological roles in conceptus implantation, uterine receptivity, and decidualization. *The International journal of developmental biology,* 58**,** 107.

FILANT, J., ZHOU, H. & SPENCER, T. E. 2012. Progesterone inhibits uterine gland development in the neonatal mouse uterus. *Biology of reproduction,* 86**,** 146, 1-9.

FITZGERALD, H. C., DHAKAL, P., BEHURA, S. K., SCHUST, D. J. & SPENCER, T. E. 2019. Self-renewing endometrial epithelial organoids of the human uterus. *Proceedings of the National Academy of Sciences,* 116**,** 23132-23142.

FITZGERALD, H. C., SCHUST, D. J. & SPENCER, T. E. 2021. In vitro models of the human endometrium: evolution and application for women's health. *Biology of Reproduction,* 104**,** 282-293.

FLEISCHER, A. C. Sonographic assessment of endometrial disorders. Seminars in Ultrasound, CT and MRI, 1999. Elsevier, 259-266.

FORBES, K., WESTWOOD, M., BAKER, P. N. & APLIN, J. D. 2008. Insulin-like growth factor I and II regulate the life cycle of trophoblast in the developing human placenta. *Am J Physiol Cell Physiol,* 294**,** C1313-22.

FORD, H. B. & SCHUST, D. J. 2009. Recurrent pregnancy loss: etiology, diagnosis, and therapy. *Reviews in obstetrics and gynecology,* 2**,** 76.

FRASER, A. M., BROCKERT, J. E. & WARD, R. H. 1995. Association of young maternal age with adverse reproductive outcomes. *New England journal of medicine,* 332**,** 1113-1118.

FREEDMAN, B. S., BROOKS, C. R., LAM, A. Q., FU, H., MORIZANE, R., AGRAWAL, V., SAAD, A. F., LI, M. K., HUGHES, M. R., WERFF, R. V., PETERS, D. T., LU, J., BACCEI, A., SIEDLECKI, A. M., VALERIUS, M. T., MUSUNURU, K., MCNAGNY, K. M., STEINMAN, T. I., ZHOU, J., LEROU, P. H. & BONVENTRE, J. V. 2015. Modelling kidney disease with CRISPR-mutant kidney organoids derived from human pluripotent epiblast spheroids. *Nat Commun,* 6**,** 8715.

FRETTS, R. C., SCHMITTDIEL, J., MCLEAN, F. H., USHER, R. H. & GOLDMAN, M. B. 1995. Increased maternal age and the risk of fetal death. *New England Journal of Medicine,* 333**,** 953-957.

FRIEDMAN, J. R. & KAESTNER, K. H. 2006. The Foxa family of transcription factors in development and metabolism. *Cell Mol Life Sci,* 63**,** 2317-28.

GANAPATHY-KANNIAPPAN, S. & GESCHWIND, J.-F. H. 2013. Tumor glycolysis as a target for cancer therapy: progress and prospects. *Molecular cancer,* 12**,** 1-11.

GARCIA-ALONSO, L., HANDFIELD, L.-F., ROBERTS, K., NIKOLAKOPOULOU, K., FERNANDO, R. C., GARDNER, L., WOODHAMS, B., ARUTYUNYAN, A., POLANSKI, K., HOO, R., SANCHO-SERRA, C., LI, T., KWAKWA, K., TUCK, E., KLESHCHEVNIKOV, V., TARKOWSKA, A., PORTER, T., MAZZEO, C. I., VAN DONGEN, S., DABROWSKA, M., VASKIVSKYI, V., MAHBUBANI, K. T., PARK, J.-E., JIMENEZ-LINAN, M., CAMPOS, L., KISELEV, V., LINDSKOG, C., AYUK, P., PRIGMORE, E., STRATTON, M. R., SAEB-PARSY, K., MOFFETT, A., MOORE, L., BAYRAKTAR, O. A., TEICHMANN, S. A.,

TURCO, M. Y. & VENTO-TORMO, R. 2021. Mapping the temporal and spatial dynamics of the human endometrium in vivo and in vitro. *bioRxiv***,** 2021.01.02.425073.

GARGETT, C. E., SCHWAB, K. E., ZILLWOOD, R. M., NGUYEN, H. P. T. & WU, D. 2009. Isolation and culture of epithelial progenitors and mesenchymal stem cells from human endometrium. *Biology of reproduction,* 80**,** 1136-1145.

GARRY, R., HART, R., KARTHIGASU, K. & BURKE, C. 2010. Structural changes in endometrial basal glands during menstruation. *BJOG: An International Journal of Obstetrics & Gynaecology,* 117**,** 1175-1185.

GARRY, R., HART, R., KARTHIGASU, K. A. & BURKE, C. 2009. A re-appraisal of the morphological changes within the endometrium during menstruation: a hysteroscopic, histological and scanning electron microscopic study. *Human reproduction,* 24**,** 1393-1401.

GELLERSEN, B. & BROSENS, J. 2003. Cyclic AMP and progesterone receptor cross-talk in human endometrium: a decidualizing affair. *Journal of Endocrinology,* 178**,** 357-372.

GELLERSEN, B. & BROSENS, J. J. 2014. Cyclic decidualization of the human endometrium in reproductive health and failure. *Endocrine reviews,* 35**,** 851-905.

GERRETSEN, G., HUISJES, H. J. & ELEMA, J. D. 1981. Morphological changes of the spiral arteries in the placental bed in relation to pre-eclampsia and fetal growth retardation. *Br J Obstet Gynaecol,* 88**,** 876-81.

GHOSH, J., PAPADOPOULOU, A., DEVALL, A. J., JEFFERY, H. C., BEESON, L. E., DO, V., PRICE, M. J., TOBIAS, A., TUNÇALP, Ö., LAVELANET, A., GÜLMEZOGLU, A. M., COOMARASAMY, A. & GALLOS, I. D. 2021. Methods for managing miscarriage: a network meta-analysis. *Cochrane Database Syst Rev,* 6**,** Cd012602.

GIL-SANCHIS, C., CERVELLÓ, I., MAS, A., FAUS, A., PELLICER, A. & SIMÓN, C. 2013. Leucine-rich repeat-containing G-protein-coupled receptor 5 (Lgr5) as a putative human endometrial stem cell marker. *Molecular human reproduction,* 19**,** 407-414.

GOAD, J., KO, Y.-A., KUMAR, M., SYED, S. M. & TANWAR, P. S. 2017. Differential Wnt signaling activity limits epithelial gland development to the anti-mesometrial side of the mouse uterus. *Developmental biology,* 423**,** 138-151.

GOVINDASAMY, N., LONG, H., JEONG, H. W., RAMAN, R., ÖZCIFCI, B., PROBST, S., ARNOLD, S. J., RIEHEMANN, K., RANGA, A., ADAMS, R. H.,

TRAPPMANN, B. & BEDZHOV, I. 2021. 3D biomimetic platform reveals the first interactions of the embryo and the maternal blood vessels. *Dev Cell,* 56**,** 3276-3287.e8.

GRAY, C., BURGHARDT, R., JOHNSON, G., BAZER, F. & SPENCER, T. 2002. Evidence that absence of endometrial gland secretions in uterine gland knockout ewes compromises conceptus survival and elongation. *REPRODUCTION-CAMBRIDGE-,* 124**,** 289-300.

GRAY, C. A., BARTOL, F. F., TARLETON, B. J., WILEY, A. A., JOHNSON, G. A., BAZER, F. W. & SPENCER, T. E. 2001. Developmental biology of uterine glands. *Biology of reproduction,* 65**,** 1311-1323.

GRAY, C. A., BARTOL, F. F., TAYLOR, K. M., WILEY, A. A., RAMSEY, W. S., OTT, T. L., BAZER, F. W. & SPENCER, T. E. 2000. Ovine uterine gland knock-out model: effects of gland ablation on the estrous cycle. *Biology of reproduction,* 62**,** 448-456.

GROLL, J. M., USADI, R. S., LESSEY, B. A., LININGER, R., YOUNG, S. L. & FRITZ, M. A. 2009. Effects of variations in serum estradiol concentrations on secretory endometrial development and function in experimentally induced cycles in normal women. *Fertility and sterility,* 92**,** 2058-2061.

GROOTHUIS, P., DASSEN, H., ROMANO, A. & PUNYADEERA, C. 2007. Estrogen and the endometrium: lessons learned from gene expression profiling in rodents and human. *Human reproduction update,* 13**,** 405-417.

GRUHN, J. R., ZIELINSKA, A. P., SHUKLA, V., BLANSHARD, R., CAPALBO, A., CIMADOMO, D., NIKIFOROV, D., CHAN, A. C., NEWNHAM, L. J., VOGEL, I., SCARICA, C., KRAPCHEV, M., TAYLOR, D., KRISTENSEN, S. G., CHENG, J., ERNST, E., BJØRN, A. B., COLMORN, L. B., BLAYNEY, M., ELDER, K., LISS, J., HARTSHORNE, G., GRØNDAHL, M. L., RIENZI, L., UBALDI, F., MCCOY, R., LUKASZUK, K., ANDERSEN, C. Y., SCHUH, M. & HOFFMANN, E. R. 2019. Chromosome errors in human eggs shape natural fertility over reproductive life span. *Science,* 365**,** 1466-1469.

GUDE, N. M., STEVENSON, J., ROGERS, S., BEST, J., KALIONIS, B., HUISMAN, M., ERWICH, J., TIMMER, A. & KING, R. G. 2003. GLUT12 expression in human placenta in first trimester and term. *Placenta,* 24**,** 566-570.

GUDMUNDSSON, S. & THIELE, I. 2010. Computationally efficient flux variability analysis. *BMC bioinformatics,* 11**,** 1-3.

GUO, R., GU, J., ZONG, S., WU, M. & YANG, M. 2018. Structure and mechanism of mitochondrial electron transport chain. *Biomedical journal,* 41**,** 9-20.

HAIDER, S., GAMPERL, M., BURKARD, T. R., KUNIHS, V., KAINDL, U., JUNTTILA, S., FIALA, C., SCHMIDT, K., MENDJAN, S., KNÖFLER, M. & LATOS, P. A. 2019. Estrogen Signaling Drives Ciliogenesis in Human Endometrial Organoids. *Endocrinology,* 160**,** 2282-2297.

HAIDER, S., MEINHARDT, G., SALEH, L., KUNIHS, V., GAMPERL, M., KAINDL, U., ELLINGER, A., BURKARD, T. R., FIALA, C., POLLHEIMER, J., MENDJAN, S., LATOS, P. A. & KNÖFLER, M. 2018. Self-Renewing Trophoblast Organoids Recapitulate the Developmental Program of the Early Human Placenta. *Stem Cell Reports,* 11**,** 537-551.

HALDER, A. & FAUZDAR, A. 2006. Skewed sex ratio and low aneuploidy in recurrent early missed abortion. *Indian J Med Res,* 124**,** 41-50.

HAMILTON, W. & BOYD, J. 1960. Development of the human placenta in the first three months of gestation. *Journal of anatomy,* 94**,** 297.

HAN, B., BHOWMICK, N., QU, Y., CHUNG, S., GIULIANO, A. E. & CUI, X. 2017. FOXC1: an emerging marker and therapeutic target for cancer. *Oncogene,* 36**,** 3957-3963.

HAOUZI, D., MAHMOUD, K., FOURAR, M., BENDHAOU, K., DECHAUD, H., DE VOS, J., REME, T., DEWAILLY, D. & HAMAMAH, S. 2009. Identification of new biomarkers of human endometrial receptivity in the natural cycle. *Human reproduction,* 24**,** 198-205.

HAPANGAMA, D., KAMAL, A. & SARETZKI, G. 2017. Implications of telomeres and telomerase in endometrial pathology. *Human reproduction update,* 23**,** 166-187.

HASSOLD, T. & HUNT, P. 2001. To err (meiotically) is human: the genesis of human aneuploidy. *Nature Reviews Genetics,* 2**,** 280-291.

HAUSERMANN, H. M., DONNELLY, K. M., BELL, S. C., VERHAGE, H. G. & FAZLEABAS, A. T. 1998. Regulation of the glycosylated β-lactoglobulin homolog, glycodelin [placental protein 14:(PP14)] in the baboon (Papio anubis) uterus. *The Journal of Clinical Endocrinology & Metabolism,* 83**,** 1226-1233.

HEMBERGER, M., UDAYASHANKAR, R., TESAR, P., MOORE, H. & BURTON, G. J. 2010. ELF5-enforced transcriptional networks define an epigenetically regulated trophoblast stem cell compartment in the human placenta. *Hum Mol Genet,* 19**,** 2456-67.

HEMPSTOCK, J., CINDROVA-DAVIES, T., JAUNIAUX, E. & BURTON, G. J. 2004. Endometrial glands as a source of nutrients, growth factors and cytokines

during the first trimester of human pregnancy: a morphological and immunohistochemical study. *Reproductive Biology and Endocrinology,* 2**,** 58.

HOMBACH-KLONISCH, S., KEHLEN, A., FOWLER, P. A., HUPPERTZ, B., JUGERT, J. F., BISCHOFF, G., SCHLÜTER, E., BUCHMANN, J. & KLONISCH, T. 2005. Regulation of functional steroid receptors and ligand-induced responses in telomerase-immortalized human endometrial epithelial cells. *Journal of molecular endocrinology,* 34**,** 517-534.

HOUTEN, S. M., VIOLANTE, S., VENTURA, F. V. & WANDERS, R. J. 2016. The biochemistry and physiology of mitochondrial fatty acid β-oxidation and its genetic disorders. *Annual review of physiology,* 78**,** 23-44.

HOUTEN, S. M. & WANDERS, R. J. 2010. A general introduction to the biochemistry of mitochondrial fatty acid β-oxidation. *Journal of inherited metabolic disease,* 33**,** 469-477.

HU, S., YAO, G., WANG, Y., XU, H., JI, X., HE, Y., ZHU, Q., CHEN, Z. & SUN, Y. 2014. Transcriptomic changes during the pre-receptive to receptive transition in human endometrium detected by RNA-Seq. *J Clin Endocrinol Metab,* 99**,** E2744-53.

HUPPERTZ, B. 2020. Traditional and new routes of trophoblast invasion and their implications for pregnancy diseases. *International journal of molecular sciences,* 21**,** 289.

HUSTIN, J., JAUNIAUX, E. & SCHAAPS, J. P. 1990. Histological study of the materno-embryonic interface in spontaneous abortion. *Placenta,* 11**,** 477-86.

JASLOW, C. R., CARNEY, J. L. & KUTTEH, W. H. 2010. Diagnostic factors identified in 1020 women with two versus three or more recurrent pregnancy losses. *Fertility and sterility,* 93**,** 1234-1243.

JAUNIAUX, E., GULBIS, B. & BURTON, G. J. 2003a. Physiological implications of the materno–fetal oxygen gradient in human early pregnancy. *Reproductive biomedicine online,* 7**,** 250-253.

JAUNIAUX, E., HEMPSTOCK, J., GREENWOLD, N. & BURTON, G. J. 2003b. Trophoblastic oxidative stress in relation to temporal and regional differences in maternal placental blood flow in normal and abnormal early pregnancies. *Am J Pathol,* 162**,** 115-25.

JAUNIAUX, E., VAN OPPENRAAIJ, R. H. & BURTON, G. J. 2010. Obstetric outcome after early placental complications. *Curr Opin Obstet Gynecol,* 22**,** 452-7.

JAUNIAUX, E., WATSON, A. & BURTON, G. 2001. Evaluation of respiratory gases and acid-base gradients in human fetal fluids and uteroplacental tissue

between 7 and 16 weeks' gestation. *American journal of obstetrics and gynecology,* 184**,** 998-1003.

JEONG, J.-W., KWAK, I., LEE, K. Y., KIM, T. H., LARGE, M. J., STEWART, C. L., KAESTNER, K. H., LYDON, J. P. & DEMAYO, F. J. 2010. Foxa2 is essential for mouse endometrial gland development and fertility. *Biology of reproduction,* 83**,** 396-403.

JHO, E.-H., ZHANG, T., DOMON, C., JOO, C.-K., FREUND, J.-N. & COSTANTINI, F. 2002. Wnt/β-catenin/Tcf signaling induces the transcription of Axin2, a negative regulator of the signaling pathway. *Molecular and cellular biology,* 22**,** 1172-1183.

JOHNS, J. & JAUNIAUX, E. 2006. Threatened miscarriage as a predictor of obstetric outcome. *Obstet Gynecol,* 107**,** 845-50.

JOHNSON, G. A., BURGHARDT, R. C., BAZER, F. W. & SPENCER, T. E. 2003. Osteopontin: roles in implantation and placentation. *Biology of reproduction,* 69**,** 1458-1471.

JONES, C., CHOUDHURY, R. & APLIN, J. 2015. Tracking nutrient transfer at the human maternofetal interface from 4 weeks to term. *Placenta,* 36**,** 372-380.

JONES, R. L., CRITCHLEY, H. O. D., BROOKS, J., JABBOUR, H. & MCNEILLY, A. 1998. Localization and temporal expression of prolactin receptor in human endometrium. *The Journal of Clinical Endocrinology & Metabolism,* 83**,** 258-262.

JUNG, K. B., KWON, O., LEE, M. O., LEE, H., SON, Y. S., HABIB, O., OH, J. H., CHO, H. S., JUNG, C. R., KIM, J. & SON, M. Y. 2019. Blockade of STAT3 Causes Severe In Vitro and In Vivo Maturation Defects in Intestinal Organoids Derived from Human Embryonic Stem Cells. *J Clin Med,* 8.

KAIKO, G. E., RYU, S. H., KOUES, O. I., COLLINS, P. L., SOLNICA-KREZEL, L., PEARCE, E. J., PEARCE, E. L., OLTZ, E. M. & STAPPENBECK, T. S. 2016. The colonic crypt protects stem cells from microbiota-derived metabolites. *Cell,* 165**,** 1708-1720.

KAM, E. P., GARDNER, L., LOKE, Y. W. & KING, A. 1999. The role of trophoblast in the physiological change in decidual spiral arteries. *Hum Reprod,* 14**,** 2131-8.

KELLEHER, A. M., DEMAYO, F. J. & SPENCER, T. E. 2019. Uterine glands: developmental biology and functional roles in pregnancy. *Endocrine reviews,* 40**,** 1424-1445.

KESSLER, M., HOFFMANN, K., BRINKMANN, V., THIECK, O., JACKISCH, S., TOELLE, B., BERGER, H., MOLLENKOPF, H. J., MANGLER, M., SEHOULI,

J., FOTOPOULOU, C. & MEYER, T. F. 2015. The Notch and Wnt pathways regulate stemness and differentiation in human fallopian tube organoids. *Nat Commun,* 6**,** 8989.

KIM, H., PARK, H. J., CHOI, H., CHANG, Y., PARK, H., SHIN, J., KIM, J., LENGNER, C. J., LEE, Y. K. & KIM, J. 2019. Modeling G2019S-LRRK2 Sporadic Parkinson's Disease in 3D Midbrain Organoids. *Stem Cell Reports,* 12**,** 518-531.

KIM, J., KOO, B.-K. & KNOBLICH, J. A. 2020. Human organoids: model systems for human biology and medicine. *Nature Reviews Molecular Cell Biology,* 21**,** 571-584.

KIM, K. M., NOH, J. H., BODOGAI, M., MARTINDALE, J. L., YANG, X., INDIG, F. E., BASU, S. K., OHNUMA, K., MORIMOTO, C., JOHNSON, P. F., BIRAGYN, A., ABDELMOHSEN, K. & GOROSPE, M. 2017. Identification of senescent cell surface targetable protein DPP4. *Genes Dev,* 31**,** 1529-1534.

KNOBLOCH, M., PILZ, G.-A., GHESQUIÈRE, B., KOVACS, W. J., WEGLEITER, T., MOORE, D. L., HRUZOVA, M., ZAMBONI, N., CARMELIET, P. & JESSBERGER, S. 2017. A fatty acid oxidation-dependent metabolic shift regulates adult neural stem cell activity. *Cell reports,* 20**,** 2144-2155.

KNUDSEN, U. B., HANSEN, V., JUUL, S. & SECHER, N. J. 1991. Prognosis of a new pregnancy following previous spontaneous abortions. *European Journal of Obstetrics & Gynecology and Reproductive Biology,* 39**,** 31-36.

KOFF, A. K. 1933. Development of the vagina in the human fetus. *Contributions to embryology,* 24**,** 59-91.

KOLTE, A. M., BERNARDI, L. A., CHRISTIANSEN, O. B., QUENBY, S., FARQUHARSON, R. G., GODDIJN, M. & STEPHENSON, M. D. 2015. Terminology for pregnancy loss prior to viability: a consensus statement from the ESHRE early pregnancy special interest group. *Hum Reprod,* 30**,** 495-8.

KOLTE, A. M., WESTERGAARD, D., LIDEGAARD, Ø., BRUNAK, S. & NIELSEN, H. S. 2021. Chance of live birth: a nationwide, registry-based cohort study. *Hum Reprod,* 36**,** 1065-1073.

KONG, C. S., ORDOÑEZ, A. A., TURNER, S., TREMAINE, T., MUTER, J., LUCAS, E. S., SALISBURY, E., VASSENA, R., TISCORNIA, G., FOULADI-NASHTA, A. A., HARTSHORNE, G., BROSENS, J. J. & BRIGHTON, P. J. 2021. Embryo biosensing by uterine natural killer cells determines endometrial fate decisions at implantation. *Faseb j,* 35**,** e21336.

KOPPER, O., DE WITTE, C. J., LÕHMUSSAAR, K., VALLE-INCLAN, J. E., HAMI, N., KESTER, L., BALGOBIND, A. V., KORVING, J., PROOST, N., BEGTHEL, H., VAN WIJK, L. M., REVILLA, S. A., THEEUWSEN, R., VAN DE VEN, M., VAN ROOSMALEN, M. J., PONSIOEN, B., HO, V. W. H., NEEL, B. G., BOSSE, T., GAARENSTROOM, K. N., VRIELING, H., VREESWIJK, M. P. G., VAN DIEST, P. J., WITTEVEEN, P. O., JONGES, T., BOS, J. L., VAN OUDENAARDEN, A., ZWEEMER, R. P., SNIPPERT, H. J. G., KLOOSTERMAN, W. P. & CLEVERS, H. 2019. An organoid platform for ovarian cancer captures intra- and interpatient heterogeneity. *Nat Med,* 25**,** 838-849.

KRETZSCHMAR, K. & CLEVERS, H. 2016. Organoids: modeling development and the stem cell niche in a dish. *Developmental cell,* 38**,** 590-600.

LAEDERICH, M. B., FUNES-DURAN, M., YEN, L., INGALLA, E., WU, X., CARRAWAY III, K. L. & SWEENEY, C. 2004. The leucine-rich repeat protein LRIG1 is a negative regulator of ErbB family receptor tyrosine kinases. *Journal of Biological Chemistry,* 279**,** 47050-47056.

LAM, K. K., CHIU, P. C., LEE, C.-L., PANG, R. T., LEUNG, C. O., KOISTINEN, H., SEPPALA, M., HO, P.-C. & YEUNG, W. S. 2011. Glycodelin-A protein interacts with Siglec-6 protein to suppress trophoblast invasiveness by down-regulating extracellular signal-regulated kinase (ERK)/c-Jun signaling pathway. *Journal of Biological Chemistry,* 286**,** 37118-37127.

LANCASTER, M. A. & KNOBLICH, J. A. 2014. Organogenesis in a dish: modeling development and disease using organoid technologies. *Science,* 345.

LANCASTER, M. A., RENNER, M., MARTIN, C.-A., WENZEL, D., BICKNELL, L. S., HURLES, M. E., HOMFRAY, T., PENNINGER, J. M., JACKSON, A. P. & KNOBLICH, J. A. 2013. Cerebral organoids model human brain development and microcephaly. *Nature,* 501**,** 373-379.

LASH, G. E., BULMER, J. N., LI, T. C., INNES, B. A., MARIEE, N., PATEL, G., SANDERSON, J., QUENBY, S. & LAIRD, S. M. 2016. Standardisation of uterine natural killer (uNK) cell measurements in the endometrium of women with recurrent reproductive failure. *Journal of reproductive immunology,* 116**,** 50-59.

LEACH, R. E., KHALIFA, R., RAMIREZ, N. D., DAS, S. K., WANG, J., DEY, S. K., ROMERO, R. & ARMANT, D. R. 1999. Multiple roles for heparin-binding epidermal growth factor-like growth factor are suggested by its cell-specific

expression during the human endometrial cycle and early placentation. *J Clin Endocrinol Metab,* 84**,** 3355-63.

LEE, C.-L., LAM, K. K., KOISTINEN, H., SEPPALA, M., KURPISZ, M., FERNANDEZ, N., PANG, R. T., YEUNG, W. S. & CHIU, P. C. 2011. Glycodelin-A as a paracrine regulator in early pregnancy. *Journal of reproductive immunology,* 90**,** 29-34.

LEE, C.-L., VIJAYAN, M., WANG, X., LAM, K. K., KOISTINEN, H., SEPPALA, M., LI, R. H., NG, E. H., YEUNG, W. S. & CHIU, P. C. 2019. Glycodelin-A stimulates the conversion of human peripheral blood CD16− CD56bright NK cell to a decidual NK cell-like phenotype. *Human Reproduction,* 34**,** 689-701.

LEITAO, B., JONES, M. C., FUSI, L., HIGHAM, J., LEE, Y., TAKANO, M., GOTO, T., CHRISTIAN, M., LAM, E. W. F. & BROSENS, J. J. 2010. Silencing of the JNK pathway maintains progesterone receptor activity in decidualizing human endometrial stromal cells exposed to oxidative stress signals. *The FASEB Journal,* 24**,** 1541-1551.

LI, J., POI, M. J. & TSAI, M.-D. 2011. Regulatory mechanisms of tumor suppressor P16INK4A and their relevance to cancer. *Biochemistry,* 50**,** 5566-5582.

LI, Z. 2013. CD133: a stem cell biomarker and beyond. *Experimental hematology & oncology,* 2**,** 1-8.

LIANG, H. & WARD, W. F. 2006. PGC-1α: a key regulator of energy metabolism. *Advances in physiology education*.

LONG, J., TOKHUNTS, R., OLD, W. M., HOUEL, S., RODGRIGUEZ-BLANCO, J., SINGH, S., SCHILLING, N., CAPOBIANCO, A. J., AHN, N. G. & ROBBINS, D. J. 2015. Identification of a family of fatty-acid-speciated sonic hedgehog proteins, whose members display differential biological properties. *Cell reports,* 10**,** 1280-1287.

LUCAS, E. S., DYER, N. P., MURAKAMI, K., LEE, Y. H., CHAN, Y. W., GRIMALDI, G., MUTER, J., BRIGHTON, P. J., MOORE, J. D., PATEL, G., CHAN, J. K., TAKEDA, S., LAM, E. W., QUENBY, S., OTT, S. & BROSENS, J. J. 2016. Loss of Endometrial Plasticity in Recurrent Pregnancy Loss. *Stem Cells,* 34**,** 346-56.

LUCAS, E. S., VRLJICAK, P., MUTER, J., DINIZ-DA-COSTA, M. M., BRIGHTON, P. J., KONG, C. S., LIPECKI, J., FISHWICK, K. J., ODENDAAL, J., EWINGTON, L. J., QUENBY, S., OTT, S. & BROSENS, J. J. 2020. Recurrent pregnancy loss is associated with a pro-senescent decidual response during the peri-implantation window. *Commun Biol,* 3**,** 37.

LUDWIG, H. & SPORNITZ, U. 1991. Microarchitecture of the human endometrium by scanning electron microscopy: menstrual desquamation and remodeling. *Annals of the New York Academy of Sciences,* 622**,** 28-46.

MACONOCHIE, N., DOYLE, P., PRIOR, S. & SIMMONS, R. 2007. Risk factors for first trimester miscarriage—results from a UK-population-based case–control study. *BJOG: An International Journal of Obstetrics & Gynaecology,* 114**,** 170-186.

MACOSKO, E. Z., BASU, A., SATIJA, R., NEMESH, J., SHEKHAR, K., GOLDMAN, M., TIROSH, I., BIALAS, A. R., KAMITAKI, N., MARTERSTECK, E. M., TROMBETTA, J. J., WEITZ, D. A., SANES, J. R., SHALEK, A. K., REGEV, A. & MCCARROLL, S. A. 2015. Highly Parallel Genome-wide Expression Profiling of Individual Cells Using Nanoliter Droplets. *Cell,* 161**,** 1202-1214.

MAENHOUDT, N., DEFRAYE, C., BORETTO, M., JAN, Z., HEREMANS, R., BOECKX, B., HERMANS, F., ARIJS, I., COX, B., VAN NIEUWENHUYSEN, E., VERGOTE, I., VAN ROMPUY, A. S., LAMBRECHTS, D., TIMMERMAN, D. & VANKELECOM, H. 2020. Developing Organoids from Ovarian Cancer as Experimental and Preclinical Models. *Stem Cell Reports,* 14**,** 717-729.

MAGNUS, M. C., WILCOX, A. J., MORKEN, N.-H., WEINBERG, C. R. & HÅBERG, S. E. 2019. Role of maternal age and pregnancy history in risk of miscarriage: prospective register based study. *bmj,* 364.

MARQUÉS-TORREJÓN, M., WILLIAMS, C. A. C., SOUTHGATE, B., ALFAZEMA, N., CLEMENTS, M. P., GARCIA-DIAZ, C., BLIN, C., ARRANZ-EMPARAN, N., FRASER, J., GAMMOH, N., PARRINELLO, S. & POLLARD, S. M. 2021. LRIG1 is a gatekeeper to exit from quiescence in adult neural stem cells. *Nat Commun,* 12**,** 2594.

MARU, Y., KAWATA, A., TAGUCHI, A., ISHII, Y., BABA, S., MORI, M., NAGAMATSU, T., ODA, K., KUKIMOTO, I., OSUGA, Y., FUJII, T. & HIPPO, Y. 2020. Establishment and Molecular Phenotyping of Organoids from the Squamocolumnar Junction Region of the Uterine Cervix. *Cancers (Basel),* 12.

MARUO, T., MATSUO, H., MURATA, K. & MOCHIZUKI, M. 1992. Gestational age-dependent dual action of epidermal growth factor on human placenta early in gestation. *J Clin Endocrinol Metab,* 75**,** 1362-7.

MENON, R. 2016. Human fetal membranes at term: Dead tissue or signalers of parturition? *Placenta,* 44**,** 1-5.

MIYAZAKI, M., DOBRZYN, A., ELIAS, P. M. & NTAMBI, J. M. 2005. Stearoyl-CoA desaturase-2 gene expression is required for lipid synthesis during early skin

and liver development. *Proceedings of the National Academy of Sciences,* 102**,** 12501-12506.

MOKHTAR, N. M., CHENG, C.-W., COOK, E., BIELBY, H., SMITH, S. K. & CHARNOCK-JONES, D. S. 2009. Progestin regulates chemokine (CXC motif) ligand 14 transcript level in human endometrium. *MHR: Basic science of reproductive medicine,* 16**,** 170-177.

MOORE, L., LEONGAMORNLERT, D., COORENS, T. H. H., SANDERS, M. A., ELLIS, P., DENTRO, S. C., DAWSON, K. J., BUTLER, T., RAHBARI, R., MITCHELL, T. J., MAURA, F., NANGALIA, J., TARPEY, P. S., BRUNNER, S. F., LEE-SIX, H., HOOKS, Y., MOODY, S., MAHBUBANI, K. T., JIMENEZ-LINAN, M., BROSENS, J. J., IACOBUZIO-DONAHUE, C. A., MARTINCORENA, I., SAEB-PARSY, K., CAMPBELL, P. J. & STRATTON, M. R. 2020. The mutational landscape of normal human endometrial epithelium. *Nature,* 580**,** 640-646.

MOSER, G., GAUSTER, M., ORENDI, K., GLASNER, A., THEUERKAUF, R. & HUPPERTZ, B. 2010. Endoglandular trophoblast, an alternative route of trophoblast invasion? Analysis with novel confrontation co-culture models. *Human reproduction,* 25**,** 1127-1136.

MOSER, G., WEISS, G., GAUSTER, M., SUNDL, M. & HUPPERTZ, B. 2015. Evidence from the very beginning: endoglandular trophoblasts penetrate and replace uterine glands in situ and in vitro. *Human reproduction,* 30**,** 2747-2757.

MOSER, G., WINDSPERGER, K., POLLHEIMER, J., DE SOUSA LOPES, S. C. & HUPPERTZ, B. 2018. Human trophoblast invasion: new and unexpected routes and functions. *Histochemistry and cell biology,* 150**,** 361-370.

MOTE, P., BALLEINE, R., MCGOWAN, E. & CLARKE, C. 1999. Colocalization of progesterone receptors A and B by dual immunofluorescent histochemistry in human endometrium during the menstrual cycle. *The Journal of Clinical Endocrinology & Metabolism,* 84**,** 2963-2971.

MULHOLLAND, J., WINTERHAGER, E. & BEIER, H. M. 1988. Changes in proteins synthesized by rabbit endometrial epithelial cells following primary culture. *Cell and tissue research,* 252**,** 123-132.

MUTER, J., ALAM, M. T., VRLJICAK, P., BARROS, F. S., RUANE, P. T., EWINGTON, L. J., APLIN, J. D., WESTWOOD, M. & BROSENS, J. J. 2018. The glycosyltransferase EOGT regulates adropin expression in decidualizing human endometrium. *Endocrinology,* 159**,** 994-1004.

MUÑOZ-ESPÍN, D. & SERRANO, M. 2014. Cellular senescence: from physiology to pathology. *Nature reviews Molecular cell biology,* 15**,** 482-496.

NAGAOKA, S. I., HASSOLD, T. J. & HUNT, P. A. 2012. Human aneuploidy: mechanisms and new insights into an age-old problem. *Nature Reviews Genetics,* 13**,** 493-504.

NAKAMURA, M., TAKAKURA, M., FUJII, R., MAIDA, Y., BONO, Y., MIZUMOTO, Y., ZHANG, X., KIYONO, T. & KYO, S. 2013. The PRB-dependent FOXO1/IGFBP-1 axis is essential for progestin to inhibit endometrial epithelial growth. *Cancer Lett,* 336**,** 68-75.

NAKANO, T., ANDO, S., TAKATA, N., KAWADA, M., MUGURUMA, K., SEKIGUCHI, K., SAITO, K., YONEMURA, S., EIRAKU, M. & SASAI, Y. 2012. Self-formation of optic cups and storable stratified neural retina from human ESCs. *Cell stem cell,* 10**,** 771-785.

NANJAPPA, M. K., MEDRANO, T. I., MARCH, A. G. & COOKE, P. S. 2015. Neonatal uterine and vaginal cell proliferation and adenogenesis are independent of estrogen receptor 1 (ESR1) in the mouse. *Biology of reproduction,* 92**,** 78, 1-10.

NGUYEN, H. P., SPRUNG, C. N. & GARGETT, C. E. 2012. Differential expression of Wnt signaling molecules between pre-and postmenopausal endometrial epithelial cells suggests a population of putative epithelial stem/progenitor cells reside in the basalis layer. *Endocrinology,* 153**,** 2870-2883.

NGUYEN, H. P. T., XIAO, L., DEANE, J. A., TAN, K.-S., COUSINS, F. L., MASUDA, H., SPRUNG, C. N., ROSAMILIA, A. & GARGETT, C. E. 2017. N-cadherin identifies human endometrial epithelial progenitor cells by in vitro stem cell assays. *Human Reproduction,* 32**,** 2254-2268.

NICE. 2020. *PALBOCICLIB* [Online]. NICE. Available: https://bnf.nice.org.uk/drug/palbociclib.html [Accessed 7th July 2021].

NIEC, R. E., RUDENSKY, A. Y. & FUCHS, E. 2021. Inflammatory adaptation in barrier tissues. *Cell,* 184**,** 3361-3375.

NOYES, R., HERTIG, A. & ROCK, J. 1950. Dating the endometrial biopsy. *Obstetrical & Gynecological Survey,* 5**,** 561-564.

NUSSE, R., FUERER, C., CHING, W., HARNISH, K., LOGAN, C., ZENG, A., TEN BERGE, D. & KALANI, Y. Wnt signaling and stem cell control. Cold Spring Harbor symposia on quantitative biology, 2008. Cold Spring Harbor Laboratory Press, 59-66.

O'RAHILLY, R. 1973. The embryology and anatomy of the uterus. *The uterus.* The Williams & Wilkins Co. Baltimore.

OBER, W. B. & BERNSTEIN, J. 1955. Observations on the endometrium and ovary in the newborn. *Pediatrics,* 16**,** 445-460.

OEFNER, C., SHARKEY, A., GARDNER, L., CRITCHLEY, H., OYEN, M. & MOFFETT, A. 2015. Collagen type IV at the fetal–maternal interface. *Placenta,* 36**,** 59-68.

OGASAWARA, M., AOKI, K., OKADA, S. & SUZUMORI, K. 2000. Embryonic karyotype of abortuses in relation to the number of previous miscarriages. *Fertility and sterility,* 73**,** 300-304.

OGRODNIK, M., MIWA, S., TCHKONIA, T., TINIAKOS, D., WILSON, C. L., LAHAT, A., DAY, C. P., BURT, A., PALMER, A., ANSTEE, Q. M., GRELLSCHEID, S. N., HOEIJMAKERS, J. H. J., BARNHOORN, S., MANN, D. A., BIRD, T. G., VERMEIJ, W. P., KIRKLAND, J. L., PASSOS, J. F., VON ZGLINICKI, T. & JURK, D. 2017. Cellular senescence drives age-dependent hepatic steatosis. *Nat Commun,* 8**,** 15691.

OHTSUKA, T., ISHIBASHI, M., GRADWOHL, G., NAKANISHI, S., GUILLEMOT, F. & KAGEYAMA, R. 1999. Hes1 and Hes5 as notch effectors in mammalian neuronal differentiation. *Embo j,* 18**,** 2196-207.

OJOSNEGROS, S., SERIOLA, A., GODEAU, A. L. & VEIGA, A. 2021. Embryo implantation in the laboratory: an update on current techniques. *Human Reproduction Update*.

ORTH, J. D., THIELE, I. & PALSSON, B. Ø. 2010. What is flux balance analysis? *Nature biotechnology,* 28**,** 245-248.

OWUSU-AKYAW, A., KRISHNAMOORTHY, K., GOLDSMITH, L. T. & MORELLI, S. S. 2019. The role of mesenchymal–epithelial transition in endometrial function. *Human reproduction update,* 25**,** 114-133.

PADYKULA, H. A. 1989. Regeneration in the primate uterus. *Biology of the uterus***,** 279-288.

PAIVA, P., MENKHORST, E., SALAMONSEN, L. & DIMITRIADIS, E. 2009. Leukemia inhibitory factor and interleukin-11: critical regulators in the establishment of pregnancy. *Cytokine & growth factor reviews,* 20**,** 319-328.

PARIA, B. C., LIM, H., WANG, X.-N., LIEHR, J., DAS, S. K. & DEY, S. K. 1998. Coordination of differential effects of primary estrogen and catecholestrogen on two distinct targets mediates embryo implantation in the mouse. *Endocrinology,* 139**,** 5235-5246.

PARVANOV, D., GANEVA, R., VIDOLOVA, N. & STAMENOV, G. 2021. Decreased number of p16-positive senescent cells in human endometrium as a marker of miscarriage. *Journal of Assisted Reproduction and Genetics***,** 1-9.

PATRA, K. C. & HAY, N. 2014. The pentose phosphate pathway and cancer. *Trends in biochemical sciences,* 39**,** 347-354.

PECINA, P., HOUST KOVA, H., ZEMAN, J. & HOUSTEK, J. 2004. Genetic defects of cytochrome c oxidase assembly. *Physiological Research,* 53**,** S213-224.

PEGG, A. E. 2008. Spermidine/spermine-N 1-acetyltransferase: a key metabolic regulator. *American Journal of Physiology-Endocrinology and Metabolism,* 294**,** E995-E1010.

POTTEN, C. S. & LOEFFLER, M. 1990. Stem cells: attributes, cycles, spirals, pitfalls and uncertainties. Lessons for and from the crypt. *Development,* 110**,** 1001-1020.

PRACTICE COMMITTEE OF THE AMERICAN SOCIETY FOR REPRODUCTIVE, M. 2012. Evaluation and treatment of recurrent pregnancy loss: a committee opinion. *Fertility and Sterility,* 98**,** 1103-1111.

PÅLSSON-MCDERMOTT, E. M. & O'NEILL, L. A. 2020. Targeting immunometabolism as an anti-inflammatory strategy. *Cell research,* 30**,** 300-314.

QUENBY, S., GALLOS, I. D., DHILLON-SMITH, R. K., PODESEK, M., STEPHENSON, M. D., FISHER, J., BROSENS, J. J., BREWIN, J., RAMHORST, R., LUCAS, E. S., MCCOY, R. C., ANDERSON, R., DAHER, S., REGAN, L., AL-MEMAR, M., BOURNE, T., MACINTYRE, D. A., RAI, R., CHRISTIANSEN, O. B., SUGIURA-OGASAWARA, M., ODENDAAL, J., DEVALL, A. J., BENNETT, P. R., PETROU, S. & COOMARASAMY, A. 2021. Miscarriage matters: the epidemiological, physical, psychological, and economic costs of early pregnancy loss. *Lancet,* 397**,** 1658-1667.

RADOVIĆ JANOŠEVIĆ, D., POPOVIĆ, J., KRSTIĆ, M., TUBIĆ-PAVLOVIĆ, A., STEFANOVIĆ, M. & POP-TRAJKOVIĆ, S. 2016. The structure of immunocompetent decidual cells in recurrent missed abortions. *Vojnosanit Pregl,* 73**,** 306-11.

RASMARK ROEPKE, E., MATTHIESEN, L., RYLANCE, R. & CHRISTIANSEN, O. B. 2017. Is the incidence of recurrent pregnancy loss increasing? A retrospective register-based study in Sweden. *Acta obstetricia et gynecologica Scandinavica,* 96**,** 1365-1372.

RAWLINGS, T. 2020. *Three-Dimensional Modelling of the Human Peri-Implantation Endometrium.* Doctor of Philosophy, University of Warwick.

RAWLINGS, T. M., MAKWANA, K., TAYLOR, D. M., MOLÈ, M. A., FISHWICK, K. J., TRYFONOS, M., ODENDAAL, J., HAWKES, A., ZERNICKA-GOETZ, M., HARTSHORNE, G. M., BROSENS, J. J. & LUCAS, E. S. 2021a. Modelling the impact of decidual senescence on embryo implantation in human endometrial assembloids. *Elife,* 10**,** e69603.

RAWLINGS, T. M., MAKWANA, K., TRYFONOS, M. & LUCAS, E. S. 2021b. Organoids to model the endometrium: implantation and beyond. *Reproduction and Fertility,* 2**,** R85-R101.

RAY, P. D., HUANG, B.-W. & TSUJI, Y. 2012. Reactive oxygen species (ROS) homeostasis and redox regulation in cellular signaling. *Cellular signalling,* 24**,** 981-990.

REED, B. G. & CARR, B. R. 2015. The Normal Menstrual Cycle and the Control of Ovulation. *De Groot LJ, Chrousos G, Dungan K, et al., editors. Endotext.* South Dartmouth (MA): MDText.com, Inc.

RINEHART, C. A., LYN-COOK, B. D. & KAUFMAN, D. G. 1988. Gland formation from human endometrial epithelial cells in vitro. *In vitro cellular & developmental biology,* 24**,** 1037-1041.

RISCH, H. A., WEISS, N. S., AILEEN CLARKE, E. & MILLER, A. B. 1988. Risk factors for spontaneous abortion and its recurrence. *American journal of epidemiology,* 128**,** 420-430.

ROSARIO, G. X. & STEWART, C. L. 2016. The multifaceted actions of leukaemia inhibitory factor in mediating uterine receptivity and embryo implantation. *American Journal of Reproductive Immunology,* 75**,** 246-255.

ROSSI, G., MANFRIN, A. & LUTOLF, M. P. 2018. Progress and potential in organoid research. *Nature Reviews Genetics,* 19**,** 671-687.

ROTKO, D., KUDIN, A. P., ZSURKA, G., KULAWIAK, B., SZEWCZYK, A. & KUNZ, W. S. 2021. Molecular and Functional Effects of Loss of Cytochrome c Oxidase Subunit 8A. *Biochemistry (Moscow),* 86**,** 33-43.

RUIZ-ALONSO, M., BLESA, D., DÍAZ-GIMENO, P., GÓMEZ, E., FERNÁNDEZ-SÁNCHEZ, M., CARRANZA, F., CARRERA, J., VILELLA, F., PELLICER, A. & SIMÓN, C. 2013. The endometrial receptivity array for diagnosis and personalized embryo transfer as a treatment for patients with repeated implantation failure. *Fertility and sterility,* 100**,** 818-824.

RUIZ-ALONSO, M., BLESA, D. & SIMÓN, C. 2012. The genomics of the human endometrium. *Biochimica et Biophysica Acta (BBA)-Molecular Basis of Disease,* 1822**,** 1931-1942.

RYALL, J. G., DELL'ORSO, S., DERFOUL, A., JUAN, A., ZARE, H., FENG, X., CLERMONT, D., KOULNIS, M., GUTIERREZ-CRUZ, G., FULCO, M. & SARTORELLI, V. 2015. The NAD(+)-dependent SIRT1 deacetylase translates a metabolic switch into regulatory epigenetics in skeletal muscle stem cells. *Cell Stem Cell,* 16**,** 171-83.

SALKER, M. S., NAUTIYAL, J., STEEL, J. H., WEBSTER, Z., SUĆUROVIĆ, S., NICOU, M., SINGH, Y., LUCAS, E. S., MURAKAMI, K., CHAN, Y. W., JAMES, S., ABDALLAH, Y., CHRISTIAN, M., CROY, B. A., MULAC-JERICEVIC, B., QUENBY, S. & BROSENS, J. J. 2012. Disordered IL-33/ST2 activation in decidualizing stromal cells prolongs uterine receptivity in women with recurrent pregnancy loss. *PLoS One,* 7**,** e52252.

SATO, T., VRIES, R. G., SNIPPERT, H. J., VAN DE WETERING, M., BARKER, N., STANGE, D. E., VAN ES, J. H., ABO, A., KUJALA, P., PETERS, P. J. & CLEVERS, H. 2009. Single Lgr5 stem cells build crypt-villus structures in vitro without a mesenchymal niche. *Nature,* 459**,** 262-5.

SCHEFFLER, I. E. & YADAVA, N. 2001. Molecular genetics of the mammalian NADH–ubiquinone oxidoreductase. *Journal of bioenergetics and biomembranes,* 33**,** 243-250.

SCHOLZ, C., TOTH, B., BRUNNHUBER, R., RAMPF, E., WEISSENBACHER, T., SANTOSO, L., FRIESE, K. & JESCHKE, U. 2008. Glycodelin A induces a tolerogenic phenotype in monocyte-derived dendritic cells in vitro. *American Journal of Reproductive Immunology,* 60**,** 501-512.

SEISHIMA, R., LEUNG, C., YADA, S., MURAD, K. B. A., TAN, L. T., HAJAMOHIDEEN, A., TAN, S. H., ITOH, H., MURAKAMI, K., ISHIDA, Y., NAKAMIZO, S., YOSHIKAWA, Y., WONG, E. & BARKER, N. 2019. Neonatal Wnt-dependent Lgr5 positive stem cells are essential for uterine gland development. *Nat Commun,* 10**,** 5378.

SEPPÄLÄ, M., TAYLOR, R. N., KOISTINEN, H., KOISTINEN, R. & MILGROM, E. 2002. Glycodelin: a major lipocalin protein of the reproductive axis with diverse actions in cell recognition and differentiation. *Endocrine reviews,* 23**,** 401-430.

SHELTON, D. N., FORNALIK, H., NEFF, T., PARK, S. Y., BENDER, D., DEGEEST, K., LIU, X., XIE, W., MEYERHOLZ, D. K., ENGELHARDT, J. F. &

GOODHEART, M. J. 2012. The role of LEF1 in endometrial gland formation and carcinogenesis. *PLoS One,* 7**,** e40312.

SHEN-ORR, S. S. & GAUJOUX, R. 2013. Computational deconvolution: extracting cell type-specific information from heterogeneous samples. *Current opinion in immunology,* 25**,** 571-578.

SHUYA, L. L., MENKHORST, E. M., YAP, J., LI, P., LANE, N. & DIMITRIADIS, E. 2011. Leukemia inhibitory factor enhances endometrial stromal cell decidualization in humans and mice. *PLoS One,* 6**,** e25288.

SIEBEL, C. & LENDAHL, U. 2017. Notch signaling in development, tissue homeostasis, and disease. *Physiological reviews,* 97**,** 1235-1294.

SIKDER, H. A., DEVLIN, M. K., DUNLAP, S., RYU, B. & ALANI, R. M. 2003. Id proteins in cell growth and tumorigenesis. *Cancer Cell,* 3**,** 525-30.

SIMIAN, M. & BISSELL, M. J. 2017. Organoids: a historical perspective of thinking in three dimensions. *Journal of Cell Biology,* 216**,** 31-40.

SIMINTIRAS, C. A., DHAKAL, P., RANJIT, C., FITZGERALD, H. C., BALBOULA, A. Z. & SPENCER, T. E. 2021. Capture and metabolomic analysis of the human endometrial epithelial organoid secretome. *Proceedings of the National Academy of Sciences,* 118.

SINGH, H. & APLIN, J. D. 2009. Adhesion molecules in endometrial epithelium: tissue integrity and embryo implantation. *Journal of anatomy,* 215**,** 3-13.

SINHA, A., FAN, V. B., RAMAKRISHNAN, A.-B., ENGELHARDT, N., KENNELL, J. & CADIGAN, K. M. 2021. Repression of Wnt/β-catenin signaling by SOX9 and Mastermind-like transcriptional coactivator 2. *Science Advances,* 7**,** eabe0849.

SMITH, S. & KELLY, R. 1988. The release of PGF2α and PGE2 from separated cells of human endometrium and decidua. *Prostaglandins, leukotrienes and essential fatty acids,* 33**,** 91-96.

SMITS, M. A. J., VAN MAARLE, M., HAMER, G., MASTENBROEK, S., GODDIJN, M. & VAN WELY, M. 2020. Cytogenetic testing of pregnancy loss tissue: a meta-analysis. *Reprod Biomed Online,* 40**,** 867-879.

SOSA, M. S., PARIKH, F., MAIA, A. G., ESTRADA, Y., BOSCH, A., BRAGADO, P., EKPIN, E., GEORGE, A., ZHENG, Y., LAM, H. M., MORRISSEY, C., CHUNG, C. Y., FARIAS, E. F., BERNSTEIN, E. & AGUIRRE-GHISO, J. A. 2015. NR2F1 controls tumour cell dormancy via SOX9- and RARβ-driven quiescence programmes. *Nat Commun,* 6**,** 6170.

STEPHENSON, M. & KUTTEH, W. 2007. Evaluation and management of recurrent early pregnancy loss. *Clin Obstet Gynecol,* 50**,** 132-45.

STEWART, C. L., KASPAR, P., BRUNET, L. J., BHATT, H., GADI, I., KÖNTGEN, F. & ABBONDANZO, S. J. 1992. Blastocyst implantation depends on maternal expression of leukaemia inhibitory factor. *Nature,* 359**,** 76-79.

STRIKOUDIS, A., CIEŚLAK, A., LOFFREDO, L., CHEN, Y. W., PATEL, N., SAQI, A., LEDERER, D. J. & SNOECK, H. W. 2019. Modeling of Fibrotic Lung Disease Using 3D Organoids Derived from Human Pluripotent Stem Cells. *Cell Rep,* 27**,** 3709-3723.e5.

STUART, T., BUTLER, A., HOFFMAN, P., HAFEMEISTER, C., PAPALEXI, E., MAUCK III, W. M., HAO, Y., STOECKIUS, M., SMIBERT, P. & SATIJA, R. 2019. Comprehensive integration of single-cell data. *Cell,* 177**,** 1888-1902. e21.

SUHORUTSHENKO, M., KUKUSHKINA, V., VELTHUT-MEIKAS, A., ALTMÄE, S., PETERS, M., MÄGI, R., KRJUTŠKOV, K., KOEL, M., CODOÑER, F. M., MARTINEZ-BLANCH, J. F., VILELLA, F., SIMÓN, C., SALUMETS, A. & LAISK, T. 2018. Endometrial receptivity revisited: endometrial transcriptome adjusted for tissue cellular heterogeneity. *Hum Reprod,* 33**,** 2074-2086.

SYLVESTER, J. E., FISCHEL-GHODSIAN, N., MOUGEY, E. B. & O'BRIEN, T. W. 2004. Mitochondrial ribosomal proteins: candidate genes for mitochondrial disease. *Genetics in Medicine,* 6**,** 73-80.

TAKASATO, M., ER, P., BECROFT, M., VANSLAMBROUCK, J. M., STANLEY, E., ELEFANTY, A. G. & LITTLE, M. H. 2014. Directing human embryonic stem cell differentiation towards a renal lineage generates a self-organizing kidney. *Nature cell biology,* 16**,** 118-126.

TALBI, S., HAMILTON, A. E., VO, K. C., TULAC, S., OVERGAARD, M. T., DOSIOU, C., LE SHAY, N., NEZHAT, C. N., KEMPSON, R., LESSEY, B. A., NAYAK, N. R. & GIUDICE, L. C. 2006. Molecular phenotyping of human endometrium distinguishes menstrual cycle phases and underlying biological processes in normo-ovulatory women. *Endocrinology,* 147**,** 1097-121.

TANAKA, M., KYO, S., KANAYA, T., YATABE, N., NAKAMURA, M., MAIDA, Y., OKABE, M. & INOUE, M. 2003. Evidence of the monoclonal composition of human endometrial epithelial glands and mosaic pattern of clonal distribution in luminal epithelium. *The American journal of pathology,* 163**,** 295-301.

TEKLENBURG, G., SALKER, M., MOLOKHIA, M., LAVERY, S., TREW, G., AOJANEPONG, T., MARDON, H. J., LOKUGAMAGE, A. U., RAI, R.,

LANDLES, C., ROELEN, B. A., QUENBY, S., KUIJK, E. W., KAVELAARS, A., HEIJNEN, C. J., REGAN, L., BROSENS, J. J. & MACKLON, N. S. 2010. Natural selection of human embryos: decidualizing endometrial stromal cells serve as sensors of embryo quality upon implantation. *PLoS One,* 5**,** e10258.

TEMPEST, N., BAKER, A., WRIGHT, N. & HAPANGAMA, D. 2018a. Does human endometrial LGR5 gene expression suggest the existence of another hormonally regulated epithelial stem cell niche? *Human Reproduction,* 33**,** 1052-1062.

TEMPEST, N., JANSEN, M., BAKER, A. M., HILL, C. J., HALE, M., MAGEE, D., TREANOR, D., WRIGHT, N. A. & HAPANGAMA, D. K. 2020. Histological 3D reconstruction and in vivo lineage tracing of the human endometrium. *The Journal of Pathology,* 251**,** 440-451.

TEMPEST, N., MACLEAN, A. & HAPANGAMA, D. K. 2018b. Endometrial stem cell markers: current concepts and unresolved questions. *International journal of molecular sciences,* 19**,** 3240.

TEWARY, S., LUCAS, E. S., FUJIHARA, R., KIMANI, P. K., POLANCO, A., BRIGHTON, P. J., MUTER, J., FISHWICK, K. J., DA COSTA, M., EWINGTON, L. J., LACEY, L., TAKEDA, S., BROSENS, J. J. & QUENBY, S. 2020. Impact of sitagliptin on endometrial mesenchymal stem-like progenitor cells: A randomised, double-blind placebo-controlled feasibility trial. *EBioMedicine,* 51**,** 102597.

THELLIN, O., ZORZI, W., LAKAYE, B., DE BORMAN, B., COUMANS, B., HENNEN, G., GRISAR, T., IGOUT, A. & HEINEN, E. 1999. Housekeeping genes as internal standards: use and limits. *Journal of biotechnology,* 75**,** 291-295.

TOJO, M., HAMASHIMA, Y., HANYU, A., KAJIMOTO, T., SAITOH, M., MIYAZONO, K., NODE, M. & IMAMURA, T. 2005. The ALK-5 inhibitor A-83-01 inhibits Smad signaling and epithelial-to-mesenchymal transition by transforming growth factor-β. *Cancer science,* 96**,** 791-800.

TOTHOVA, Z., KOLLIPARA, R., HUNTLY, B. J., LEE, B. H., CASTRILLON, D. H., CULLEN, D. E., MCDOWELL, E. P., LAZO-KALLANIAN, S., WILLIAMS, I. R., SEARS, C., ARMSTRONG, S. A., PASSEGUÉ, E., DEPINHO, R. A. & GILLILAND, D. G. 2007. FoxOs are critical mediators of hematopoietic stem cell resistance to physiologic oxidative stress. *Cell,* 128**,** 325-39.

TURCO, M. Y., GARDNER, L., HUGHES, J., CINDROVA-DAVIES, T., GOMEZ, M. J., FARRELL, L., HOLLINSHEAD, M., MARSH, S. G. E., BROSENS, J. J., CRITCHLEY, H. O., SIMONS, B. D., HEMBERGER, M., KOO, B. K.,

MOFFETT, A. & BURTON, G. J. 2017. Long-term, hormone-responsive organoid cultures of human endometrium in a chemically defined medium. *Nat Cell Biol,* 19**,** 568-577.

TURCO, M. Y., GARDNER, L., KAY, R. G., HAMILTON, R. S., PRATER, M., HOLLINSHEAD, M. S., MCWHINNIE, A., ESPOSITO, L., FERNANDO, R., SKELTON, H., REIMANN, F., GRIBBLE, F. M., SHARKEY, A., MARSH, S. G. E., O'RAHILLY, S., HEMBERGER, M., BURTON, G. J. & MOFFETT, A. 2018. Trophoblast organoids as a model for maternal-fetal interactions during human placentation. *Nature,* 564**,** 263-267.

TÜMPEL, S. & RUDOLPH, K. L. 2019. Quiescence: good and bad of stem cell aging. *Trends in cell biology,* 29**,** 672-685.

UCHIDA, H., MARUYAMA, T., OHTA, K., ONO, M., ARASE, T., KAGAMI, M., ODA, H., KAJITANI, T., ASADA, H. & YOSHIMURA, Y. 2007. Histone deacetylase inhibitor-induced glycodelin enhances the initial step of implantation. *Human reproduction,* 22**,** 2615-2622.

VALDES-DAPENA, M. A. 1973. The development of the uterus in late fetal life, infancy, and childhood. *The Uterus (International Academy of Pathology Monograph Series). Melbourne, FL: Krieger Pub Co***,** 40-67.

VALENTIJN, A., SARETZKI, G., TEMPEST, N., CRITCHLEY, H. & HAPANGAMA, D. 2015. Human endometrial epithelial telomerase is important for epithelial proliferation and glandular formation with potential implications in endometriosis. *Human Reproduction,* 30**,** 2816-2828.

VALENTIJN, A. J., PALIAL, K., AL-LAMEE, H., TEMPEST, N., DRURY, J., VON ZGLINICKI, T., SARETZKI, G., MURRAY, P., GARGETT, C. E. & HAPANGAMA, D. K. 2013. SSEA-1 isolates human endometrial basal glandular epithelial cells: phenotypic and functional characterization and implications in the pathogenesis of endometriosis. *Human reproduction,* 28**,** 2695-2708.

VANDER HEIDEN, M. G., CANTLEY, L. C. & THOMPSON, C. B. 2009. Understanding the Warburg effect: the metabolic requirements of cell proliferation. *science,* 324**,** 1029-1033.

WAGNER, G. P., KIN, K. & LYNCH, V. J. 2012. Measurement of mRNA abundance using RNA-seq data: RPKM measure is inconsistent among samples. *Theory in biosciences,* 131**,** 281-285.

WAGNER, V. & GIL, J. 2020. Senescence as a therapeutically relevant response to CDK4/6 inhibitors. *Oncogene,* 39**,** 5165-5176.

WANG, H., CRITCHLEY, H. O., KELLY, R. W., SHEN, D. & BAIRD, D. T. 1998. Progesterone receptor subtype B is differentially regulated in human endometrial stroma. *Molecular human reproduction,* 4**,** 407-412.

WANG, H., PILLA, F., ANDERSON, S., MARTÍNEZ-ESCRIBANO, S., HERRER, I., MORENO-MOYA, J. M., MUSTI, S., BOCCA, S., OEHNINGER, S. & HORCAJADAS, J. A. 2012. A novel model of human implantation: 3D endometrium-like culture system to study attachment of human trophoblast (Jar) cell spheroids. *Molecular human reproduction,* 18**,** 33-43.

WANG, Y., HANIFI-MOGHADDAM, P., HANEKAMP, E. E., KLOOSTERBOER, H. J., FRANKEN, P., VELDSCHOLTE, J., VAN DOORN, H. C., EWING, P. C., KIM, J. J., GROOTEGOED, J. A., BURGER, C. W., FODDE, R. & BLOK, L. J. 2009. Progesterone inhibition of Wnt/beta-catenin signaling in normal endometrium and endometrial cancer. *Clin Cancer Res,* 15**,** 5784-93.

WEIMAR, C. H. E., KAVELAARS, A., BROSENS, J. J., GELLERSEN, B., DE VREEDEN-ELBERTSE, J. M. T., HEIJNEN, C. J. & MACKLON, N. S. 2012. Endometrial stromal cells of women with recurrent miscarriage fail to discriminate between high-and low-quality human embryos. *PLoS One,* 7**,** e41424.

WIRA, C. R., RODRIGUEZ-GARCIA, M. & PATEL, M. V. 2015. The role of sex hormones in immune protection of the female reproductive tract. *Nature reviews Immunology,* 15**,** 217.

WIWATPANIT, T., MURPHY, A. R., LU, Z., URBANEK, M., BURDETTE, J. E., WOODRUFF, T. K. & KIM, J. J. 2020. Scaffold-free endometrial organoids respond to excess androgens associated with polycystic ovarian syndrome. *The Journal of Clinical Endocrinology & Metabolism,* 105**,** 769-780.

WOODING, P. & BURTON, G. 2008. *Comparative placentation: structures, functions and evolution*, Springer Science & Business Media.

WU, Z., JIN, L., ZHENG, W., ZHANG, C., ZHANG, L., CHEN, Y., GUAN, J. & FEI, H. 2018. NMR-based serum metabolomics study reveals a innovative diagnostic model for missed abortion. *Biochemical and Biophysical Research Communications*.

WYNN, R. M. 1989. The human endometrium: cyclic and gestational changes. *Biology of the Uterus,* 2**,** 289-331.

XIONG, S., SHARKEY, A. M., KENNEDY, P. R., GARDNER, L., FARRELL, L. E., CHAZARA, O., BAUER, J., HIBY, S. E., COLUCCI, F. & MOFFETT, A. 2013.

Maternal uterine NK cell–activating receptor KIR2DS1 enhances placentation. *The Journal of clinical investigation,* 123**,** 4264-4272.

XU, L., LIN, W., WEN, L. & LI, G. 2019. Lgr5 in cancer biology: functional identification of Lgr5 in cancer progression and potential opportunities for novel therapy. *Stem cell research & therapy,* 10**,** 1-9.

YAMAGUCHI, M., YOSHIHARA, K., SUDA, K., NAKAOKA, H., YACHIDA, N., UEDA, H., SUGINO, K., MORI, Y., YAMAWAKI, K., TAMURA, R., ISHIGURO, T., MOTOYAMA, T., WATANABE, Y., OKUDA, S., TAINAKA, K. & ENOMOTO, T. 2021. Three-dimensional understanding of the morphological complexity of the human uterine endometrium. *iScience,* 24**,** 102258.

YOSHIDA, G. J. 2015. Metabolic reprogramming: the emerging concept and associated therapeutic strategies. *Journal of experimental & clinical cancer research,* 34**,** 1-10.

YU, Y., FANG, L., WANG, S., LI, Y., GUO, Y. & SUN, Y.-P. 2019. Amphiregulin promotes trophoblast invasion and increases MMP9/TIMP1 ratio through ERK1/2 and Akt signal pathways. *Life sciences,* 236**,** 116899.

ZAFARULLAH, M., LI, W., SYLVESTER, J. & AHMAD, M. 2003. Molecular mechanisms of N-acetylcysteine actions. *Cellular and Molecular Life Sciences CMLS,* 60**,** 6-20.

ZAKRZEWSKI, W., DOBRZYŃSKI, M., SZYMONOWICZ, M. & RYBAK, Z. 2019. Stem cells: past, present, and future. *Stem cell research & therapy,* 10**,** 1-22.

ZAMMIT, V. A. 2008. Carnitine palmitoyltransferase 1: central to cell function. *IUBMB life,* 60**,** 347-354.

ZEINEDDINE, D., ABOU HAMMOUD, A., MORTADA, M. & BOEUF, H. 2014. The Oct4 protein: more than a magic stemness marker. *American journal of stem cells,* 3**,** 74.

ZHANG, L., REES, M. & BICKNELL, R. 1995. The isolation and long-term culture of normal human endometrial epithelium and stroma. Expression of mRNAs for angiogenic polypeptides basally and on oestrogen and progesterone challenges. *Journal of cell science,* 108**,** 323-331.

ZHENG, Y., XUE, X., SHAO, Y., WANG, S., ESFAHANI, S. N., LI, Z., MUNCIE, J. M., LAKINS, J. N., WEAVER, V. M., GUMUCIO, D. L. & FU, J. 2019. Controlled modelling of human epiblast and amnion development using stem cells. *Nature,* 573**,** 421-425.

ZHOU, S., XIE, Y., PUSCHECK, E. E. & RAPPOLEE, D. A. 2011. Oxygen levels that optimize TSC culture are identified by maximizing growth rates and minimizing stress. *Placenta,* 32**,** 475-81.

ZHOU, X.-L., LEI, Z. & RAO, C. V. 1999. Treatment of human endometrial gland epithelial cells with chorionic gonadotropin/luteinizing hormone increases the expression of the cyclooxygenase-2 gene. *The Journal of Clinical Endocrinology & Metabolism,* 84**,** 3364-3377.

ZHU, Q., DONG, Y. C., ZHANG, L., MA, X. & XIA, H. F. 2020. miR-98 is involved in missed abortion by targeting GDF6 and FAPP2. *Reproduction,* 159**,** 525-537.

ZHU, Z., CAO, F. & LI, X. 2019. Epigenetic programming and fetal metabolic programming. *Frontiers in endocrinology,* 10**,** 764.

Publications

RESEARCH ARTICLE

Modelling the impact of decidual senescence on embryo implantation in human endometrial assembloids

Thomas M Rawlings[1,2], Komal Makwana[1,2], Deborah M Taylor[1,2,3], Matteo A Molè[4], Katherine J Fishwick[1], Maria Tryfonos[1,2], Joshua Odendaal[1,5], Amelia Hawkes[1,5], Magdalena Zernicka-Goetz[4,6], Geraldine M Hartshorne[1,2,3], Jan J Brosens[1,2,5]*, Emma S Lucas[1,2]

[1]Division of Biomedical Sciences, Warwick Medical School, University of Warwick, Coventry, United Kingdom; [2]Centre for Early Life, Warwick Medical School, University of Warwick, Coventry, United Kingdom; [3]Centre for Reproductive Medicine, University Hospitals Coventry and Warwickshire NHS Trust, Coventry, United Kingdom; [4]Department of Physiology, Development and Neuroscience, University of Cambridge, Cambridge, United Kingdom; [5]Tommy's National Centre for Miscarriage Research, University Hospitals Coventry & Warwickshire NHS Trust, Coventry, United Kingdom; [6]Synthetic Mouse and Human Embryology Group, California Institute of Technology (Caltech), Division of Biology and Biological Engineering, Pasadena, United Kingdom

***For correspondence:** J.J.Brosens@warwick.ac.uk

Competing interest: The authors declare that no competing interests exist.

Funding: See page 19

Preprinted: 02 March 2021
Received: 20 April 2021
Accepted: 03 September 2021
Published: 06 September 2021

Reviewing Editor: Thomas E Spencer, Fred Hutchinson Cancer Research Center, United States

Abstract Decidual remodelling of midluteal endometrium leads to a short implantation window after which the uterine mucosa either breaks down or is transformed into a robust matrix that accommodates the placenta throughout pregnancy. To gain insights into the underlying mechanisms, we established and characterized endometrial assembloids, consisting of gland-like organoids and primary stromal cells. Single-cell transcriptomics revealed that decidualized assembloids closely resemble midluteal endometrium, harbouring differentiated and senescent subpopulations in both glands and stroma. We show that acute senescence in glandular epithelium drives secretion of multiple canonical implantation factors, whereas in the stroma it calibrates the emergence of anti-inflammatory decidual cells and pro-inflammatory senescent decidual cells. Pharmacological inhibition of stress responses in pre-decidual cells accelerated decidualization by eliminating the emergence of senescent decidual cells. In co-culture experiments, accelerated decidualization resulted in entrapment of collapsed human blastocysts in a robust, static decidual matrix. By contrast, the presence of senescent decidual cells created a dynamic implantation environment, enabling embryo expansion and attachment, although their persistence led to gradual disintegration of assembloids. Our findings suggest that decidual senescence controls endometrial fate decisions at implantation and highlight how endometrial assembloids may accelerate the discovery of new treatments to prevent reproductive failure.

Introduction

Upon embryo implantation, the cycling human endometrium transforms into the decidua of pregnancy to accommodate the placenta (***Gellersen and Brosens, 2014***). Transition between these physiological endometrial states requires intensive tissue remodelling, a process termed decidualization. Notwithstanding that decidualization in early pregnancy cannot be studied directly, a spectrum of prevalent reproductive disorders is attributed to perturbations in this process, including recurrent

eLife digest At the beginning of a human pregnancy, the embryo implants into the uterus lining, known as the endometrium. At this point, the endometrium transforms into a new tissue that helps the placenta to form. Problems in this transformation process are linked to pregnancy disorders, many of which can lead to implantation failure (the embryo fails to invade the endometrium altogether) or recurrent miscarriages (the embryo implants successfully, but the interface between the placenta and the endometrium subsequently breaks down).

Studying the implantation of human embryos directly is difficult due to ethical and technical barriers, and animals do not perfectly mimic the human process, making it challenging to determine the causes of pregnancy disorders. However, it is likely that a form of cellular arrest called senescence, in which cells stop dividing but remain metabolically active, plays a role. Indeed, excessive senescence in the cells that make up the endometrium is associated with recurrent miscarriage, while a lack of senescence is associated with implantation failure.

To study this process, Rawlings et al. developed a new laboratory model of the human endometrium by assembling two of the main cell types found in the tissue into a three-dimensional structure. When treated with hormones, these 'assembloids' successfully mimic the activity of genes in the cells of the endometrium during implantation. Rawlings et al. then exposed the assembloids to the drug dasatinib, which targets and eliminates senescent cells. This experiment showed that assembloids become very robust and static when devoid of senescent cells.

Rawlings et al. then studied the interaction between embryos and assembloids using time-lapse imaging. In the absence of dasatinib treatment, cells in the assembloid migrated towards the embryo as it expanded, a process required for implantation. However, when senescent cells were eliminated using dasatinib, this movement of cells towards the embryo stopped, and the embryo failed to expand, in a situation that mimicks implantation failure.

The assembloid model of the endometrium may help scientists to study endometrial defects in the lab and test potential treatments. Further work will include other endometrial cell types in the assembloids, and could help increase the reliability of the model. However, any drug treatments identified using this model will need further research into their safety and effectiveness before they can be offered to patients.

implantation failure and recurrent pregnancy loss (***Dimitriadis et al., 2020***; ***Macklon, 2017***; ***Zhou et al., 2019***). By contrast, the sequence of events that renders the endometrium receptive to embryo implantation has been investigated extensively, starting with obligatory oestrogen-dependent tissue growth following menstrual repair. As a consequence of rapid proliferation of stromal fibroblasts and glandular epithelial cells (EpCs), which peaks in the upper third of the functional layer (***Ferenczy et al., 1979***), endometrial volume and thickness increases multifold prior to ovulation (***Raine-Fenning et al., 2004***; ***Dallenbach-Hellweg, 1981***). After the postovulatory rise in progesterone levels, proliferation of EpCs first decreases and then ceases altogether in concert with the onset of apocrine glandular secretions, heralding the start of the midluteal window of implantation (***Dallenbach-Hellweg, 1981***). Concurrently, uterine natural killer (uNK) cells accumulate and endometrial stromal cells (EnSCs) start decidualizing in a process that can be described as 'inflammatory programming' (***Brighton et al., 2017***; ***Chavan et al., 2021***; ***Erkenbrack et al., 2018***; ***Salker et al., 2012***). Morphological decidual cells, characterized by abundant cytoplasm and enlarged nuclei, emerge upon closure of the 4 -day implantation window, meaning that the endometrium has become refractory to embryo implantation (***Gellersen and Brosens, 2014***). In pregnancy, decidual cells form a robust, tolerogenic matrix in which invading trophoblast cells cooperate with local immune cells to form a haemochorial placenta (***Aplin et al., 2020***; ***Vento-Tormo et al., 2018***). In non-conception cycles, however, falling progesterone levels and influx of neutrophils lead to breakdown of the superficial endometrial layer and menstrual shedding (***Jabbour et al., 2006***).

Recently, we highlighted the importance of cellular senescence in endometrial remodelling during the midluteal implantation window (***Brighton et al., 2017***; ***Lucas et al., 2020***; ***Kong et al., 2021***). Senescence denotes a cellular stress response triggered by replicative exhaustion or other stressors that cause macromolecular damage (***Muñoz-Espín and Serrano, 2014***). Activation of tumour

suppressor pathways and upregulation of cyclin-dependent kinase inhibitors $p16^{INK4a}$ (encoded by *CDKN2A*) and $p21^{CIP1}$ (*CDKN1A*) lead to permanent cell cycle arrest, induction of survival genes, and production of a bioactive secretome, referred to as the senescence-associated secretory phenotype (SASP). The composition of the SASP is tissue-specific but typically includes proinflammatory and immunomodulatory cytokines, chemokines, growth factors, and extracellular matrix (ECM) proteins and proteases (***Birch and Gil, 2020***). Acute senescence, characterized by transient SASP production and rapid immune-mediated clearance of senescent cells, is widely implicated in processes involving physiological tissue remodelling, including during embryo development, placenta formation, and wound healing (***Muñoz-Espín and Serrano, 2014***; ***Van, 2014***). By contrast, persisting senescent cells cause chronic inflammation or 'inflammaging' (***Birch and Gil, 2020***), a pathological state that underpins ageing and age-related disorders. We demonstrated that inflammatory reprogramming of EnSC burdened by replication stress leads to the emergence of acute senescent cells during the implantation window (***Brighton et al., 2017***; ***Lucas et al., 2020***; ***Kong et al., 2021***). Upon successful implantation and continuous progesterone signalling, decidual cells co-opt uNK cells to eliminate their senescent counterparts through granule exocytosis (***Brighton et al., 2017***; ***Lucas et al., 2020***; ***Kong et al., 2021***). Clearance of senescent decidual cells likely necessitates recruitment of bone marrow-derived decidual precursor cells, which confer tissue plasticity for rapid decidual expansion in early pregnancy (***Diniz-da-Costa et al., 2021***). Importantly, lack of clonogenic decidual precursor cells and a pro-senescent decidual response are linked to recurrent pregnancy loss (***Lucas et al., 2016***; ***Lucas et al., 2020***; ***Tewary et al., 2020***).

Based on these insights, we hypothesized that acute senescence is integral to successful implantation by creating conditions for anchorage of the conceptus in an otherwise tightly adherent decidual matrix. To test this hypothesis, we developed an 'assembloid' model, consisting of endometrial gland-like organoids and primary EnSC, which recapitulates the complexity in cell states and gene expression of the midluteal implantation window, improving resemblance to endometrial tissue in comparison with existing co-culture models (***Cheung et al., 2021***; ***Rawlings, 2021***). We used this model to establish co-cultures with human blastocysts and demonstrate that aspects of different pathological states associated with implantation failure and miscarriage can be recapitulated in endometrial assembloids by modulating decidual senescence.

Results

Establishment of endometrial assembloids

Organoids consisting of gland-like structures are established by culturing endometrial EpCs seeded in Matrigel in a chemically defined medium containing growth factors and signal transduction pathway modulators (***Supplementary file 1***: Table 1; ***Turco et al., 2017***; ***Boretto et al., 2017***). Gland-like organoids grown in this medium, termed expansion medium, are genetically stable, easily passaged, and can be maintained in long-term cultures (***Boretto et al., 2017***; ***Turco et al., 2017***). Oestradiol (E2) promotes proliferation of gland-like organoids and cooperates with NOTCH signalling to activate ciliogenesis in a subpopulation of EpC (***Haider et al., 2019***). Further, treatment with a progestin (e.g. medroxyprogesterone acetate [MPA]) and a cyclic AMP analogue (e.g. 8-bromo-cAMP) induces secretory transformation of gland-like organoids in parallel with expression of luteal-phase marker genes (***Turco et al., 2017***; ***Boretto et al., 2017***).

We modified the gland-like organoid model to incorporate EnSC. To this end, midluteal endometrial biopsies (***Supplementary file 1***: Table 2) were digested and gland-like organoids established from isolated EpC (***Figure 1A***). In parallel, purified EnSC were propagated in standard monolayer cultures. At passage 2, single-cell suspensions of EnSC were combined with organoid EpC, seeded in hydrogel, and cultured in expansion medium supplemented with E2 (***Figure 1A***). The hydrogel matrix comprised 97% type I and 3% type III collagens, which are both present in midluteal endometrium (***Oefner et al., 2015***; ***Aplin et al., 1988***; ***Aplin and Jones, 1989***; ***Iwahashi et al., 1996***), and has a predicted in-use elastic modulus (Pa) of comparable magnitude to non-pregnant endometrium (***Abbas et al., 2019***; ***Bagley, 2019***). As shown in ***Figure 1B***, gland formation was unperturbed by the presence of EnSC and assembloids resembled the architecture of native endometrium more closely than organoids. Further, decidualization of assembloids with 8-bromo-cAMP and MPA for 4 days (***Figure 1C***) resulted in robust secretion of decidual prolactin (PRL) and C-X-C motif chemokine ligand

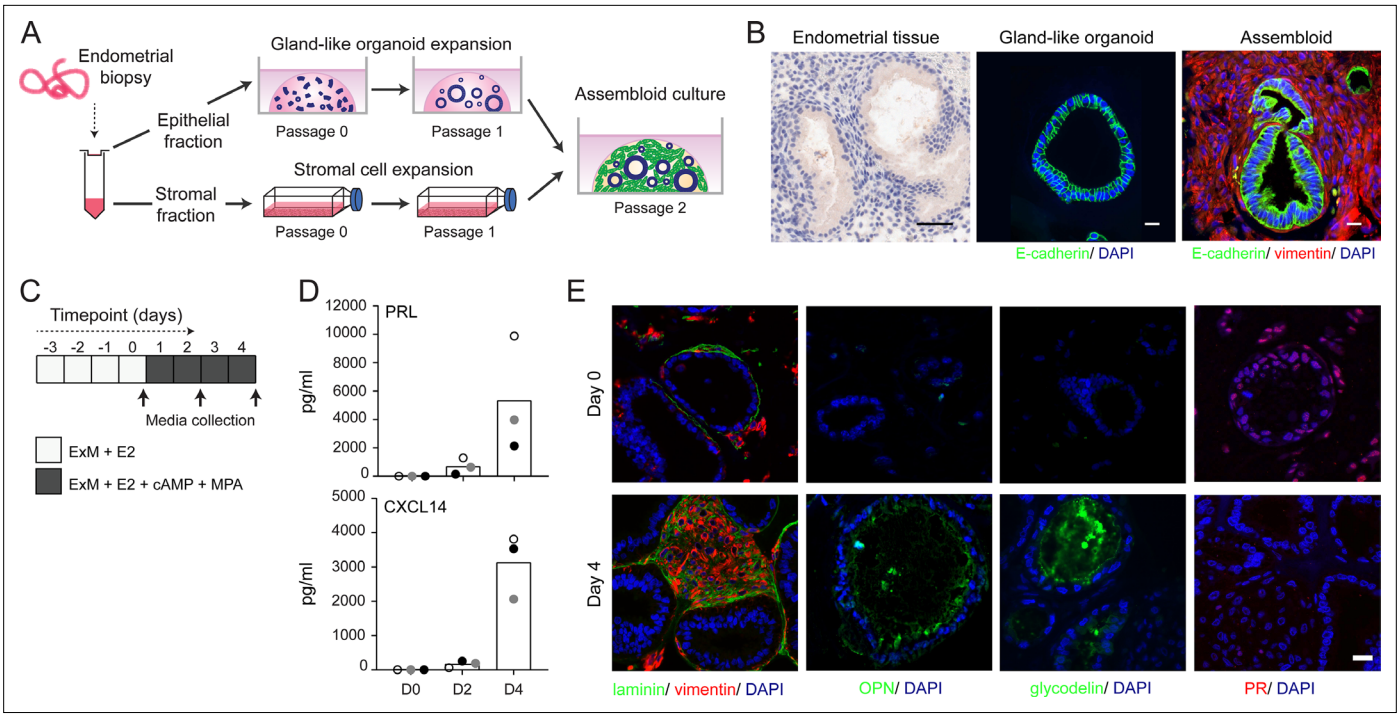

Figure 1. Establishment of endometrial assembloids. (**A**) Schematic for establishing endometrial assembloids. (**B**) Structural appearance of hematoxylin and eosin stained secretory endometrium, E-cadherin labelled gland-like organoids, and E-cadherin and vimentin stained endometrial assembloids. Scale bar = 50 µm. (**C**) Schematic summary of experimental design. (**D**) Secreted levels of PRL and CXCL14 were measured by ELISA in spent medium at the indicated timepoints. Data points are coloured to indicate secretion in assembloids established from different endometrial biopsies (n = 3). (**E**) Representative immunofluorescence labelling of laminin and vimentin, progesterone receptor (PR), glycodelin, and osteopontin (OPN) in undifferentiated (day 0, top panels) and decidualized (day 4; bottom panels) assembloids. Nuclei were counterstained with DAPI. Scale bar = 50 µm. ELISA data in (**B**) are available in ***Figure 1—source data 1***.

The online version of this article includes the following figure supplement(s) for figure 1:

Source data 1. Secretion of PRL and CXCL14 by endometrial assembloids.

14 (CXCL14) (***Figure 1D***). Immunofluorescence microscopy provided further evidence that decidualizing assembloids mimic luteal phase endometrium, exemplified by laminin deposition by decidualizing EnSC, induction of osteopontin (*SPP1*) and accumulation of glycodelin (encoded by *PAEP*) in the lumen of secretory glands, and downregulation of the progesterone receptor (*PGR*) in both stromal and glandular compartments (***Figure 1E***).

We reasoned that once established assembloids may no longer require exogenous growth factors and pathway modulators for differentiation because of the presence of EnSC. To test this hypothesis, parallel gland-like organoids and assembloids were established from three endometrial biopsies and decidualized with E2, 8-bromo-cAMP, and MPA for 4 days in either expansion medium, base medium (***Supplementary file 1***: Table 1), or base medium with each exogeneous factor added back individually. Induction of *PAEP* and *SPP1* was used to monitor the glandular differentiation response. As shown in ***Figure 2***, differentiation of gland-like organoids in base medium markedly blunted the induction of *PAEP* and *SPP1* when compared to expansion medium. Add-back of individual factors did not restore the glandular response, with the exception of N-acetyl-L-cysteine (NAC). Addition of NAC at low concentration (1.25 mM) to base medium resulted in a robust glandular response in assembloids. Thus, in subsequent experiments assembloids were grown in expansion medium supplemented with E2 and then decidualized in minimal differentiation medium (MDM), consisting of base medium containing NAC, E2, 8-bromo-cAMP, and MPA.

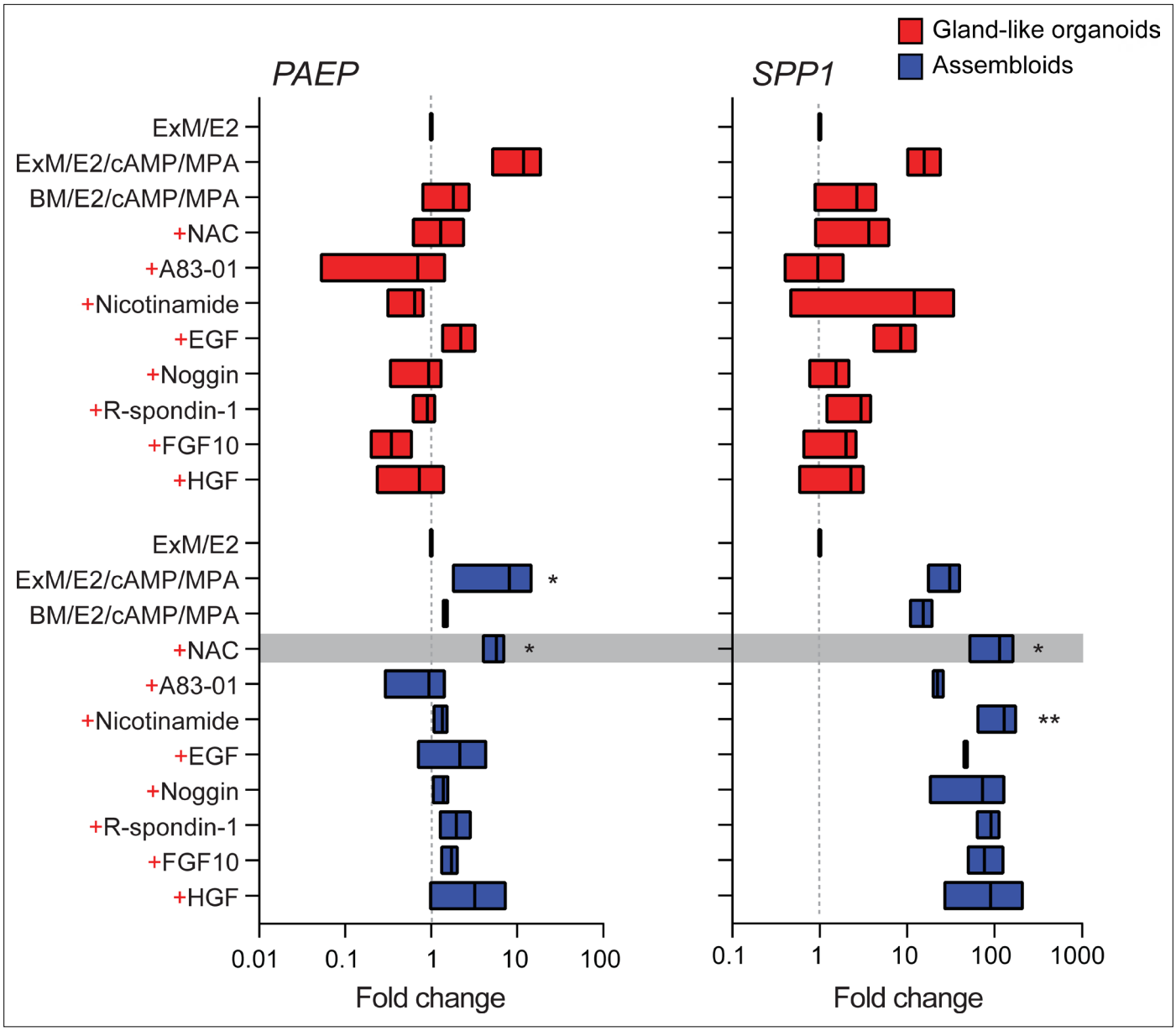

Figure 2. Characterization of a minimal differentiation medium for endometrial assembloids. Parallel gland-like organoids (red) and assembloids (blue) were established from three endometrial biopsies and decidualized with 8-bromo-cAMP and MPA for 4 days in either expansion medium (ExM), base medium (BM), or BM with each exogeneous factor added back individually (+). Induction of *PAEP* and *SPP1* was used to monitor the glandular differentiation. The grey bar indicates the composition of the minimal differentiation medium selected for further use (BM supplemented with NAC, E2, cAMP, and MPA). Data are presented as fold-change relative to expression levels in undifferentiated organoids or assembloids cultured in ExM+ E2. Bars present minimal, maximal, and median fold-change. * and ** indicate $p<0.05$ and $p<0.01$ obtained by Friedman's test for matched samples. Relative expression values for biological replicates are available in ***Figure 2—source data 1***.

The online version of this article includes the following figure supplement(s) for figure 2:

Source data 1. RTqPCR data associated with the minimal differentiation medium (MDM) experiments.

Cellular complexity of decidualizing assembloids mimics midluteal endometrium

We hypothesized that, depending on the level of replicative stress (***Lucas et al., 2020***; ***Abbas et al., 2019***), individual EpC and EnSC adopt distinct cellular states upon decidualization of endometrial assembloids. Based on previous time-course experiments in 2D cultures, we further speculated that divergence of cells into distinct subpopulations would be apparent by day 4 of differentiation (***Brosens***

et al., 1999; *Lucas et al., 2020*). To test this hypothesis, we performed single-cell RNA sequencing (scRNA-seq) on undifferentiated assembloids grown for 4 days in expansion medium and assembloids decidualized in MDM for four additional days (*Figure 3A*). Eleven distinct cell clusters were identified by Shared Nearest Neighbour (SNN) and Uniform Manifold Approximation and Projection (UMAP) analysis, segregating broadly into epithelial and stromal populations within the UMAP-1 dimension and into undifferentiated and differentiated subpopulations within the UMAP-2 dimension (*Figure 3B*). Each cell cluster was annotated based on expression of curated marker genes, which were cross-referenced with a publicly available data set (GEO: GSE4888) to determine their relative expression across the menstrual cycle in vivo (*Talbi et al., 2006*).

We identified five unambiguous EpC subsets. The glandular component of undifferentiated assembloids harboured actively dividing EpC (EpS1; n = 198) as well as EpC-expressing marker genes of E2-responsive proliferative phase endometrium (EpS2; n = 692), including *PGR* and *CPM* (*Figure 3C*). EpS3 (n = 29) consisted of ciliated EpC, expressing an abundance of genes involved in cilium assembly and organization, including *DNAI1* and *TUBA4B* (*Figure 3C*). Ciliated cells are the only glandular subpopulation present in both undifferentiated and decidualized assembloids. In vivo, EpS3 marker genes transiently peak during the early-luteal phase (*Figure 3C*). Decidualization of endometrial assembloids led to the emergence of two distinct EpC subsets, EpS4 (n = 434) and EpS5 (n = 208). Both clusters expressed canonical endometrial 'receptivity genes' (annotated in green in *Figure 3C*), that is, genes used in a clinical test to aid the timing of embryo transfer to the window of implantation in IVF patients (*Díaz-Gimeno et al., 2011*). In agreement, induction of EpS4 and EpS5 marker genes in vivo coincides with the transition from early- to midluteal phase. However, while expression of EpS4 marker genes, including *SOD2*, *MAOA*, and *PTGS1*, generally peaks during the midluteal window of implantation, EpS5 genes tend to persist or peak during the late-luteal phase (*Figure 3C*). Additional mining of the data revealed that transition from EpS4 to EpS5 coincides with induction of $p16^{INK4a}$ and $p21^{CIP1}$ in parallel with upregulation of 56 genes encoding secretory factors (*Figure 3—figure supplement 1*). Notably, several canonical implantation factors secreted by this subpopulation are also well-characterized SASP components, including dipeptidyl peptidase 4 (*DPP4; Kim et al., 2017*), growth differentiation factor 15 (*GDF15; Basisty et al., 2020*), and insulin-like growth factor binding protein 3 (*IGFBP3; Elzi et al., 2012*). Thus, EpS5 consists of senescent EpC producing an implantation-specific SASP.

Decidualized endometrial assembloids also harboured a sizable population of ambiguous cells expressing both epithelial and stromal genes (*Figure 3C* and *Figure 3—figure supplement 2*). A hallmark of this subset, termed 'transitional population' (TP; n = 472), is the induction of long non-coding RNAs involved in mesenchymal-epithelial and epithelial-mesenchymal transition (MET/EMT), such as *NEAT1* (nuclear paraspeckle assembly transcript 1) and *KCNQ1OT1* (KCNQ1 opposite strand/antisense transcript 1) (*Bian et al., 2019*; *Chen et al., 2021*). GO analysis showed that both EpS5 and the transitional population comprised secretory cells involved in ECM organization (*Figure 3D*). However, while EpS5 genes are implicated in neutrophil activation (a hallmark of premenstrual endometrium), genes expressed by the transitional population are uniquely enriched in GO terms such as 'wound healing', 'regulation of stem cell proliferation', 'blood coagulation', and 'blood vessel development' (*Figure 3D*), which points towards a putative role in tissue repair and regeneration.

The stromal fraction of undifferentiated assembloids consisted of actively dividing EnSC (stromal subpopulation 1 [SS1]; n = 434) and E2-responsive EnSC (SS2; n = 874) expressing proliferative phase marker genes, such as *PGR*, *MMP11*, and *CRABP2* (*Figure 3E*). As anticipated, decidualization of assembloids for 4 days led to a preponderance of pre-decidual cells (SS3; n = 495) as well as emerging decidual cells (SS4; n = 87) and senescent decidual cells (SS5; n = 118) (*Figure 3E*). Each of these subpopulations expressed marker genes identified previously by scRNA-seq reconstruction of the decidual pathway in standard primary EnSC cultures (*Lucas et al., 2020*). Pre-decidual cells in SS3 express *HAND2*, a key decidual transcription factor (*Marinić et al., 2021*), as well as previously identified genes encoding secreted factors, including *VEGFA* (vascular endothelial growth factor A), *CRISPLD2* (a progesterone-dependent anti-inflammatory response gene coding cysteine-rich secretory protein LCCL domain containing 2), *IL15* (interleukin 15), and *TIMP3* (TIMP metallopeptidase inhibitor 3) (*Lucas et al., 2020*). Novel candidate pre-decidual genes were also identified, such as *DDIT4* (DNA damage-inducible transcript 4), encoding a stress response protein intimately involved in autophagy, stemness, and antioxidative defences (*Ho et al., 2020*; *Miller et al., 2020*). Decidual

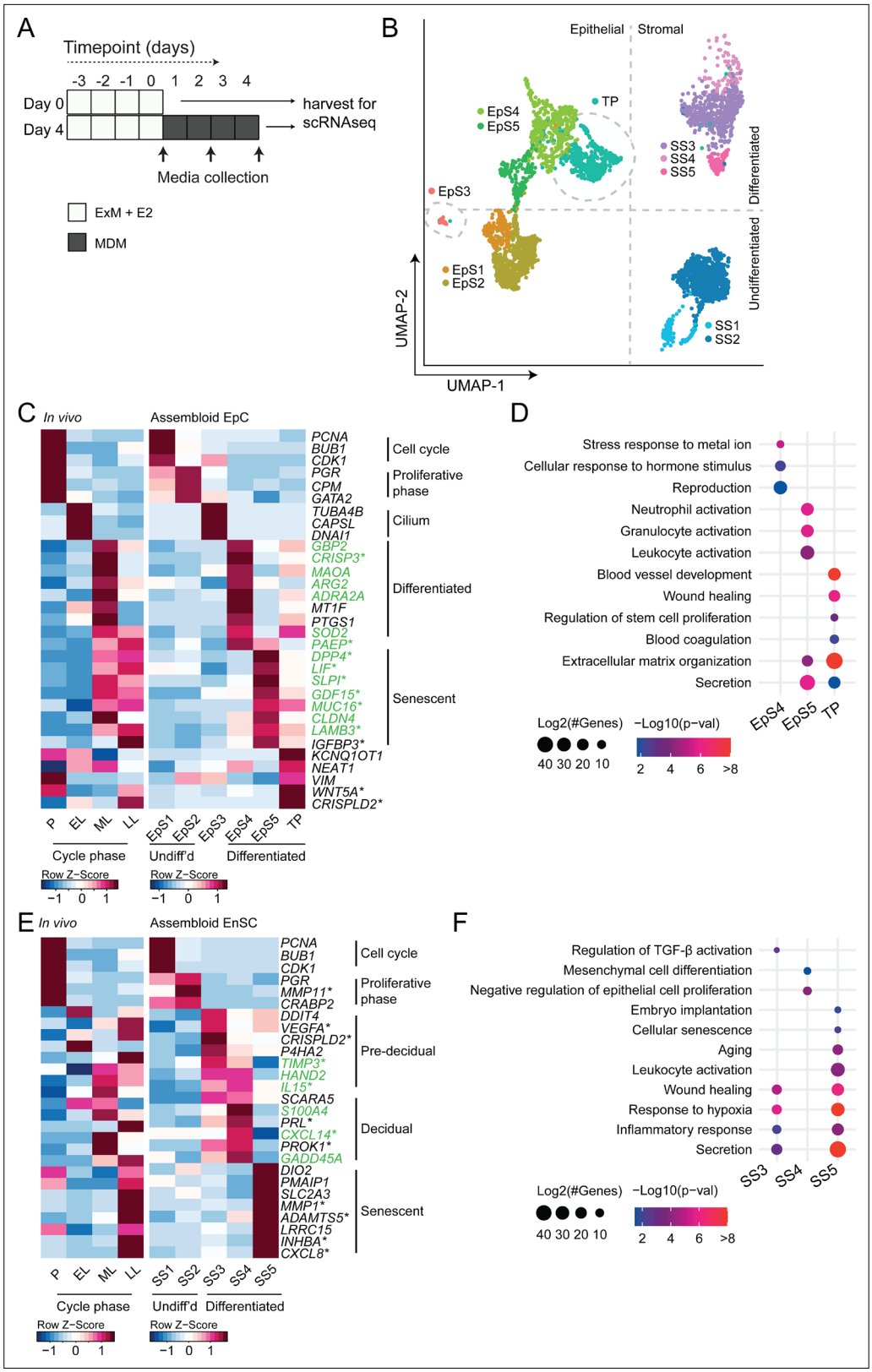

Figure 3. Decidualizing assembloids mimic midluteal endometrium. (**A**) Schematic overview of experimental design. ExM: expansion medium; MDM: minimal differentiation medium. (**B**) Uniform Manifold Approximation and Projection (UMAP) visualizing epithelial and stromal subsets (EpS and SS, respectively) identified by single-cell transcriptomic analysis of undifferentiated and decidualized assembloids. A transitional population (TP) consisting

Figure 3 continued on next page

Figure 3 continued

of cells expressing epithelial and stromal markers is also shown. Dotted lines indicate the separation of EpS and SS in UMAP_1 and of undifferentiated and differentiated subpopulations in UMAP_2. Dotted circles indicate ciliated (EpS3) and TP, which did not fit these broad segregations. (**C**) Composite heatmaps showing relative expression (Z-scores) of epithelial marker genes across the menstrual cycle in vivo and in undifferentiated and decidualized assembloids. Highlighted in green are genes that mark the midluteal window of implantation (***Díaz-Gimeno et al., 2011***), whereas genes encoding secreted proteins are indicated by * (***Uhlén et al., 2015***). See also ***Figure 3—figure supplement 1***. (**D**) Dot plots showing GO terms related to biological processes enriched in different epithelial populations in decidualizing assembloids. The dot size represents the number of genes in each GO term and the colour indicates FDR-corrected p-value. (**E**) Composite heatmaps showing relative expression (Z-scores) of stromal marker genes across the menstrual cycle in vivo and in undifferentiated and decidualized assembloids. Highlighted in green are genes that mark the midluteal window of implantation (***Díaz-Gimeno et al., 2011***), whereas genes encoding secreted proteins are indicated by * (***Uhlén et al., 2015***). (**F**) Dot plots showing GO terms related to biological processes enriched in different stromal subpopulations in decidualizing assembloids. See also ***Figure 3—figure supplements 1 and 2*** and 3. Complete epithelial subpopulation marker lists can be found in ***Figure 3—source data 1***. GO analysis outputs can be found in . Complete stromal subpopulation marker lists can be found in .

The online version of this article includes the following figure supplement(s) for figure 3:

Source data 1. Epithelial subpopulation markers.

Source data 2. GO analysis of differentiated subpopulations.

Source data 3. Stromal sub-population markers.

Figure supplement 1. Heatmap showing relative expression (Z-scores) of genes encoding the cyclin-dependent kinase inhibitors $p16^{INK4a}$ and $p21^{CIP1}$ as well as SASP-related genes in epithelial and transitional subpopulations in decidualizing assembloids.

Figure supplement 2. Heatmap showing relative expression (Z-scores) of epithelial-mesenchymal transition/mesenchymal-epithelial transition (EMT/MET), epithelial and mesenchymal marker genes in the transitional population (TP), epithelial (EpS4-5) and stromal (SS3-5) subpopulations in decidualizing assembloids.

Figure supplement 3. Heatmap showing relative expression (Z-scores) of genes encoding the cyclin-dependent kinase inhibitors $p16^{INK4a}$ and $p21^{CIP1}$ as well as secretory and SASP-related genes in stromal subpopulations (SS3-5) in decidualizing assembloids.

cells (SS4) and senescent decidual cells (SS5) express *SCARA5* and *DIO2*, respectively (***Figure 3E***), two stroma-specific marker genes identified by scRNA-seq analysis of mid- and late-luteal endometrial biopsies (***Lucas et al., 2020***). SS3 and SS4 genes mapped to the early- and midluteal phase of the cycle, whereas SS5 genes peak in the late-luteal phase, that is, prior to menstrual breakdown. Notably, the transcriptomic profiles of SS3 and SS5 are enriched in GO terms such as 'Wound healing', 'Response to hypoxia', and 'Inflammatory response', suggesting that both clusters comprise stressed cells (***Figure 3F***). However, the nature of the cellular stress response differs between these populations with only senescent decidual cells (SS5) expressing genes enriched in categories such as 'Embryo implantation', 'Cellular senescence', 'Aging', and 'Leukocyte activation'. By contrast, few notable categories were selectively enriched in decidual cells (e.g. 'Mesenchymal cell differentiation'), rendering the lack of GO terms that pertain to stress, inflammation, or wound healing perhaps the most striking observation. In keeping with the GO analysis, senescent decidual cells (SS5) express a multitude of SASP-related genes (***Figure 3—figure supplement 3***), including matrix metallopeptidases (e.g. *MMP3*, *7*, *9*, *10*, *11*, and *14*), insulin-like growth factor binding proteins (e.g. *IGFBP1*, *3*, *6*, and *7*), growth factors (e.g. *AREG*, *FGF2*, *FGF7*, *HGF*, and *VEGFA*) and growth factor receptors (*PDGFRA* and *PDGFRB*), cytokines (e.g. *LIF*, *IL6*, *IL1A*, and *IL11*), chemokines (e.g. *CXCL8* and *CXCL1*), and members of the TGF-β superfamily of proteins (e.g. *GDF15*, *INHBA*, and *BMP2*). By contrast, decidual cells are characterized by expression of a unique network of secretory genes, some encoding ECM proteins (e.g. *COL1A1*, *COL3A1*, and *LAMA4*) and other known decidual markers (e.g. *PRL*, *PROK1*, and *WNT4*) as well as factors involved in uNK cell chemotaxis and activation (e.g. *CCL2*, *CXCL14*, and *IL15*) (***Figure 3—figure supplement 3***).

Taken together, single-cell analysis of undifferentiated and decidualized assembloids revealed a surprising level of cellular complexity. Each epithelial and stromal subpopulation appears functionally distinct and maps to a specific phase of the menstrual cycle. Transition between cellular states is

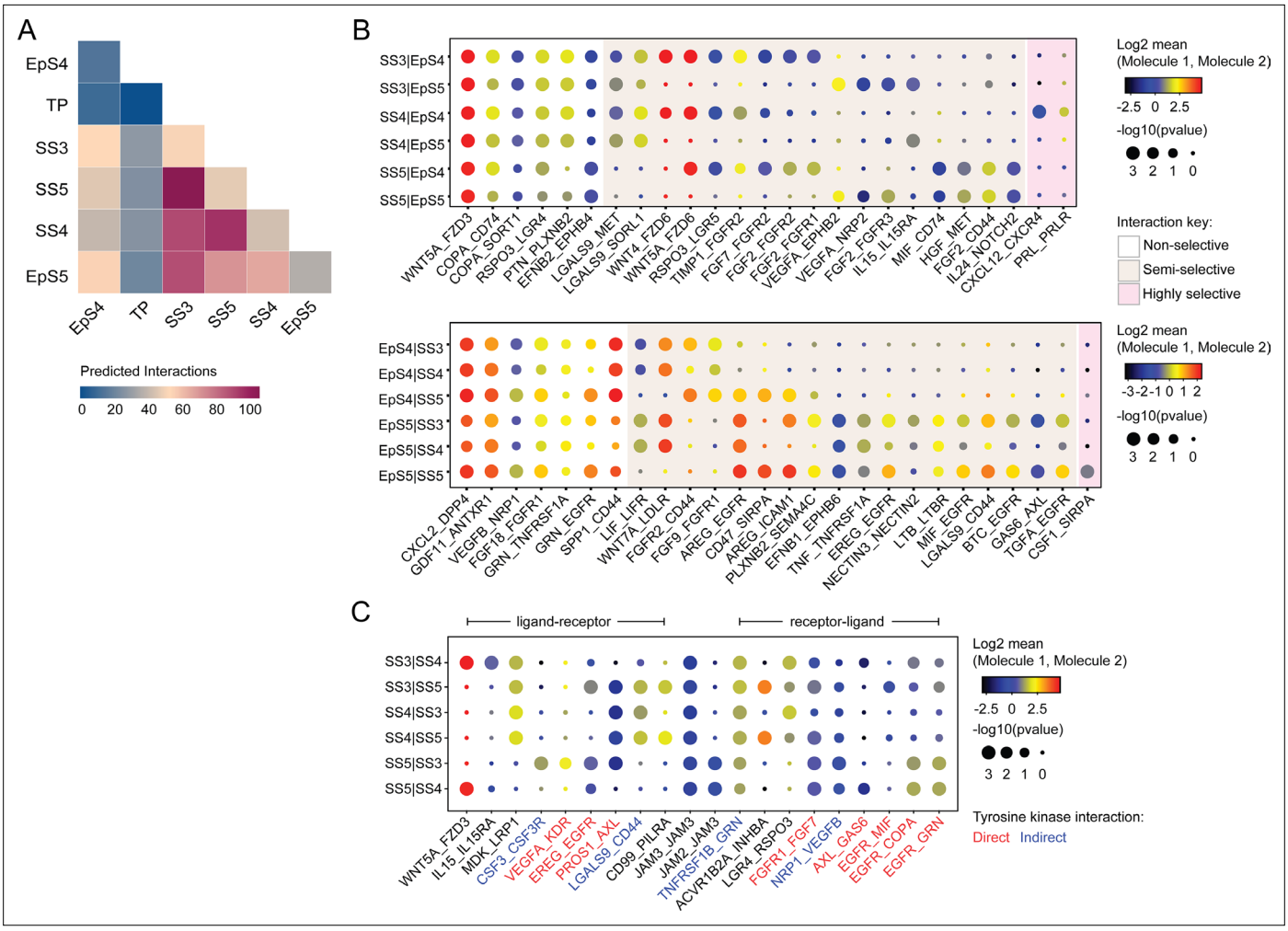

Figure 4. Putative receptor-ligand interactions in decidualizing assembloids. (**A**) Heatmap showing the total number of cell-cell interactions predicted by CellPhoneDB between different subpopulations in decidualizing assembloids. (**B**) Dot plots of representative ligand-receptor interactions between stromal subsets (SS) and epithelial subsets (EpS) (upper panel) and EpS and SS (lower panel) in decidualizing assembloids. Circle size and colour indicate p-value and the means of the average expression value of the interacting molecules, respectively. Shaded boxes were used to group putative interactions by level of selectivity. (**C**) Dot plot of representative ligand-receptor and receptor-ligand interactions between stromal subpopulations in decidualizing assembloids. Direct and indirect tyrosine kinase interactions are indicated by red and blue labels, respectively. Complete tables of predicted ligand-receptor interactions can be found in ***Figure 4—source data 1***.

The online version of this article includes the following figure supplement(s) for figure 4:

Source data 1. CellPhoneDB prediction of cell-cell interactions.

predicated on changes in cell cycle status, ranging from actively dividing cells in proliferating assembloids to the emergence upon differentiation of highly secretory senescent epithelial and decidual subpopulations, resembling premenstrual endometrium. However, the dominant subpopulations on day 4 of decidualization are EpS4 and SS3, which map to the midluteal implantation window in vivo.

Receptor-ligand interactions in decidualizing assembloids

We used CellPhoneDB, a publicly available online repository of highly curated receptor-ligand interactions, to explore putative interactions between subpopulations in decidualizing assembloids. This computational tool also takes into account the subunit architecture of both ligands and receptors in heteromeric complexes (***Efremova et al., 2020***; ***Vento-Tormo et al., 2018***). The number of predicted interactions is depicted in ***Figure 4A***, showing a conspicuous lack of crosstalk between the transitional population and any other populations. Conversely, the most abundant interactions centre around the secretory subpopulations, EpS5 and SS5.

A total of 270 significantly enriched (non-integrin) receptor-ligand interactions (FDR-corrected p<0.05) were identified between epithelial and stromal subsets in decidualizing assembloids (***Figure 4—source data 1***), a representative selection of which are shown in ***Figure 4B***. Within the multitude of predicted complex interactions, three broad categories can be discerned. First, there are non-selective interactions involving ligands produced by all subpopulations in one compartment acting on receptors expressed by all subsets in the other compartment. Second, there are semi-selective stromal-epithelial interactions involving three or four subpopulations across both compartments. For example, binding of WNT5A secreted by all decidual stromal subsets to FZD3 (frizzled class receptor 3) expressed on all EpCs represents a non-selective receptor-ligand interaction, whereas binding of WNT5A or WNT4 to FZD6 is a predicted semi-selective interaction, involving all stromal subsets (SS3-5) and EpS4 but not EpS5 (***Figure 4B***). While FZD3 activates the canonical β-catenin pathway, FZD6 functions as a negative regulator of this signalling cascade (***Corda and Sala, 2017***). Finally, we identified only three highly selective receptor-ligand interactions (***Figure 4B***), two of which involved secretion of decidual ligands, prolactin (PRL) and C-X-C motif chemokine ligand 12 (CXCL12), acting on their cognate receptors expressed on receptive EpC (EpS4). CXCL12-dependent activation of C-X-C motif chemokine receptor 4 (CXCR4) has been shown to promote motility of EpC (***Zheng et al., 2020***), whereas PRL is a lactogenic hormone that stimulates glandular secretion in early pregnancy (***Burton et al., 2020***).

In contrast to stromal-epithelial communication, non-selective interactions are predicted to be rare between decidual subsets. Instead, communication appears governed largely by a combinatorial network of receptor-ligand interactions (***Figure 4C***). For example, colony stimulating factor 3 (CSF3) and vascular endothelial growth factor A (VEGFA) produced by senescent decidual cells (SS5) are predicted to impact selectively on pre-decidual cells (SS3), whereas secretion of inhibin A (INHBA) may engage both pre-decidual and decidual cells (SS4). Other interactions are predicted to govern crosstalk between SS3 and SS4, such as modulation of the WNT pathway in response to binding of R-spondin 3 (RSPO3) to leucine-rich repeat-containing G protein-coupled receptor 4 (LGR4). A striking observation is the overrepresentation of receptor tyrosine kinases implicated in SS3 and SS5 signal transduction as well as the involvement of receptors that signal through downstream cytoplasmic tyrosine kinases, including CSF3 receptor (CSF3R) and CD44 (***Figure 4C***; ***Corey et al., 1998***; ***van der Voort et al., 1999***).

Tyrosine kinase-dependent stress responses determine the fate of decidual cells

The CellPhoneDB analysis inferred that epithelial-stromal crosstalk in assembloids is robust, buffered by numerous non-selective interactions, whereas decidual subsets are reliant on selective receptor-ligand interactions and activation of distinct signal transduction pathways. For example, the predicted tyrosine kinase dependency of pre-decidual (SS3) and senescent decidual cells (SS5) raised the possibility that these subpopulations can be targeted by tyrosine kinase inhibitors, such as dasatinib (***Brighton et al., 2017***; ***Zhu et al., 2015***), a second-generation, broad-spectrum ATP-competitive protein tyrosine kinase inhibitor (***Aguilera and Tsimberidou, 2009***; ***Li et al., 2010***). To test this supposition, we generated single-cell transcriptomic profiles of assembloids decidualized for 4 days in the presence of dasatinib (***Figure 5A***). We found that decidualization in the presence of dasatinib had a dramatic impact on stromal subpopulations, virtually eliminating senescent decidual cells (SS5, n = 7) and increasing the abundance of decidual cells ninefold (SS4, n = 882; ***Figure 5B***). Apart from a modest reduction in pre-decidual cells (SS3), dasatinib also impacted markedly on transitional cells, reducing their numbers by 76% . By contrast, the effect on epithelial populations was confined to a modest reduction in senescent EpC (EpS5) (***Figure 5B***). Further, relatively few genes were perturbed significantly (FDR-corrected p<0.05) upon dasatinib treatment in epithelial populations (***Figure 5C***). In the stroma, dasatinib triggered a conspicuous transcriptional response in pre-decidual (SS3) and transitional cells, whereas gene expression in decidual cells (SS4) and the few remaining senescent decidual cells (SS5) was largely unaffected (***Figure 5C***). In transitional cells, dasatinib simultaneously upregulated genes encoding canonical mesenchymal markers (e.g. *SNAI2*, *TWIST2*, *ZEB1*, *COL1A1*, and *FBN1*; ***Owusu-Akyaw et al., 2019***) and decidual factors (e.g. *SCARA5*, *FOXO1*, *GADD45A*, *IL15*, *CXCL14*, and *SGK1*; ***Gellersen and Brosens, 2014***), suggesting that MET accounts for the emergence of this population upon decidualization (***Figure 5—source data 1***). In pre-decidual cells,

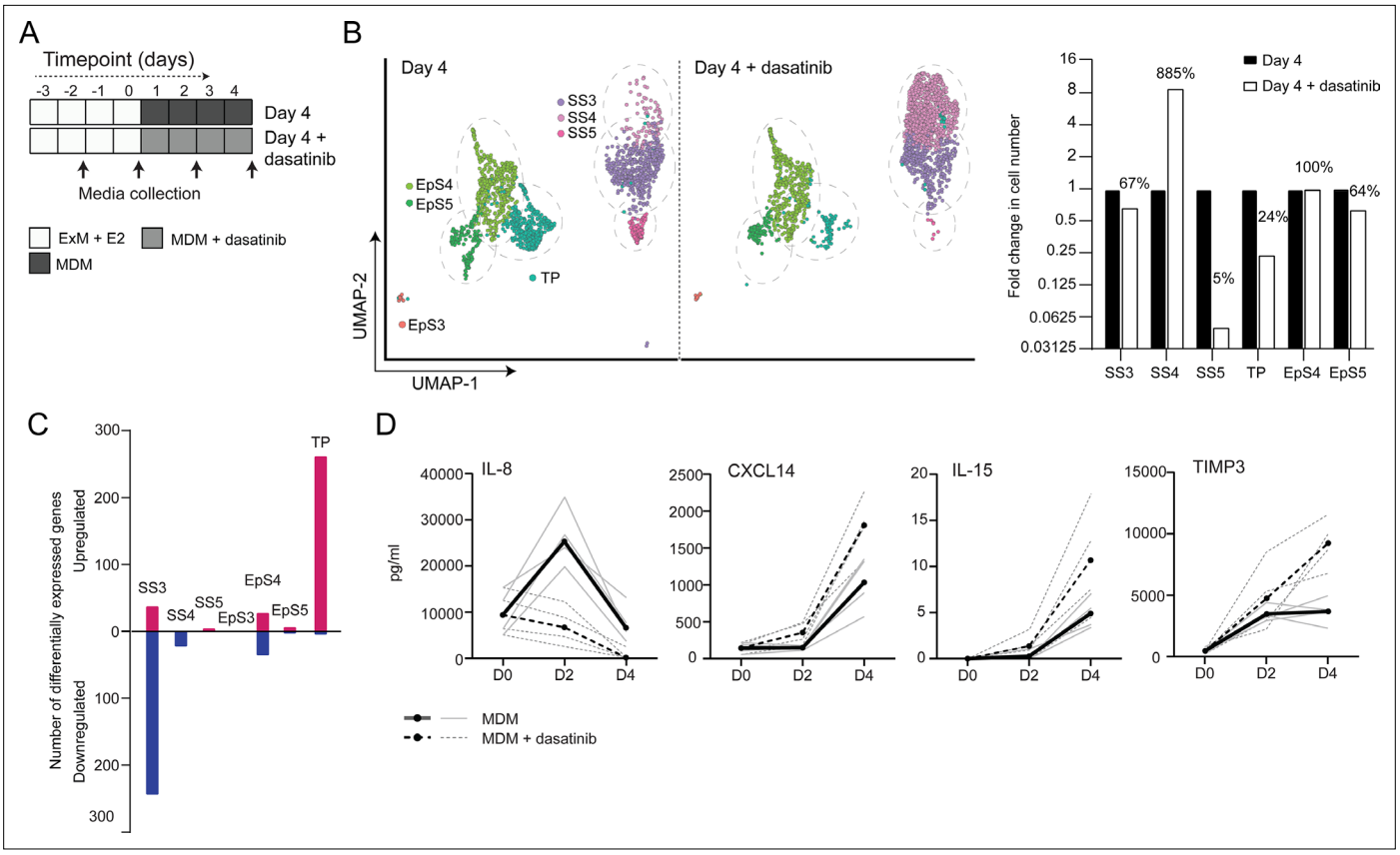

Figure 5. Tyrosine kinase-dependent stress responses determine the fate of decidual cells. (**A**) Schematic overview of experimental design. ExM: expansion medium; MDM: minimal differentiation medium. (**B**) Uniform Manifold Approximation and Projection (UMAP) visualization (left panel) and relative proportions (right panel) of subpopulations in endometrial assembloid decidualized in the presence or absence of dasatinib. (**C**) Number of differentially expressed genes (DEGs) in each subpopulation in response to dasatinib pre-treatment. (**D**) Secreted levels of CXCL8 and decidual cell factors in spent medium from assembloids treated with or without dasatinib. Secreted levels in individual assembloids established from four different endometrial assembloids decidualized with or without dasatinib are shown by dotted and solid lines, respectively. Full lists of DEGs and associated GO analysis can be found in ***Figure 5—source data 1*** and ***Figure 5—source data 2***, respectively. Data used in (**D**) are available in ***Figure 5—source data 3***.

The online version of this article includes the following figure supplement(s) for figure 5:

Source data 1. Differentially expressed genes for day 4 populations treated with and without dasatinib.

Source data 2. GO analysis for day 4 populations treated with and without dasatinib.

Source data 3. ELISA data.

dasatinib inhibited the expression of a network of genes enriched in GO categories such as 'Response to wounding' (FDR-corrected $p=3.5 \times 10^{-5}$), 'Response to stress' (FDR-corrected $p=3.8 \times 10^{-5}$), and 'Response to oxidative stress' (FDR-corrected $p=1.3 \times 10^{-4}$), indicative of a blunted stress response. To substantiate this finding, we measured the secreted levels of CXCL8 (IL-8), a potent inflammatory mediator implicated in autocrine/paracrine propagation of cellular senescence (***Acosta et al., 2008***; ***Kuilman et al., 2008***), in assembloids decidualized with or without dasatinib. CXCL14, IL-15, and TIMP3 levels were also measured to monitor the decidual response. As shown in ***Figure 5D***, dasatinib completely abrogated the release of CXCL8 by pre-decidual cells while markedly enhancing subsequent secretion of CXCL14, IL-15, and TIMP3, which are involved in effecting immune clearance of senescent decidual cells (***Brighton et al., 2017***; ***Lucas et al., 2020***; ***Kong et al., 2021***). Together, these observations not only support the CellPhoneDB predictions but also indicate that the amplitude of the cellular stress response during the pre-decidual phase determines the subsequent decidual trajectory, with low levels accelerating differentiation and high levels promoting cellular senescence and MET.

Modelling the impact of decidual subpopulations on human embryos

We postulated that decidual invasion by human embryos that have breached the luminal endometrial epithelium depends on an acute cellular senescence and transient SASP production, rich in growth factors and proteases. Conversely, we reasoned that lack of senescent decidual cells or unconstrained SASP should simulate pathological implantation environments associated with implantation failure and early pregnancy loss, respectively. To test this hypothesis, we constructed a simple implantation

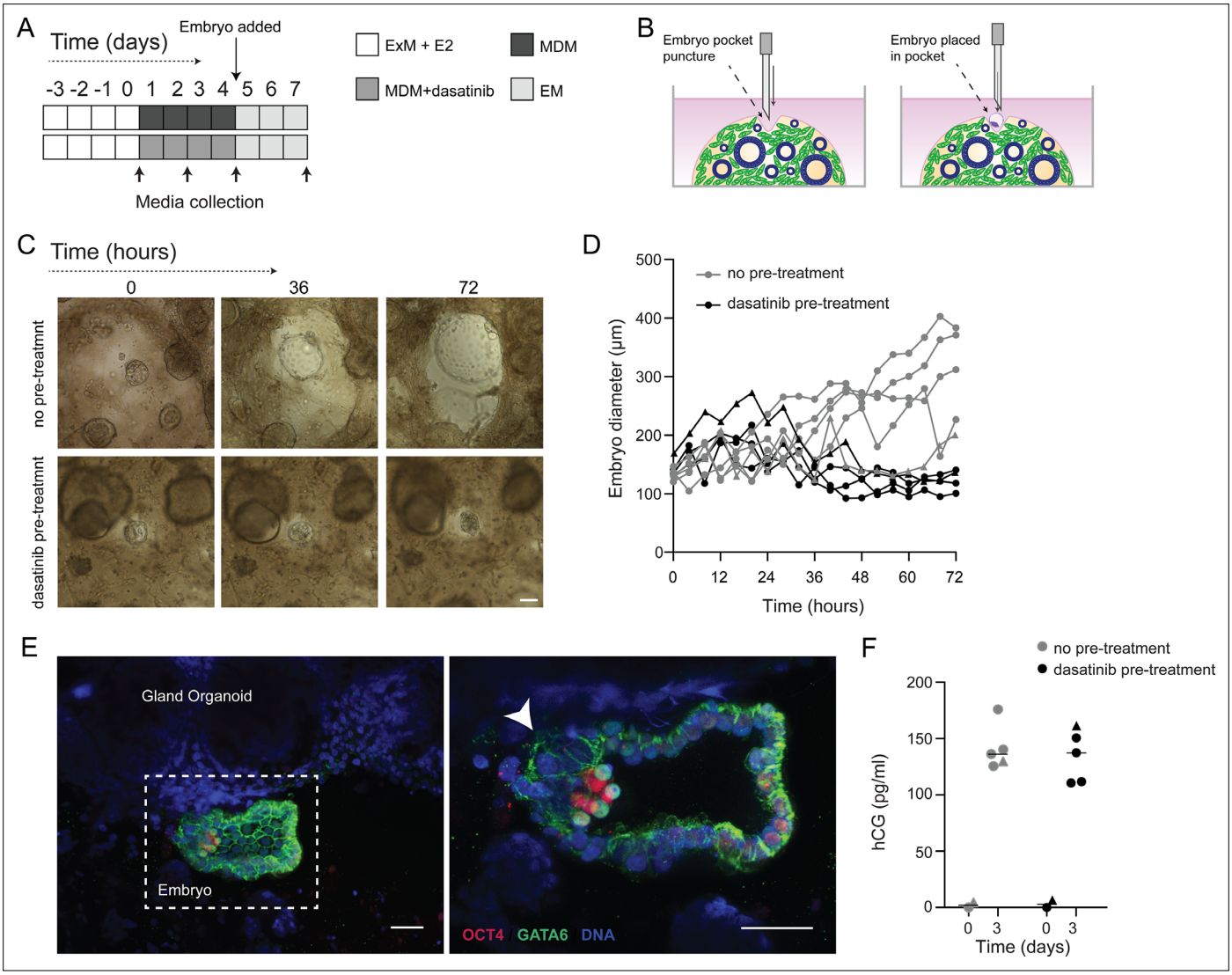

Figure 6. Impact of decidual senescence in assembloids on co-cultured human blastocysts. (**A**) Diagram showing experimental design. ExM: expansion medium; MDM: minimal differentiation medium; EM: embryo medium. (**B**) Schematic drawing of co-culture method. (**C**) Representative time-lapse images of blastocysts embedded in assembloids following decidualization for 96 hr in the absence (upper panels) or presence (lower panels) of dasatinib. Scale bar = 100 µm. See also ***Figure 6—figure supplement 1***. (**D**) Embryo diameters (µm) measured over 72 hr when embedded in decidualizing assembloids pre-treated with or without dasatinib. (**E**) OCT4 and GATA6 immunofluorescence marking the epiblast and hypoblast, respectively, in a blastocyst attached by proliferating polar trophectoderm (arrowhead) to decidual assembloids. Scale bar = 50 µM. (**F**) Secreted levels of human chorionic gonadotropin (hCG) in blastocyst-endometrial assembloid co-cultures. Individual embryo diameter measurements for biological replicates in (**D**) are available in ***Figure 6—source data 1***. Individual ELISA data used in (**F**) are available in ***Figure 6—source data 2***.

The online version of this article includes the following figure supplement(s) for figure 6:

Source data 1. Embryo expansion measurement.

Source data 2. Embryo human chorionic gonadotropin (hCG) secretion.

Figure supplement 1. Stromal migration towards the polar trophectoderm of expanding embryos in differentiated endometrial assembloids.

Figure supplement 2. Dasatinib prevents disintegration of decidualizing assembloids.

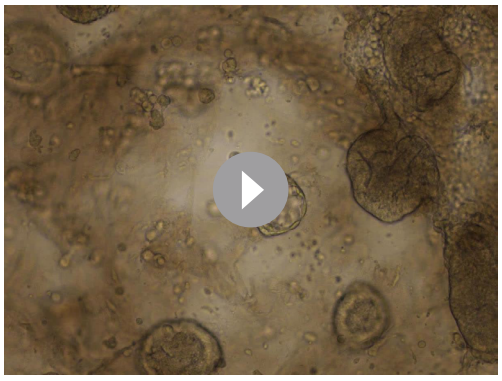

Video 1. Time-lapse microscopy of a human blastocyst embedded in a decidualizing assembloid. Representative video of a human blastocyst embedded in an assembloid, as imaged by time-lapse microscopy over 72 hr with images captured every 60 min.
https://elifesciences.org/articles/69603/figures#video1

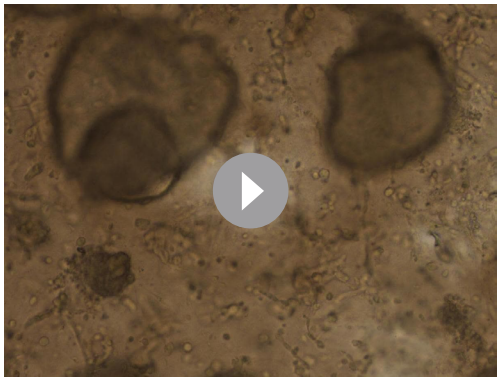

Video 2. Time-lapse microscopy of a human blastocyst embedded in a decidualizing assembloid pre-treated with dasatinib. Representative video of a human blastocyst embedded in an assembloid which had been pre-treated with dasatinib, as imaged by time-lapse microscopy over 72 hr with images captured every 60 min.
https://elifesciences.org/articles/69603/figures#video2

model by embedding human embryos in endometrial assembloids. To this end, assembloids were first decidualized for 96 hr in the presence or absence of dasatinib, washed and cultured in embryo medium, consisting of MDM with added supplements (***Figure 6A*** and ***Supplementary file 1***: Table 1). Day 5 human blastocysts were placed into small pockets created in the decidualized assembloids (***Figure 6B***), one embryo per assembloid, and individual co-cultures imaged using time-lapse microscopy over 72 hr. Co-cultured blastocysts (n = 5) expanded markedly when placed in decidualized assembloids that were not pre-treated with dasatinib (***Figure 6C and D***). Time-lapse microscopy revealed intense cellular movement in the stromal compartment as well as evidence that interaction between migratory decidual cells and polar trophectoderm promotes adherence and early invasion of the embryo (SI ***Video 1*** and ***Figure 6—figure supplement 1***). Retrieval and processing of one attached embryo demonstrated proliferating polar trophectoderm and expression of OCT4 and GATA6 in the epiblast and hypoblast, respectively (***Figure 6E***). A major limitation of this implantation model is that persistence of senescent decidual cells also causes gradual disintegration of the assembloids (***Figure 6—figure supplement 2***). By contrast, pre-treatment with dasatinib, which accelerates decidualization and all but eliminates decidual senescence, resulted in much more robust assembloids. However, all embedded blastocysts (n = 5) failed to expand in this model (***Figure 6C and D***). Further, movement of the decidual matrix was greatly reduced and directed migration or attachment of decidual cells to the blastocyst was not observed (SI ***Video 2***). Secreted levels of human chorionic gonadotropin (hCG) did not differ between co-cultures (***Figure 6E***), suggesting that all embryos remained viable over the 72 hr observation period. Thus, while our experimental design precluded modelling of physiological embryo implantation, aspects of different pathological endometrial states underlying reproductive failure, that is, implantation failure and miscarriage, were recapitulated in assembloids.

Discussion

Here we report on the development of endometrial assembloids, consisting of gland-like organoids surrounded by a matrix rich in primary EnSC, as novel model to parse the cellular dynamics that govern embryo implantation in cycling human endometrium. While assembloids complement and advance other recently described endometrial organoid models (***Boretto et al., 2017***; ***Cheung et al., 2021***; ***Fitzgerald et al., 2019***; ***Luddi et al., 2020***; ***Turco et al., 2017***), they still lack the cellular complexity of native endometrium, including uNK cells, macrophages, and vascular cells. Nevertheless, we demonstrated that aspects of pathological implantation events can be recapitulated in assembloids, rendering them useful as novel models to study mechanisms of reproductive failure and evaluate potential therapeutic interventions.

Single-cell analysis of differentiating endometrial assembloids indicates that the sequence of events leading up to the implantation window, and beyond, requires divergence of both glandular EpC and EnSC into differentiated and senescent subpopulations, a process likely determined by the level of replication stress incurred by individual cells in the preceding proliferative phase (**Brighton et al., 2017**). Importantly, we demonstrate that acute senescence in glandular EpC (EpS5) underpins production of an implantation-specific SASP, comprising canonical implantation factors and growth factors, such as amphiregulin (*AREG*) and epiregulin (*EREG*), implicated in transforming cytotrophoblasts into extravillous trophoblasts (**Cui et al., 2020**; **Yu et al., 2019**). On the other hand, the transcriptome profile of differentiated EpC (EpS4) revealed a pivotal role for this subpopulation in prostaglandin and glycodelin synthesis. Prostaglandins, and specifically PGE2, are indispensable for implantation (**Ruan et al., 2012**), whereas glycodelin is an abundantly secreted, multifaceted glycoprotein involved in blastocyst attachment, trophoblast differentiation, and immune modulation in early pregnancy (**Lee et al., 2016**). Further, differentiated EpC highly express *SLC2A1*, encoding the major glucose transporter GLUT1. Glucose is required for glycogen synthesis, an essential component of glandular secretions that nourishes the conceptus prior to the onset of placental perfusion around 10 weeks of pregnancy (**Burton et al., 2020**). The fate and function of senescent EpC in pregnancy are unknown. Arguably, localized secretion of proteinases by senescent EpC may promote breakdown of the surrounding basement membrane, thereby facilitating endoglandular trophoblast invasion and access to histotrophic nutrition in early gestation (**Huppertz, 2019**; **Moser et al., 2010**). In non-conception cycles, the abundance of $p16^{INK4}$-positive glandular EpC rises markedly during the late-luteal phase (**Brighton et al., 2017**), indicating that senescent EpC are progesterone-independent and likely responsible for glandular breakdown in the superficial endometrial layer at menstruation.

Decidual transformation of EnSC in assembloids unfolded largely as anticipated from previous studies, that is, starting with an acute pre-decidual stress response and leading to the emergence of both decidual and senescent decidual subpopulations (**Brighton et al., 2017**; **Lucas et al., 2020**; **Kong et al., 2021**). Like their epithelial counterparts, senescent decidual cells have a conspicuous secretory phenotype. We identified 56 and 72 genes encoding secreted factors upregulated in senescent epithelial and decidual subpopulations, respectively. However, only 15 genes were shared, indicating that the SASP generated in both cellular compartments is distinct. As glandular secretions drain into the uterine cavity, the embryonic microenvironment is therefore predicted to change abruptly upon breaching of the luminal epithelium. Recent comparative metabolomics of apical and basolateral endometrial gland-like organoid secretomes also supports the prediction of an asymmetrical profile of glandular secretions in the pre- and post-implantation microenvironments (**Simintiras et al., 2021**).

Based on computational predictions of ligand-receptor interactions, we demonstrated that the decidual response in assembloids can be targeted pharmacologically with only modest impact on glandular function and, by extension, the preimplantation embryo milieu. Specifically, dasatinib, a tyrosine kinase inhibitor, was highly effective in blunting the pre-decidual stress response, leading to a dramatic expansion of anti-inflammatory decidual cells and near-total elimination of senescent decidual cells. Dasatinib also inhibited the emergence of TP and shifted the transcriptional profile of the remaining transitional cells towards a decidual phenotype. An analogous population of ambiguous cells expressing both epithelial and mesenchymal marker genes was recently identified in midluteal endometrium by scRNA-seq analysis (**Lucas et al., 2020**). Further, based on CellPhoneDB and GO analyses, transitional cells are predicted to be highly autonomous and involved in tissue regeneration, in line with experimental evidence that MET drives re-epithelization of the endometrium following menstruation and parturition (**Owusu-Akyaw et al., 2019**; **Patterson et al., 2013**). Thus, the level of endogenous cellular stress generated by the endometrium during the window of implantation calibrates the subsequent decidual trajectory, either promoting the formation of a robust decidual matrix or facilitating tissue breakdown and repair. Further, an in-built feature of both trajectories is self-enforcement as decidual cells recruit and activate uNK cells to eliminate their senescent counterparts (**Brighton et al., 2017**; **Lucas et al., 2020**; **Kong et al., 2021**), whereas senescent decidual cells induce secondary senescence in neighbouring decidual (**Brighton et al., 2017**; **Ozaki et al., 2017**) and, plausibly, uNK cells (**Rajagopalan and Long, 2012**).

Clinically, recurrent pregnancy loss, defined as multiple miscarriages, is associated with loss of endometrial clonogenicity (**Lucas et al., 2016**; **Diniz-da-Costa et al., 2021**), uNK cell deficiency and

excessive decidual senescence (**Lucas et al., 2020**; **Tewary et al., 2020**), and rapid conceptions (also referred to as 'superfertility') (**Dimitriadis et al., 2020**; **Ticconi et al., 2020**). Conversely, lack of a proliferative gene signature in midluteal endometrium and premature expression of decidual PRL have been linked to recurrent implantation failure (**Berkhout et al., 2020b**; **Koler et al., 2009**; **Koot et al., 2016**), a pathological condition defined by a failure to achieve a pregnancy following transfer of one or more high-quality embryos in multiple IVF cycles (**Polanski et al., 2014**). We reasoned that these aberrant implantation environments can be recapitulated in assembloids by manipulating the level of decidual senescence. In line with these predictions, the presence of senescent decidual cells created a permissive environment in which migratory decidual cells interacted with expanding blastocysts, although continuous SASP production also promoted breakdown of the assembloids. Conversely, in the absence of senescent decidual cells, non-expanding embryos became entrapped in a robust but stagnant decidual matrix. These observations are in keeping with previous studies demonstrating that implantation of human embryos depends critically on the invasive and migratory capacities of decidual cells (**Berkhout et al., 2020a**; **Gellersen et al., 2010**; **Grewal et al., 2008**; **Weimar et al., 2012**). Our co-culture experiments also highlighted the shortcomings of assembloids as an implantation model, including the lack of a surface epithelium to create distinct pre- and post-implantation microenvironments and the absence of key cellular constituents, such as innate immune cells.

In summary, parsing the mechanisms that control implantation has been hampered by the overwhelming complexity of factors involved in endometrial receptivity. Our single-cell analysis of decidualizing assembloids suggests that this complexity reflects the reliance of the human endometrium on rapid E2-dependent proliferation and replicative exhaustion to generate both differentiated and senescent epithelial and stromal subpopulations in response to the postovulatory rise in progesterone. We demonstrate that senescent cells in both cellular compartments produce distinct bioactive secretomes, which plausibly prime pre-implantation embryos for interaction with the luminal epithelium and then stimulate encapsulation by underlying decidual stromal cells. Based on our co-culture observations, we predict that a blunted pre-decidual stress response causes implantation failure because of a lack of senescence-induced tissue remodelling and accelerated decidualization. Conversely, a heightened stress response leading to excessive decidual senescence may render embryo implantation effortless, albeit in a decidual matrix destined for breakdown and repair. Finally, we demonstrated that pre-decidual stress responses can be modulated pharmacologically, highlighting the potential of endometrial assembloids as a versatile system to evaluate new or repurposed drugs aimed at preventing reproductive failure.

Materials and methods

Ethical approvals, endometrial samples, and human blastocysts

Endometrial biopsies were obtained from women attending the Implantation Research Clinic, University Hospitals Coventry and Warwickshire National Health Service Trust. Written informed consent was obtained in accordance with the Declaration of Helsinki 2000. The study was approved by the NHS National Research Ethics Committee of Hammersmith and Queen Charlotte's Hospital NHS Trust (1997/5065) and Tommy's Reproductive Health Biobank (Project TSR19-002E, REC Reference: 18/WA/0356). Timed endometrial biopsies were obtained 6–11 days after the post-ovulatory LH surge using a Wallach Endocell Endometrial Cell Sampler. Patient demographics for the samples used in each experiment are detailed in **Supplementary file 1**: Table 2.

The use of vitrified human blastocysts was carried out under a Human Fertilisation and Embryology Authority research licence (HFEA: R0155) with local National Health Service Research Ethics Committee approval (04/Q2802/26). Spare blastocysts were donated to research following informed consent by couples who had completed their fertility treatment at the Centre for Reproductive Medicine, University Hospitals Coventry and Warwickshire National Health Service Trust. Briefly, women underwent ovarian stimulation and oocytes were collected by transvaginal ultrasound-guided aspiration and inseminated with prepared sperm (day 0). All oocytes examined 16–18 hr after insemination and classified as normally fertilized were incubated under oil in 20–25 µl drops of culture media (ORIGIO Sequential Cleav and Blast media, CooperSurgical, Denmark) at 5% O_2, 6% CO_2, 89% N_2 at 37 °C. Following culture to day 5 of development, the embryo(s) with the highest quality was selected for transfer, whereas surplus embryos considered top-quality blastocysts were cryopreserved

on day 5 or 6 by vitrification using Kitazato vitrification media (Dibimed, Spain) and stored in liquid nitrogen. Prior to their use in the co-culture, vitrified blastocysts were warmed using the Kitazato vitrification warming media (Dibimed, Spain) and underwent zona pellucida removal using a Saturn 5 Laser (CooperSurgical). Blastocysts were then incubated for 1 hr under oil in 20 µl drops of culture media (ORIGIO Sequential Blast media, CooperSurgical) at 5% O_2, 6% CO_2, 89% N_2 at 37 °C and allowed to re-expand.

Processing of endometrial biopsies and primary EnSC cultures

Unless otherwise stated, reagents were obtained from Life Technologies (Paisley, UK). Cell cultures were incubated at 37 °C, 5% CO_2 in a humidified incubator. Centrifugation and incubation steps were performed at room temperature unless stated otherwise. Fresh endometrial biopsies were processed as described previously (***Barros et al., 2016***). Briefly, tissue was finely minced for 5 min using a scalpel blade. Minced tissue was then digested enzymatically with 0.5 mg/ml collagenase I (Sigma-Aldrich, Gillingham, UK) and 0.1 mg/ml deoxyribonuclease (DNase) type I (Lorne Laboratories, Reading, UK) in 5 ml phenol red-free Dulbecco's Modified Eagle Medium (DMEM)/F12 for 1 hr at 37 °C, with regular vigorous shaking. Dissociated cells were washed with growth medium (DMEM/F12 containing 10% dextran-coated charcoal stripped FBS [DCC-FBS], 1% penicillin-streptomycin, 2 mM L-glutamine, 1 nM E2 [Sigma-Aldrich] and 2 mg/ml insulin [Sigma-Aldrich]). Samples were passed through a 40 µm cell sieve. EnSCs were collected from the flowthrough, while epithelial clumps remained in the sieve and were collected by backwashing into a 50 ml Falcon tube. Samples were resuspended in growth medium and centrifuged at 400× *g* for 5 min. EnSC pellets were resuspended in 10 ml growth medium and plated in tissue culture flasks. To isolate EnSC from other (non-adherent) cells collected in the flowthrough, medium was refreshed after 24 hr. Thereafter, medium was refreshed every 48 hr. Sub-confluent monolayers were passaged using 0.25% Trypsin-EDTA and split at a ratio of 1:3.

Endometrial gland-like organoid culture

Endometrial gland-like organoids were established as described previously (***Turco et al., 2017***), with adaptations. Freshly isolated endometrial gland fragments were resuspended in 500 µl phenol red-free DMEM/F12 medium in a microcentrifuge tube and centrifuged at 600× *g* for 5 min. The medium was aspirated and ice-cold, growth factor-reduced Matrigel (Corning Life Sciences B.V., Amsterdam, Netherlands) was added at a ratio of 1:20 (cell pellet: Matrigel). Samples mixed in Matrigel were kept on ice until plating at which point the suspension was aliquoted in 20 µl volumes to a 48-well plate, one drop per well, and allowed to cure for 15 min. Expansion medium supplemented with E2 (***Supplementary file 1***: Table 1; ***Turco et al., 2017***) was then added and samples cultured for up to 7 days. For passaging, Matrigel droplets containing gland-like organoids were collected into microcentrifuge tubes and centrifuged at 600× *g* for 6 min at 4 °C. Samples were resuspended in ice-cold, phenol red-free DMEM/F12 and subjected to manual pipetting to disrupt the organoids. Suspensions were centrifuged again, resuspended in ice-cold additive-free DMEM/F12, and then subjected to further manual pipetting. Suspensions were centrifuged again and either resuspended in Matrigel and plated as described above for continued expansion or used to establish assembloid cultures.

Establishment of assembloid cultures

At passage 2, EnSC and gland-like organoid pellets were mixed at a ratio of 1:1 (v/v) and ice-cold PureCol EZ Gel (Sigma-Aldrich) added at a ratio of 1:20 (cell pellet: hydrogel). Samples were kept on ice until plating. The suspension was aliquoted in 20 µl volumes using ice-cold pipette tips into a 48-well plate, one droplet per well, and allowed to cure in the cell culture incubator for 45 min. Expansion medium supplemented with 10 nM E2 was overlaid and the medium was refreshed every 48 hr. For decidualization experiments, assembloid cultures were grown in expansion medium supplemented with E2 for 4 days to allow for growth and expansion. Assembloids were then either harvested or decidualized using different media as tabulated in ***Supplementary file 1***: Table 1 for a further 4 days. Again, the medium was refreshed every 48 hr and spent medium stored for further analysis. For tyrosine kinase inhibition, MDM was supplemented with 250 nM dasatinib (Cell Signaling Technology, Leiden, NL).

Fluorescence microscopy

For fluorescent microscopy, assembloids were removed from culture wells and transferred into tubes for fixation. Samples were washed in PBS and fixed in 10% neutral buffered formalin in the tube for 15 min, then washed three times with PBS, and stored for use. Samples were dehydrated in increasing concentrations of ethanol (70% then 90% for 1 hr each, followed by 100% for 90 min), then incubated in xylene for 1 hr. After paraffin wax embedding, 5 µm sections were cut and mounted, then incubated overnight at 60 °C. Slides were then stored at 4 °C until further processing. De-paraffinization and rehydration were performed through xylene, 100% isopropanol, 70% isopropanol, and distilled water incubations. Following antigen retrieval, permeabilization was performed where appropriate by incubation with 0.1% Triton X-100 for 30 min. Slides were then washed, blocked, and incubated in primary antibodies overnight at 4 °C. Antibody details are presented in ***Supplementary file 1***: Table 3. After washing three times, slides were incubated with secondary antibodies for 2 hr, then washed as before and mounted in ProLong Gold Antifade Reagent with DAPI (Cell Signaling Technology). Slides were visualized using the EVOS Auto system, with imaging parameters maintained throughout image acquisition. Images were merged in ImageJ and any adjustments to brightness or contrast were applied equally within comparisons.

Real-time quantitative polymerase chain reaction

After removal of spent medium, gland-like organoid cultures were washed in PBS and harvested in 200 µl Cell Recovery Solution (Corning). Gel droplets were transferred to nuclease-free microcentrifuge tubes and placed at 4 °C for 30 min. Samples were then washed in PBS, centrifuged at 600× *g* for 6 min twice, and snap frozen as cell pellets. Assembloid cultures were washed with PBS and then recovered by directly scraping the samples into nuclease-free microcentrifuge tubes. Samples were centrifuged at 600× *g* for 6 min. The cellular pellet was resuspended in 500 µl of 500 µg/ml collagenase I diluted in additive-free DMEM/F12 and incubated at 37 °C for 10 min with regular manual shaking. Samples were washed twice in PBS, with centrifugation at 600× *g* for 6 min, then cell pellets were snap frozen. RNA extraction was performed using the RNeasy Micro Kit (QIAGEN, Manchester, UK) according to the manufacturer's instructions. RNA concentration and purity were determined using a NanoDrop ND-1000. All RNA samples were stored at –80 °C until use. Reverse transcription was performed using the QuantiTect Reverse Transcription (RT) Kit according to the manufacturer's protocol (QIAGEN). Input RNA was determined by the sample with lowest concentration within each experiment. Genes of interest were amplified using PrecisionPlus SYBR Green Mastermix (PrimerDesign, Southampton, UK). Amplification was performed in 10 µl reactions containing 5 µl PrecisionPlus 2× master mix, 300 nM each of forward and reverse primer, nuclease-free water, and 1 µl of cDNA or water control. Amplification was performed for 40 cycles on an Applied Biosystems QuantStudio 5 Real-Time PCR System (qPCR). Data were analysed using the Pffafl method (***Pfaffl, 2001***) and *L19* was used as a reference gene. Primer sequences were as follows: *L19* forward: 5′-GCG GAA GGG TAC AGC CAA T-3′, *L19* reverse: 5′-GCA GCC GGC GCA AA-3′, *PAEP* forward: 5′-GAG CAT GAT GTG CCA GTA CC-3′, *PAEP* reverse: 5′-CCT GAA AGC CCT GAT GAA TCC-3′, *SPP1* forward: 5′-TGC AGC CTT CTC AGC CAA A-3′, *SPP1* reverse: 5′-GGA GGC AAA AGC AAA TCA CTG-3′.

Enzyme-linked immunosorbent assay

Spent medium was collected every two days during a 4- day decidual time course, with or without dasatinib treatment. Duoset solid-phase sandwich enzyme-linked immunosorbent assay (ELISA) kits (Bio-Techne, Abingdon, UK) were used for the detection of PRL (DY682), TIMP3 (DY973), IL-8 (DY208), IL-15 (DY247), CXCL14 (DY866), and HCG (DY9034). Assays were performed according to the manufacturer's instructions. Absorbance at 450 nm was measured on a PheraStar microplate reader (BMG LABTECH Ltd, Aylesbury, UK), with background subtraction from absorbance measured at 540 nm. Protein concentration was obtained using a four-parameter logistic regression analysis and interpolation from the curve. As medium was collected at different timepoints in a time-course culture, secreted levels were not normalized to total cell or protein contents.

Single-cell capture, library preparation, and sequencing

Assembloids were dissociated to single cells by incubation of gel droplets with 0.5 mg/ml collagenase I for 10 min in a 37 °C water bath for 10 min with regular vigorous shaking. Samples were washed with

additive-free DMEM/F12 phenol-free medium and incubated with 5× TrypLE Select diluted in additive-free DMEM/F12 phenol-free medium for 5 min in a 37 °C water bath. Cell clumps were disrupted by manual pipetting, then suspended in 0.1% bovine serum albumin (BSA) in PBS and passed through a 35 µm cell sieve. Droplet generation was performed using a Nadia Instrument (Dolomite Bio, Cambridge, UK) according to the manufacturer's guidelines and using reagents as described by ***Macosko et al., 2015*** and the scRNAseq v1.8 protocol (Dolomite Bio). Pooled beads were processed as described previously (***Lucas et al., 2020***) and sequenced using a NextSeq 500 with high-output 75-cycle cartridge (Illumina, Cambridge, UK) by the University of Warwick Genomics Facility.

Bioinformatics analysis

Initial single-cell RNAseq data processing was performed using Drop-Seq_tools-2.3.0 (DropseqAlignmentCookbook_v2Sept2018, http://mccarrolllab.com/dropseq) and as described previously (***Lucas et al., 2020***). To select high-quality data for analysis, cells were included when at least 200 genes were detected, while genes were included if they were detected in at least three cells. Cells with more than 5000 genes were excluded from the analysis as were cells with more than 5% mitochondrial gene transcripts to minimize doublets and low quality (broken or damaged) cells, respectively. The Seurat v3 standard workflow (***Stuart et al., 2019***) was used to integrate datasets from biological replicates. Clustering and nearest-neighbour analysis was performed on the full integrated dataset using principal components 1:15 and a resolution of 0.6. The 'subset' function was applied for interrogation of specific experimental conditions and timepoints. Gene Ontology (GO) analysis was performed on differentially expressed genes from specified 'FindMarkers' comparisons in Seurat v3 using the Gene Ontology Consortium database (***Ashburner, 2000***; ***THE GENE ONTOLOGY, 2019***; ***THE GENE ONTOLOGY, 2019***; ***Mi et al., 2013***). Dot plots of significantly enriched GO terms (FDR-adjusted $p<0.05$) were generated in RStudio (version 1.2.5042). CellPhoneDB was used to predict enriched receptor-ligand interactions between subpopulations in decidualizing assembloids (***Efremova et al., 2020***; ***Vento-Tormo et al., 2018***). Significance was set at $p<0.05$. Annotated tyrosine kinase interactions were curated manually.

Co-culture of human blastocyst and endometrial assembloids

Prior to co-culture, decidualized assembloids were washed in PBS and medium was replaced with embryo medium (***Supplementary file 1***: Table 1). Assembloids were lightly punctured with a needle to create a small pocket, to enable one re-expanded day 5 human blastocyst to be co-cultured per assembloid. The plate was transferred to a pre-warmed and gassed (humidified 5% CO_2 in air) environment chamber placed on an automated X-Y stage (EVOS FL Auto Imaging System with onstage incubator) for time-lapse imaging. Brightfield images were captured every 60 min over 72 hr. Captured images were converted into videos using ImageJ.

For fixation, assembloid co-cultures were removed from culture wells and transferred into tubes. Samples were washed in PBS and fixed in 10% neutral buffered formalin in the tube for 15 min, then washed three times with PBS. Assembloids were permeabilized for 30 min in PBS containing 0.3% Triton X-100 and 0.1 M glycine for 30 min at room temperature. Samples were incubated overnight at 4 °C in primary antibodies diluted in PBS containing 10% FBS, 2% BSA, and 0.1% Tween-20. Samples were then washed in PBS (0.1% Tween-20) and incubated for 2 hr at room temperature protected from light in fluorescently conjugated Alexa Fluor secondary antibodies 1:500 (ThermoFisher Scientific) and DAPI (D3571, ThermoFisher Scientific, dilution 1/500), diluted in PBS containing 10% FBS, 2% BSA, and 0.1% Tween-20. Samples were imaged on a Leica SP8 confocal microscope using a ×25 water objective, with a 0.6 µm z-step and 2× line averaging.

Statistical analysis

Data were analysed using GraphPad Prism. Pairwise comparison of non-parametric data was performed using Mann–Whitney U test. For paired, non-parametric significance testing between multiple groups, the Friedman test, and Dunn's multiple comparisons *post hoc* test were performed. Only values of $p<0.05$ were considered statistically significant.

Acknowledgements

We are grateful to the women and couples who participated in this research. We are indebted to Dr. Siobhan Quenby and all the staff in the Centre for Reproductive Medicine and Biomedical

Research Unit, University Hospitals Coventry and Warwickshire National Health Service Trust, for facilitating sample collection. This work was supported by a Wellcome Trust Investigator Award to JJB (212233/Z/18/Z). TMR was supported by the MRC Doctoral Training Partnership (MR/N014294/1) and a fellowship from Warwick-Wellcome Trust Translational Partnership initiative.

Additional information

Funding

Funder	Grant reference number	Author
Wellcome Trust	212233/Z/18/Z	Jan Joris Brosens
MRC Doctoral Training Partnership	MR/N014294/1	Thomas M Rawlings
Warwick-Wellcome Trust Translational Partnership		Thomas M Rawlings

The funders had no role in study design, data collection and interpretation, or the decision to submit the work for publication.

Author contributions

Thomas M Rawlings, Formal analysis, Investigation, Methodology, Project administration, Visualization, Writing – original draft, Writing – review and editing; Komal Makwana, Formal analysis, Investigation, Writing – review and editing; Deborah M Taylor, Joshua Odendaal, Amelia Hawkes, Geraldine M Hartshorne, Resources, Writing – review and editing; Matteo A Molè, Katherine J Fishwick, Maria Tryfonos, Investigation, Writing – review and editing; Magdalena Zernicka-Goetz, Supervision, Writing – review and editing; Jan J Brosens, Conceptualization, Formal analysis, Funding acquisition, Project administration, Resources, Supervision, Visualization, Writing – original draft, Writing – review and editing; Emma S Lucas, Formal analysis, Investigation, Methodology, Project administration, Supervision, Visualization, Writing – original draft, Writing – review and editing

Author ORCIDs

Magdalena Zernicka-Goetz http://orcid.org/0000-0002-7004-2471
Jan J Brosens http://orcid.org/0000-0003-0116-9329
Emma S Lucas http://orcid.org/0000-0002-8571-8921

Ethics

Human subjects: Endometrial biopsies were obtained from women attending the Implantation Research Clinic, University Hospitals Coventry and Warwickshire National Health Service Trust. Written informed consent was obtained in accordance with the Declaration of Helsinki 2000. The study was approved by the NHS National Research Ethics Committee of Hammersmith and Queen Charlotte's Hospital NHS Trust (1997/5065) and Tommy's Reproductive Health Biobank (Project TSR19-002E, REC Reference: 18/WA/0356). The use of vitrified human blastocysts was carried out under a Human Fertilisation and Embryology Authority research licence (HFEA: R0155) with local National Health Service Research Ethics Committee approval (04/Q2802/26). Spare blastocysts were donated to research following informed consent by couples who had completed their fertility treatment at the Centre for Reproductive Medicine, University Hospitals Coventry and Warwickshire National Health Service Trust.

Decision letter and Author response

Decision letter https://doi.org/10.7554/eLife.69603.sa1
Author response https://doi.org/10.7554/eLife.69603.sa2

Additional files

Supplementary files

- Supplementary file 1. Supplementary tables 1-3.
Table 1. Culture media composition. Table 2. Patient demographics for endometrial samples. Table

3. Antibody details for immunofluorescence labelling.

- Transparent reporting form

Data availability

Single cell RNAseq data presented in this paper are openly available as a Gene Expression Omnibus DataSet (https://www.ncbi.nlm.nih.gov/gds) under accession number GSE168405. Other source data are presented in the Source Data tables as indicated in the corresponding Figure legends.

The following dataset was generated:

Author(s)	Year	Dataset title	Dataset URL	Database and Identifier
Brosens JJ, Lucas ES, Rawlings TM	2021	Single-cell RNA Sequencing of Endometrial Assembloid Cultures	https://www.ncbi.nlm.nih.gov/geo/query/acc.cgi?acc=GSE168405	NCBI Gene Expression Omnibus, GSE168405

The following previously published datasets were used:

Author(s)	Year	Dataset title	Dataset URL	Database and Identifier
Talbi S, Hamilton AE, Kc Vo, Tulac S, Overgaard MT, Dosiou C, Le Shay N, Le Shay N, Kimpson R, Lessey BA, Nayak NR, Giudice LC	2006	Molecular phenotyping of human endometrium	https://www.ncbi.nlm.nih.gov/geo/query/acc.cgi?acc=GSE4888	NCBI Gene Expression Omnibus, GSE4888

References

Abbas Y, Carnicer-Lombarte A, Gardner L, Thomas J, Brosens JJ, Moffett A, Sharkey AM, Franze K, Burton GJ, Oyen ML. 2019. Tissue stiffness at the human maternal-fetal interface. *Human Reproduction* **34**: 1999–2008. DOI: https://doi.org/10.1093/humrep/dez139, PMID: 31579915

Acosta JC, O'Loghlen A, Banito A, Guijarro MV, Augert A, Raguz S, Fumagalli M, Da Costa M, Brown C, Popov N, Takatsu Y, Melamed J, d'Adda di Fagagna F, Bernard D, Hernando E, Gil J. 2008. Chemokine signaling via the cxcr2 receptor reinforces senescence. *Cell* **133**: 1006–1018. DOI: https://doi.org/10.1016/j.cell.2008.03.038, PMID: 18555777

Aguilera DG, Tsimberidou AM. 2009. Dasatinib in chronic myeloid leukemia: A review. *Therapeutics and Clinical Risk Management* **5**: 281–289. DOI: https://doi.org/10.2147/tcrm.s3425, PMID: 19536317

Aplin JD, Charlton AK, Ayad S. 1988. An immunohistochemical study of human endometrial extracellular matrix during the menstrual cycle and first trimester of pregnancy. *Cell and Tissue Research* **253**: 231–240. DOI: https://doi.org/10.1007/BF00221758, PMID: 3416340

Aplin JD, Jones CJP. 1989. Extracellular matrix in endometrium and decidua. Klopper A, Beaconsfield R (Eds). *Placenta as a Model and a Source*. Springer. p. 23–25. DOI: https://doi.org/10.1007/978-1-4613-0823-2

Aplin JD, Myers JE, Timms K, Westwood M. 2020. Tracking placental development in health and disease. *Nature Reviews. Endocrinology* **16**: 479–494. DOI: https://doi.org/10.1038/s41574-020-0372-6, PMID: 32601352

Ashburner M. 2000. Gene ontology: Tool for the unification of biology. *The Gene Ontology Consortium. Nat Genet* **25**: 25–29. DOI: https://doi.org/10.1038/75556

Bagley B. 2019. Advanced Biomatrix. Collagen Gelation Kinetics and Shear Modulus. https://advancedbiomatrix.com/3d-collagen-hydrogel-stiffness.html

Barros FS, Brosens JJ, Brighton PJ. 2016. Isolation and primary culture of various cell types from whole human endometrial biopsies. *Bio-Protocol* **6**: e2028. DOI: https://doi.org/10.21769/BioProtoc.2028

Basisty N, Kale A, Jeon OH, Kuehnemann C, Payne T, Rao C, Holtz A, Shah S, Sharma V, Ferrucci L, Campisi J, Schilling B. 2020. A proteomic atlas of senescence-associated secretomes for aging biomarker development. *PLOS Biology* **18**: e3000599. DOI: https://doi.org/10.1371/journal.pbio.3000599, PMID: 31945054

Berkhout RP, Keijser R, Repping S, Lambalk CB, Afink GB, Mastenbroek S, Hamer G. 2020a. High-quality human preimplantation embryos stimulate endometrial stromal cell migration via secretion of microrna HSA-MIR-320A. *Human Reproduction* **35**: 1797–1807. DOI: https://doi.org/10.1093/humrep/deaa149, PMID: 32644109

Berkhout RP, Lambalk CB, Repping S, Hamer G, Mastenbroek S. 2020b. Premature expression of the decidualization marker prolactin is associated with repeated implantation failure. *Gynecological Endocrinology* **36**: 360–364. DOI: https://doi.org/10.1080/09513590.2019.1650344, PMID: 31389284

Bian Y, Gao G, Zhang Q, Qian H, Yu L, Yao N, Qian J, Liu B, Qian X. 2019. Kcnq1ot1/mir-217/zeb1 feedback loop facilitates cell migration and epithelial-mesenchymal transition in colorectal cancer. *Cancer Biology & Therapy* **20**: 886–896. DOI: https://doi.org/10.1080/15384047.2019.1579959, PMID: 30794031

Birch J, Gil J. 2020. Senescence and the SASP: Many therapeutic avenues. *Genes & Development* **34**: 1565–1576. DOI: https://doi.org/10.1101/gad.343129.120, PMID: 33262144

Boretto M, Cox B, Noben M, Hendriks N, Fassbender A, Roose H, Amant F, Timmerman D, Tomassetti C, Vanhie A, Meuleman C, Ferrante M, Vankelecom H. 2017. Development of organoids from mouse and human endometrium showing endometrial epithelium physiology and long-term expandability. *Development* **144**: 1775–1786. DOI: https://doi.org/10.1242/dev.148478, PMID: 28442471

Brighton PJ, Maruyama Y, Fishwick K, Vrljicak P, Tewary S, Fujihara R, Muter J, Lucas ES, Yamada T, Woods L, Lucciola R, Hou Lee Y, Takeda S, Ott S, Hemberger M, Quenby S, Brosens JJ. 2017. Clearance of senescent decidual cells by uterine natural killer cells in cycling human endometrium. *eLife* **6**: e31274. DOI: https://doi.org/10.7554/eLife.31274, PMID: 29227245

Brosens JJ, Hayashi N, White JO. 1999. Progesterone receptor regulates decidual prolactin expression in differentiating human endometrial stromal cells. *Endocrinology* **140**: 4809–4820. DOI: https://doi.org/10.1210/endo.140.10.7070, PMID: 10499541

Burton GJ, Cindrova-Davies T, Turco MY. 2020. Review: Histotrophic nutrition and the placental-endometrial dialogue during human early pregnancy. *Placenta* **102**: 21–26. DOI: https://doi.org/10.1016/j.placenta.2020.02.008, PMID: 33218574

Chavan AR, Griffith OW, Stadtmauer DJ, Maziarz J, Pavlicev M, Fishman R, Koren L, Romero R, Wagner GP. 2021. Evolution of embryo implantation was enabled by the origin of decidual stromal cells in eutherian mammals. *Molecular Biology and Evolution* **38**: 1060–1074. DOI: https://doi.org/10.1093/molbev/msaa274, PMID: 33185661

Chen Y, Li J, Xiao J-K, Xiao L, Xu B-W, Li C. 2021. The LNCRNA neat1 promotes the epithelial-mesenchymal transition and metastasis of osteosarcoma cells by sponging mir-483 to upregulate stat3 expression. *Cancer Cell International* **21**: 90. DOI: https://doi.org/10.1186/s12935-021-01780-8, PMID: 33546665

Cheung VC, Peng C-Y, Marinić M, Sakabe NJ, Aneas I, Lynch VJ, Ober C, Nobrega MA, Kessler JA. 2021. Pluripotent stem cell-derived endometrial stromal fibroblasts in a cyclic, hormone-responsive, coculture model of human decidua. *Cell Reports* **35**: : S2211-1247(21)00477-0. DOI: https://doi.org/10.1016/j.celrep.2021.109138, PMID: 34010658

Corda G, Sala A. 2017. Non-canonical WNT/PCP signalling in cancer: Fzd6 takes centre stage. *Oncogenesis* **6**: e364. DOI: https://doi.org/10.1038/oncsis.2017.69, PMID: 28737757

Corey SJ, Dombrosky-Ferlan PM, Zuo S, Krohn E, Donnenberg AD, Zorich P, Romero G, Takata M, Kurosaki T. 1998. Requirement of SRC kinase lyn for induction of DNA synthesis by granulocyte colony-stimulating factor. *The Journal of Biological Chemistry* **273**: 3230–3235. DOI: https://doi.org/10.1074/jbc.273.6.3230, PMID: 9452436

Cui X, Wang H, Li Y, Chen T, Liu S, Yan Q. 2020. Epiregulin promotes trophoblast epithelial-mesenchymal transition through pofut1 and o-fucosylation by pofut1 on UPA. *Cell Proliferation* **53**: e12745. DOI: https://doi.org/10.1111/cpr.12745, PMID: 31889361

Dallenbach-Hellweg G. 1981. *Histopathology of the Endometrium*. Springer. DOI: https://doi.org/10.1007/978-3-642-96638-5

Díaz-Gimeno P, Horcajadas JA, Martínez-Conejero JA, Esteban FJ, Alamá P, Pellicer A, Simón C. 2011. A genomic diagnostic tool for human endometrial receptivity based on the transcriptomic signature. *Fertility and Sterility* **95**: 50–60, . DOI: https://doi.org/10.1016/j.fertnstert.2010.04.063, PMID: 20619403

Dimitriadis E, Menkhorst E, Saito S, Kutteh WH, Brosens JJ. 2020. Recurrent pregnancy loss. *Nature Reviews. Disease Primers* **6**: 98. DOI: https://doi.org/10.1038/s41572-020-00228-z, PMID: 33303732

Diniz-da-Costa M, Kong CS, Fishwick KJ, Rawlings T, Brighton PJ, Hawkes A, Odendaal J, Quenby S, Ott S, Lucas ES, Vrljicak P, Brosens JJ. 2021. Characterization of highly proliferative decidual precursor cells during the window of implantation in human endometrium. *Stem Cells* **39**: 1067–1080. DOI: https://doi.org/10.1002/stem.3367, PMID: 33764639

Efremova M, Vento-Tormo M, Teichmann SA, Vento-Tormo R. 2020. Cellphonedb: Inferring cell-cell communication from combined expression of multi-subunit ligand-receptor complexes. *Nature Protocols* **15**: 1484–1506. DOI: https://doi.org/10.1038/s41596-020-0292-x, PMID: 32103204

Elzi DJ, Lai Y, Song M, Hakala K, Weintraub ST, Shiio Y. 2012. PLASMINOGEN activator inhibitor 1--insulin-like growth factor binding protein 3 Cascade regulates stress-induced senescence. *PNAS* **109**: 12052–12057. DOI: https://doi.org/10.1073/pnas.1120437109, PMID: 22778398

Erkenbrack EM, Maziarz JD, Griffith OW, Liang C, Chavan AR, Nnamani MC, Wagner GP. 2018. The mammalian decidual cell evolved from a cellular stress response. *PLOS Biology* **16**: e2005594. DOI: https://doi.org/10.1371/journal.pbio.2005594, PMID: 30142145

Ferenczy A, Bertrand G, Gelfand MM. 1979. Proliferation kinetics of human endometrium during the normal menstrual cycle. *American Journal of Obstetrics and Gynecology* **133**: 859–867. DOI: https://doi.org/10.1016/0002-9378(79)90302-8, PMID: 434029

Fitzgerald HC, Dhakal P, Behura SK, Schust DJ, Spencer TE. 2019. Self-renewing endometrial epithelial organoids of the human uterus. *PNAS* **116**: 23132–23142. DOI: https://doi.org/10.1073/pnas.1915389116, PMID: 31666317

Gellersen B, Reimann K, Samalecos A, Aupers S, Bamberger A-M. 2010. Invasiveness of human endometrial stromal cells is promoted by decidualization and by trophoblast-derived signals. *Human Reproduction* **25**: 862–873. DOI: https://doi.org/10.1093/humrep/dep468, PMID: 20118488

Gellersen B, Brosens JJ. 2014. Cyclic decidualization of the human endometrium in reproductive health and failure. *Endocrine Reviews* **35**: 851–905. DOI: https://doi.org/10.1210/er.2014-1045, PMID: 25141152

Grewal S, Carver JG, Ridley AJ, Mardon HJ. 2008. Implantation of the human embryo requires rac1-dependent endometrial stromal cell migration. *PNAS* **105**: 16189–16194. DOI: https://doi.org/10.1073/pnas.0806219105, PMID: 18838676

Haider S, Gamperl M, Burkard TR, Kunihs V, Kaindl U, Junttila S, Fiala C, Schmidt K, Mendjan S, Knöfler M, Latos PA. 2019. Estrogen signaling drives ciliogenesis in human endometrial organoids. *Endocrinology* **160**: 2282–2297. DOI: https://doi.org/10.1210/en.2019-00314, PMID: 31290979

Ho K-H, Chen P-H, Chou C-M, Shih C-M, Lee Y-T, Cheng C-H, Chen K-C. 2020. A key role of DNA damage-inducible Transcript 4 (ddit4) connects autophagy and glut3-mediated stemness to desensitize temozolomide efficacy in glioblastomas. *Neurotherapeutics* **17**: 1212–1227. DOI: https://doi.org/10.1007/s13311-019-00826-0, PMID: 31916238

Huppertz B. 2019. Traditional and New Routes of Trophoblast Invasion and Their Implications for Pregnancy Diseases. *International Journal of Molecular Sciences* **21**: E289. DOI: https://doi.org/10.3390/ijms21010289, PMID: 31906245

Iwahashi M, Muragaki Y, Ooshima A, Yamoto M, Nakano R. 1996. Alterations in distribution and composition of the extracellular matrix during decidualization of the human endometrium. *Journal of Reproduction and Fertility* **108**: 147–155. DOI: https://doi.org/10.1530/jrf.0.1080147, PMID: 8958841

Jabbour HN, Kelly RW, Fraser HM, Critchley HOD. 2006. Endocrine regulation of menstruation. *Endocrine Reviews* **27**: 17–46. DOI: https://doi.org/10.1210/er.2004-0021, PMID: 16160098

Kim KM, Noh JH, Bodogai M, Martindale JL, Yang X, Indig FE, Basu SK, Ohnuma K, Morimoto C, Johnson PF, Biragyn A, Abdelmohsen K, Gorospe M. 2017. Identification of senescent cell surface targetable protein DPP4. *Genes & Development* **31**: 1529–1534. DOI: https://doi.org/10.1101/gad.302570.117, PMID: 28877934

Koler M, Achache H, Tsafrir A, Smith Y, Revel A, Reich R. 2009. Disrupted gene pattern in patients with repeated in vitro fertilization (IVF) failure. *Human Reproduction* **24**: 2541–2548. DOI: https://doi.org/10.1093/humrep/dep193, PMID: 19542175

Kong C-S, Ordoñez AA, Turner S, Tremaine T, Muter J, Lucas ES, Salisbury E, Vassena R, Tiscornia G, Fouladi-Nashta AA, Hartshorne G, Brosens JJ, Brighton PJ. 2021. Embryo biosensing by uterine natural killer cells determines endometrial fate decisions at implantation. *FASEB Journal* **35**: e21336. DOI: https://doi.org/10.1096/fj.202002217R, PMID: 33749894

Koot YEM, van Hooff SR, Boomsma CM, van Leenen D, Groot Koerkamp MJA, Goddijn M, Eijkemans MJC, Fauser BCJM, Holstege FCP, Macklon NS. 2016. An endometrial gene expression signature accurately predicts recurrent implantation failure after IVF. *Scientific Reports* **6**: 19411. DOI: https://doi.org/10.1038/srep19411, PMID: 26797113

Kuilman T, Michaloglou C, Vredeveld LCW, Douma S, van Doorn R, Desmet CJ, Aarden LA, Mooi WJ, Peeper DS. 2008. Oncogene-induced senescence relayed by an interleukin-dependent inflammatory network. *Cell* **133**: 1019–1031. DOI: https://doi.org/10.1016/j.cell.2008.03.039, PMID: 18555778

Lee C-L, Lam KKW, Vijayan M, Koistinen H, Seppala M, Ng EHY, Yeung WSB, Chiu PCN. 2016. The pleiotropic effect of glycodelin-a in early pregnancy. *American Journal of Reproductive Immunology* **75**: 290–297. DOI: https://doi.org/10.1111/aji.12471, PMID: 26757357

Li J, Rix U, Fang B, Bai Y, Edwards A, Colinge J, Bennett KL, Gao J, Song L, Eschrich S, Superti-Furga G, Koomen J, Haura EB. 2010. A chemical and phosphoproteomic characterization of dasatinib action in lung cancer. *Nature Chemical Biology* **6**: 291–299. DOI: https://doi.org/10.1038/nchembio.332, PMID: 20190765

Lucas ES, Dyer NP, Murakami K, Lee YH, Chan Y-W, Grimaldi G, Muter J, Brighton PJ, Moore JD, Patel G, Chan JKY, Takeda S, Lam EW-F, Quenby S, Ott S, Brosens JJ. 2016. Loss of endometrial plasticity in recurrent pregnancy loss. *Stem Cells* **34**: 346–356. DOI: https://doi.org/10.1002/stem.2222, PMID: 26418742

Lucas ES, Vrljicak P, Muter J, Diniz-da-Costa MM, Brighton PJ, Kong CS, Lipecki J, Fishwick KJ, Odendaal J, Ewington LJ, Quenby S, Ott S, Brosens JJ. 2020. Recurrent pregnancy loss is associated with a pro-senescent decidual response during the peri-implantation window. *Communications Biology* **3**: 37. DOI: https://doi.org/10.1038/s42003-020-0763-1, PMID: 31965050

Luddi A, Pavone V, Semplici B, Governini L, Criscuoli M, Paccagnini E, Gentile M, Morgante G, Leo VD, Belmonte G, Zarovni N, Piomboni P. 2020. Organoids of human endometrium: A powerful in vitro model for the endometrium-embryo cross-talk at the implantation site. *Cells* **9**: E1121. DOI: https://doi.org/10.3390/cells9051121, PMID: 32366044

Macklon N. 2017. Recurrent implantation failure is a pathology with a specific transcriptomic signature. *Fertility and Sterility* **108**: 9–14. DOI: https://doi.org/10.1016/j.fertnstert.2017.05.028, PMID: 28602479

Macosko EZ, Basu A, Satija R, Nemesh J, Shekhar K, Goldman M, Tirosh I, Bialas AR, Kamitaki N, Martersteck EM, Trombetta JJ, Weitz DA, Sanes JR, Shalek AK, Regev A, McCarroll SA. 2015. Highly parallel genome-wide expression profiling of individual cells using nanoliter droplets. *Cell* **161**: 1202–1214. DOI: https://doi.org/10.1016/j.cell.2015.05.002, PMID: 26000488

Marinić M, Mika K, Chigurupati S, Lynch VJ. 2021. Evolutionary transcriptomics implicates HAND2 in the origins of implantation and regulation of gestation length. *eLife* **10**: e61257. DOI: https://doi.org/10.7554/eLife.61257, PMID: 33522483

Mi H, Muruganujan A, Casagrande JT, Thomas PD. 2013. Large-scale gene function analysis with the PANTHER classification system. *Nature Protocols* **8**: 1551–1566. DOI: https://doi.org/10.1038/nprot.2013.092, PMID: 23868073

Miller WP, Sunilkumar S, Giordano JF, Toro AL, Barber AJ, Dennis MD. 2020. The stress response protein redd1 promotes diabetes-induced oxidative stress in the retina by keap1-independent nrf2 degradation. *The Journal of Biological Chemistry* **295**: 7350–7361. DOI: https://doi.org/10.1074/jbc.RA120.013093, PMID: 32295843

Moser G, Gauster M, Orendi K, Glasner A, Theuerkauf R, Huppertz B. 2010. Endoglandular trophoblast, an alternative route of trophoblast invasion? Analysis with novel confrontation co-culture models. *Human Reproduction* **25**: 1127–1136. DOI: https://doi.org/10.1093/humrep/deq035, PMID: 20176592

Muñoz-Espín D, Serrano M. 2014. Cellular senescence: from physiology to pathology. *Nature Reviews. Molecular Cell Biology* **15**: 482–496. DOI: https://doi.org/10.1038/nrm3823, PMID: 24954210

Oefner CM, Sharkey A, Gardner L, Critchley H, Oyen M, Moffett A. 2015. Collagen type IV at the fetal-maternal interface. *Placenta* **36**: 59–68. DOI: https://doi.org/10.1016/j.placenta.2014.10.012, PMID: 25465704

Owusu-Akyaw A, Krishnamoorthy K, Goldsmith LT, Morelli SS. 2019. The role of mesenchymal-epithelial transition in endometrial function. *Human Reproduction Update* **25**: 114–133. DOI: https://doi.org/10.1093/humupd/dmy035, PMID: 30407544

Ozaki R, Kuroda K, Ikemoto Y, Ochiai A, Matsumoto A, Kumakiri J, Kitade M, Itakura A, Muter J, Brosens JJ, Takeda S. 2017. Reprogramming of the retinoic acid pathway in decidualizing human endometrial stromal cells. *PLOS ONE* **12**: e0173035. DOI: https://doi.org/10.1371/journal.pone.0173035, PMID: 28253328

Patterson AL, Zhang L, Arango NA, Teixeira J, Pru JK. 2013. Mesenchymal-to-epithelial transition contributes to endometrial regeneration following natural and artificial decidualization. *Stem Cells and Development* **22**: 964–974. DOI: https://doi.org/10.1089/scd.2012.0435, PMID: 23216285

Pfaffl MW. 2001. A new mathematical model for relative quantification in real-time RT-PCR. *Nucleic Acids Research* **29**: e45. DOI: https://doi.org/10.1093/nar/29.9.e45, PMID: 11328886

Polanski LT, Baumgarten MN, Quenby S, Brosens J, Campbell BK, Raine-Fenning NJ. 2014. What exactly do we mean by "recurrent implantation failure"? A systematic review and opinion. *Reproductive Biomedicine Online* **28**: 409–423. DOI: https://doi.org/10.1016/j.rbmo.2013.12.006, PMID: 24581986

Raine-Fenning NJ, Campbell BK, Clewes JS, Kendall NR, Johnson IR. 2004. Defining endometrial growth during the menstrual cycle with three-dimensional ultrasound. *BJOG* **111**: 944–949. DOI: https://doi.org/10.1111/j.1471-0528.2004.00214.x, PMID: 15327609

Rajagopalan S, Long EO. 2012. Cellular senescence induced by CD158D reprograms natural killer cells to promote vascular remodeling. *PNAS* **109**: 20596–20601. DOI: https://doi.org/10.1073/pnas.1208248109, PMID: 23184984

Rawlings TM. 2021. Organoids to model the endometrium: Implantation and beyond. Reproduction and Fertility.DOI: https://doi.org/10.1530/RAF-21-0023

Ruan YC, Guo JH, Liu X, Zhang R, Tsang LL, Dong JD, Chen H, Yu MK, Jiang X, Zhang XH, Fok KL, Chung YW, Huang H, Zhou WL, Chan HC. 2012. Activation of the epithelial Na+ channel triggers prostaglandin E_2 release and production required for embryo implantation. *Nature Medicine* **18**: 1112–1117. DOI: https://doi.org/10.1038/nm.2771, PMID: 22729284

Salker MS, Nautiyal J, Steel JH, Webster Z, Sućurović S, Nicou M, Singh Y, Lucas ES, Murakami K, Chan Y-W, James S, Abdallah Y, Christian M, Croy BA, Mulac-Jericevic B, Quenby S, Brosens JJ. 2012. Disordered il-33/st2 activation in decidualizing stromal cells prolongs uterine receptivity in women with recurrent pregnancy loss. *PLOS ONE* **7**: e52252. DOI: https://doi.org/10.1371/journal.pone.0052252, PMID: 23300625

Simintiras CA, Dhakal P, Ranjit C, Fitzgerald HC, Balboula AZ, Spencer TE. 2021. Capture and metabolomic analysis of the human endometrial epithelial organoid secretome. *PNAS* **118**: e2026804118. DOI: https://doi.org/10.1073/pnas.2026804118, PMID: 33876774

Stuart T, Butler A, Hoffman P, Hafemeister C, Papalexi E, Mauck WM, Hao Y, Stoeckius M, Smibert P, Satija R. 2019. Comprehensive integration of single-cell data. *Cell* **177**: 1888–1902. DOI: https://doi.org/10.1016/j.cell.2019.05.031, PMID: 31178118

Talbi S, Hamilton AE, Vo KC, Tulac S, Overgaard MT, Dosiou C, Le Shay N, Nezhat CN, Kempson R, Lessey BA, Nayak NR, Giudice LC. 2006. Molecular phenotyping of human endometrium distinguishes menstrual cycle phases and underlying biological processes in normo-ovulatory women. *Endocrinology* **147**: 1097–1121. DOI: https://doi.org/10.1210/en.2005-1076, PMID: 16306079

Tewary S, Lucas ES, Fujihara R, Kimani PK, Polanco A, Brighton PJ, Muter J, Fishwick KJ, Da Costa M, Ewington LJ, Lacey L, Takeda S, Brosens JJ, Quenby S. 2020. Impact of sitagliptin on endometrial mesenchymal stem-like progenitor cells: A randomised, double-blind placebo-controlled feasibility trial. *EBioMedicine* **51**: 102597. DOI: https://doi.org/10.1016/j.ebiom.2019.102597, PMID: 31928963

THE GENE ONTOLOGY. 2019. The Gene Ontology Resource: 20 years and still GOing strong. *Nucleic Acids Research* **47**: D330–D338. DOI: https://doi.org/10.1093/nar/gky1055, PMID: 30395331

Ticconi C, Pietropolli A, D'Ippolito S, Chiaramonte C, Piccione E, Scambia G, Di Simone N. 2020. Time-to-pregnancy in women with unexplained recurrent pregnancy loss: A controlled study. *Reproductive Sciences* **27**: 1121–1128. DOI: https://doi.org/10.1007/s43032-019-00122-4, PMID: 32046416

Turco MY, Gardner L, Hughes J, Cindrova-Davies T, Gomez MJ, Farrell L, Hollinshead M, Marsh SGE, Brosens JJ, Critchley HO, Simons BD, Hemberger M, Koo B-K, Moffett A, Burton GJ. 2017. Long-term, hormone-responsive organoid cultures of human endometrium in a chemically defined medium. *Nature Cell Biology* **19**: 568–577. DOI: https://doi.org/10.1038/ncb3516, PMID: 28394884

Uhlén M, Fagerberg L, Hallström BM, Lindskog C, Oksvold P, Mardinoglu A, Sivertsson Å, Kampf C, Sjöstedt E, Asplund A, Olsson I, Edlund K, Lundberg E, Navani S, Szigyarto CA-K, Odeberg J, Djureinovic D, Takanen JO, Hober S, Alm T, et al. 2015. Proteomics Tissue-based map of the human proteome. *Science* **347**: 1260419. DOI: https://doi.org/10.1126/science.1260419, PMID: 25613900

Van JM. 2014. The role of senescent cells in ageing. *Nature* **509**: 439–446. DOI: https://doi.org/10.1038/nature13193, PMID: 24848057

van der Voort R, Taher TE, Wielenga VJ, Spaargaren M, Prevo R, Smit L, David G, Hartmann G, Gherardi E, Pals ST. 1999. HepaRan sulfate-modified CD44 promotes hepatocyte growth factor/scatter factor-induced signal transduction through the receptor tyrosine kinase C-met. *The Journal of Biological Chemistry* **274**: 6499–6506. DOI: https://doi.org/10.1074/jbc.274.10.6499, PMID: 10037743

Vento-Tormo R, Efremova M, Botting RA, Turco MY, Vento-Tormo M, Meyer KB, Park J-E, Stephenson E, Polański K, Goncalves A, Gardner L, Holmqvist S, Henriksson J, Zou A, Sharkey AM, Millar B, Innes B, Wood L, Wilbrey-Clark A, Payne RP, et al. 2018. Single-cell reconstruction of the early maternal-fetal interface in humans. *Nature* **563**: 347–353. DOI: https://doi.org/10.1038/s41586-018-0698-6, PMID: 30429548

Weimar CHE, Kavelaars A, Brosens JJ, Gellersen B, de Vreeden-Elbertse JMT, Heijnen CJ, Macklon NS. 2012. Endometrial stromal cells of women with recurrent miscarriage fail to discriminate between high- and low-quality human embryos. *PLOS ONE* **7**: e41424. DOI: https://doi.org/10.1371/journal.pone.0041424, PMID: 22848492

Yu Y, Fang L, Wang S, Li Y, Guo Y, Sun Y-P. 2019. Amphiregulin promotes trophoblast invasion and increases mmp9/timp1 ratio through ERK1/2 and AKT signal pathways. *Life Sciences* **236**: : 4. DOI: https://doi.org/10.1016/j.lfs.2019.116899, PMID: 31614145

Zheng J, Qu D, Wang C, Ding L, Zhou W. 2020. Involvement of cxcl12/cxcr4 in the motility of human first-trimester endometrial epithelial cells through an autocrine mechanism by activating PI3K/AKT signaling. *BMC Pregnancy and Childbirth* **20**: 87. DOI: https://doi.org/10.1186/s12884-020-2788-3, PMID: 32041571

Zhou Q, Yan G, Ding L, Liu J, Yu X, Kong S, Zhang M, Wang Z, Liu Y, Jiang Y, Kong N, Sun J, Sun H. 2019. EHD1 impairs decidualization by regulating the Wnt4/β-catenin signaling pathway in recurrent implantation failure. *EBioMedicine* **50**: 343–354. DOI: https://doi.org/10.1016/j.ebiom.2019.10.018, PMID: 31707150

Zhu Y, Tchkonia T, Pirtskhalava T, Gower AC, Ding H, Giorgadze N, Palmer AK, Ikeno Y, Hubbard GB, Lenburg M, O'Hara SP, LaRusso NF, Miller JD, Roos CM, Verzosa GC, LeBrasseur NK, Wren JD, Farr JN, Khosla S, Stout MB, et al. 2015. The Achilles' heel of senescent cells: from transcriptome to senolytic drugs. *Aging Cell* **14**: 644–658. DOI: https://doi.org/10.1111/acel.12344, PMID: 25754370

REVIEW

Organoids to model the endometrium: implantation and beyond

Thomas M Rawlings[1], Komal Makwana[1], Maria Tryfonos[1] and **Emma S Lucas[1,2]**

[1]Division of Biomedical Sciences, Warwick Medical School, University of Warwick, Coventry, UK
[2]Centre for Early Life, Warwick Medical School, University of Warwick, Coventry, UK

Correspondence should be addressed to E S Lucas: E.S.Lucas@warwick.ac.uk

Abstract

Despite advances in assisted reproductive techniques in the 4 decades since the first human birth after *in vitro* fertilisation, 1–2% of couples experience recurrent implantation failure, and some will never achieve a successful pregnancy even in the absence of a confirmed dysfunction. Furthermore, 1–2% of couples who do conceive, either naturally or with assistance, will experience recurrent early loss of karyotypically normal pregnancies. In both cases, embryo-endometrial interaction is a clear candidate for exploration. The impossibility of studying implantation processes within the human body has necessitated the use of animal models and cell culture approaches. Recent advances in 3-dimensional modelling techniques, namely the advent of organoids, present an exciting opportunity to elucidate the unanswerable within human reproduction. In this review, we will explore the ontogeny of implantation modelling and propose a roadmap to application and discovery.

Lay summary

A significant number of couples experience either recurrent implantation failure or recurrent pregnancy loss. Often, no underlying disorder can be identified. In both cases, the interaction of the embryo and maternal tissues is key. The lining of the womb, the endometrium, becomes receptive to embryo implantation during each menstrual cycle and provides a nourishing and supportive environment to support ongoing pregnancy. It is not possible to study early pregnancy directly, therefore, modelling embryo-endometrium interactions in the laboratory is essential if we wish to understand where this goes wrong. Advances in the lab have resulted in the development of organoids in culture: 3D cellular structures that represent the characteristics of a particular tissue or organ. We describe past and present models of the endometrium and propose a roadmap for future work with organoid models, from fundamental understanding of the endometrial function and implantation processes to the development of therapeutics to improve pregnancy outcomes and gynaecological health.

Key Words: ▶ embryo implantation ▶ endometrium ▶ organoid ▶ assembloid

Reproduction and Fertility (2021) **2** R85–R101

Introduction

Although reported success rates in assisted reproduction approach or even surpass natural conceptions, 1–2% of couples will experience recurrent implantation failure, defined as the absence of a positive pregnancy test after three transfers of high-quality embryos (Mascarenhas *et al.* 2021). Some will never achieve a successful pregnancy even in the absence of a confirmed dysfunction. Furthermore, 1–2% of couples who do conceive, either naturally or

https://raf.bioscientifica.com
https://doi.org/10.1530/RAF-21-0023

with assistance, will experience recurrent early loss of karyotypically normal pregnancies with no identifiable cause even after extensive clinical investigation (Bender Atik *et al.* 2018). In both cases, the loss of overtly 'normal' embryos suggests that defects of embryo-endometrial interaction might be a plausible explanation.

The purpose of any model system is to generate a physical, theoretical, or mathematical representation of a real phenomenon that is difficult or impractical to observe directly (Rogers 2012), a situation entirely descriptive of the study of human implantation. The ethical and practical impossibility of studying implantation processes within the human body has necessitated the use of animal models and cell culture approaches. These approaches have revealed considerable detail about the requirements for successful implantation but remain far from ideal. Recent advances in 3-dimensional (3D) modelling techniques, namely the advent of organoids, present an exciting opportunity to elucidate the unanswerable within human reproduction. In this review, we will explore the ontogeny of implantation modelling and propose a roadmap to application and discovery.

The endometrium and implantation

The mucosal lining of the uterus, the endometrium, is a complex tissue comprising luminal and glandular epithelium, as well as stromal, endothelial, and immune cells and provides a nourishing, immune-privileged environment to support successful embryo implantation (Gellersen & Brosens 2014). Formed of two distinct layers, the endometrium undergoes hormone-dependent cyclic renewal with proliferation, differentiation, shedding (menstruation), and regeneration of the upper functional layer in each cycle. Spontaneous, embryo-independent transformation of the tissue, termed decidualisation, occurs in the midluteal phase of each cycle facilitating the development of the decidua of pregnancy to support placentation and foetal development until parturition. Humans are one of only a handful of species in which spontaneous decidualisation has evolved. This is proposed to reflect the need for maternal control over the challenge posed by genetically diverse and mosaic embryos in species where deep haemochorial placentation requires complete maternal investment in the pregnancy (Gellersen & Brosens 2014).

Functional defects in the endometrium, and particularly in the decidualisation process, have been associated with a spectrum of reproductive disorders, ranging from implantation failure and miscarriages to major obstetrical syndromes such as preeclampsia, foetal growth restriction, and preterm birth (reviewed by Lucas *et al.* 2013). However, other than histological descriptions of embryo implantation in hysterectomy samples from the early and mid-20th century (Hertig *et al.* 1956), we know very little about the earliest stages of implantation of the human blastocyst and the pivotal interactions taking place between the midluteal endometrium and the embryo. *In vivo* studies of dynamic implantation processes have been dependent on the use of animal models, while the generation of *in vitro* systems has facilitated the study of human embryo development and endometrial physiology and pathology, albeit largely in isolation. The development of embryo-endometrium co-cultures that faithfully mimic *in vivo* processes will truly unlock the black box of human reproduction.

Modelling implantation

Animal models

In the absence of human *in vivo* studies, murine, ovine, and bovine models, among others, have contributed much to the study of endometrial biology and pregnancy. However, the extent to which animal models represent human physiology is limited due to marked interspecies differences in reproductive strategy, implantation, and placentation. These have been reviewed extensively elsewhere (Lee & DeMayo 2004, Carter 2007, 2020, Morrison *et al.* 2018).

Livestock models have been utilised to pioneer many techniques used in modern assisted reproductive technologies (ART) (reviewed by Morrison *et al.* 2018). Sheep and cattle have been used to model human pregnancy while also advancing their commercial productivity with similar goals to human ART: to improve conception and live birth rates and reduce the incidence of pregnancy loss. Considerable differences in maternal recognition of pregnancy, implantation timing, and placental morphology make direct inference to human implantation difficult, nonetheless, conserved mechanisms are present (Tinning *et al.* 2020). Notwithstanding the value of sheep to model human foetal development (Morrison *et al.* 2018), the utility of large domestic animals to model early human pregnancy is limited (Carter 2020). Mouse models have been used to explore all aspects of reproduction, including implantation and the establishment of pregnancy. The mouse has been a preferred model for researchers for a number of reasons including litter-bearing status, rapid conception and gestation, haemochorial placentation, and genetic tractability; all of which provide an abundance

https://raf.bioscientifica.com
https://doi.org/10.1530/RAF-21-0023

of material for study and the ability to target specific pathways of interest to determine the impact on fecundity and fertility (Carter 2020). However, progesterone receptor expression dynamics vary greatly between humans and mice (Teilmann *et al.* 2006), and decidualisation in mouse is dependent on an embryonic stimulus (Lopes *et al.* 2004) rather than a spontaneous cyclic process. Overall, despite the many advances in our understanding of early pregnancy from animal models, interspecies differences have hindered the translation of understanding to human embryo implantation research.

In vitro models

To circumvent interspecies variability at implantation, *in vitro* models have been developed using primary endometrial epithelial or stromal cell cultures as well as endometrium-derived cell lines. *In vitro* endometrial models aim to represent at least certain aspects of the human implantation environment while retaining levels of experimental control and manipulability (Fig. 1 and Table 1). In combination with a range of molecular techniques and other assays, these models present effective tools to close the knowledge gap regarding human embryo implantation and answer a diverse panel of questions.

Monolayer cultures

Two-dimensional (2D) cultures of endometrial stromal and epithelial cells have both been utilised to investigate implantation processes (Fig. 1). Since the first report using monolayer epithelial cells to describe interactions between the luminal epithelium and an implanting embryo (Lindenberg *et al.* 1985), many studies have used this approach to study early feto-maternal interactions (Weimar *et al.* 2013, Aplin & Ruane 2017). In response to embryonic signals, co-cultured epithelial cells upregulate expression of the receptivity genes CXC chemokine receptor type 1 (CXCR1), CXCR4, and CXCR5, and the chemokine interleukin (IL)-8 (Caballero-Campo *et al.* 2002, Dominguez *et al.* 2003), encoded by *CXCL8*, as well as epithelial cell surface molecules implicated in embryo implantation, such as mucin 1 (MUC1) (Simón *et al.* 1997, Meseguer *et al.* 2001) and osteopontin (OPN) (von Wolff *et al.* 2001, Erikson *et al.* 2009, Berneau *et al.* 2019) (Table 1). Co-culture of *in vitro* fertilised (IVF) embryos with an autologous epithelial monolayer prior to embryo transfer increased the frequency of high-quality blastocyst formation and implantation rates (Simón *et al.* 1999, Le Saint *et al.* 2019). However, a significant benefit of the co-culture to live birth rates remains to be confirmed (Le Saint *et al.* 2019). Trophoblast

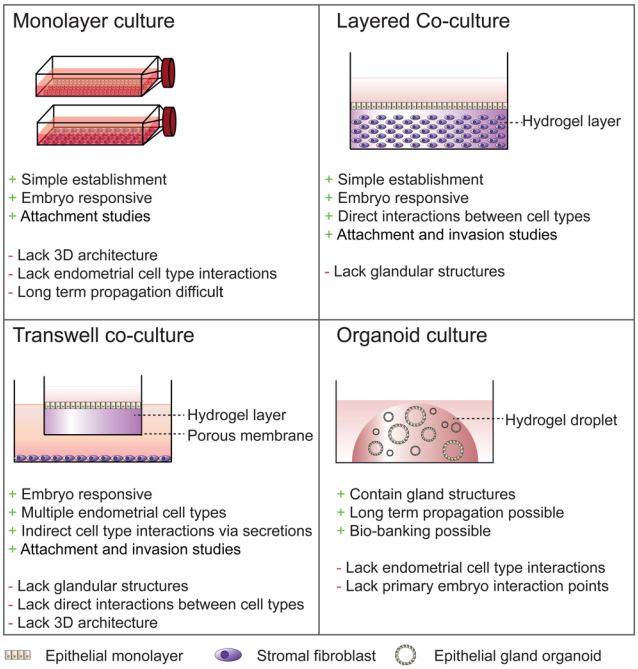

Figure 1 *In vitro* endometrial models to study implantation. Schematic representations of existing models for modelling endometrium-embryo interactions. The main benefits (+) and shortfalls (-) of each system are indicated.

spheroids, as a surrogate for human blastocysts, have also been used successfully in co-culture with epithelial monolayers to investigate embryo attachment to the luminal epithelium (Weimar *et al.* 2013, Lee *et al.* 2015, Huang *et al.* 2017, Evans *et al.* 2020, Ruane *et al.* 2020) (Table 1). These studies demonstrate the reciprocal relationship between luminal epithelium and preimplantation embryos in preparation for human implantation. However, endometrial epithelial cells are technically challenging to propagate as monolayers and cannot be cultured long-term (Varma *et al.* 1982, Fitzgerald *et al.* 2021). They also do not represent the normal physiology and architecture of glands *in vivo* (Gray *et al.* 2001).

Primary human endometrial stromal cells have been used extensively to study human decidualisation and the peri-implantation endometrial environment. Studies of primary stromal monolayers have demonstrated embryo-stroma interactions and the retention of patient phenotypes by these cells. Carver and colleagues (2003) co-cultured stromal cell monolayers with hatched day five human blastocysts for 3 days and demonstrated that blastocysts could attach to and invade a decidualised stromal monolayer but did not interact with undifferentiated cells. In midluteal endometrium, decidualising stromal cells transiently attain a myo-fibroblastic phenotype, in which they become

https://raf.bioscientifica.com
https://doi.org/10.1530/RAF-21-0023

Table 1 *In vitro* models to study human endometrium-embryo interaction.

Model format/cell types	Embryo/spheroid	Measures of interaction				References
		Embryo/spheroid	Stromal cells	Epithelial cells	Trophoblast	
Monolayer						
Primary human endometrial stromal cells	Hatched human blastocysts, high- and low-quality human embryos, human embryo-conditioned media, mouse blastocysts, human trophoblast spheroids, embryonic stem cell-derived trophoblast spheroids	Attachment (apposition and anchoring), trophoblast outgrowth and invasion, hCG secretion	Cell migration, secretion of implantation-associated cytokines, gene expression profiles, calcium signalling, 'biosensing' embryo quality			Carver *et al.* (2003), Grewal *et al.* (2008, 2010), Teklenburg *et al.* (2010), Weimar *et al.* (2012), Brosens *et al.* (2014), Lee *et al.* (2015), Berkhout *et al.* (2018)
Human endometrial stromal cell lines (T-HESC; hTERT-immortalised endometrial stromal cells)	Human trophoblast spheroids (AC-1M88, Sw.71)	*Attachment, expansion, outgrowth and invasion, CEACAM1 expression	Mmigration			Holmberg *et al.* (2012), Gellersen *et al.* (2013)
Primary human endometrial epithelial cells	Cleavage stage human embryos and blastocysts, human embryo-conditioned media, mouse blastocysts, human trophoblast spheroids (trophoblast stem cell-, embryonic stem cell-and/or choriocarcinoma -derived)	Blastocyst rate and quality, blastocyst adhesion, spheroid attachment and outgrowth		Gene expression and secretion of implantation-associated chemokines, chemokine receptor expression and localisation, gene expression profiles, morphological assessment		Lindenberg *et al.* (1985), Simón *et al.* (1997, 1999), Meseguer *et al.* (2001), Caballero-Campo *et al.* (2002), Dominguez *et al.* (2003), Lee *et al.* (2015), Le Saint *et al.* (2019), Evans *et al.* (2020).
Human endometrial epithelial cell lines (Ishikawa, RL95-2)	Hatched and unhatched human blastocysts, hatched mouse blastocysts, human trophoblast spheroids (trophoblast stem cell-, embryonic stem cell-and/or choriocarcinoma -derived)	Attachment and outgrowth/invasion		Gene expression profiles		Lee *et al.* (2015), Huang *et al.* (2017), Berneau *et al.* (2019), Evans *et al.* (2020), Ruane *et al.* (2020).
Layered culture						
Primary human endometrial epithelial and stromal cells	Expanded/hatching human blastocysts, trophoblast spheroids (choriocarcinoma, JAr)	Embryo attachment, trophoblast invasion and syncytium formation, spheroid attachment and outgrowth/invasion				Bentin-Ley *et al.* (2000), Wang *et al.* (2012)

https://raf.bioscientifica.com
https://doi.org/10.1530/RAF-21-0023

		*Attachment and outgrowth/invasion					
Human endometrial epithelial cell lines (RL95-2, HEC-1A, Ishikawa), immortalised and primary human endometrial stromal cells	Trophoblast spheroids (Jar choriocarcinoma)						Evron *et al.* (2011), Wang *et al.* (2012)
Transwell culture							
Primary human endometrial stromal cells and immortalised cell lines (St-T1b; T-HESC)	Trophoblast cells (AC-1M88)		Mmotility and invasion	Invasiveness			Gellersen *et al.* (2010, 2013)
Organoids							
Primary human endometrial epithelial cells	Embryo conditioned media				Pinopode development, glycodelin secretion profile.		Luddi *et al.* (2021)
Assembloid		†Expansion and attachment; EM cells: morphology and motility					
Primary human endometrial epithelial and stromal cells	Hatched human blastocysts						Rawlings *et al.* (2021)

*Spheroid; †Embryos.
EM cells, endometrial cells.

migratory and can produce extracellular matrix (ECM)-degrading matrix metallopeptidases (MMP) (Anacker *et al.* 2011), a process which is essential to allow trophoblast outgrowth (Grewal *et al.* 2008, 2010). Decidualised stromal cells are sensitive to embryo quality, selectively migrating towards high-quality human embryos but downregulating implantation-associated genes and the migratory phenotype in the presence of poor-quality or arresting embryos or conditioned media (Teklenburg *et al.* 2010, Weimar *et al.* 2012, Brosens *et al.* 2014, Berkhout *et al.* 2018) (Table 1).

Monolayer stromal co-cultures with blastocysts have also been used to investigate endometrial function and dysfunction in reproductive failure. Decidualising stromal cells of recurrent pregnancy loss (RPL) patients fail to inhibit implantation genes when co-cultured with poor-quality embryos (Weimar *et al.* 2012). This suggests a defect in embryo quality 'biosensing' in the endometrium of these women, manifesting as a loss of embryo selectivity. Also referred to as the 'selection failure hypothesis, this failure to prevent implantation of poor-quality embryos is predicted to lead to subsequent miscarriage (Aplin *et al.* 1996, Macklon & Brosens 2014).

Overall, monolayer endometrial cell models provide a simple and robust model for studying early embryo implantation and embryo-endometrial interactions in humans. A major disadvantage of monolayer models is the restriction to a single endometrial cell type, disregarding stromal-epithelial interactions within the *in vivo* environment, as well as the roles of resident immune and endothelial cell populations. Additionally, although these models have been utilised to study the initial attachment and invasion of embryos, they lack the 3D architecture essential to study trophoblast invasion and the foundations of placentation.

Layered co-cultures

Glandular development and differentiation are dependent on stromal secretions (reviewed by Fitzgerald *et al.* 2021), exemplifying the dependence of the peri-implantation endometrial environment on synchronous paracrine signals, cell–cell, and cell-matrix interactions between multiple cell types of the decidualising endometrium. To study these interactions, more complex co-culture models have been developed (Fig. 1 and Table 1) and these will be explored briefly here.

To establish 3D cultures, cells are seeded into or on top of a scaffold to mimic their spatial environment within the structure of the ECM. The most common scaffold is the hydrogel, a hydrophilic polymer chain network that can be easily fine-tuned to mimic the structural

https://raf.bioscientifica.com
https://doi.org/10.1530/RAF-21-0023

properties of a native tissue ECM. Layered co-cultures of endometrial epithelial cells grown over a stromal cell-containing collagen hydrogel resemble a simplified human endometrium and aim to replicate the complexity of the *in vivo* endometrium more closely (Bentin-Ley *et al.* 1994, Evron *et al.* 2011, Wang *et al.* 2012). Luminal epithelium polarisation and embryo attachment within 48 h were revealed in one such model by scanning electron microscopy, with apparent penetration of syncytiotrophoblast through the epithelium into the underlying stromal layer (Bentin-Ley *et al.* 2000). In place of embryos, trophoblast cell line spheroids, such as the JAr cell line (John *et al.* 1993), have also been utilised to study implantation in layered co-culture models (Evron *et al.* 2011, Wang *et al.* 2012). The attachment of trophoblast spheroids to epithelial cell lines was improved by co-culturing with stromal cells (Wang *et al.* 2012) and dependent on the receptivity status of the stromal cells (Evron *et al.* 2011). Occasional spontaneous gland-like structures were observed in these cultures (Wang *et al.* 2012) although layered models generally fail to form glandular structures reproducibly and thus while useful for studying very early implantation processes, are not truly representative of the tissue at implantation.

Transwell co-culture models enhanced the ability to study trophoblast invasion: using dual-chambered systems containing an extracellular matrix (Matrigel™)-coated porous filter insert, adherent trophoblast cells can invade the matrix and migrate through the filter (Aplin 2006, Lash *et al.* 2007) (Fig. 1). By seeding endometrial epithelial cells on top of the Matrigel™ in the transwell insert and culturing stromal cells in the well beneath the filter (Arnold *et al.* 2001, Pierro *et al.* 2001, Bläuer *et al.* 2005), the transwell approach provides an easily manipulatable assay to assess trophoblast invasion in the presence of endometrial cells. The presence of trophoblasts also improves the invasiveness of decidualised stromal cells in transwell systems (Gellersen *et al.* 2010, 2013). However, cell–cell contact between epithelial and stromal cells is not established in these models and so critical interactions to orchestrate trophoblast invasion and endometrial tissue remodelling are likely to be missing.

Clearly, layered and transwell co-culture approaches improve upon monolayer cultures by incorporating both stromal and epithelial cells into a 3D space, providing the architecture for a more physiological model to study implantation. However, these models conspicuously lack glandular structures, a functional unit of the endometrium essential for embryo implantation.

Modelling endometrial glands: the missing link?

Secretory transformation of endometrial glands results in the production of histotroph, or 'uterine milk'. Histotroph composition has been studied extensively during the menstrual cycle, consisting largely of glycogen and glycoproteins, as well as other components such as amino acids and lipid droplets (Burton *et al.* 2002). This rich secreted product provides nutrition for the embryo until the onset of placental perfusion (Burton *et al.* 2007, 2010). Studies using animal models, such as the uterine gland knockout sheep, produced by a progestin-induced gland knock out, demonstrate that without endometrial glands, embryo implantation is inhibited (Gray *et al.* 2001). Progestin uterine gland knockout mice also exhibit implantation failure, with reduced expression of key implantation genes (Kelleher *et al.* 2016).

Besides providing nutritional support to the implanting embryo, endometrial glands upregulate genes required for embryo receptivity and implantation, including numerous secreted factors essential for implantation (Fig. 2). For example, osteopontin (OPN), encoded by phosphoprotein 1 (*SPP1*), contains the integrin-binding motif RGD, a tripeptide of amino acids arginine, glycine, and aspartate, which facilitates embryo adhesion to the luminal epithelium (Singh & Aplin 2009, Berneau *et al.* 2019). Leukaemia inhibitory factor, encoded by *LIF*, is a protein related to blastocyst adhesion, as well as having roles in embryonic development and trophoblast differentiation (Salleh & Giribabu 2014). Glycodelin, a dimeric glycoprotein, encoded by progestogen-associated endometrial protein (*PAEP*), also participates in interactions between the implanting blastocyst and luminal epithelium. *In vitro*, induction of glycodelin secretion improves trophoblast spheroid attachment while silencing *PAEP* inhibits attachment (Uchida *et al.* 2007, So *et al.* 2012).

Human endometrial glands also secrete the growth factors EGF, vascular endothelial growth factor (VEGF), and transforming growth factor-beta (TGFB), the cognate receptors for which are expressed by the trophectoderm of the implanting blastocyst. EGF stimulates proliferation of cytotrophoblast and secretion of human chorionic gonadotropin (hCG) and human placental lactogen (hPL) by the syncytiotrophoblast (Ladines-Llave *et al.* 1991, Maruo *et al.* 1997) (Fig. 2). VEGF enhances the adhesion of the trophoblast to the luminal epithelium (Binder *et al.* 2014), while TGFB increases ECM remodelling, via the secretion of fibronectin, for example, thereby facilitating

https://raf.bioscientifica.com
https://doi.org/10.1530/RAF-21-0023

endometrial adhesion for invading trophoblasts (Feinberg *et al.* 1994).

Overall, the glands and their secretions are essential for implantation, and therefore, being able to model the glands *in vitro* is an essential step towards studying and understanding human embryo implantation and early pregnancy events. Recent development of glandular organoid models may have brought us closer than ever to establish a physiological model of the human endometrium.

Organoids of the reproductive system

'Organoid' describes 3D structures that resemble organs or tissues *ex vivo* in a supportive hydrogel droplet, such as Matrigel™, replacing the ECM of the originating tissue. Organoids arise from single cells or small clusters of cells with stem or progenitor properties in cultures with complex growth media designed to mimic organ- or tissue-specific signalling pathways and recapitulate the niche environment (Kim *et al.* 2020*b*). Organoids differ from previous *in vitro* model systems in that they spontaneously organise into architectures that resemble their corresponding *in vivo* tissue or organ in a culture plate. Additionally, organoid models functionally mimic their tissue of origin and can recapitulate developmental processes that take place *in vivo*, thus allowing the study of developing and differentiating cells in real time. Growth factor and inhibitor combinations in these complex media support proliferation and renewal as well as differentiation and substitute for the absence of the tissue complexity present *in vivo*. Most reported models employ a consistent core set of factors that are reviewed elsewhere (Kretzschmar & Clevers 2016, Alzamil *et al.* 2021). Organoids have been generated from the vast majority of endoderm-derived tissues including the colon (Sato *et al.* 2011), intestine (Fujii *et al.* 2018), stomach (Bartfeld *et al.* 2015, Schlaermann *et al.* 2016), liver (Huch *et al.* 2015, Hu *et al.* 2018), pancreas (Loomans *et al.* 2018), lung/airway (Sachs *et al.* 2019) and bladder (Lee *et al.* 2018).

Several recent reports have demonstrated progress in modelling human reproductive epithelia using organoid systems. In the female reproductive system, endometrium (Boretto *et al.* 2017, Turco *et al.* 2017), fallopian tube (Kessler *et al.* 2015), cervix (Chumduri *et al.* 2021, Maru *et al.* 2020, Lohmussaar *et al.* 2021), and ovarian cancer (Kopper *et al.* 2019, Maenhoudt *et al.* 2020) models have been described (Fig. 3), as well as mammary gland (Linnemann *et al.* 2015). These models facilitate the study of the general biology and histology of the reproductive tissues since they recapitulate epithelial cell morphology, function, and cellular heterogeneity while being genetically stable. These organoids are hormone-responsive and can be differentiated under specific conditions (reviewed by Alzamil *et al.* 2021). In the male reproductive tract, organoid systems are described for both testis (Alves-Lopes *et al.* 2017, Baert *et al.* 2017, Pendergraft *et al.* 2017) and prostate (Chua *et al.* 2014, Karthaus *et al.* 2014). Trophoblast organoids to model placental development (Haider *et al.* 2018, Turco *et al.* 2018), as well as embryo-like organoids, known as blastoids have also been described (Zheng *et al.* 2019, Liu *et al.* 2021,

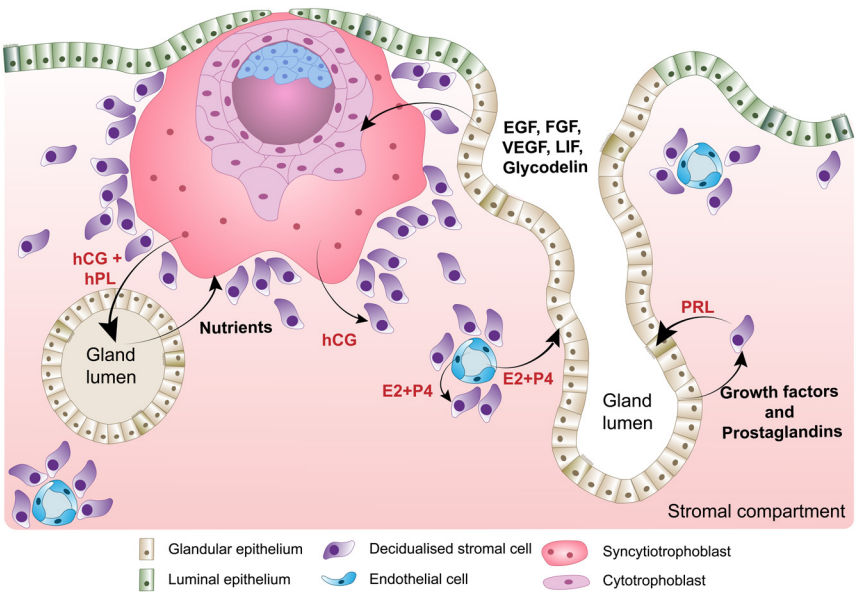

Figure 2 Embryo-endometrium crosstalk at implantation. Schematic representation of the crosstalk between endometrial glands, decidualised stromal cells, corpus luteum, and trophoblasts cells of the invading embryo. During pregnancy, the syncytiotrophoblast cells produce hCG to maintain the corpus luteum so progesterone can be continually produced. Progesterone is essential for the maintenance of the decidualised cell and differentiated glands. A key secretion of the decidual cells at implantation is PRL, which acts on the glands through PRLR to maintain the glandular secretory phenotype. Additionally, trophoblast cells act directly on the glands through hCG and hPL secretion, resulting in the production of growth factors, nutrients, and receptivity markers such as LIF and glycodelin. In turn, these factors improve trophoblast invasion, thus forming a positive feedback loop.

https://raf.bioscientifica.com
https://doi.org/10.1530/RAF-21-0023

Yu *et al.* 2021). Human blastoids recapitulate the key morphology of preimplantation blastocysts, including cell-lineage composition and allocation, with transcriptomic similarities but lack important structures like the zona pellucida (Liu *et al.* 2021, Yu *et al.* 2021). Blastoids and trophoblast organoids both offer the opportunity to study implantation and early developmental processes at a greater scale than possible with research embryos, and in cases where embryos are unavailable for research use or such applications are prohibited.

The emergence of these organoid models for human reproduction and fertility represents a huge leap forward for the field, presenting a considerable opportunity to advance our knowledge of many 'hidden' processes within these systems. Limitations remain, for example, ease of accessibility means comparisons with healthy tissue are limited in some cases, while optimisation of other models is still required.

Endometrial gland organoids

Organoid-like structures established from endometrial epithelial cells were first reported in 1988, derived from primary gland fragments seeded into Matrigel™ (Rinehart *et al.* 1988). Glandular structures were retained after tissue digest collapsed and monolayer colony outgrowth was observed within 7 to 10 days. Following several weeks of culture, these colonies formed large cystic organoid structures of polarised columnar epithelial cells with luminal microvilli and could be maintained in culture for at least 6 months. Endometrial gland organoids were also produced in Matrigel™ and grown in a transwell system, in co-culture with stromal cells grown in the lower chamber (Bläuer *et al.* 2005). In this system, the organoids were responsive to oestradiol treatment in the presence of the stromal cell layer. These reports failed to recapitulate the gland phenotype fully, and genetic stability was not confirmed, nor were the culture conditions chemically defined. Renewed interest in endometrial gland organoids was stimulated recently by parallel reports delivering a step-change in our ability to study the function of these structures (Boretto *et al.* 2017, Turco *et al.* 2017) (Fig. 3). The resulting organoids are genetically stable, have the clonogenic capacity, cellular heterogeneity, and can recapitulate molecular and histological similarities of the glands *in vivo* (Boretto *et al.* 2017, Turco *et al.* 2017, Fitzgerald *et al.* 2019). They can be derived from physiologically diverse endometrial tissues throughout the menstrual cycle, after menopause, and from decidual pregnancy samples (Turco *et al.* 2017). Like other organoid models,

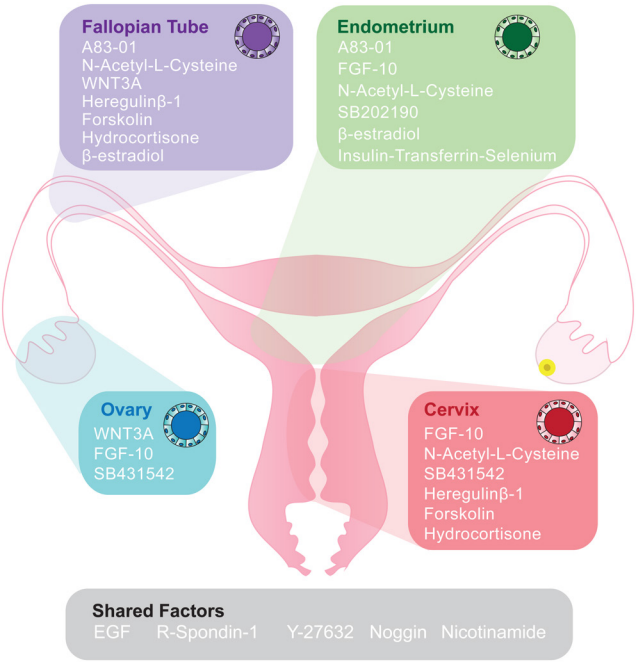

Figure 3 Organoid models of the female reproductive tract. In the human female reproductive tract, organoid models have been derived from the endometrium, fallopian tube, ovary, and cervix tissues and recapitulate the epithelial structure of the tissue of origin. All systems have been cultured in basal medium including Advanced DMEM/F12, B-27, and N-2 supplements, antibiotics, and L-Glutamine but also include a cocktail of growth factors and inhibitors to promote proliferation and maintain undifferentiated or progenitor cell-like conditions. Common to all models is the growth factor EGF and the WNT signalling activator R-Spondin-1, as well as the ROCK inhibitor Y-27632 and BMP pathway inhibitor Noggin, and Nicotinamide, a survival factor, and ROCK inhibitor. Other factors which are often added include the TGFB receptor inhibitor A83-01, the activin/ BMP/TGFB inhibitor, SB431542, and the p38 MAPK inhibitor SB202190; Growth factors FGF-10 (fibroblast growth factor) and WNT3A as well as other factors such as N-acetyl-L-cysteine (antioxidant), β-estradiol (mitogen), heregulin-β (growth factor), forskolin (adenylyl cyclase activator), and hydrocortisone (glucocorticoid).

endometrial gland organoids are cultured in Matrigel™ and are dependent on a chemically defined complex 'expansion medium' containing a variety of growth factors required to promote proliferation and inhibit differentiation, including fibroblast growth factor 10 (FGF10), EGF, Wingless and Int1 (WNT) signalling activator R-spondin 1 (RSPO1), bone morphogenetic protein (BMP) inhibitor Noggin, and the TGFβ antagonist, A83-01. Unlike the initial report (Rinehart *et al.* 1988), these recent models see rapid organoid formation from gland fragments within 7–10 days. Oestrogen treatment induces proliferation of the cells with an increase in Ki67+ cells (Boretto *et al.* 2017) as well as stimulating ciliogenesis (Haider *et al.* 2019) and, when combined with progesterone, secretion of glycodelin-A corresponds to tissue profiles in mid-secretory endometrium (Luddi *et al.* 2020). Glycodelin

https://raf.bioscientifica.com
https://doi.org/10.1530/RAF-21-0023

profiles were further modulated after incubation of organoids with embryo-conditioned medium (Luddi *et al.* 2021), confirming embryo-endometrial crosstalk is possible within the model (Table 1). Metabolomic analysis of the secretome of endometrial organoids also demonstrates unique characteristics of the apical (inter-organoid) and basolateral (extra-organoid) secretory profiles, characteristic of that predicted *in vivo* (Simintiras *et al.* 2021). Through exposure to pregnancy signals of the stroma (cyclic AMP and prolactin (PRL)) and trophoblast (hCG and hPL), the organoids acquired a decidual-like phenotype akin to early pregnancy (Turco *et al.* 2017).

Thus far, endometrial gland organoid models are still in their infancy, albeit one that surpasses prior systems physiologically. The opportunity to address questions of normal endometrial physiology and implantation processes, therefore, lies along our path.

Endometrial gland organoids and the future: a roadmap to utility

Endometrial gland organoids, assembloids, and modelling embryo implantation

Despite their structural and functional recapitulation of endometrial gland phenotypes, endometrial organoid models do not faithfully represent the midluteal endometrium, due to being grown in isolation without the influence of other endometrial cell types present in the tissue. Endometrial stromal cells are essential for glandular regeneration, expansion, and differentiation throughout the menstrual cycle. For example, through the secretion of PRL, decidualising stroma regulates gland differentiation via the PRL receptor (PRLR), whose expression peaks in the endometrial glands during the mid-secretory phase (Jones *et al.* 1998). PRL induces glandular differentiation by stimulating the Janus kinase (JAK)/STATs and mitogen-activated protein kinase (MAPK) pathways. In parallel, apoptosis in the glandular epithelium is inhibited by activation of the phosphatidylinositol 3 kinase (PI3K) pathway (Jabbour *et al.* 2002).

Recently, several protocols have described stromal-epithelial co-cultures retaining physiological structure. Slices of full thickness endometrial tissue cultured in collagen gel maintain true histoarchitecture of the endometrium, and a decidual response similar to the *in vivo* profile can be induced following differentiation with oestradiol (E2) and progesterone (P4) (Muruganandan *et al.* 2020). Others have reported the use of porous 3D scaffolds to establish co-cultures. Using a collagen-based scaffold, Abbas and colleagues demonstrated that stromal cells were able to proliferate within the scaffold pores and deposit their own ECM, while fragments of endometrial gland organoids seeded on top of the scaffolds formed a luminal epithelium reminiscent of the tissue structure *in vivo* (Abbas *et al.* 2020). As well as solid scaffolds, synthetic hydrogels, such as polyethylene glycol (PEG), functionalised with ECM- and integrin-binding peptides have been utilised as a replacement for animal-derived hydrogels. When cultured in PEG hydrogels, endometrial stromal cells proliferate and decidualise in response to hormonal stimulation (Cook *et al.* 2017). Modulating the PEG hydrogel altered cell behaviour, highlighting the importance of matrix conditions when developing a representative model of the endometrium (Cook *et al.* 2017). Finally, another recent protocol reported self-aggregation of epithelial and stromal cells in a scaffold-free environment to form structures containing a stromal cell centre and an outer layer of epithelial cells within an agarose mould (Wiwatpanit *et al.* 2020).

An alternative approach to produce a structurally and functionally physiological model of the endometrium is to incorporate endometrial stromal cells into endometrial organoid cultures. Co-culturing of organoids with stromal cells has been reported in other organoid systems, such as the bladder and brain, and these models are designated as 'assembloids' (Kim *et al.* 2020*a*, Andersen *et al.* 2020, Miura *et al.* 2020). In the case of bladder, the applicability of organoids to *in vivo* pathology and disease is uncertain because, in isolation, they do not recapitulate the native tissue architecture and microenvironment. To overcome these limitations, bladder organoids were mixed with components of the bladder stroma, such as stromal, endothelial, and immune cells, and a muscle layer to form bladder assembloids (Kim *et al.* 2020). The assembloids represent a more physiological model of the native organ or tissue, and therefore, should provide a more faithful model for testing drug responses and mimicking disease phenotypes.

Recently, we have reported the establishment of endometrial assembloids whereby the gland organoid model was modified to incorporate stromal cells (Rawlings *et al.* 2021). Gland organoids were expanded from primary epithelial cells while in parallel the stromal fraction was propagated by standard monolayer culture (Fig. 4). Single-cell stromal suspensions were combined with manually digested organoids, seeded into a collagen hydrogel, and cultured in an expansion medium supplemented with E2. In this model, gland organoid formation was unperturbed by stromal co-culture, and assembloids

https://raf.bioscientifica.com
https://doi.org/10.1530/RAF-21-0023

resemble the architecture of native endometrium more closely than the gland organoids alone. The addition of stromal cells should abrogate the need for many components of the complex medium of growth factors and inhibitors to maintain secretory gland organoids, and indeed a minimal differentiation medium supported robust glandular differentiation in the assembloid model (Rawlings *et al.* 2021). Based on single-cell transcriptomic analysis, decidualised assembloids closely resemble the mid-secretory endometrium, containing several subpopulations of both stromal and epithelial cells, including senescent stromal and epithelial cells, which secrete many canonical implantation factors. Co-culturing human blastocysts with decidualised assembloids demonstrated that in the presence of senescent decidual cells, the assembloids engender a dynamic implantation environment, enabling embryo expansion and attachment, although persistent endometrial senescence led to the gradual disintegration of the assembloid matrix, likely through the actions of MMPs (Freitas-Rodriguez *et al.* 2017). Pharmacological inhibition of stress responses in pre-decidual cells by a tyrosine kinase inhibitor inhibited the propagation of decidual senescence, impeding assembloid breakdown. However, the lack of senescent cells resulted in the entrapment of the blastocysts in the largely static assembloid matrix. This study not only demonstrated that the endometrial assembloid model could be used as a novel embryo implantation model but also confirms previous reports that decidual senescence controls endometrial fate decisions during implantation and early pregnancy (Brighton *et al.* 2017, Lucas *et al.* 2020). Challenges for the endometrial assembloid model are to introduce a luminal epithelium, in order to study sequential blastocyst attachment and invasion, as well as the incorporation of immune cells such as uterine natural killer cells to mimic tissue remodelling processes predicted to take place during implantation (Brighton *et al.* 2017, Kong *et al.* 2021). Moreover, long-term maintenance and propagation of endometrial assembloids to mimic the cycling tissue have yet to be developed.

The major challenge in increasing complexity for a physiological model of the endometrium suitable for use in implantation studies is being able to balance the needs of different cell types within the model. For example, the basement membrane preparation Matrigel™, used frequently for organoid culture, is unsuitable as an extracellular matrix for stromal cells (Arnold *et al.* 2001). Beyond the co-culture of stromal cells with epithelial organoids, endothelial cells may be required to directly invade trophoblasts for placentation (Weiss *et al.* 2016). Additionally, immune cells, such as resident uterine natural killer cells, have been demonstrated to be essential for providing a robust decidual matrix suitable for successful embryo implantation (Kong *et al.* 2021). A microfluidic approach may be the solution to this potential dilemma.

Endometrial pathologies, genetic manipulation, and biomarker discovery

Beyond understanding the fundamentals of embryo implantation, endometrial pathologies that impede fertility must also be studied to advance the provision of therapeutics (Fig. 5). The development of medical treatments for many human diseases is limited by patient variation, difficulties in predicting outcomes, and lengthy preclinical drug testing. This is restricted further for applications in human reproduction by our limited ability to study *in vivo* processes in normal tissues. Therefore, organoid and assembloid cultures based on specific

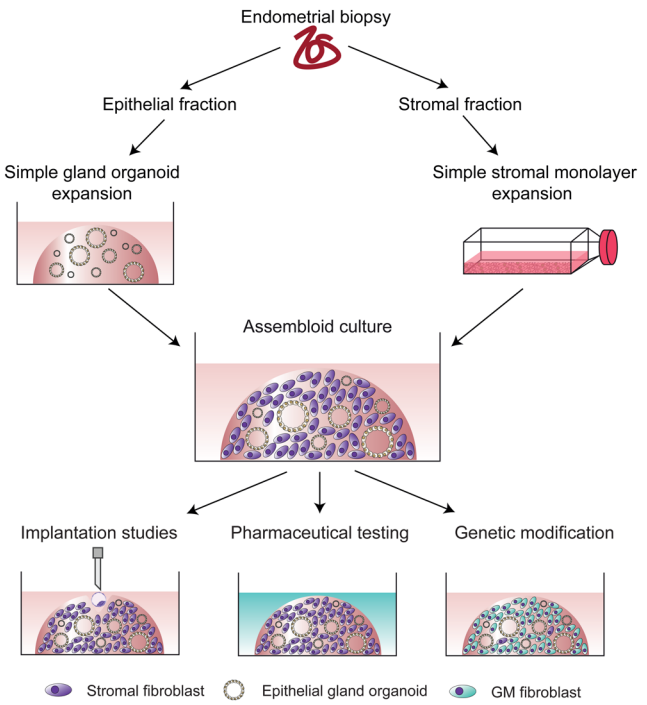

Figure 4 Establishment of an endometrial assembloid model. Schematic representation of the establishment of the endometrial assembloid model. Endometrial pipelle biopsies are digested and separated into epithelial and stromal fractions. Epithelial cells are expanded in Matrigel using the simple gland organoid culture approach for two passages, while stromal cells are expanded in monolayer culture. At passage 2, digested organoids and stromal cells are combined and encapsulated in collagen hydrogel to form an assembloid culture which then follows growth and differentiation protocols as required. Current and future applications for the assembloids include, but are not limited to embryo implantation studies, pharmaceutical testing (e.g. drugs or small molecules) and genetic modification of the different cell populations.

https://raf.bioscientifica.com
https://doi.org/10.1530/RAF-21-0023

pathologies and even on individual patients are expected to develop into powerful tools for precision therapy, permitting a personalised approach to drug discovery, development, and screening. Primary cancers, infectious diseases, and developmental diseases can be replicated with *ex vivo* biopsy samples from patients. Testing prospective pharmacological treatments on human organoids could facilitate the identification of patient group-specific responses and lead to targeted therapeutic approaches. Indeed, initial explorations into the utility of gland organoids in studying endometrial pathology have been reported, demonstrating the value of patient-specific cultures to study pathologies such as endometriosis and cancer (Boretto *et al.* 2017, 2019).

Endometriosis is an endometrial disorder characterised by the ectopic growth of endometrial tissue. Endometriosis is associated with infertility and affects 10% of women of reproductive age. The aetiology and pathogenesis of this disease remain unclear, and therefore, effective treatments are limited. Mouse models of endometriosis, while useful, do not model the complexity of the disease fully (Greaves *et al.* 2017). Gland organoids established from endometriotic lesions have been shown to differ from organoids derived in parallel from patient-matched eutopic endometrium, maintaining a heterogeneous disease profile, including aberrant signalling in integrin, PI3K-AKT, and WNT pathways, and thus identifying potential drug targets (Boretto *et al.* 2019). Furthermore, differences in glycodelin secretion mirror those in patients and controls (Luddi *et al.* 2020). However, this model is limited to only glandular epithelial cells. Sampson's theory of retrograde menstruation proposes that endometriotic lesions derive from endometrial cells seeding the peritoneum at menstruation (Filby *et al.* 2020). Incorporating decidualised stromal cells from endometriotic lesions to generate endometriosis assembloids could provide a more encompassing model for lesion establishment and behaviour, while crossover experiments with healthy and pathological cell subpopulations could also aid in pinpointing the exact mechanisms for endometrial diseases.

Endometrial cancer is another potential candidate for organoid modelling since the pathology of endometrial cancer is largely unknown, and treatment is limited, mainly due to a lack of reliable preclinical models. Tumour-derived cell lines do not recapitulate clinical cancer heterogeneity, and genetic mouse models show aberrations inconsistent with clinical endometrial cancer (Boretto *et al.* 2019). Tumour-derived organoids from endometrial cancers have been shown to maintain clinical heterogeneity under long-term expansion but required medium optimisation to recapitulate the tumour niche, owing to non-cancerous organoids outcompeting cancerous organoids in the standard protocol (Boretto *et al.* 2019). This key observation highlights the necessity to consider the nuances of the local environment when developing future endometrial organoid-based disease models. Pre-cancerous organoid models have also been developed, such as organoids derived from hyperplastic endometrium, which faithfully reproduced the disease genotype. These organoids may provide a model that can be used to identify patient-specific biomarkers for early detection and intervention (Boretto *et al.* 2019).

The development of pathological endometrial organoid and assembloid models, in concert with healthy controls, provides promising tools to interrogate endometrial biology and pathology. In models that are physiologically or pathologically relevant, single-cell omics and functional assays may provide initial targets for gene editing. Owing to their clonal capacity, organoids provide an excellent candidate model for gene editing through CRISPR/Cas9 (Jinek *et al.* 2012, Cong *et al.* 2013, Mali *et al.* 2013) and this has been achieved in numerous organoid systems already, including the brain (Wang *et al.* 2015, Ogawa *et al.* 2018), liver (Artegiani *et al.* 2019), kidney (Freedman *et al.* 2015), and intestine (Matano *et al.* 2015, Roper *et al.* 2018). To our knowledge, only one study has demonstrated CRISPR/Cas9 in endometrial organoids (Chen *et al.* 2021), derived from mouse tissue, and therefore, efforts to advance the manipulation of human endometrial organoids will be

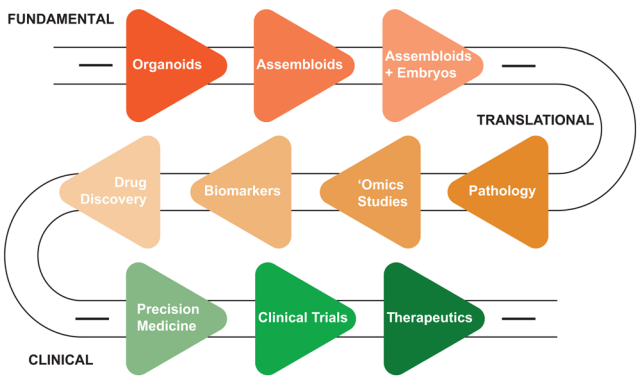

Figure 5 A roadmap to application for endometrial organoids. Schematic representation of the proposed roadmap to application for the endometrial organoids. The roadmap is divided into fundamental (red), translational (orange) and clinical (green) approaches to implantation research. This roadmap presents the trajectory from defining the embryo-endometrial interactions during and after implantation to disease modelling and biomarker- and drug- discovery, through developing successful therapeutic interventions for pathologies that impede successful pregnancy.

https://raf.bioscientifica.com
https://doi.org/10.1530/RAF-21-0023

welcomed. Genetic and gene regulatory manipulations will be essential for underpinning the key mechanisms and aberrations that lead to disease states, and as well as to open new avenues for biomarker investigation and drug discovery.

Endometrial precision medicine, clinical trials, and therapeutic potential

The clearest benefit of patient-derived organoids and assembloids is to provide a novel opportunity to discover personalised treatments. Unlike previous models, patient-derived organoids have been demonstrated to maintain the heterogeneity and complexity of their clinical derivatives, allowing for the study of patient-specific phenotypes. Therefore, the next step in the development of pathological endometrial organoid models is to utilise them in preclinical drug screening tools. Organoids from other systems have already been used for drug screening. For example, cystic fibrosis (CF) is a genetic disorder caused by mutations in the cystic fibrosis transmembrane conductance regulator (CFTR) gene and causes particularly severe damage to the pulmonary and digestive systems (Dekkers *et al.* 2013). Clinical trials with CFTR-targeting drugs have shown variable efficacy among individuals. Organoids can be harnessed to target different mutations in the CFTR protein with the intention to discover personalised and effective treatments for CF (Dekkers *et al.* 2013, 2016, Berkers *et al.* 2019, Ramalho *et al.* 2021).

Endometrial organoids have already been used in pre-clinical drug screening studies for endometrial cancer (Chen *et al.* 2021). Unbiased drug screening of tumour organoids from mouse endometrial cancer identified MI-136 as a potential inhibitor of endometrial cancer through regulation of the HIF pathway, a novel mechanism distinct from those in acute myeloid leukaemia and prostate cancer (Chen *et al.* 2021). Additionally, the study reported that MI-136 also inhibited growth significantly in primary cancer organoids derived from patients (Chen *et al.* 2021). This provides evidence that endometrial organoids could be used as in pre-clinical drug screening studies.

To maximise the effective use of therapeutics, stratification of subjects in clinical trials is essential, especially in the case of a heterogeneous disease. Stratification and personalised medicine could be extrapolated to endometrial organoids and assembloids and the treatment of infertility. Our recent research has demonstrated that excessive decidual cellular senescence is associated with recurrent pregnancy loss (Lucas *et al.* 2020). Biomarkers for excessive decidual senescence could be utilised for screening for organoid- and assembloid-based pre-clinical drug interventions to reduce senescence and possibly reduce the burden of miscarriage. Only patients experiencing cycles with excessive senescence would likely see a benefit in reducing senescence, and therefore, it is essential to target this subset of patients. Primary endometrial stromal cells *in vitro* retain phenotypic characteristics of the donating patient. For example, endometrial stromal cells from women with recurrent pregnancy loss exhibit an imbalance of mature decidual and senescent decidual cells and an inability to recognise poor-quality embryos (Weimar *et al.* 2012, Lucas *et al.* 2020). Therefore, endometrial assembloid models should be able to mimic the behaviour of the tissue *in vivo* and provide a first step approach to patient-specific testing and stratification for treatment. Indeed, since organoid cultures can be bio-banked for future drug testing (Boretto *et al.* 2019), reducing the requirement for repeated biopsies, directed testing should be possible on specified cohorts of bio-banked samples.

Overall, organoids appear to be a promising model for drug discovery, pre-clinical evaluation, and stratification of subject groups for clinical trials and our challenge lie in driving the models from the fundamental study into the translational application to realise their full potential (Fig. 5).

Conclusions

Organoid and assembloid models of the endometrium offer the opportunity to study embryo-endometrium interactions at the earliest timepoints in implantation, with increased physiological relevance, and thus present a promising tool for future research. Advancing our knowledge of the mechanisms and requirements for successful implantation also offers the prospect of identifying the routes through which the process fails, thus indicating possible therapeutic avenues. Through the ongoing development and characterisation of patient-specific organoid and assembloid models, targeted pre-conception therapies can be developed and tested extensively in pre-clinical studies. These exciting possibilities mean much work ahead: the full potential of organoid and assembloid models has not yet been realised, and the challenge now is to ensure that we drive the models forward to translational outcomes.

Declaration of interest
E S L is an ordinary member of SRF council. The authors have no financial interests to declare.

https://raf.bioscientifica.com
https://doi.org/10.1530/RAF-21-0023

Funding

T M R is supported by a fellowship from the Warwick-Wellcome Trust Translational Partnership initiative. K M is funded by a Warwick Medical School scholarship. M T is funded by a EUTOPIA Co-tutelle PhD Scholarship between the University of Warwick and Vrije Universiteit Brussel (VUB). E S L is funded through a Wellcome Trust Investigator Award to Professor Jan Brosens (212233/Z/18/Z).

Author contribution statement

T M R and E S L conceptualised the article. T M R, K M, M T, and E S L drafted the article. K M, M T, T M R, and E S L prepared the figures. E S L edited the article. All authors approved the final version.

References

Abbas Y, Brunel LG, Hollinshead MS, Fernando RC, Gardner L, Duncan I, Moffett A, Best S, Turco MY, Burton GJ, *et al*. 2020 Generation of a three-dimensional collagen scaffold-based model of the human endometrium. *Interface Focus* **10** 20190079. (https://doi.org/10.1098/rsfs.2019.0079)

Alves-Lopes JP, Söder O & Stukenborg JB 2017 Testicular organoid generation by a novel in vitro three-layer gradient system. *Biomaterials* **130** 76–89. (https://doi.org/10.1016/j.biomaterials.2017.03.025)

Alzamil L, Nikolakopoulou K & Turco MY 2021 Organoid systems to study the human female reproductive tract and pregnancy. *Cell Death and Differentiation* **28** 35–51. (https://doi.org/10.1038/s41418-020-0565-5)

Anacker J, Segerer SE, Hagemann C, Feix S, Kapp M, Bausch R & Kämmerer U 2011 Human decidua and invasive trophoblasts are rich sources of nearly all human matrix metalloproteinases. *Molecular Human Reproduction* **17** 637–652. (https://doi.org/10.1093/molehr/gar033)

Andersen J, Revah O, Miura Y, Thom N, Amin ND, Kelley KW, Singh M, Chen X, Thete MV, Walczak EM, *et al*. 2020 Generation of functional human 3D cortico-motor assembloids. *Cell* **183** 1913.e26–1929.e26. (https://doi.org/10.1016/j.cell.2020.11.017)

Aplin JD 2006 In vitro analysis of trophoblast invasion. In *Placenta and Trophoblast: Methods and Protocols*, Vol. 2. Eds **MJ Soares & JS Hunt**. Totowa, NJ: Humana Press. (https://doi.org/10.1385/1-59259-989-3:45)

Aplin JD & Ruane PT 2017 Embryo-epithelium interactions during implantation at a glance. *Journal of Cell Science* **130** 15–22. (https://doi.org/10.1242/jcs.175943)

Aplin JD, Hey NA & Li TC 1996 MUC1 as a cell surface and secretory component of endometrial epithelium: reduced levels in recurrent miscarriage. *American Journal of Reproductive Immunology* **35** 261–266. (https://doi.org/10.1111/j.1600-0897.1996.tb00042.x)

Arnold JT, Kaufman DG, Seppälä M & Lessey BA 2001 Endometrial stromal cells regulate epithelial cell growth in vitro: a new co-culture model. *Human Reproduction* **16** 836–845. (https://doi.org/10.1093/humrep/16.5.836)

Artegiani B, Van Voorthuijsen L, Lindeboom RGH, Seinstra D, Heo I, Tapia P, López-Iglesias C, Postrach D, Dayton T, Oka R, *et al*. 2019 Probing the tumor suppressor function of BAP1 in CRISPR-engineered human liver organoids. *Cell Stem Cell* **24** 927.e6–943.e6. (https://doi.org/10.1016/j.stem.2019.04.017)

Baert Y, De Kock J, Alves-Lopes JP, Söder O, Stukenborg JB & Goossens E 2017 Primary human testicular cells self-organize into organoids with testicular properties. *Stem Cell Reports* **8** 30–38. (https://doi.org/10.1016/j.stemcr.2016.11.012)

Bartfeld S, Bayram T, Van De Wetering M, Huch M, Begthel H, Kujala P, Vries R, Peters PJ & Clevers H 2015 In vitro expansion of human gastric epithelial stem cells and their responses to bacterial infection. *Gastroenterology* **148** 126.e6–136.e6. (https://doi.org/10.1053/j.gastro.2014.09.042)

Bentin-Ley U, Pedersen B, Lindenberg S, Larsen JF, Hamberger L & Horn T 1994 Isolation and culture of human endometrial cells in a three-dimensional culture system. *Journal of Reproduction and Fertility* **101** 327–332. (https://doi.org/10.1530/jrf.0.1010327)

Bentin-Ley U, Horn T, Sjogren A, Sorensen S, Falck Larsen J & Hamberger L 2000 Ultrastructure of human blastocyst-endometrial interactions in vitro. *Journal of Reproduction and Fertility* **120** 337–350. (https://doi.org/10.1530/jrf.0.1200337)

Berkers G, Van Mourik P, Vonk AM, Kruisselbrink E, Dekkers JF, De Winter-De Groot KM, Arets HGM, Marck-Van Der Wilt REP, Dijkema JS, Vanderschuren MM, *et al*. 2019 Rectal organoids enable personalized treatment of cystic fibrosis. *Cell Reports* **26** 1701.e3–1708.e3. (https://doi.org/10.1016/j.celrep.2019.01.068)

Berkhout RP, Lambalk CB, Huirne J, Mijatovic V, Repping S, Hamer G & Mastenbroek S 2018 High-quality human preimplantation embryos actively influence endometrial stromal cell migration. *Journal of Assisted Reproduction and Genetics* **35** 659–667. (https://doi.org/10.1007/s10815-017-1107-z)

Berneau SC, Ruane PT, Brison DR, Kimber SJ, Westwood M & Aplin JD 2019 Characterisation of osteopontin in an in vitro model of embryo implantation. *Cells* **8** 432. (https://doi.org/10.3390/cells8050432)

Binder NK, Evans J, Gardner DK, Salamonsen LA & Hannan NJ 2014 Endometrial signals improve embryo outcome: functional role of vascular endothelial growth factor isoforms on embryo development and implantation in mice. *Human Reproduction* **29** 2278–2286. (https://doi.org/10.1093/humrep/deu211)

Bläuer M, Heinonen PK, Martikainen PM, Tomás E & Ylikomi T 2005 A novel organotypic culture model for normal human endometrium: regulation of epithelial cell proliferation by estradiol and medroxyprogesterone acetate. *Human Reproduction* **20** 864–871. (https://doi.org/10.1093/humrep/deh722)

Boretto M, Cox B, Noben M, Hendriks N, Fassbender A, Roose H, Amant F, Timmerman D, Tomassetti C, Vanhie A, *et al*. 2017 Development of organoids from mouse and human endometrium showing endometrial epithelium physiology and long-term expandability. *Development* **144** 1775–1786. (https://doi.org/10.1242/dev.148478)

Boretto M, Maenhoudt N, Luo X, Hennes A, Boeckx B, Bui B, Heremans R, Perneel L, Kobayashi H, Van Zundert I, *et al*. 2019 Patient-derived organoids from endometrial disease capture clinical heterogeneity and are amenable to drug screening. *Nature Cell Biology* **21** 1041–1051. (https://doi.org/10.1038/s41556-019-0360-z)

Brighton PJ, Maruyama Y, Fishwick K, Vrljicak P, Tewary S, Fujihara R, Muter J, Lucas ES, Yamada T, Woods L, *et al*. 2017 Clearance of senescent decidual cells by uterine natural killer cells in cycling human endometrium. *eLife* **6** e31274. (https://doi.org/10.7554/eLife.31274)

Brosens JJ, Salker MS, Teklenburg G, Nautiyal J, Salter S, Lucas ES, Steel JH, Christian M, Chan YW, Boomsma CM, *et al*. 2014 Uterine selection of human embryos at implantation. *Scientific Reports* **4** 3894. (https://doi.org/10.1038/srep03894)

Burton GJ, Watson AL, Hempstock J, Skepper JN & Jauniaux E 2002 Uterine glands provide histiotrophic nutrition for the human fetus during the first trimester of pregnancy. *Journal of Clinical Endocrinology and Metabolism* **87** 2954–2959. (https://doi.org/10.1210/jcem.87.6.8563)

Burton GJ, Jauniaux E & Charnock-Jones DS 2007 Human early placental development: potential roles of the endometrial glands.

Placenta **28** (Supplement A) S64–S69. (https://doi.org/10.1016/j.placenta.2007.01.007)

Burton GJ, Jauniaux E & Charnock-Jones DS 2010 The influence of the intrauterine environment on human placental development. *International Journal of Developmental Biology* **54** 303–312. (https://doi.org/10.1387/ijdb.082764gb)

Caballero-Campo P, Domínguez F, Coloma J, Meseguer M, Remohí J, Pellicer A & Simón C 2002 Hormonal and embryonic regulation of chemokines IL-8, MCP-1 and RANTES in the human endometrium during the window of implantation. *Molecular Human Reproduction* **8** 375–384. (https://doi.org/10.1093/molehr/8.4.375)

Carter AM 2007 Animal models of human placentation – a review. *Placenta* **28** (Supplement A) S41–S47. (https://doi.org/10.1016/j.placenta.2006.11.002)

Carter AM 2020 Animal models of human pregnancy and placentation: alternatives to the mouse. *Reproduction* **160** R129–R143. (https://doi.org/10.1530/REP-20-0354)

Carver J, Martin K, Spyropoulou I, Barlow D, Sargent I & Mardon H 2003 An in-vitro model for stromal invasion during implantation of the human blastocyst. *Human Reproduction* **18** 283–290. (https://doi.org/10.1093/humrep/deg072)

Chen J, Zhao L, Peng H, Dai S, Quan Y, Wang M, Wang J, Bi Z, Zheng Y, Zhou S, *et al*. 2021 An organoid-based drug screening identified a menin-MLL inhibitor for endometrial cancer through regulating the HIF pathway. *Cancer Gene Therapy* **28** 112–125. (https://doi.org/10.1038/s41417-020-0190-y)

Chua CW, Shibata M, Lei M, Toivanen R, Barlow LJ, Bergren SK, Badani KK, Mckiernan JM, Benson MC, Hibshoosh H, *et al*. 2014 Single luminal epithelial progenitors can generate prostate organoids in culture. *Nature Cell Biology* **16** 951–961. (https://doi.org/10.1038/ncb3047)

Chumduri C, Gurumurthy RK, Berger H, Dietrich O, Kumar N, Koster S, Brinkmann V, Hoffmann K, Drabkina M, Arampatzi P *et al*. 2021 Opposing Wnt signals regulate cervical squamocolumnar homeostasis and emergence of metaplasia *Nature Cell Biology* **23** 184-197. (https://doi.org/10.1038/s41556-020-00619-0)

Cong L, Ran FA, Cox D, Lin S, Barretto R, Habib N, Hsu PD, Wu X, Jiang W, Marraffini LA, *et al*. 2013 Multiplex genome engineering using CRISPR/Cas systems. *Science* **339** 819–823. (https://doi.org/10.1126/science.1231143)

Cook CD, Hill AS, Guo M, Stockdale L, Papps JP, Isaacson KB, Lauffenburger DA & Griffith LG 2017 Local remodeling of synthetic extracellular matrix microenvironments by co-cultured endometrial epithelial and stromal cells enables long-term dynamic physiological function. *Integrative Biology* **9** 271–289. (https://doi.org/10.1039/c6ib00245e)

Dekkers JF, Van Der Ent CK & Beekman JM 2013 Novel opportunities for CFTR-targeting drug development using organoids. *Rare Diseases* **1** e27112. (https://doi.org/10.4161/rdis.27112)

Dekkers JF, Berkers G, Kruisselbrink E, Vonk A, de Jonge HR, Janssens HM, Bronsveld I, van de Graaf EA, Nieuwenhuis EE, Houwen RH, *et al*. 2016 Characterizing responses to CFTR-modulating drugs using rectal organoids derived from subjects with cystic fibrosis. *Science Translational Medicine* **8** 344ra84. (https://doi.org/10.1126/scitranslmed.aad8278)

Dominguez F, Galan A, Martin JJL, Remohi J, Pellicer A & Simón C 2003 Hormonal and embryonic regulation of chemokine receptors CXCR1, CXCR4, CCR5 and CCR2B in the human endometrium and the human blastocyst. *Molecular Human Reproduction* **9** 189–198. (https://doi.org/10.1093/molehr/gag024)

Erikson DW, Burghardt RC, Bayless KJ & Johnson GA 2009 Secreted phosphoprotein 1 (SPP1, osteopontin) binds to integrin Alphavbeta6 on porcine trophectoderm cells and integrin Alphavbeta3 on uterine luminal epithelial cells, and promotes trophectoderm. *Biology of Reproduction* **81** 814–825. (https://doi.org/10.1095/biolreprod.109.078600)

ESHRE Guideline Group on RPL, **Bender Atik R, Christiansen OB, Elson J, Kolte AM, Lewis S, Middeldorp S, Nelen W, Peramo B, Quenby S, *et al*.** 2018 ESHRE guideline: recurrent pregnancy loss. *Human Reproduction Open* **2018** hoy004. (https://doi.org/10.1093/hropen/hoy004)

Evans J, Walker KJ, Bilandzic M, Kinnear S & Salamonsen LA 2020 A novel 'embryo-endometrial' adhesion model can potentially predict 'receptive' or 'non-receptive' endometrium. *Journal of Assisted Reproduction and Genetics* **37** 5–16. (https://doi.org/10.1007/s10815-019-01629-0)

Evron A, Goldman S & Shalev E 2011 Effect of primary human endometrial stromal cells on epithelial cell receptivity and protein expression is dependent on menstrual cycle stage. *Human Reproduction* **26** 176–190. (https://doi.org/10.1093/humrep/deq296)

Feinberg RF, Kliman HJ & Wang CL 1994 Transforming growth factor-beta stimulates trophoblast oncofetal fibronectin synthesis in vitro: implications for trophoblast implantation in vivo. *Journal of Clinical Endocrinology and Metabolism* **78** 1241–1248. (https://doi.org/10.1210/jcem.78.5.8175984)

Filby CE, Rombauts L, Montgomery GW, Giudice LC & Gargett CE 2020 Cellular origins of endometriosis: towards novel diagnostics and therapeutics. *Seminars in Reproductive Medicine* **38** 201–215. (https://doi.org/10.1055/s-0040-1713429)

Fitzgerald HC, Dhakal P, Behura SK, Schust DJ & Spencer TE 2019 Self-renewing endometrial epithelial organoids of the human uterus. *PNAS* **116** 23132–23142. (https://doi.org/10.1073/pnas.1915389116)

Fitzgerald HC, Schust DJ & Spencer TE 2021 In vitro models of the human endometrium: evolution and application for women's health. *Biology of Reproduction* **104** 282–293. (https://doi.org/10.1093/biolre/ioaa183)

Freedman BS, Brooks CR, Lam AQ, Fu H, Morizane R, Agrawal V, Saad AF, Li MK, Hughes MR, Werff RV, *et al*. 2015 Modelling kidney disease with CRISPR-mutant kidney organoids derived from human pluripotent epiblast spheroids. *Nature Communications* **6** 8715. (https://doi.org/10.1038/ncomms9715)

Freitas-Rodriguez S, Folgueras AR & Lopez-Otin C 2017 The role of matrix metalloproteinases in aging: tissue remodeling and beyond. *Biochimica et Biophysica Acta: Molecular Cell Research* **1864** 2015–2025. (https://doi.org/10.1016/j.bbamcr.2017.05.007)

Fujii M, Matano M, Toshimitsu K, Takano A, Mikami Y, Nishikori S, Sugimoto S & Sato T 2018 Human intestinal organoids maintain self-renewal capacity and cellular diversity in niche-inspired culture condition. *Cell Stem Cell* **23** 787.e6–793.e6. (https://doi.org/10.1016/j.stem.2018.11.016)

Gellersen B & Brosens JJ 2014 Cyclic decidualization of the human endometrium in reproductive health and failure. *Endocrine Reviews* **35** 851–905. (https://doi.org/10.1210/er.2014-1045)

Gellersen B, Reimann K, Samalecos A, Aupers S & Bamberger AM 2010 Invasiveness of human endometrial stromal cells is promoted by decidualization and by trophoblast-derived signals. *Human Reproduction* **25** 862–873. (https://doi.org/10.1093/humrep/dep468)

Gellersen B, Wolf A, Kruse M, Schwenke M & Bamberger A-M 2013 Human endometrial stromal cell-trophoblast interactions: mutual stimulation of chemotactic migration and promigratory roles of cell surface molecules CD82 and CEACAM11. *Biology of Reproduction* **88** 80. (https://doi.org/10.1095/biolreprod.112.106724)

Gray CA, Bartol FF, Tarleton BJ, Wiley AA, Johnson GA, Bazer FW & Spencer TE 2001 Developmental biology of uterine glands. *Biology of Reproduction* **65** 1311–1323. (https://doi.org/10.1095/biolreprod65.5.1311)

Greaves E, Critchley HOD, Horne AW & Saunders PTK 2017 Relevant human tissue resources and laboratory models for use in endometriosis research. *Acta Obstetricia et Gynecologica Scandinavica* **96** 644–658. (https://doi.org/10.1111/aogs.13119)

Grewal S, Carver JG, Ridley AJ & Mardon HJ 2008 Implantation of the human embryo requires Rac1-dependent endometrial stromal

https://raf.bioscientifica.com
https://doi.org/10.1530/RAF-21-0023

cell migration. *PNAS* **105** 16189–16194. (https://doi.org/10.1073/pnas.0806219105)

Grewal S, Carver J, Ridley AJ & Mardon HJ 2010 Human endometrial stromal cell rho GTPases have opposing roles in regulating focal adhesion turnover and embryo invasion in vitro. *Biology of Reproduction* **83** 75–82. (https://doi.org/10.1095/biolreprod.109.080630)

Haider S, Meinhardt G, Saleh L, Kunihs V, Gamperl M, Kaindl U, Ellinger A, Burkard TR, Fiala C, Pollheimer J, *et al*. 2018 Self-renewing trophoblast organoids recapitulate the developmental program of the early human placenta. *Stem Cell Reports* **11** 537–551. (https://doi.org/10.1016/j.stemcr.2018.07.004)

Haider S, Gamperl M, Burkard TR, Kunihs V, Kaindl U, Junttila S, Fiala C, Schmidt K, Mendjan S, Knöfler M, *et al*. 2019 Estrogen signaling drives ciliogenesis in human endometrial organoids. *Endocrinology* **160** 2282–2297. (https://doi.org/10.1210/en.2019-00314)

Hertig AT, Rock J & Adams EC 1956 A description of 34 human ova within the first 17 days of development. *American Journal of Anatomy* **98** 435–493. (https://doi.org/10.1002/aja.1000980306)

Holmberg JC, Haddad S, Wünsche V, Yang Y, Aldo PB, Gnainsky Y, Granot I, Dekel N & Mor G 2012 An in vitro model for the study of human implantation. *American Journal of Reproductive Immunology* **67** 169–178. (https://doi.org/10.1111/j.1600-0897.2011.01095.x)

Hu H, Gehart H, Artegiani B, Löpez-Iglesias C, Dekkers F, Basak O, van Es J, Chuva de Sousa Lopes SM, Begthel H, Korving J, *et al*. 2018 Long-term expansion of functional mouse and human hepatocytes as 3D organoids. *Cell* **175** 1591.e19–1606.e19. (https://doi.org/10.1016/j.cell.2018.11.013)

Huang X, Liu H & Li R 2017 Prostaglandin E2 promotes BeWo spheroids implantation in RL95-2 cell monolayers. *Gynecological Endocrinology* **33** 548–552. (https://doi.org/10.1080/09513590.2017.1296125)

Huch M, Gehart H, Van Boxtel R, Hamer K, Blokzijl F, Verstegen MM, Ellis E, Van Wenum M, Fuchs SA, De Ligt J, *et al*. 2015 Long-term culture of genome-stable bipotent stem cells from adult human liver. *Cell* **160** 299–312. (https://doi.org/10.1016/j.cell.2014.11.050)

Jabbour HN, Gubbay O & Critchley HOD 2002 Prolactin action and signalling in the human endometrium. *Reproductive Medicine Review* **10** 117–132. (https://doi.org/10.1017/S0962279902000236)

Jinek M, Chylinski K, Fonfara I, Hauer M, Doudna JA & Charpentier E 2012 A programmable dual-RNA-guided DNA endonuclease in adaptive bacterial immunity. *Science* **337** 816–821. (https://doi.org/10.1126/science.1225829)

John NJ, Linke M & Denker HW 1993 Quantitation of human choriocarcinoma spheroid attachment to uterine epithelial cell monolayers. *In Vitro Cellular and Developmental Biology: Animal* **29** 461–468. (https://doi.org/10.1007/BF02639380)

Jones RL, Critchley HOD, Brooks J, Jabbour HN & Mcneilly AS 1998 Localization and temporal expression of prolactin receptor in human endometrium. *Journal of Clinical Endocrinology and Metabolism* **83** 258–262. (https://doi.org/10.1210/jcem.83.1.4506)

Karthaus WR, Iaquinta PJ, Drost J, Gracanin A, Van Boxtel R, Wongvipat J, Dowling CM, Gao D, Begthel H, Sachs N, *et al*. 2014 Identification of multipotent luminal progenitor cells in human prostate organoid cultures. *Cell* **159** 163–175. (https://doi.org/10.1016/j.cell.2014.08.017)

Kelleher AM, Burns GW, Behura S, Wu G & Spencer TE 2016 Uterine glands impact uterine receptivity, luminal fluid homeostasis and blastocyst implantation. *Scientific Reports* **6** 38078–38078. (https://doi.org/10.1038/srep38078)

Kessler M, Hoffmann K, Brinkmann V, Thieck O, Jackisch S, Toelle B, Berger H, Mollenkopf HJ, Mangler M, Sehouli J, *et al*. 2015 The Notch and Wnt pathways regulate stemness and differentiation in human Fallopian tube organoids. *Nature Communications* **6** 8989. (https://doi.org/10.1038/ncomms9989)

Kim E, Choi S, Kang B, Kong J, Kim Y, Yoon WH, Lee HR, Kim S, Kim HM, Lee H, *et al*. 2020*a* Creation of bladder assembloids mimicking tissue regeneration and cancer. *Nature* **588** 664–669. (https://doi.org/10.1038/s41586-020-3034-x)

Kim J, Koo BK & Knoblich JA 2020*b* Human organoids: model systems for human biology and medicine. *Nature Reviews: Molecular Cell Biology* **21** 571–584. (https://doi.org/10.1038/s41580-020-0259-3)

Kong CS, Ordonez AA, Turner S, Tremaine T, Muter J, Lucas ES, Salisbury E, Vassena R, Tiscornia G, Fouladi-Nashta AA, *et al*. 2021 Embryo biosensing by uterine natural killer cells determines endometrial fate decisions at implantation. *FASEB Journal* **35** e21336. (https://doi.org/10.1096/fj.202002217R)

Kopper O, De Witte CJ, Lõhmussaar K, Valle-Inclan JE, Hami N, Kester L, Balgobind AV, Korving J, Proost N, Begthel H, *et al*. 2019 An organoid platform for ovarian cancer captures intra-and interpatient heterogeneity. *Nature Medicine* **25** 838–849. (https://doi.org/10.1038/s41591-019-0422-6)

Kretzschmar K & Clevers H 2016 Organoids: modeling development and the stem cell niche in a dish. *Developmental Cell* **38** 590–600. (https://doi.org/10.1016/j.devcel.2016.08.014)

Ladines-Llave CA, Maruo T, Manalo AS & Mochizuki M 1991 Cytologic localization of epidermal growth factor and its receptor in developing human placenta varies over the course of pregnancy. *American Journal of Obstetrics and Gynecology* **165** 1377–1382. (https://doi.org/10.1016/0002-9378(91)90372-x)

Lash GE, Hornbuckle J, Brunt A, Kirkley M, Searle RF, Robson SC & Bulmer JN 2007 Effect of low oxygen concentrations on trophoblast-like cell line invasion. *Placenta* **28** 390–398. (https://doi.org/10.1016/j.placenta.2006.06.001)

Le Saint C, Crespo K, Bourdiec A, Bissonnette F, Buzaglo K, Couturier B, Bisotto S, Phillips SJ, Stutz M, Gouze JN, *et al*. 2019 Autologous endometrial cell co-culture improves human embryo development to high-quality blastocysts: a randomized controlled trial. *Reproductive Biomedicine Online* **38** 321–329. (https://doi.org/10.1016/j.rbmo.2018.12.039)

Lee KY & DeMayo FJ 2004 Animal models of implantation. *Reproduction* **128** 679–695. (https://doi.org/10.1530/rep.1.00340)

Lee YL, Fong SW, Chen ACH, Li T, Yue C, Lee CL, Ng EHY, Yeung WSB & Lee KF 2015 Establishment of a novel human embryonic stem cell-derived trophoblastic spheroid implantation model. *Human Reproduction* **30** 2614–2626. (https://doi.org/10.1093/humrep/dev223)

Lee SH, Hu W, Matulay JT, Silva MV, Owczarek TB, Kim K, Chua CW, Barlow LJ, Kandoth C, Williams AB, *et al*. 2018 Tumor evolution and drug response in patient-derived organoid models of bladder cancer. *Cell* **173** 515.e17–528.e17. (https://doi.org/10.1016/j.cell.2018.03.017)

Lindenberg S, Nielsen MH & Lenz S 1985 In vitro studies of human blastocyst Implantationa. *Annals of the New York Academy of Sciences* **442** 368–374. (https://doi.org/10.1111/j.1749-6632.1985.tb37541.x)

Linnemann JR, Miura H, Meixner LK, Irmler M, Kloos UJ, Hirschi B, Bartsch HS, Sass S, Beckers J, Theis FJ, *et al*. 2015 Quantification of regenerative potential in primary human mammary epithelial cells. *Development* **142** 3239–3251. (https://doi.org/10.1242/dev.123554)

Liu X, Tan JP, Schröder J, Aberkane A, Ouyang JF, Mohenska M, Lim SM, Sun YBY, Chen J, Sun G, *et al*. 2021 Modelling human blastocysts by reprogramming fibroblasts into iBlastoids. *Nature* **591** 627–632. (https://doi.org/10.1038/s41586-021-03372-y)

Lohmussaar K, Oka R, Espejo Valle-Inclan J, Smits MHH, Wardak H, Korving J, Begthel H, Proost N, Van De Ven M, Kranenburg OW, *et al*. 2021 Patient-derived organoids model cervical tissue dynamics and viral oncogenesis in cervical cancer. *Cell Stem Cell* **28** 1380.e6–1396.e6. (https://doi.org/10.1016/j.stem.2021.03.012)

Loomans CJM, Giuliani NW, Balak J, Ringnalda F, Van Gurp L, Huch M, Boj SF, Sato T, Kester L, De Sousa Lopes SMC,

et al. 2018 Expansion of adult human pancreatic tissue yields organoids harboring progenitor cells with endocrine differentiation potential. *Stem Cell Reports* **10** 712–724. (https://doi.org/10.1016/j.stemcr.2018.02.005)

Lopes FL, Desmarais JA & Murphy BD 2004 Embryonic diapause and its regulation. *Reproduction* **128** 669–678. (https://doi.org/10.1530/rep.1.00444)

Lucas ES, Salker MS & Brosens JJ 2013 Uterine plasticity and reproductive fitness. *Reproductive Biomedicine Online* **27** 506–514. (https://doi.org/10.1016/j.rbmo.2013.06.012)

Lucas ES, Vrljicak P, Muter J, Diniz-Da-Costa MM, Brighton PJ, Kong CS, Lipecki J, Fishwick KJ, Odendaal J, Ewington LJ, *et al*. 2020 Recurrent pregnancy loss is associated with a pro-senescent decidual response during the peri-implantation window. *Communications Biology* **3** 37. (https://doi.org/10.1038/s42003-020-0763-1)

Luddi A, Pavone V, Semplici B, Governini L, Criscuoli M, Paccagnini E, Gentile M, Morgante G, Leo V, Belmonte G, *et al*. 2020 Organoids of human endometrium: a powerful in vitro model for the endometrium-embryo cross-talk at the implantation site. *Cells* **9** 1121. (https://doi.org/10.3390/cells9051121)

Luddi A, Pavone V, Governini L, Capaldo A, Landi C, Ietta F, Paccagnini E, Morgante G, De Leo V & Piomboni P 2021 Emerging role of embryo secretome in the paracrine communication at the implantation site: a proof of concept. *Fertility and Sterility* **115** 1054–1062. (https://doi.org/10.1016/j.fertnstert.2020.10.058)

Macklon NS & Brosens JJ 2014 The human endometrium as a sensor of embryo quality. *Biology of Reproduction* **91** 98. (https://doi.org/10.1095/biolreprod.114.122846)

Maenhoudt N, Defraye C, Boretto M, Jan Z, Heremans R, Boeckx B, Hermans F, Arijs I, Cox B, Van Nieuwenhuysen E, *et al*. 2020 Developing organoids from ovarian cancer as experimental and preclinical models. *Stem Cell Reports* **14** 717–729. (https://doi.org/10.1016/j.stemcr.2020.03.004)

Mali P, Yang L, Esvelt KM, Aach J, Guell M, Dicarlo JE, Norville JE & Church GM 2013 RNA-guided human genome engineering via Cas9. *Science* **339** 823–826. (https://doi.org/10.1126/science.1232033)

Maru Y, Kawata A, Taguchi A, Ishii Y, Baba S, Mori M, Nagamatsu T, Oda K, Kukimoto I, Osuga Y, *et al*. 2020 Establishment and molecular phenotyping of organoids from the squamocolumnar junction region of the uterine cervix. *Cancers* **12** 694. (https://doi.org/10.3390/cancers12030694)

Maruo T, Matsuo H, Otani T & Mochizuki M 1997 Epidermal growth factor (EGF) regulates trophoblast proliferation and endocrine function in synergy with thyroid hormone. *Placenta* **18** 27–39. (https://doi.org/10.1016/S0143-4004(05)80158-4)

Mascarenhas M, Jeve Y, Polanski L, Sharpe A, Yasmin E & Bhandari HM 2021 Management of recurrent implantation failure: British Fertility Society Policy and Practice Guideline. *Human Fertility* 1–25. (https://doi.org/10.1080/14647273.2021.1905886)

Meseguer M, Aplin JD, Caballero-Campo P, O'Connor JE, Martín JC, Remohí J, Pellicer A & Simón C 2001 Human endometrial mucin MUC1 is up-regulated by progesterone and down-regulated in vitro by the human blastocyst. *Biology of Reproduction* **64** 590–601. (https://doi.org/10.1095/biolreprod64.2.590)

Miura Y, Li MY, Birey F, Ikeda K, Revah O, Thete MV, Park JY, Puno A, Lee SH, Porteus MH, *et al*. 2020 Generation of human striatal organoids and cortico-striatal assembloids from human pluripotent stem cells. *Nature Biotechnology* **38** 1421–1430. (https://doi.org/10.1038/s41587-020-00763-w)

Morrison JL, Berry MJ, Botting KJ, Darby JRT, Frasch MG, Gatford KL, Giussani DA, Gray CL, Harding R, Herrera EA, *et al*. 2018 Improving pregnancy outcomes in humans through studies in sheep. *American Journal of Physiology: Regulatory, Integrative and Comparative Physiology* **315** R1123–R1153. (https://doi.org/10.1152/ajpregu.00391.2017)

Muruganandan S, Fan X, Dhal S & Nayak NR 2020 Development of A 3D tissue slice culture model for the study of human endometrial repair and regeneration. *Biomolecules* **10** 136. (https://doi.org/10.3390/biom10010136)

Ogawa J, Pao GM, Shokhirev MN & Verma IM 2018 Glioblastoma model using human cerebral organoids. *Cell Reports* **23** 1220–1229. (https://doi.org/10.1016/j.celrep.2018.03.105)

Pendergraft SS, Sadri-Ardekani H, Atala A & Bishop CE 2017 Three-dimensional testicular organoid: a novel tool for the study of human spermatogenesis and gonadotoxicity in vitro. *Biology of Reproduction* **96** 720–732. (https://doi.org/10.1095/biolreprod.116.143446)

Pierro E, Minici F, Alesiani O, Miceli F, Proto C, Screpanti I, Mancuso S & Lanzone A 2001 Stromal-epithelial interactions modulate estrogen responsiveness in normal human endometrium. *Biology of Reproduction* **64** 831–838. (https://doi.org/10.1095/biolreprod64.3.831)

Ramalho AS, Fürstová E, Vonk AM, Ferrante M, Verfaillie C, Dupont L, Boon M, Proesmans M, Beekman JM, Sarouk I, *et al*. 2021 Correction of CFTR function in intestinal organoids to guide treatment of cystic fibrosis. *European Respiratory Journal* **57** 1902426. (https://doi.org/10.1183/13993003.02426-2019)

Rawlings TM, Makwana K, Taylor DM, Molè MA, Fishwick KJ, Tryfonos M, Odendaal J, Hawkes A, Zernicka-Goetz M, Hartshorne GM, *et al*. 2021 Modelling the impact of decidual senescence on embryo implantation in human endometrial assembloids. *bioRxiv* 2021.03.02.433560. (https://doi.org/10.1101/2021.03.02.433560)

Rinehart CA, Lyn-Cook BD & Kaufman DG 1988 Gland formation from human endometrial epithelial cells in vitro. *In Vitro Cellular and Developmental Biology* **24** 1037–1041. (https://doi.org/10.1007/BF02620878)

Rogers K 2012 *Scientific Modeling [Online]*. Encyclopedia Britannica. (available at: https://www.britannica.com/science/scientific-modeling). Accessed on 21 February 2021.

Ruane PT, Buck CJ, Babbington PA, Aboussahoud W, Berneau SC, Westwood M, Kimber SJ, Aplin JD & Brison DR 2020 The effects of hyaluronate-containing medium on human embryo attachment to endometrial epithelial cells in vitro. *Human Reproduction Open* **2020** hoz033. (https://doi.org/10.1093/hropen/hoz033)

Sachs N, Papaspyropoulos A, Zomer-Van Ommen DD, Heo I, Böttinger L, Klay D, Weeber F, Huelsz-Prince G, Iakobachvili N, Amatngalim GD, *et al*. 2019 Long-term expanding human airway organoids for disease modeling. *EMBO Journal* **38** e100300. (https://doi.org/10.15252/embj.2018100300)

Salleh N & Giribabu N 2014 Leukemia inhibitory factor: roles in embryo implantation and in nonhormonal contraception. *ScientificWorldJournal* **2014** 201514. (https://doi.org/10.1155/2014/201514)

Schlaermann P, Toelle B, Berger H, Schmidt SC, Glanemann M, Ordemann J, Bartfeld S, Mollenkopf HJ & Meyer TF 2016 A novel human gastric primary cell culture system for modelling Helicobacter pylori infection in vitro. *Gut* **65** 202–213. (https://doi.org/10.1136/gutjnl-2014-307949)

Simintiras CA, Dhakal P, Ranjit C, Fitzgerald HC, Balboula AZ & Spencer TE 2021 Capture and metabolomic analysis of the human endometrial epithelial organoid secretome. *PNAS* **118** e2026804118. (https://doi.org/10.1073/pnas.2026804118)

Simón C, Gimeno MJ, Mercader A, O'Connor JE, Remohí J, Polan ML & Pellicer A 1997 Embryonic regulation of integrins β3,α 4, and α1 in human endometrial epithelial cells in vitro. *Journal of Clinical Endocrinology and Metabolism* **82** 2607–2616. (https://doi.org/10.1210/jcem.82.8.4153)

Simón C, Mercader A, Garcia-Velasco J, Nikas G, Moreno C, Remohí J & Pellicer A 1999 Coculture of human embryos with autologous human endometrial epithelial cells in patients with

implantation failure. *Journal of Clinical Endocrinology and Metabolism* **84** 2638–2646. (https://doi.org/10.1210/jcem.84.8.5873)

Singh H & Aplin JD 2009 Adhesion molecules in endometrial epithelium: tissue integrity and embryo implantation. *Journal of Anatomy* **215** 3–13. (https://doi.org/10.1111/j.1469-7580.2008.01034.x)

So KH, Lee CL, Yeung WS & Lee KF 2012 Glycodelin suppresses endometrial cell migration and invasion but stimulates spheroid attachment. *Reproductive Biomedicine Online* **24** 639–645. (https://doi.org/10.1016/j.rbmo.2012.03.004)

Teilmann SC, Clement CA, Thorup J, Byskov AG & Christensen ST 2006 Expression and localization of the progesterone receptor in mouse and human reproductive organs. *Journal of Endocrinology* **191** 525–535. (https://doi.org/10.1677/joe.1.06565)

Teklenburg G, Salker M, Molokhia M, Lavery S, Trew G, Aojanepong T, Mardon HJ, Lokugamage AU, Rai R, Landles C, *et al*. 2010 Natural selection of human embryos: decidualizing endometrial stromal cells serve as sensors of embryo quality upon implantation. *PLoS ONE* **5** e10258. (https://doi.org/10.1371/journal.pone.0010258)

Tinning H, Taylor A, Wang D, Constantinides B, Sutton R, Oikonomou G, Velazquez MA, Thompson P, Treumann A, O'Connell MJ, *et al*. 2020 The role of CAPG in molecular communication between the embryo and the uterine endometrium: is its function conserved in species with different implantation strategies? *FASEB Journal* **34** 11015–11029. (https://doi.org/10.1096/fj.202000882RR)

Turco MY, Gardner L, Hughes J, Cindrova-Davies T, Gomez MJ, Farrell L, Hollinshead M, Marsh SGE, Brosens JJ, Critchley HO, *et al*. 2017 Long-term, hormone-responsive organoid cultures of human endometrium in a chemically defined medium. *Nature Cell Biology* **19** 568–577. (https://doi.org/10.1038/ncb3516)

Turco MY, Gardner L, Kay RG, Hamilton RS, Prater M, Hollinshead MS, Mcwhinnie A, Esposito L, Fernando R, Skelton H, *et al*. 2018 Trophoblast organoids as a model for maternal–fetal interactions during human placentation. *Nature* **564** 263–267. (https://doi.org/10.1038/s41586-018-0753-3)

Uchida H, Maruyama T, Ono M, Ohta K, Kajitani T, Masuda H, Nagashima T, Arase T, Asada H & Yoshimura Y 2007 Histone deacetylase inhibitors stimulate cell migration in human endometrial adenocarcinoma cells through up-regulation of glycodelin. *Endocrinology* **148** 896–902. (https://doi.org/10.1210/en.2006-0896)

Varma VA, Melin SA, Adamec TA, Dorman BH, Siegfried JM, Walton LA, Carney CN, Norton CR & Kaufman DG 1982 Monolayer culture of human endometrium: methods of culture and identification of cell types. *In Vitro* **18** 911–918. (https://doi.org/10.1007/BF02796347)

von Wolff M, Strowitzki T, Becker V, Zepf C, Tabibzadeh S & Thaler CJ 2001 Endometrial osteopontin, a ligand of beta3-integrin, is maximally expressed around the time of the 'implantation window'. *Fertility and Sterility* **76** 775–781. (https://doi.org/10.1016/s0015-0282(01)02015-5)

Wang H, Pilla F, Anderson S, Martínez-Escribano S, Herrer I, Moreno-Moya JM, Musti S, Bocca S, Oehninger S & Horcajadas JA 2012 A novel model of human implantation: 3D endometrium-like culture system to study attachment of human trophoblast (Jar) cell spheroids. *Molecular Human Reproduction* **18** 33–43. (https://doi.org/10.1093/molehr/gar064)

Wang P, Lin M, Pedrosa E, Hrabovsky A, Zhang Z, Guo W, Lachman HM & Zheng D 2015 CRISPR/Cas9-mediated heterozygous knockout of the autism gene CHD8 and characterization of its transcriptional networks in neurodevelopment. *Molecular Autism* **6** 55. (https://doi.org/10.1186/s13229-015-0048-6)

Weimar CH, Kavelaars A, Brosens JJ, Gellersen B, De Vreeden-Elbertse JM, Heijnen CJ & Macklon NS 2012 Endometrial stromal cells of women with recurrent miscarriage fail to discriminate between high- and low-quality human embryos. *PLoS ONE* **7** e41424. (https://doi.org/10.1371/journal.pone.0041424)

Weimar CH, Post Uiterweer ED, Teklenburg G, Heijnen CJ & Macklon NS 2013 In-vitro model systems for the study of human embryo-endometrium interactions. *Reproductive Biomedicine Online* **27** 461–476. (https://doi.org/10.1016/j.rbmo.2013.08.002)

Weiss G, Huppertz B, Siwetz M, Lang I & Moser G 2016 Arterial endothelial cytokines guide extravillous trophoblast invasion towards spiral arteries; an in-vitro study with the trophoblast cell line ACH-3P and female non-uterine endothelial cells. *Placenta* **38** 49–56. (https://doi.org/10.1016/j.placenta.2015.12.010)

Wiwatpanit T, Murphy AR, Lu Z, Urbanek M, Burdette JE, Woodruff TK & Kim JJ 2020 Scaffold-free endometrial organoids respond to excess androgens associated with polycystic ovarian syndrome. *Journal of Clinical Endocrinology and Metabolism* **105** 769–780. (https://doi.org/10.1210/clinem/dgz100)

Yu L, Wei Y, Duan J, Schmitz DA, Sakurai M, Wang L, Wang K, Zhao S, Hon GC & Wu J 2021 Blastocyst-like structures generated from human pluripotent stem cells. *Nature* **591** 620–626. (https://doi.org/10.1038/s41586-021-03356-y)

Zheng Y, Xue X, Shao Y, Wang S, Esfahani SN, Li Z, Muncie JM, Lakins JN, Weaver VM, Gumucio DL, *et al*. 2019 Controlled modelling of human epiblast and amnion development using stem cells. *Nature* **573** 421–425. (https://doi.org/10.1038/s41586-019-1535-2)

Received in final form 8 July 2021
Accepted 5 August 2021
Accepted Manuscript published online 9 August 2021